THE DEVELOPMENT AND DEMONSTRATION OF A PRACTICAL METHODOLOGY FOR FINE PARTICLE SHAPE CHARACTERISATION IN MINERALS PROCESSING

Lucy Little

A thesis submitted to the University of Cape Town
in fulfilment of the requirements for the degree of

DOCTOR OF PHILOSOPHY

15 August 2016

Centre for Minerals Research

Department of Chemical Engineering

UNIVERSITY OF CAPE TOWN

GRAPHICAL ABSTRACT

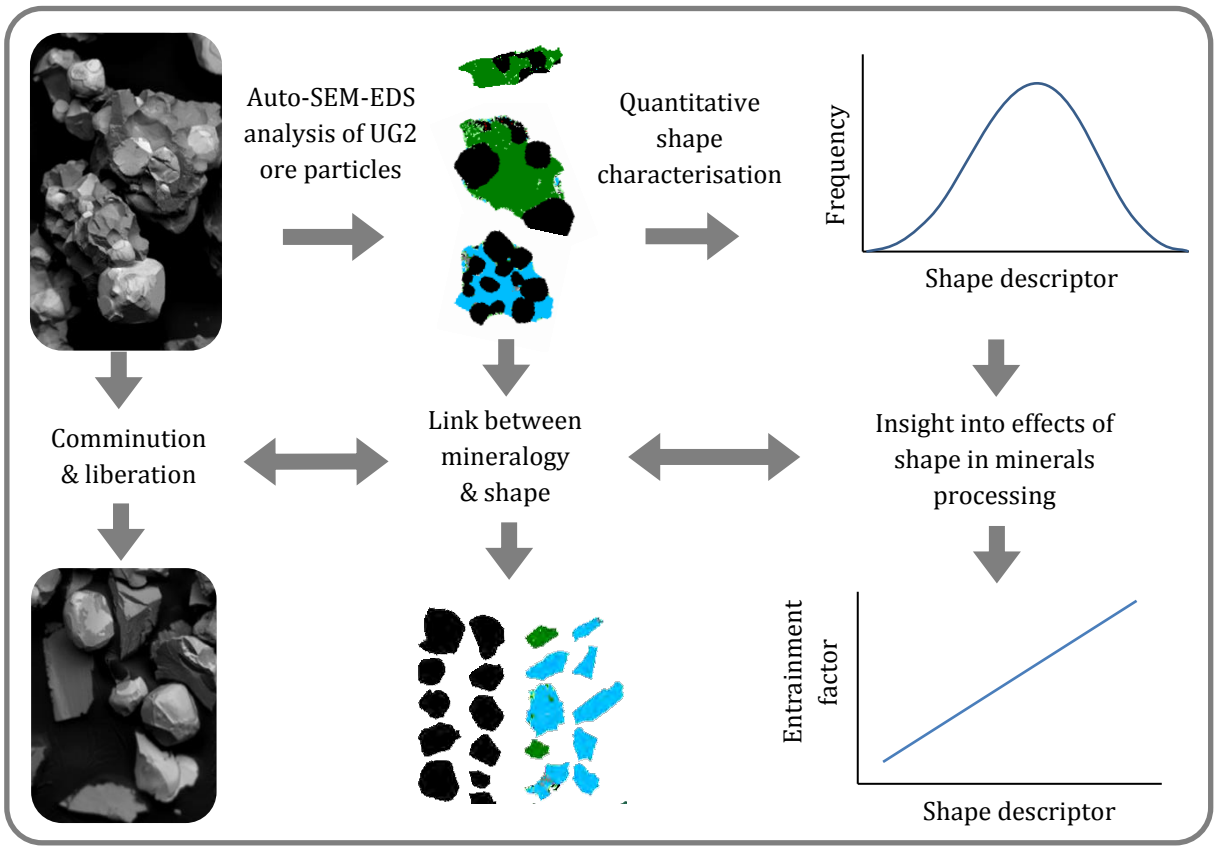

SYNOPSIS

Due to continually declining ore grades, increasing mineralogical complexity, and increasing metal demand, models for the design and optimisation of minerals processing operations are of critical importance. These models do not currently incorporate particle shape, which, although rarely quantified, is known to affect numerous unit operations. Automated Scanning Electron Microscopy (Auto-SEM-EDS) is a widely used tool for mineralogical analysis. It also provides an opportunity for simple, quantitative and mineral-specific shape characterisation. Existing mineralogical databases could therefore become useful resources to facilitate the incorporation of shape effects in minerals processing models. A robust Auto-SEM-EDS shape characterisation methodology is required to ensure that the particle shape information in these databases is interpreted appropriately.

For this work, a novel methodology for Auto-SEM-EDS shape characterisation was developed that is suitable for the analysis of fine particles (<75 μm). This involved testing the response of various shape descriptors to image resolution, and measurement with different devices and image processing routines. The most widely used shape descriptor in minerals processing, *circularity*, was found to be highly dependent on both image resolution and image processing settings, making it a poor choice for shape characterisation of fine particles. *Roundness* and *aspect ratio* were found to be more robust descriptors. However, in the interest of being able to compare particulate shape measurements across different studies, the precise definition of aspect ratio is important as variation in 'length' and 'width' definitions can significantly impact aspect ratio measurements. The possibility that preferential orientation of particles would introduce bias to the 2-D cross-sectional measurements was also addressed through comparison of roundness distributions measured from orthogonal cross-sections of a particulate sample mounted within a block of resin. The excellent repeatability of these measurements indicated that the particles were randomly orientated, and thus it can be inferred that 2-D measurements of a sufficient number of particles will be directly related to the particulate sample's 3-D properties. *Roundness* and *aspect ratio* were then used in conjunction to produce surface frequency distributions that allow for distinction between non-rounded

particles that were smooth and elongated and non-rounded particles that were neither elongated nor smooth.

Three applications of the shape characterisation methodology developed were then demonstrated, which highlighted some of the potential contributions that this methodology can make towards minerals processing. The applications were all based on a case study of the Upper Group 2 (UG2) Chromitite, a platinum group mineral (PGM) ore of key economic significance to South Africa.

The first application of the shape characterisation methodology constituted a novel approach to quantify phase boundary fracture, a mode of breakage in which cracks tend to propagate along the boundaries between mineral grains. The mineral specific shape characterisation that is possible with Auto-SEM-EDS was used to assess the conservation of grain shape during breakage, quantifying the extent to which phase boundary fracture led to liberation by detachment of the chromite grains. The critical importance of phase boundary fracture to the liberation of platinum group minerals and thus the economic processing of UG2 ore was demonstrated. Both the data presented, and the novel approach, can provide valuable evidence to support the development of liberation models.

The second application of the methodology involved fine grinding of UG2 ore in ball mills and stirred mills, with particle shape analysis used to provide insight into breakage mechanisms. The particle shape characteristics of feed and product samples from both laboratory and plant-scale ball mills and stirred mills were compared. None of the milling conditions led to product particles being more rounded than feed particles. This suggested that the common perception that fine grinding involves a higher degree of abrasion than primary grinding is inappropriate if the definition of abrasion used is that which is commonly linked to rounding of particles. Particle shape was clearly dependent on ore texture and phase boundary fracture at coarse sizes, but below the chromite grain size distribution (less than 75 μm) there were minimal differences in shape between the major mineral components. The particle roundness distributions were similar for the laboratory stirred mill sample and the ball mill and IsaMill samples taken from the plant, suggesting that ore characteristics are the dominant factor controlling particle shape. The similarity in shape characteristics of samples from the plant-scale ball mill and IsaMill led to the deduction that differences in the performance of a UG2 ore flotation circuit with an IsaMill on- or off-line are unlikely to be attributable to particle shape effects.

Finally, entrainment is an important issue in most flotation circuits as it reduces concentrate grade. It is particularly important for UG2 ore due to the negative impact of chromite gangue on

smelter performance. Little appears to exist in the published literature correlating particle shape with entrainment, and therefore, the third application for the shape characterisation methodology was focused on this topic. This required an adaptation of the methodology in order to ensure that particle size was not confounding the results. The findings based on samples taken from a UG2 ore concentrator indicated that the chromite particles recovered to the concentrate streams were significantly more rounded than chromite particles of the same size in the feed and tails streams. This suggests that shape could have a significant effect on entrainment, although in this study it was not possible to identify the mechanisms responsible, and more research would be required to determine whether the observations are generalizable. The approach to decouple the effects of shape from size could be applied to other areas of minerals processing research, and could prove particularly useful for the incorporation of effects of shape in classification models for devices such as screens, hydrocyclones, thickeners, reflux classifiers and air classifiers.

Statement of originality

The novelty of the shape characterisation methodology developed in this thesis lies in the combination of simple, robust shape descriptors appropriate for characterisation of fine mineral particles, coupled with the transparent presentation of the shape measurements, and the rigorous testing of the approach with respect to resolution, particle orientation, and measurement with different devices.

The demonstration of the shape characterisation methodology includes the following original contributions:

- A novel approach to quantify phase boundary fracture based on the conservation of grain shape;
- Confirmation that phase boundary fracture can severely enhance liberation of valuable minerals in traditional, industrial scale ball milling circuits;
- Evidence suggesting that the large difference in energy intensity between ball mills and stirred mills does not significantly impact product particle shape distributions of UG2 ore, and fine grinding does not lead to rounding of particles in either mill type;
- Evidence of differences in particle shape between entrained gangue particles of similar sizes in the feed, tails and concentrate streams of an industrial scale concentrator, with the concentrate streams comprising more rounded particles.

Plagiarism declaration

I, Lucy Little (née van de Ruit), declare that the work in this document is my own, save for that which has been properly acknowledged. Five papers are incorporated in this thesis, all comprising work that I performed as part of the scope of the PhD, under the supervision of Dr Megan Becker, Professor Aubrey Mainza and Mrs Jenny Wiese. All work referred to that was done by others is cited or acknowledged appropriately, and does not compromise the originality of this thesis. Contributions made by co-authors to the jointly authored works contained in this thesis are outlined hereafter.

Signed by candidate 15/08/2016

Signed Date

Acknowledgement of author contributions to publications incorporated in thesis

Paper 1: Little, L., Becker, M., Wiese, J., Mainza, A.N., 2015. **Auto-SEM particle shape characterisation: Investigating fine grinding of UG2 ore**. *Minerals Engineering*. 82, 92–100

L. Little completed the experiments, analysed the results and wrote the paper. Co-authors assisted with logistics and advice for the experimental test work, and critically reviewed the manuscript, making suggestions related to structure and editing.

Paper 2: Little, L., Becker, M., Wiese, J., Yorath, G., Mainza, A. N., Tonzetic I. **Shape characterisation: can different devices produce comparable data for particulate samples?** *Proceedings of the XXVIIIth International Mineral Processing Congress. Quebec, Canada, 2016*

L. Little, M. Becker, and I. Tonzetic conceptualised the work. L. Little planned and oversaw the measurements, with technical assistance from G. Yorath and I. Tonzetic. L. Little analysed the data and wrote the manuscript, which was then critically reviewed by all co-authors.

Paper 3: Little, L., Mainza, A. N., Becker, M., Wiese, J. 2016. **Using mineralogical and particle shape analysis to investigate enhanced mineral liberation through phase boundary fracture.** *Powder Technology.* 301, 794-804

L. Little developed the concept, completed the analysis, and wrote the manuscript. All co-authors critically reviewed the manuscript and assisted with editing.

Paper 4: Little, L., Mainza, A.N., Becker, M., Wiese, J. **Fine grinding: how mill type affects particle shape characteristics and mineral liberation.** *Under review for Minerals Engineering, 2016.*

L. Little carried out the experiments, analysed the data and wrote the paper. All co-authors assisted with logistics and planning during the early stages of the work. They also reviewed the manuscript and assisted with editing.

Paper 5: Little, L., Wiese, J., Becker M., Mainza, A. N., Ross, V., 2016. **Investigating the effects of particle shape on chromite entrainment at a platinum concentrator.** *Minerals Engineering. 96-97, 46-52*

L. Little developed the concept, analysed the data and wrote the paper. V. Ross assisted with logistics for sampling at the platinum concentrator, and technical discussions of the theory and analysis. All co-authors critically reviewed the manuscript and assisted with editing.

Chronological list of conference presentations associated with this thesis

van de Ruit, L., Becker, M., Wiese, J., Mainza, A. 2014. **A mineralogical investigation of the effect of particle shape on chromite entrainment for a UG2 ore.** *XXVIIth International Mineral Processing Congress. Santiago, Chile. Oct. 2014*.

L. Little (née van de Ruit) delivered an oral presentation, and received a Young Author Award for the associated paper, which is presented in Appendix A. This early work is not incorporated within this thesis, but it influenced the direction of this thesis, highlighting the need for improved shape characterisation.

Little, L., Becker, M., Wiese, J., Mainza, A.N. 2014. **Auto-SEM particle shape characterisation: Investigating fine grinding of UG2 ore.** *MEI Process Mineralogy '14, Cape Town, South Africa, Nov. 2014.*

L. Little delivered an oral presentation corresponding to the work presented in Paper 1.

Little, L., Mainza, A. N., Becker, M., Wiese, J. **Using mineralogical and particle shape analysis to investigate enhanced mineral liberation through phase boundary fracture.** *SAIMM Minproc 2015, Cape Town, South Africa, Aug. 2015.*

L. Little delivered an oral presentation corresponding to the work presented in Paper 3.

Little, L., Wiese, J., Becker M., Mainza, A. N., Ross, V. 2016. **Investigating the effects of particle shape on chromite entrainment at a platinum concentrator.** *MEI Flotation '15, Cape Town, South Africa, Nov. 2015.*

L. Little presented a poster corresponding to the work presented in Paper 5.

Little, L., Mainza, A.N., Becker, M., Wiese, J. **Fine grinding: how mill type affects particle shape characteristics and mineral liberation.** *MEI Comminution '16, Cape Town, April 2016.*

L. Little presented a poster corresponding to the work presented in Paper 4.

Little, L., Becker, M., Wiese, J., Yorath, G., Mainza, A. N., Tonzetic I. **Shape characterisation: can different devices produce comparable data for particulate samples?** *XXVIIIth International Mineral Processing Congress. Quebec, Canada. Sept. 2016*

J. Wiese delivered an oral presentation, prepared by L. Little, corresponding to the work presented in Paper 2.

Acknowledgements

The people who made this work possible

Thank you to:

- Dr Megan Becker, who is passionate about her research, encouraging, patient and excellent at giving prompt feedback – I couldn't have hoped for a better primary supervisor.
- Prof Aubrey Mainza and Jenny Wiese, I was so lucky to have such a great team of supervisors, thank you.
- My husband, Warren Little, for being wonderful, and for literally being by my side throughout this journey.
- My family for also being wonderful. I haven't tried to calculate it, but Father-dearest probably gave up as much as three quarters of his life's income towards the education of his three children. And at the same time, with help from our wonderful mum, he managed to teach us to appreciate important things in life like family holidays and mountains. I am privileged.
- Jenna, Emma and Marc for assisting with proof-reading, (now I'll use that semicolon);
- Shireen, Kenneth, Rubin, and Monde for assistance in the CMR laboratories;
- Lorraine Nkemba and Gaynor Yorath for assistance with QEMSCAN sample prep and analysis at UCT;
- Lelanie Gryffenberg for running some samples on QEMSCAN at Mintek;
- Igor Tonzetic, Benjamin Tordoff and Shaun Graham for assistance with the Mineralogic work;
- Joerg Westermann from Retsch for assistance with the CAMSIZER XT;
- Victor Ross (SAMMRI advisor) for willingly discussing ideas, assisting with logistics for the plant related work, and reviewing papers;
- Anthony Anyimadu and Grant Cockburn (also SAMMRI advisors) for their interest in the project;
- Prof Robert Schouwstra and Prof David Reid for informal reviews of Paper 3 and discussions of UG2 ore geology, mineralogy and processing;
- Adj. Prof Jeremy Mann, Prof Sandy Lambert, Prof J-P Franzidis, Prof David Deglon, Prof Kari Heiskanen and Prof Jan Nesset for discussions and advice;
- Prof Eric van Steen, Dr Belinda Mcfadzean, and Dr Adeniyi Isafiade who reviewed my PhD proposal and offered advice for the way forward;
- The anonymous reviewers of the papers incorporated within this thesis;

- Prof Dee Bradshaw for inspiration and encouragement, and for having trained Megan so well;
- Braam Durant and Bernard Oostendorp for assistance with the SMD test work at Anglo-American Technical Solutions in 2013.

The institutions and companies who contributed to the research

Thank you to the South African Minerals to Metals Research Institute (SAMMRI) and the South African Department of Science and Technology (DST) for funding the project, and ensuring that the project was relevant to industry.

The financial assistance of the National Research Foundation of South Africa (NRF) towards this research is also hereby acknowledged. This included direct financial support as well as indirect research support through Grant Numbers 86054 & 93189. Any opinions, findings and conclusions or recommendations expressed in any publication generated by the NRF supported research is that of the author(s), and the NRF accepts no liability whatsoever in this regard.

Thank you to:

- The University of Cape Town – a fantastic university;
- The Department of Chemical engineering for fantastic support and facilities;
- The Centre for Minerals Research community for meetings, seminars, Research Days and CMR-weekends-away;
- Lonmin for providing the ore samples, and facilitating site-visits and surveys;
- Anglo American Technical Solutions (in 2013) for allowing use of the laboratory SMD;
- The UCT Mountain and Ski Club for wonderful weekend excursions!

CONTENTS

List of figures that convey the key research findings (24 of 82)

List of abbreviations and acronyms

Acronym	Definition
Auto-SEM-EDS/ Auto-SEM	Automated scanning electron microscopy with energy dispersive X-ray spectrometry (e.g. QEMSCAN, MLA, TIMA, Mineralogic)
BMA	Bulk mineral analysis (QEMSCAN measurement type)
BMS	Base metal sulfides
BSE	Back scattered electrons
DEM	Discrete element method
ECD	Equivalent circle diameter (2-D)
ESD	Equivalent sphere diameter (3-D or stereologically corrected 2-D)
Fe_{max}	Maximum Feret diameter
HPGR	High pressure grinding rolls
ICP-OES	Inductively coupled plasma – optical emission spectroscopy
MIG	Mainstream inert grinding
MLA	Mineral Liberation Analyser
PGE	Platinum group elements
4E-PGE (assay)	Includes the elements platinum, palladium, rhodium and gold
PGM	Platinum group minerals
PMA	Particle mineral analysis (QEMSCAN measurement type)
PSD	Particle size distribution
PSIA	Phase specific interfacial area
PSSA	Phase specific surface area
P80	Size corresponding to 80^{th} percentile of the particle size distribution
QEMSCAN	Quantitative evaluation of minerals by scanning electron microscopy
SIBX	Sodium iso-butyl xanthate
SMD	Stirred media detritor
UFG	Ultrafine grinding
UG2	Upper Group 2 chromitite
X-CT	X-Ray computed tomography

Chapter 1

INTRODUCTION

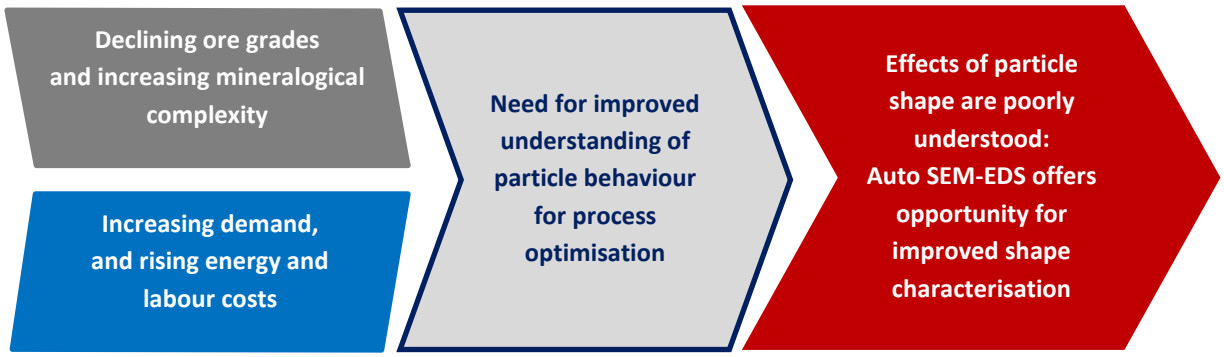

1.1 Background

1.1.1 The need for particle shape characterisation in minerals processing

Difficulties in the mining industry due to declining feed grades (Figure 1.1) and the increasing complexity of ores, coupled with increasing metal demand, result in a constant need to increase minerals processing plant capacities and optimise performance (Powell and Mainza, 2012). The major operations in minerals processing, i.e. size reduction and separation processes, are highly dependent on the mineralogy, size and shape of the ore particles. Process mineralogy involves the detailed characterisation of these particles in order to better understand their behaviour and thus optimise the design and operation of minerals processing circuits. Automated Scanning Electron Microscopy with Energy Dispersive x-ray Spectrometry (Auto-SEM-EDS) is a tool for characterising the mineralogy of particles, and has been used extensively for quantifying mineral abundance, liberation and associations (Becker et al., 2009; Cropp et al., 2013; Goodall and Scales, 2007; Goodall, 2008; Lotter et al., 2011; Rule and Schouwstra, 2011). Auto-SEM-EDS also provides information on particle shape properties, with the high resolution images obtained enabling shape characterisation of fine particles (-75 µm).

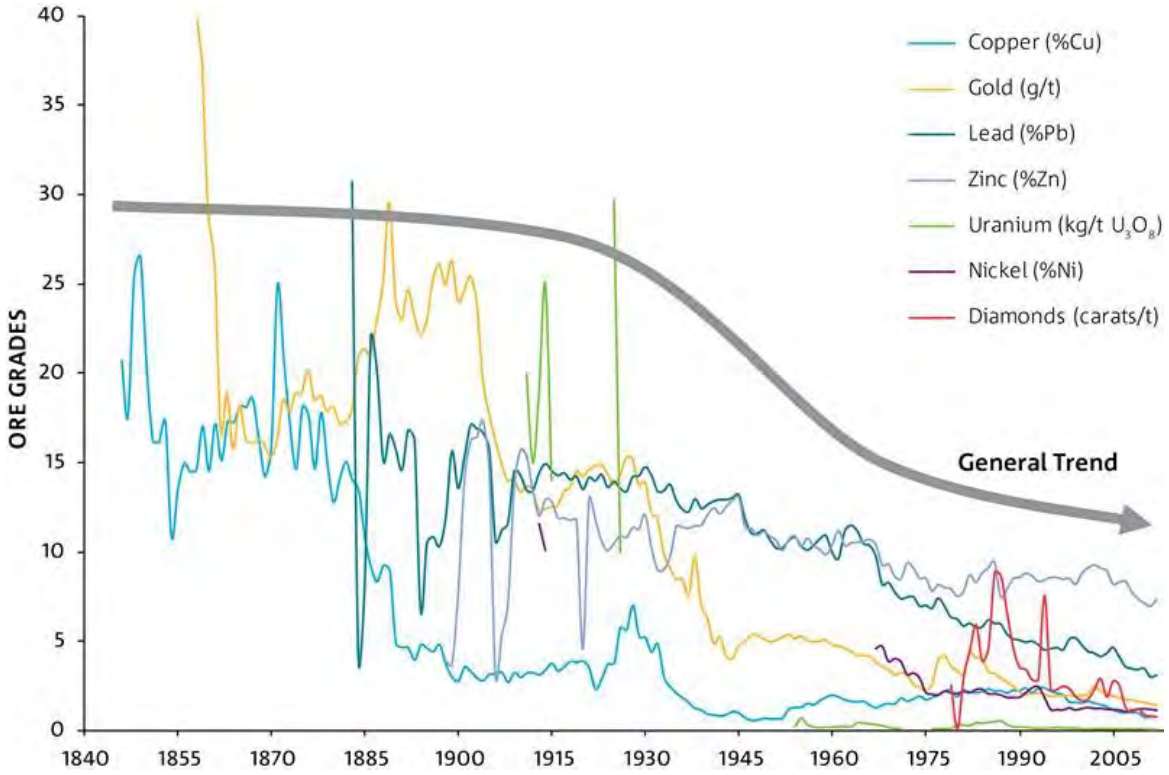

Figure 1.1: General trend of declining ore grades (Mudd, 2015).

The ability to couple quantitative shape characterisation and mineralogical analysis of ore particles within mineral processing operations could have significant benefits. For example, enhanced wear rates of mill liners over a particular time period may be attributable to a change in the feed ore mineralogy leading to an increase in particle angularity (Walker and Hambe, 2015). This problem would only be predictable with an understanding of the link between ore mineralogy and the modification of particle shape characteristics during grinding. In addition, effects due to mineral speciation or liberation on separation processes could be decoupled from effects due to particle shape (Vizcarra et al., 2011a). These types of studies have been scarce; Auto-SEM-EDS shape information has been underutilised, and increased usage could lead to significant advances in the understanding of particle behaviour in minerals processing operations.

The shape of a particle affects its fundamental interactions with other particles, water, air and equipment. Within a minerals processing circuit there are therefore numerous ways in which particle shape can affect process performance. In comminution the relationship goes both ways - different breakage mechanisms can affect progeny particle shape, and particle shape can affect breakage behaviour (Bbosa et al., 2006; Bengtsson et al., 2010; Chandramohan et al., 2010; Das and Cleary, 2010; Pourghahramani, 2012; Unland and Al-Khasawneh, 2009; Vizcarra et al., 2011b). In classification, particle shape affects the performance of screens, cyclones and

thickeners, as well as measurements of particle size distribution (Califice et al., 2013; Kashiwaya et al., 2012; Ozcan et al., 2000; Wills and Napier-Munn, 2006). Downstream, shape has been shown to impact flotation performance (Koh et al., 2009; Verrelli et al., 2014; Vizcarra et al., 2011a), and particle shape will affect slurry rheology and equipment wear rates throughout a plant (Becker et al., 2013; Walker and Hambe, 2015). Particle shape is clearly important, yet there is no routine analysis of particle shape distributions and no standard methodology for particle shape analysis and description in minerals processing.

Optimisation and design projects in minerals processing are typically facilitated by the use of models that enable the prediction of the response of process variables to proposed changes. There are many different types of models of varying complexity, which are continually being adjusted by researchers to improve model accuracy and predictive capabilities. With limited measurement of shape, it follows that most models typically used for minerals processing design and optimisation do not currently include effects of particle shape. In order to address this issue, a few requirements need to be met:

- The fundamental effects of shape on sub-processes need to be characterised and understood in order to incorporate shape parameters within models for each sub-process, and ultimately, within models of entire flow-sheets. Some progress has already been made in this area; for example the fundamental work done by Verrelli et al. investigates the effect of particle shape on particle-bubble attachment rates in flotation (Koh et al., 2009; Verrelli et al., 2012a, 2012b, 2014).
- Quantitative, abundant, accurate shape data are required in order to calibrate empirical models incorporating shape effects, or to verify computational models. These data should preferably be collected with a standardised, invariant methodology to ensure that the shape measurements are repeatable. The methodology should also be simple, as the measurement of particle shape needs to become routine in order for the value of the models to be realised.
- Ideally, the inter-relationships between mineralogy, ore hardness, particle size, particle shape, particle density, liberation and hydrophobicity need to be understood for any particular ore, in order to contextualise the outputs from the models, and understand the model limitations.

Auto-SEM-EDS databases comprising images of billions of particles from previous process mineralogy studies could be valuable resources towards meeting these requirements for the incorporation of particle shape effects into minerals processing models.

1.1.2 A case-study of UG2 ore

The need for minerals processing optimisation is evident in the platinum group element (PGE) industry in South Africa, which has suffered a severe decline over the last three years due to the collapse of the platinum price (Figure 1.2). The welfare of the platinum industry has a direct impact on the country's economy, as South Africa hosts 70% of the world's platinum group mineral (PGM) reserves (Lydall, 2009; Mudd, 2012). The Upper Group 2 chromitite ore (UG2) from the Bushveld Complex in South Africa, constitutes 40% of global PGE resources (Mudd, 2012), and the finely grained nature of the PGMs and the high chromite content of the ore lead to significant processing challenges for both comminution and flotation circuits. This makes UG2 ore a good choice for a process mineralogy case-study focused on particle shape characterisation in a minerals processing context. Specific processing issues to be addressed are associated with the requirement for fine grinding to liberate the finely grained PGMs, and the requirement to simultaneously reduce chromite entrainment during flotation, due to the adverse effects of chromite in the flotation concentrate on smelter performance.

Figure 1.2: The platinum price from the period January 2013 to June 2016 (www.platinum.matthey.com., 2016).

1.2 Problem statement

Due to continually declining ore grades, increasing ore complexity, and increasing metal demand, improving the design and optimisation of minerals processing operations is of critical importance. The models used for this purpose do not currently incorporate particle shape, which, although rarely quantified, is known to affect numerous unit operations. Auto-SEM-EDS provides an opportunity for simple, quantitative, mineral-specific shape characterisation, which will be a useful precursor to the inclusion of shape in models.

1.3 Objectives

The objectives of this study are therefore to:

1. Develop a simple, meaningful, quantitative approach for Auto-SEM-EDS particle shape characterisation that is suitable for fine particles;
2. Demonstrate how the shape characterisation methodology developed can contribute towards the understanding of:
   (a) Fracture mechanisms and the link between phase boundary fracture and liberation;
   (b) The modification of shape during fine grinding in ball mills and stirred mills;
   (c) The effects of particle shape on entrainment during flotation.

These objectives are addressed through a case study of UG2 ore involving fine grinding and flotation test work at the laboratory scale, supported by analysis of samples from an industrial UG2 ore concentrator.

1.4 Scope and limitations

Auto-SEM-EDS particle shape characterisation is the main focus of this thesis, with particular attention paid to the extraction of useful shape information from Auto-SEM-EDS databases. Given that existing Auto-SEM-EDS databases consist of two-dimensional particle data, the shape analysis used in this thesis is also limited to 2-D characterisation, although this is complemented by qualitative analysis of 3-D SEM images. The shape characterisation technique is then applied in conjunction with other process mineralogy tools, to study the physical aspects of particles produced during comminution that may affect flotation. This work was carried out using the case study of UG2 ore, so for the comminution aspect of the work, fine grinding in ball mills and stirred mills was considered of most relevance. The relationship between size reduction and liberation is also of key interest in minerals processing operations, and this relationship is directly impacted by phase boundary fracture. During initial stages of the work, observations of the shape characteristics of chromite and silicate mineral grains led to the concept of developing a novel conservation-of-shape approach to quantify phase boundary fracture.

PGE recovery and chromite entrainment were both identified as important aspects of UG2 flotation. Gangue and PGM mineralogy were investigated using Auto-SEM-EDS, although the PGM data were limited due to the resource intensive nature of locating individual PGM grains for characterisation in low grade ores (<5 g/t). The large confidence intervals associated with the limited PGM mineralogy data lead to only large differences being considered significant at a high confidence level. However, information on the gangue mineralogy is abundant, so in investigations concerning chromite, small differences were found to be statistically significant at a very high confidence level. As about 99% of the ore processed is gangue, understanding

behaviour of the gangue in both comminution and flotation is just as important as understanding the behaviour of the valuable minerals.

Models for design and optimisation of minerals processing circuits are discussed within the problem statement, but this thesis does not include a dedicated modelling component. Instead, the work done in this thesis is seen as a necessary step towards accurately incorporating effects of shape within commonly used models. There are other related areas of research, which may have been of interest to this study, but were not included in the scope. An example is classification; screens and hydrocyclones play a vital role in comminution circuits, and the effects of particle shape on the performance of these devices was not considered. Similarly, surface and pulp chemistry within a comminution circuit can have a strong influence on flotation performance, and the ceramic grinding media typically used in stirred mills results in a different chemical environment to that in ball mills with steel grinding media. However, the chemical environment within the two mill types was not considered to be related to the shape characterisation objectives of this thesis.

Figure 1.3 contextualises the scope of this work, highlighting how the topics covered fit together, and indicating the main chapter in which each topic is addressed.

1.5 Thesis layout

This thesis has been structured to include five peer-reviewed papers that convey the major findings of the work. These are preceded by generic literature review and methodology chapters to provide a cohesive introduction to the body of work as a whole. Each results chapter is prefaced with an outline of how the paper(s) within that chapter contribute to the overall objectives of this thesis. The hypotheses addressed in each paper are introduced in the relevant chapter preface, but are not referred to explicitly within the papers. Instead, each hypothesis is interrogated with respect to the findings from the test work in the concluding discussion chapter. The thesis structure is illustrated in Figure 1.4.

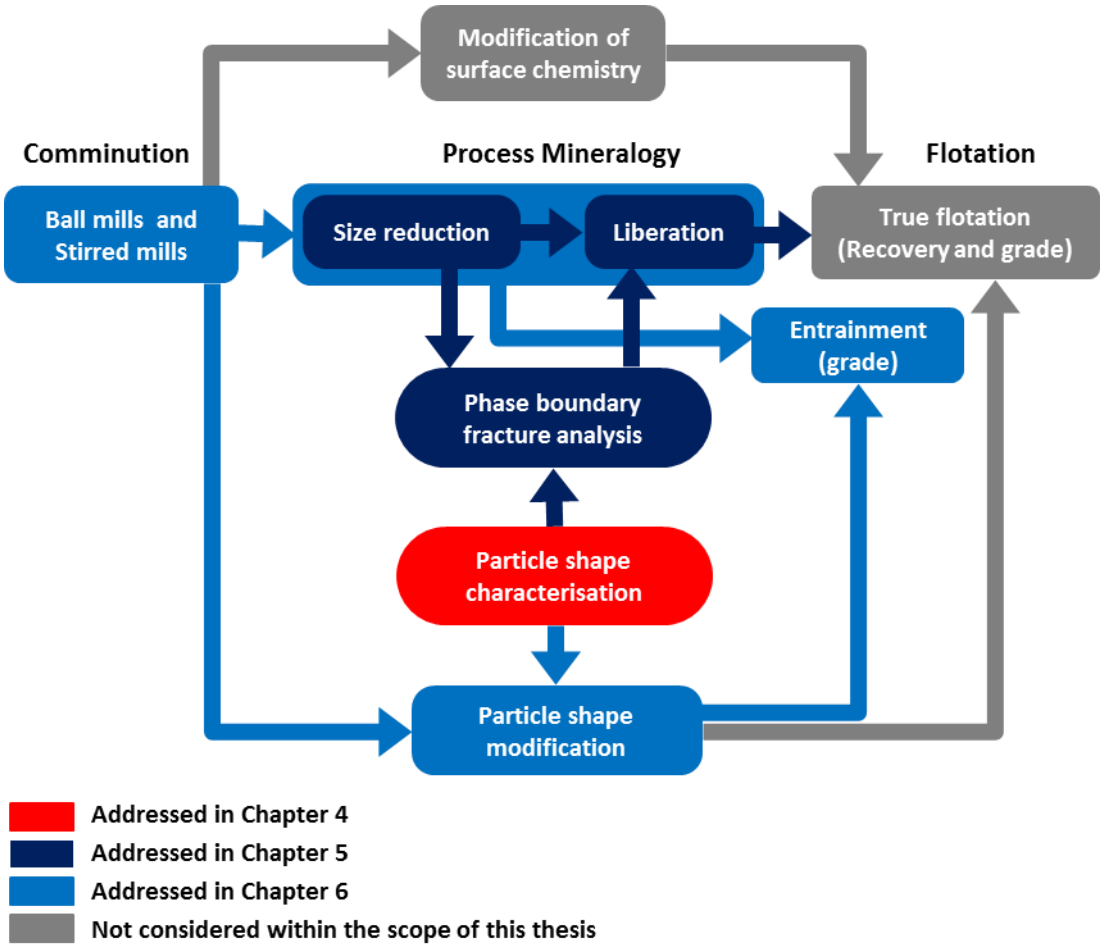

Figure 1.3: Overview of the thesis, highlighting the links between the aspects of the work that are considered in each chapter. Process mineralogy tools are used to assess the relationships between particle size, shape, and mineral liberation, which are in turn used to link comminution and flotation.

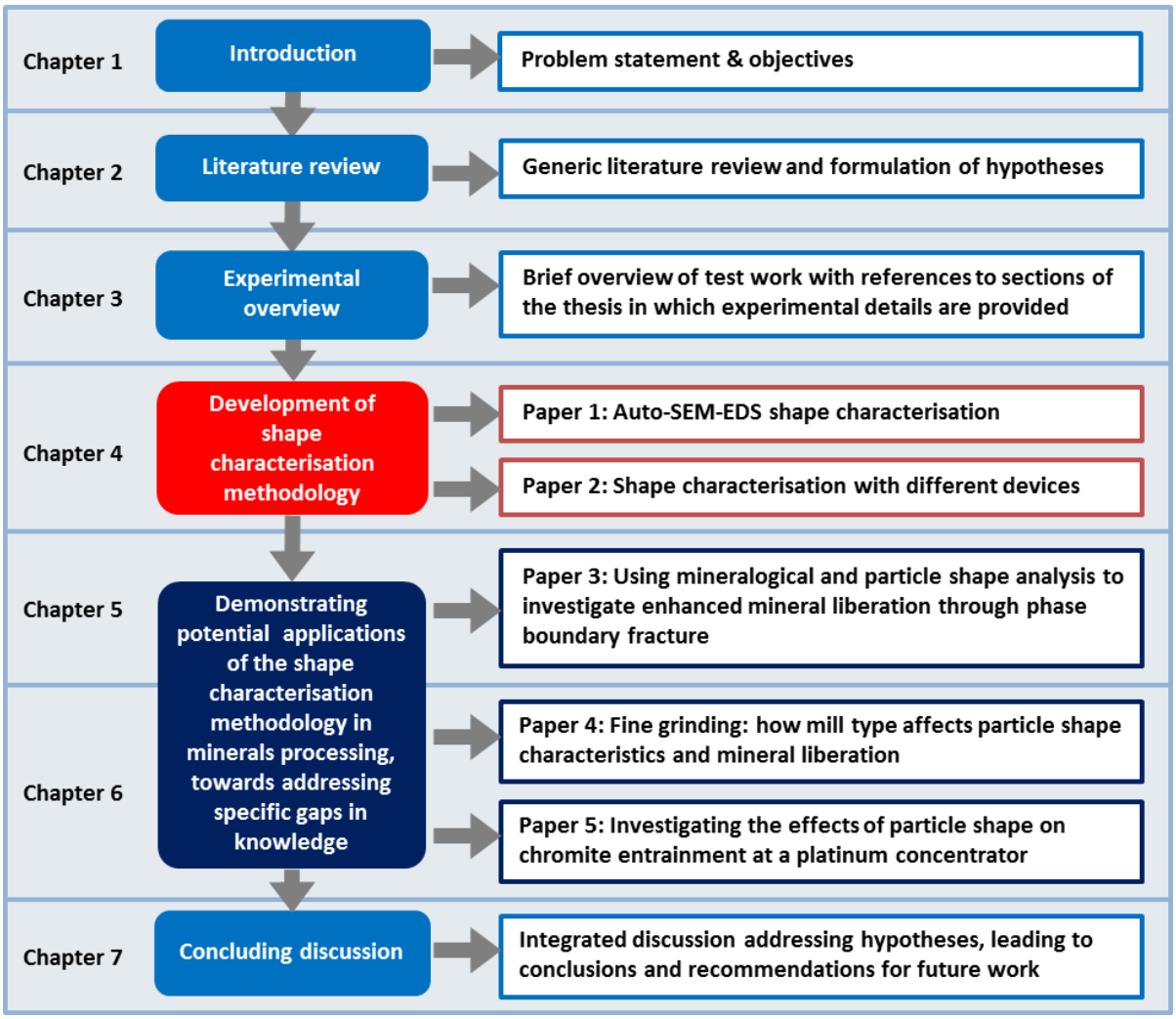

Figure 1.4: The structure of the thesis.

Chapter 2

LITERATURE REVIEW

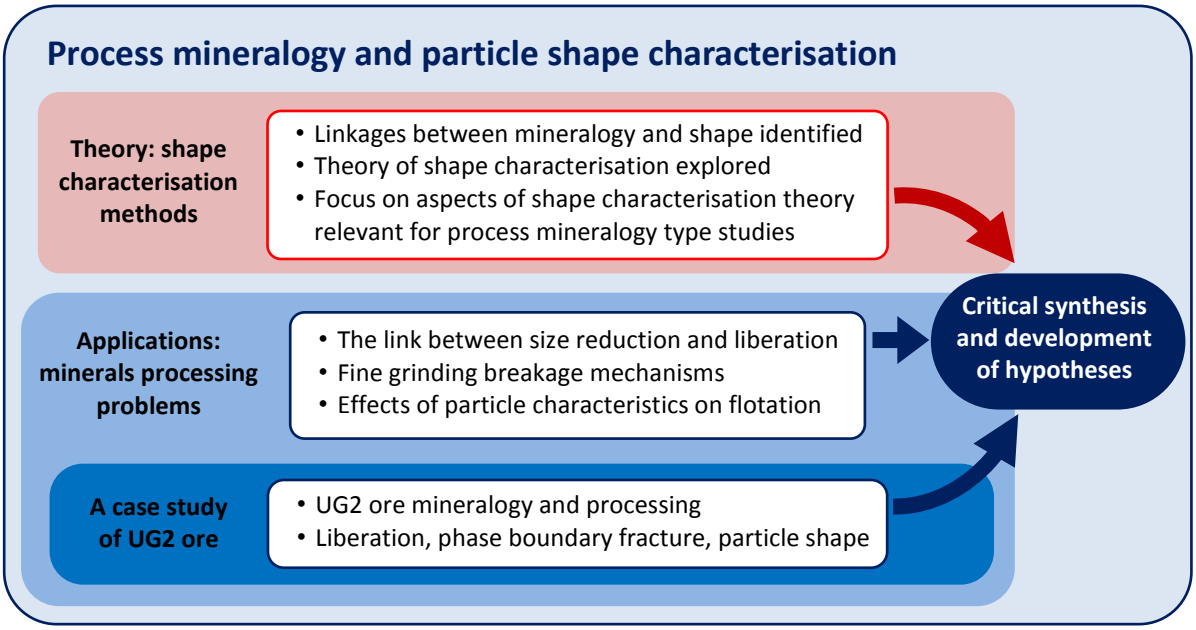

Illustration of the structure of this chapter, which explores particle shape characterisation theory, and specific minerals processing research areas that may benefit from quantitative shape characterisation.

The purpose of this chapter is to critically assess the literature related to the scope of the project, to lay the foundations for this thesis. Opportunities for particle shape characterisation are first explored within a process mineralogy context, with the objective of identifying appropriate shape characterisation techniques for Auto-SEM-EDS particle data. Specific areas of research within minerals processing that could potentially benefit from a process mineralogy approach incorporating particle shape characterisation are then considered. Finally, the potential applicability of the approach to UG2 ore is investigated.

Process mineralogy and particle shape characterisation: Theory

2.1 Background

Petruk (2000: 1) described process mineralogy as "the application of mineralogical information to understanding and solving problems encountered during the processing of ores, concentrates, smelter products and related materials." Historically, research in minerals processing has been carried out without access to detailed mineralogical information. The assessment of comminution performance was (and in many cases still is) based on size reduction, and the assessment of separation processes such as flotation was based on elemental recoveries. The need to characterise and understand mineral behaviour during minerals processing is increasingly being recognised for both optimisation and design, as it is mineralogy which to a large extent controls a process (Cropp et al., 2013; Evans et al., 2011; Goodall and Scales, 2007; Lotter, 2011; Lotter et al., 2011; Napier-Munn, 2014).

Auto-SEM-EDS systems are the 'work horses' in process mineralogy, and over two hundred Mineral Liberation Analyser (MLA) and QEMSCAN devices have been installed globally in the last decade (Gu et al., 2014). Other newer Auto-SEM-EDS systems such as the Mineralogic, TIMA and INCA Mineral, based on a variety of SEM platforms, are also now commercially available (FEI, 2015a, 2015b; Oxford Instruments, 2012; Tescan, 2012; Zeiss Microscopy, n.d.). There are numerous examples of operations that have benefitted from process mineralogy with the application of Auto-SEM-EDS, some of which have been described by Baum (2014), Evans et al. (2011), Lotter et al. (2011) and Rule and Schouwstra (2011). The particle features most commonly examined using Auto-SEM-EDS are bulk mineralogy, mineral liberation and mineral associations. Information pertaining to particle and mineral grain shape characteristics is also available, but is not being used extensively.

The requirement for accurate, quantitative particle shape characterisation in minerals processing has been acknowledged for many years (Meloy, 1990; Pirard, 1990). With the development of computer-based image analysis techniques in the 1980s, various researchers observed the potential value that automated particle shape characterisation could add to the minerals processing industry (Meloy, 1990; Pirard, 1990; Pons and Vivier, 1990) but twenty years later this potential is yet to be fully realised. Numerous studies using a variety of approaches have established that shape affects most unit operations within a minerals processing plant, including crushing, grinding, classification, flotation, size characterisation, rheology and wear rates (Bengtsson et al., 2010; Chandramohan et al., 2010; Kashiwaya et al., 2012; Koh et al., 2009; Ndlovu et al., 2011; Ozcan et al., 2000; Pourghahramani, 2012; Unland and Al-Khasawneh, 2009; Vizcarra et al., 2011a, 2011b; Walker and Hambe, 2015; Wills and

Napier-Munn, 2006). However, shape is neither routinely analysed on site, nor in typical comminution and flotation studies, and most models used for the design and optimisation of these processes do not currently incorporate effects of shape.

There is a close link between particle morphology and ore mineralogy (see Figure 2.1), as mineral properties such as hardness, ore texture, crystal structure and cleavage all impact particle shape properties (Cabri et al., 2008; Frances et al., 2001; Leroy et al., 2011; Roufail, 2011; Triffett and Bradshaw, 2008). This suggests that in minerals processing research involving shape characterisation, it would be advantageous to have insight into the mineralogy of the particles being assessed. Similarly, process mineralogy type studies could potentially benefit from quantitative shape characterisation, for example, to link the degree of liberation to particle shape (Leroy et al., 2011). Auto-SEM-EDS data includes information on both particle shape and mineralogy, presenting an opportunity that should be exploited.

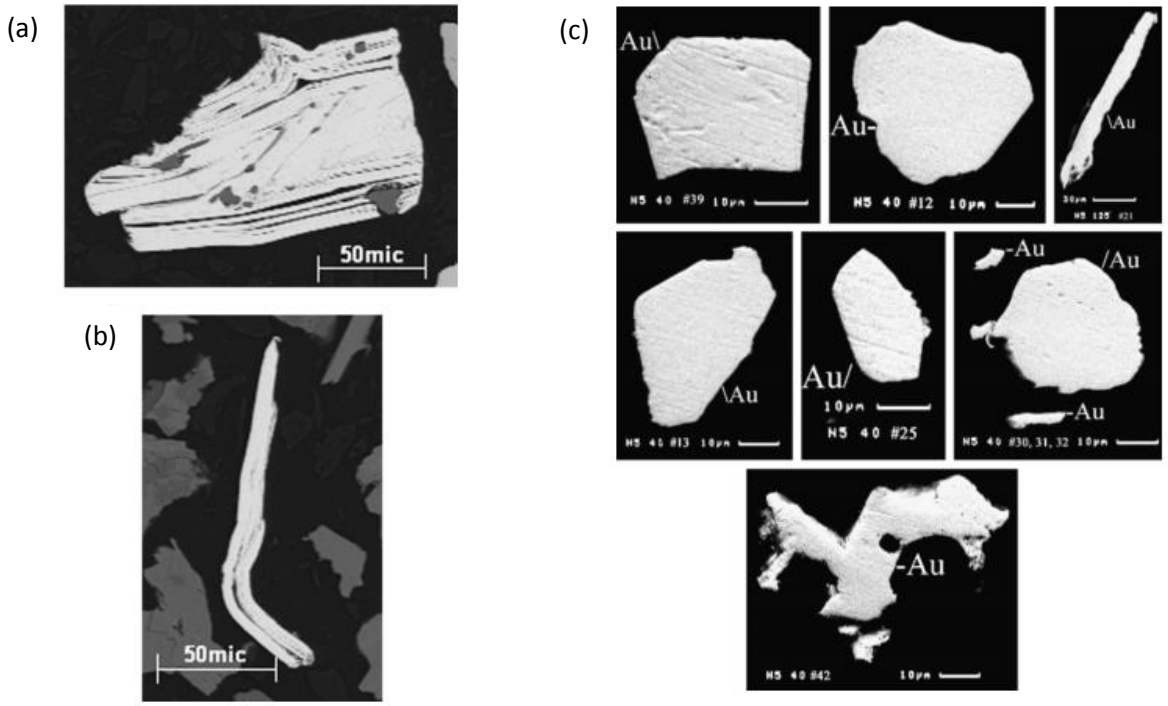

Figure 2.1: (a & b) MLA BSE images of molybdenite particles showing morphology (Triffet et al., 2008), (c) SEM images of liberated gold particles, with which qualitative assessment of shape was used to infer liberation by phase boundary fracture (Cabri et al., 2008).

Vizcarra (2010) was among the first to publish results of quantitative shape characterisation with Auto-SEM-EDS data. He plotted *angularity* distributions based on MLA images to compare the shape characteristics of ore fractured with compressive and impact breakage mechanisms (Figure 2.2). He also assessed the shape characteristics of chalcopyrite recovered to different concentrates in order to link flotation rate to particle angularity. Some examples of other

studies in which results from Auto-SEM-EDS shape characterisation have been reported include work done on dense medium separations (Grobler and Bosman, 2011; Pillay, 2015), magnetic separations (Dworzanowski, 2014), and samples of pure minerals (Wiese et al., 2015). This work has highlighted the potential for Auto-SEM-EDS shape characterisation; however the shape descriptors used in most of these studies are known to have limitations that may impact the accuracy and reproducibility of the data. These limitations need to be explored to understand the range of applicability of the shape descriptors and what level of confidence can be associated with the data.

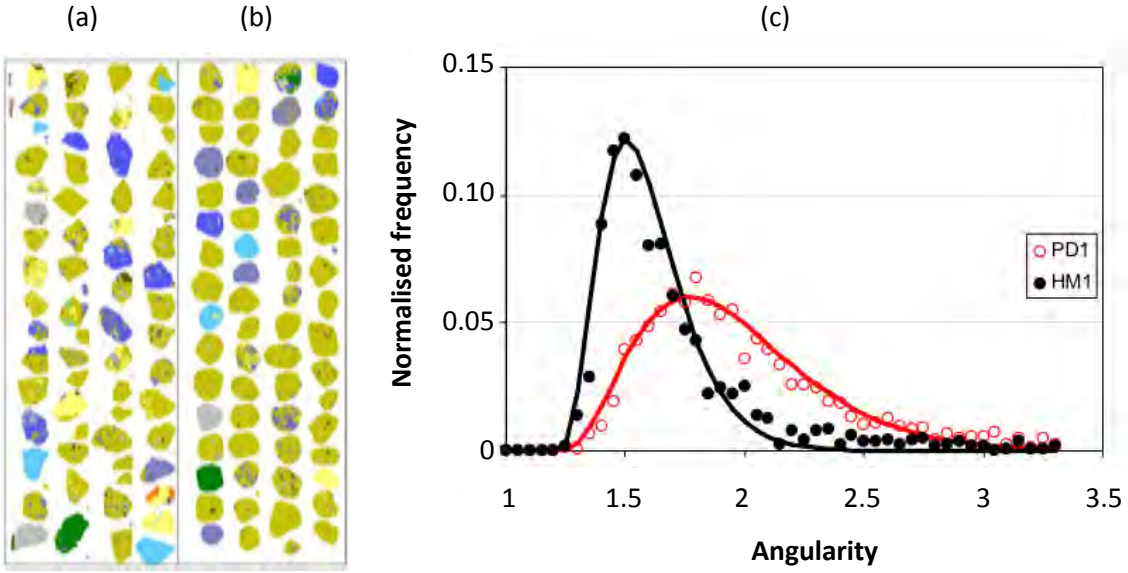

Figure 2.2: MLA false colour images of Ernest Henry ore in the -600/+500 µm size fraction after comminution with (a) Piston Die and (b) Hammer Mill. (c) Angularity frequency distributions there-of. Adapted from Vizcarra (2010).

2.2 Shape characterisation theory

Due to the wide range of applications of shape characterisation in different research fields, there is considerable variation in the approaches used to measure particle shape and morphology. There is a standard (document) for particle shape characterisation, ISO 9276-6, which is titled "Descriptive and quantitative representation of particle shape and morphology" (International Organisation for Standardisation, 2008). It is a useful document, however, it does not appear to have been widely used or cited, and even within 'the standard', there are inconsistencies in definitions and terminology. Table 2.1 has been compiled to provide an overview and critical assessment of some of the shape characterisation methods available.

Table 2.1: Overview and critical assessment of shape characterisation methods.

	Method	Reference	Critical assessment
Qualitative methods	**Words or images** 'angular' 'smooth' 'needle-shaped'	*Cabri et al. (2008)* *Kashiwaya et al. (2012)* *Makvandi et al. (2014)* *Triffett et al. (2008)*	Useful to accompany quantitative descriptors but may be subjective if used independently. Indication of image quality on which quantitative descriptors are based is useful for interpretation of results.
	Categories based on appearance Krumbein chart Manual point counting method	*Krumbein (1941)* *Roufail (2011)*	Some features of interest may be easier to determine visually than with algorithms. Method is difficult to standardise, and may be subjective.
Quantitative methods	**Geometric shape descriptors** 2-D (Image analysis): Circularity Aspect ratio Roundness	*Triffett & Bradshaw (2008)* *Vizcarra (2010)* *Kursun and Ulusoy (2006)* *Ulusoy and Kursun (2011)* *Ulusoy and Yekeler (2014)* *Pourghahramani (2012)* *Pons et al. (2002)* *Makvandi et al. (2014)*	Simple and user-friendly, most widely used in minerals processing. *Circularity or Angularity* is used most but it is dependent on perimeter and therefore not invariant with respect to image resolution. Data may be plotted as a distribution to represent populations of particles but this is rarely done; mean values are typically presented leading to minor differences being reported as significant with inadequate supporting evidence.
	3-D (micro-CT): Sphericity	*Bagheri et al. (2015)* *Garboczi et al. (2012)* *Lin and Miller (2005)* *Vonlanthen et al. (2015)*	Detailed high quality information for individual particles or small numbers of particles. High computational demand. Useful for correlating 2-D measurements or observations with 3-D.
	3D (BET surface area & size): Sphericity Roughness	*Verrelli et al. (2014)* *Rahimi et al. (2012)* *Guven et al. (2015)* *Kirjavainen (1992)*	Perhaps preferable to perimeter-based measurements, but this cannot be used to decouple roughness from shape or size as has been implied by some authors.
	Dynamic shape parameters Sedimentation velocity Pressure drop Rheology	*Lau and Chuah (2013)* *Xie and Zhang (2001)* *Medalia (1970)* *Khonthu (2012)* *Wiese et al. (2014)* *Hicyilmaz et al. (2005)*	Direct link to particulate behavior is good, but can only get an average value to represent a particulate sample, and it is difficult to decouple confounding variables.
	Mathematical shape functions Fourier analysis Fractal dimensions Tangent-angle function	*Garboczi et al, (2012*) *Ahmed, (2010)* *Bowman et al. (2001)* *Mollon and Zhao (2014)* *Pirard (1989)*	Most detail retained, good for particle reconstruction and if uniqueness is important, i.e. for image recognition. Can differentiate between surface texture and form, but only with high resolution images. High computational demand.

The terms ‘shape’ and ‘morphology’ have similar meanings, but the term ‘morphology’ generally implies more complex descriptions including characteristics such as porosity, roughness and texture. It is acknowledged that problems of shape and morphology are 3-D problems, and advances in X-Ray Computed Tomography (X-CT) are increasing the feasibility of 3-D morphological analysis (Bagheri et al., 2015; Garboczi et al., 2012; Lin and Miller, 2005). However, ISO 9276-6 is focused on shape characterisation techniques associated with 2-D image analysis because of the widespread use of image analysis methods. This thesis is also focused on 2-D image analysis methods because Auto-SEM-EDS mineral particle data sets were identified as a potential resource to be explored for fine particle shape characterisation.

Criteria for the evaluation of shape description methods include factors such as computational time, the levels of shape described, and the stability and sensitivity of the descriptor. Additional criteria are that the shape descriptors should be invariable with respect to rotation, reflection and scale (i.e. resolution), as well as independent (i.e. it is not necessary to report multiple shape descriptors that convey the same information (Ulusoy et al., 2003)). Descriptors should be economical in the number of terms required to describe a shape, and they should be easy to interpret (International Organisation for Standardisation, 2008).

Three levels of shape characterisation have been described based on the dimensions of shape features relative to particle size, as illustrated in Figure 2.3. Macro-descriptors are used to describe the overall form of a particle based on geometrical proportions, and these are calculated from size measurements of the particle silhouette. Meso-descriptors provide information on shape features that are not much smaller than the proportions of the particle, while micro-descriptors describe surface texture or roughness at a much smaller scale than the dimensions of the particle (International Organisation for Standardisation, 2008).

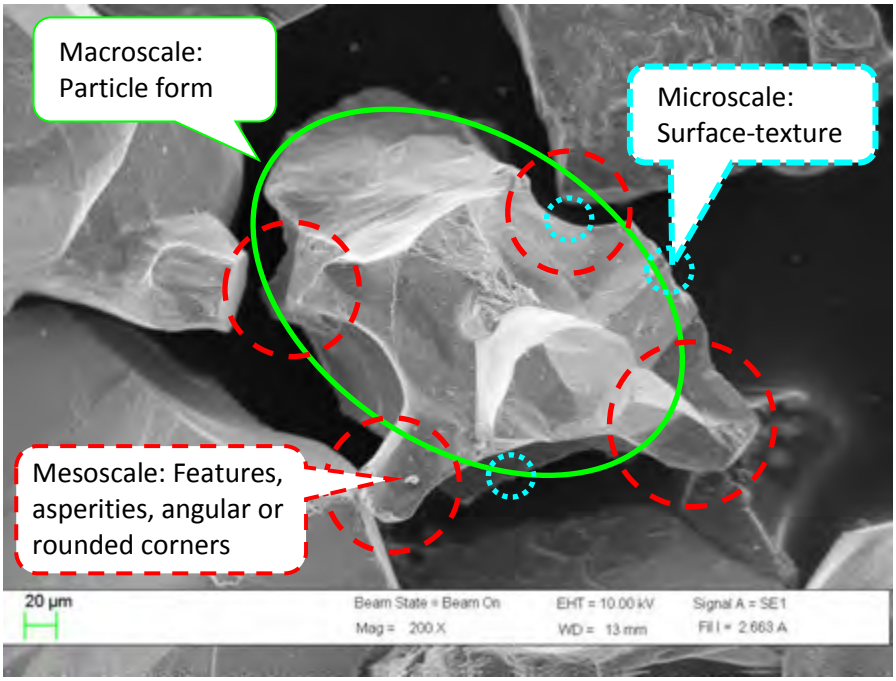

Figure 2.3: Illustration of different levels of shape characterisation (macro- and mesoscale) and morphological characterisation (microscale). Adapted from Barret (1980), illustrated on a secondary electron image of a UG2 ore particle.

Some geometric shape descriptors are presented in Tables 2.2 and 2.3, which illustrate the wide variation in shape descriptor definitions and terminology. A simple descriptor like 'aspect ratio' can have numerous definitions and a single term such as 'roundness' is commonly associated with more than one descriptor. In Tables 2.2 and 2.3 the descriptor names that were selected for this thesis are italicised, and throughout this thesis italics is used to indicate that the descriptor referred to is that with the precise definition corresponding to the selected descriptor names in Tables 2.2 and 2.3. *Roundness* is used extensively in this thesis as the name for the 2-D descriptor based on the ratio of the area of the particle cross-section to the area of a circle with diameter equivalent to the maximum Feret diameter of the particle. 'Roundness' is also commonly used to describe the radius of curvature of particle asperities. Both definitions for roundness are presented in ISO 9276-6. Ulusoy and co-authors have published widely on shape characterisation of particles using image analysis methods in the field of minerals processing. They use the term 'roundness' for the descriptor based on the perimeter of a circle with equivalent area to a particle, and 'circularity' for the descriptor based on the area of the minimum circumscribed circle of a particle (Kursun and Ulusoy, 2006; Ulusoy and Igathinathane, 2014; Ulusoy and Yekeler, 2014, 2005; Ulusoy et al., 2004, 2003).

Table 2.2: Macroscale geometric shape descriptors. Ratio definitions that give values between 0 and 1 are preferred (International Organisation for Standardisation, 2008). Underlined terms and associated descriptors are those that were selected for this thesis.

Illustration	Description	Terminology
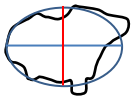	Width of Legendre ellipse/length of Legendre ellipse. The Legendre ellipse of inertia is centred at the particle's centroid, and has the same geometrical moments as the particle.	Ellipse ratio *(ISO 9276-6)* Legendre ellipse aspect ratio
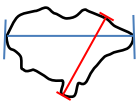	Minimum Feret diameter/maximum Feret diameter. NB: Sometimes the minimum Feret diameter is measured perpendicular to the maximum Feret diameter.	Aspect ratio *(ISO 9276-6)* Feret aspect ratio *(Ulusoy and Yekeler, 2014)*
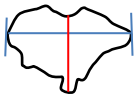	Short axis/long axis, where long axis is the maximum distance between two points on the particle contour, and short axis is the maximum width measured perpendicular to the long axis.	***Aspect ratio*** *(ASTM F1877-05)* (used by iDiscover™)
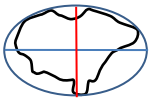	Width of bounding ellipse/length of bounding ellipse	Ellipse aspect ratio *(Ulusoy and Yekeler, 2014)* Bounding ellipse aspect ratio
	Width of bounding rectangle/length of bounding rectangle	Bounding rectangle aspect ratio *(Ulusoy and Yekeler, 2014)*
	Area of shape/area of circle with diameter equivalent to maximum Feret Diameter	***Roundness*** *(ISO 9276-6)* *(ASTM F1877-05)* Circularity *(Ulusoy and Yekeler, 2014)*
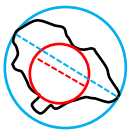	Diameter of maximum inscribed circle/diameter of minimum circumscribed circle	Irregularity Concavity *(ISO 9276-6)*

Table 2.3: Mesoscale geometric shape descriptors.

Illustration	Description	Names
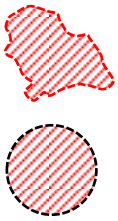	Perimeter of circle with equivalent area to shape/perimeter of shape	***Circularity*** *(Russ, 1995)* Sphericity *(CAMSIZER XT)* Angularity (inverse) Form factor *(ASTM F1877-05)* Roundness *(Ulusoy and Yekeler, 2014)* Compactness *(Mineralogic)*
	Perimeter of shape/perimeter of convex hull bounding the particle or area of shape/area of convex hull	Convexity Roughness *(ISO 9276-6)*
	Area between particle contour and smooth reference shape inscribed within particle/area of shape	Pirard roughness parameter *(Leroy et al., 2011)*
	Average radius of curvature of inscribed circles/radius of curvature of largest inscribed circle	Wadell roundness index *(Wadell, 1935)*

Fractal dimensions or low order and high order Fourier analysis methods are used to distinguish between meso-shape characteristics and micro-shape characteristics (i.e. for morphological analysis). Fractal dimensions are calculated by measuring the change in the perimeter P(λ) with lengths of the step size (λ) used to demarcate the perimeter, as illustrated in Figure 2.4. Fractal dimensions are calculated as the slope of the curve on a log–log plot, which typically has different values at high and low values of λ, representing structural and textural particle characteristics respectively (Pons et al., 1999).

There are various ways in which Fourier analysis can be applied in shape characterisation. The methods typically involve analysis of the waveform generated when the distance from the particle centroid to the contour (R) is traced through a rotation of angle θ, as illustrated in Figure 2.5. This is known as the R(θ) method (Bowman et al., 2001). Bowman et al. (2001) propose an alternative approach using Complex Fourier analysis, where the boundary of the particle is circumnavigated in the Complex plane. Compared to the simpler geometric descriptors presented in Tables 2.2 and 2.3, reports on the use of Fourier analysis and Fractal dimensions analysis in minerals processing applications have been scarce. A possible explanation for this is provided by Dumm and Hogg (1990: 286), who concluded that "Fourier analysis can provide a complete description of particle profiles but is unwieldy for practical application. Simplifications such as signature analysis seem to be insensitive to features such as angularity. Fractal analysis is excellent for describing fine-scale features but is relatively

ineffective for distinguishing between angular and rounded particles." Geometric descriptors appear to adequately provide more intuitive, less abstract shape measurements than Fourier analysis and Fractal dimensions with reduced computational time. Furthermore, very high resolution images are required in order to quantify micro-scale textural variations in morphology. Such high resolutions are not typical in image analysis systems because of both the digitization of the images, and the play-off between resolution and field of view (i.e. number of particles captured in a sample and how well they represent the population of particles). Even for simple geometric descriptors, image resolution can introduce significant errors (Kröner and Doménech Carbó, 2013). Resolutions of at least 5000 pixels per particle are recommended for descriptors that use perimeter, while resolutions of 100 to 200 pixels per particle are considered adequate for robust parameters such as projection area and ellipse ratio (International Organisation for Standardisation, 2008). An additional factor to consider is that analysis of a sample with a broad distribution of sizes will result in variation in image resolution in terms of the number of pixels per particle.

One potential application for which Fourier analysis may be useful in minerals processing research is in Discrete Element Method (DEM) modelling, where it can be used to generate accurate, realistic 3-D shapes (Mollon and Zhao, 2014).

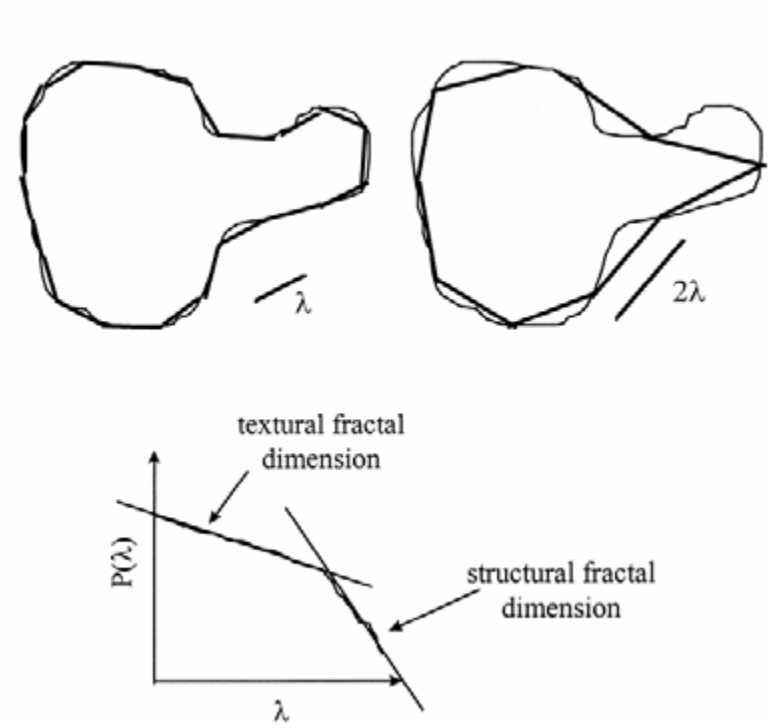

Figure 2.4: Fractal dimensions as described by Pons et al. (1999).

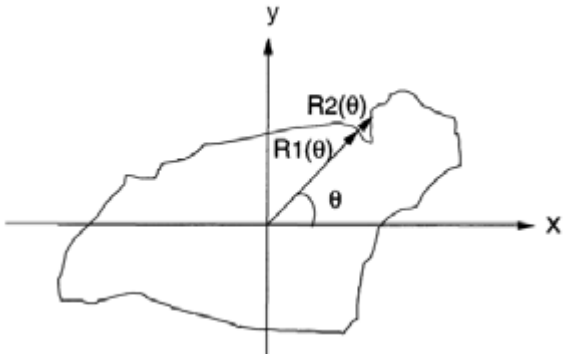

Figure 2.5: The use of Fourier analysis in closed form and difficulties encountered with re-entrant angles (Bowman et al., 2001).

2.3 Factors to be considered for Auto-SEM-EDS shape characterisation

Examples of Auto-SEM-EDS false colour images of particles are provided in Table 2.4, in comparison to some examples of images obtained with other shape characterisation methods. Qualitatively, the 3-D images of the volcanic clasts (Bagheri et al., 2015) appear to convey the most detailed information on shape, followed by the BSE images presented by Roufail (2011). However, if quantitative 2-D shape descriptors were being compared for all of the images (i.e. based on the particle silhouettes, the Auto-SEM-EDS images appear to be of similar quality to the images presented by Bagheri et al. (2015) and Roufail (2011), and of superior quality to the camera based systems. One of the key differences to consider is that Auto-SEM-EDS is done on polished sections and thus shows cross-sectional images, while most other imaging systems capture the particle silhouette or projected area. This has both advantages and disadvantages. For Auto-SEM-EDS:

- The preparation of polished sections is time-consuming but in many cases blocks are routinely prepared and measured to assess other mineralogical parameters such as bulk mineral liberation, so shape information could be considered as a useful 'by-product';
- There are well developed routines to ensure that mounted particles are adequately dispersed and statistically representative of the feed samples (Kwitko-Ribeiro, 2011);
- The particles are stationary, which ensures that motion will not impact the image quality, but this does lead to the possibility of the particles having a preferred orientation, which could introduce bias to the 2-D results;
- The polished sections allow for accurate identification of minerals, which could be used to link shape and mineralogy, but the particle size information is clearly biased due to sections that do not intersect the particle at its widest axis. This bias can be reduced through analysis of narrow size fractions and then exclusion of particle images that are significantly finer than the bottom screen size.

Table 2.4: Assessment of Auto-SEM-EDS false colour images in comparison to images from other systems. Note that false colour images have been processed, so sharpness gives an indication of resolution, but not necessarily imaging quality.

Auto-SEM-EDS system	Alternative imaging system
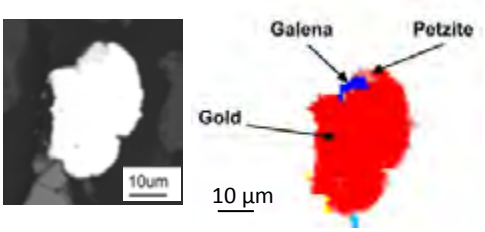 *SEM image and associated QEMSCAN false colour image of a liberated native gold grain (Coetzee et al., 2011)*	 *3-D XCT images of ~500 µm volcanic clasts (Bagheri et al., 2015)*
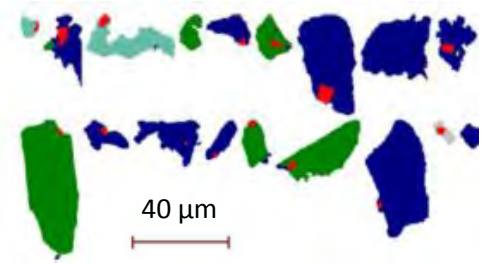 *High resolution Auto-SEM-EDS false colour images (Rule and Schouwstra, 2011)*	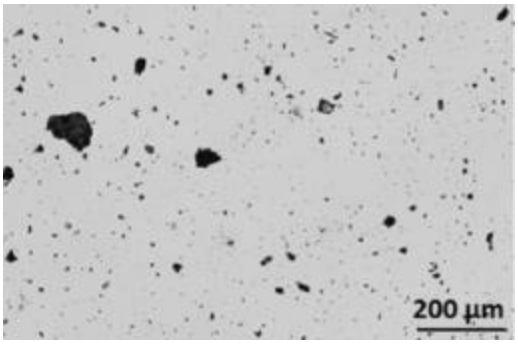 *Typical image taken by the Occhio 500-Nano (Leroy et al., 2011)*
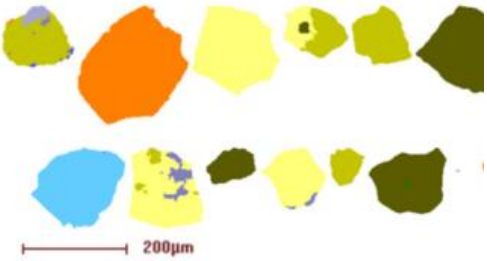 *MLA false colour images (Vizcarra et al., 2011b)*	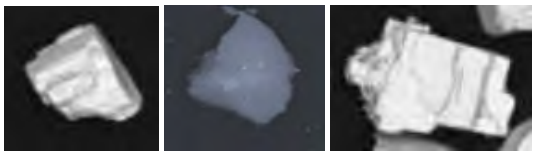 *Examples of '3-D' SEM images used by Roufail (2011) for shape characterisation*
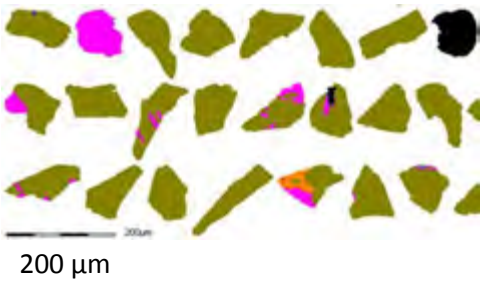 *MLA false colour images (Becker, 2009)*	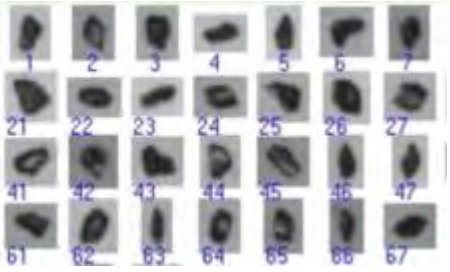 *Typical images taken by the Micrometrics® Particle Insight Dynamic Image Analyzer (Ulusoy and Yekeler, 2014)*

Appropriate size descriptors based on 2-D data are also a contentious issue. Equivalent circle diameter (ECD) is the most widely used 2-D size descriptor, described as the ideal normalisation parameter (International Organisation for Standardisation, 2008). Contrarily, Califice et al. (2013) recently concluded that ECD is not a good measure of size because it does not represent any of the physical dimensions of a flat or elongated particle. It may not represent length and width dimensions, but particle volume and thus mass could be considered more relevant size characteristics than these in many applications. Garboczi et al. (2012) compared the output from 3-D size and shape analysis to simulated 2-D analysis based on the 3-D data, and showed good correlation between the volume-equivalent sphere diameter (V-ESD) based on 3-D, and "the 2-D version of the 3-D VESD, defined as the equivalent circle diameter" (Garboczi et al., 2012: 87). In their work, ECD was obtained from the average of three orthogonal 2-D projections, which is not possible with Auto-SEM-EDS cross-sectional data. However, in spite of this limitation, ECD is the 2-D size parameter that is considered most likely to correlate to particle volume and thus particle mass for a given density.

When qualitatively assessing particles with Auto-SEM-EDS, it is possible to toggle between the false colour image representing the different minerals and the back scattered electron image showing the grey levels. It is important to note that the clarity of the false colour image gives an indication of the image resolution, but not necessarily of the image quality as image processing techniques such as thresholding will have already been applied by the software. Considerations necessary for image processing routines i.e. identification and separation of touching particles etc. still apply, however storage of the information for each particle does make it easy to check the performance of these routines, and manually adjust the output where necessary.

Based on the shape characterisation literature reviewed, the following shape descriptors were selected for consideration in this thesis:

- *Circularity* – the most widely used shape descriptor in minerals processing related research, but known to depend on image resolution;
- *Aspect ratio* – a simple, widely used shape descriptor that does not require high image resolution;
- *Roundness* – although rarely used, it is also a simple descriptor that does not require high resolution images, but it is more discriminatory than *aspect ratio* in terms of sphericity.

More complex methods such as Fourier analysis and Fractal dimensions analysis were not considered due to the resolution limitations expected for Auto-SEM-EDS false colour images of fine particulate samples.

Process mineralogy and particle shape characterisation: Applications

Comminution is an essential part of nearly all minerals processing operations, and for most ore types, the purpose of comminution is to liberate the valuable minerals for downstream separation processes. The link between size reduction and mineral liberation is critically important in both flowsheet design and comminution modelling to determine appropriate grind sizes that maximise valuable mineral recovery with the lowest possible energy consumption and operating costs (Lotter, 2011; Powell and Morrison, 2007). "Flotation is undoubtedly the most important and versatile minerals processing technique" (Wills and Napier-Munn, 2006: 267). Process mineralogy is the key to understanding the relationship between both size reduction and liberation, and thus comminution and flotation. Detailed particle shape characterisation may also have the potential to make a significant contribution to this understanding (Cabri et al., 2008; Leroy et al., 2011; Vizcarra, 2010).

Vizcarra's PhD thesis presents an excellent example of a process mineralogy study of the effects of different breakage mechanisms on particle liberation and shape characteristics, and how these in turn affect flotation performance (Vizcarra, 2010). Vizcarra studied compression and impact breakage in a piston-die compression unit and hammer mill, using Auto-SEM-EDS (MLA) to study the size-by-size liberation and shape characteristics of the feed and products. He also considered the effect of particle shape on the flotation rates of chalcopyrite at different hydrophobicities in order to determine possible effects of different breakage mechanisms on flotation performance. One of the limitations of Vizcarra's work was the use of the shape descriptor angularity. He acknowledged that the descriptor was dependent on image resolution, but he only considered the effect of scanning resolution (μm/pixel) and did not consider that for a population of particles measured with the same pixel spacing, variation in particle size will also lead to variation in the number of pixels per particle image. This means that the observation that "smaller size fractions are subject to more surface attrition events and a higher degree of particle rounding compared to larger sizes" (Vizcarra et al., 2011b: 1457), was likely biased by resolution in spite of the use of a constant scanning resolution for the different fractions (0.53 μm/pixel).

2.4 The link between size reduction and liberation is phase boundary fracture

As stated by Pérez-Barnuevo et al. (2013: 136), "texture is a critical mineralogical feature for the characterisation of ore behaviour during minerals processing. The possibility of achieving liberation by comminution, thus the potential recovery, is intimately related to textural relationships between minerals." Note that the definition of 'texture' in mineralogy differs

slightly to that in shape characterisation; here the term refers to grain size, grain boundary irregularity and the intergrowth patterns between mineral phases. It is the combination of texture and occurrence of phase boundary fracture that determine the relationship between grind size and the degree of valuable mineral liberation (Petruk, 1995, 1988).

Historically, there was an "almost universally held belief that grain-boundary fracture inevitably improves liberation" (King, 1994), however a lot of doubt as to the occurrence and relevance of phase boundary fracture has since been introduced. Firstly, King (1994: 233) used liberation model extensions to show that "…modest levels of grain-boundary fracture will not improve liberation from ores having exponentially-distributed intercept lengths." This finding was then reinforced with the following quotes: "It is known (King, 1994) that phase-boundary fracture does not influence liberation significantly unless it is severe enough to cause grain detachment and therefore no special provision is made in the models of the attainable region to accommodate this effect" (King and Schneider, 1998: 1152); "…recent theoretical studies (King, 1994) have suggested that interfacial fracture does not lead to enhanced liberation"(Fandrich et al., 1997: 187). Another comment also made by Peter King (1994: 228) has received much less attention: "However, even small improvements in liberation can lead to significant improvements in processing efficiency and ore textures that do promote increased liberation by grain-boundary fracture should be investigated".

Barbery (1991) wrote a book on mineral liberation in which he explores the theory of random uniform isotropic fragmentation (RUIF) or, more simply, random breakage. Various properties of the ore particles such as phase specific interfacial area (PSIA) would be conserved under RUIF, and liberation is relatively easy to model for this limiting case. Predicted liberation based on RUIF theory can then be compared to real observations to indicate how much non-random breakage mechanisms such as phase boundary fracture are affecting valuable mineral liberation for a particular ore type (Barbery, 1991). Unfortunately, Barbery passed away before completing the book. His colleagues compiled and published the book, and others revisited his work on stereological correction procedures (Leigh et al., 1996), but apart from this there has been no dedicated continuation of his work reported in the public domain.

Of the research that has focused on the occurrence of phase boundary fracture, most has been fundamental in nature, considering atypical comminution mechanisms such as electric pulse defragmentation, microwave cracking, thermal expansion and compressive grinding (Cabri et al., 2008; Charikinya, 2015; Kingman and Rowson, 1998; Omran et al., 2015; Song et al., 2013). Garcia et al. (2009), and Xu et al. (2013) used 3-D X-CT to quantify phase boundary fracture under controlled laboratory compression tests. Although they found evidence of phase

boundary fracture at low energy dissipation rates, these were acknowledged to be non-representative of the breakage environment experienced in traditional crushers under normal operating conditions. Garcia et al. (2009) therefore concluded that phase boundary fracture of the copper ore studied would not be achieved under such conditions. Results such as these perhaps explain why the influence of phase boundary fracture on valuable mineral liberation in normal operations has received limited attention in recent years, in spite of the increased measurement of liberation with Auto-SEM-EDS systems.

For some ores, compressive breakage mechanisms have been reported to promote fracture along phase boundaries to give enhanced mineral liberation (Apling and Bwalya, 1997; Fandrich et al., 1997; Hoşten and Özbay, 1998; King, 1992; Xiao et al., 2012), while for other ores, mineral liberation was reportedly independent of breakage mechanisms and determined by ore characteristics and particle size distribution alone (Vizcarra et al., 2010). Both microwave pre-treatment and electric pulse breakage have been shown to cause preferential cracking along phase boundaries (Charikinya, 2015; Kingman and Rowson, 1998; Omran et al., 2015; Song et al., 2013).

The research that has been done on phase boundary fracture has shown that its occurrence depends largely on ore characteristics. This suggests that the relationship between grinding and liberation will be different for each ore type. A simpler, more direct methodology for quantifying phase boundary fracture than those approaches already used would therefore be useful to develop a broad understanding as to which ore types and grinding conditions involve significantly enhanced liberation through phase boundary fracture. Work done by Leroy et al. (2011) and Cabri et al. (2008) has indicated a link between particle shape and phase boundary fracture which could potentially be exploited as a means of quantifying the extent to which phase boundary fracture can lead to liberation by detachment.

2.5 Fine grinding in ball mills and stirred mills

With the continual depletion of high grade, simple ore reserves, there is a need to process more ores in which the valuable minerals are finely grained. This has led to an increase in the requirement for fine grinding in minerals processing applications. Prior to the adoption of stirred mills into minerals processing applications in the early 1990s, ball mills were typically used for the final grinding stage of comminution circuits, and they remain a key component of most comminution circuits. In ball mills, energy for breakage is imparted to the charge by the rotating shell of the mill. The mill rotates at a speed that induces a cataracting and cascading motion in the charge, causing the grinding media (typically steel balls) to impact the toe of the charge (Wills and Napier-Munn, 2006). The small region within the toe therefore involves high

energy impact contacts, while the remainder of the charge experiences low energy impact, shear, and/or compressive contacts (Weerasekara et al., 2013). The relative contributions of these different breakage zones to the overall grinding performance is debated, with the traditional view being that impact breakage in the toe dominates, while recent DEM and PEPT studies suggest that the lower energy contacts in the bulk of the charge dominate (Weerasekara et al., 2013).

In stirred mills, energy is imparted to the charge with an impeller which enables a much higher rate of energy transfer to the charge than is possible in tumbling mills (see Figure 2.6). Stirred mills can be vertically or horizontally orientated. Different designs incorporate a variety of impeller types, and the impeller tip-speed can vary from around 3 m/s for the low energy Tower mill to 23 m/s for the high intensity IsaMills (Shi et al., 2009). In South Africa the commonly used stirred mills are the IsaMill and the Stirred Media Detritor (SMD), which are illustrated in Figure 2.7.

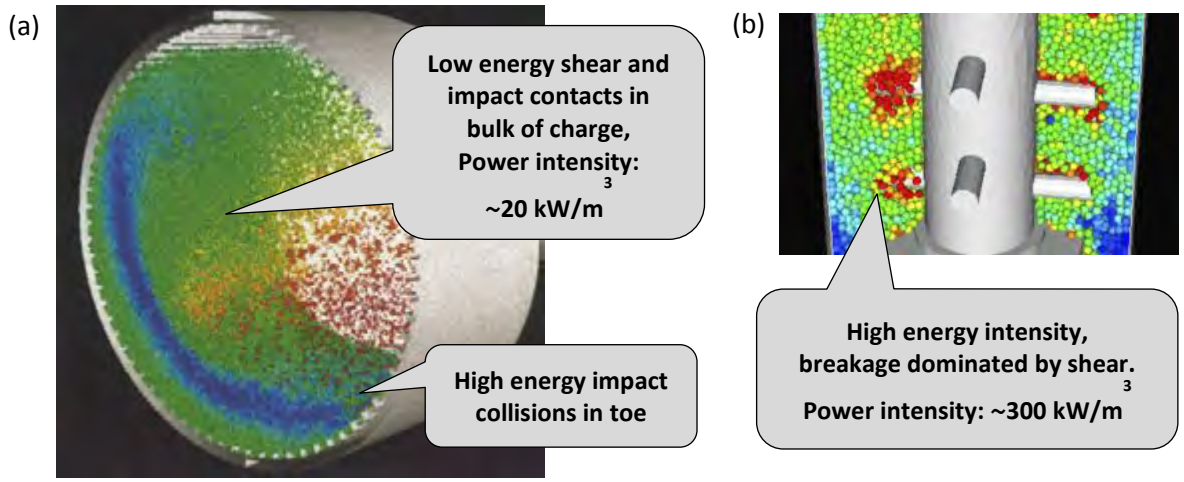

Figure 2.6: DEM-based illustration of charge motion within a ball mill (a) and a stirred mill with a pin impellor (b), indicating the difference in power intensity between the two mill types (Cleary, 2001; Shi et al., 2009; Sinnott et al., 2006).

Stirred mills are typically charged with fine ceramic grinding media (~1 – 5 mm in diameter), which afford a much higher media surface area than is possible in ball mills. 5 mm media in stirred mills would have 10 times the specific surface area of 50 mm media in ball mills. These features make stirred mills more efficient than ball mills for fine grinding (below 53 µm) and ultrafine grinding (below 10 µm), but the upper size limit at which they lose their advantage over ball mills is not clearly defined. The product fineness limit to which grinding in ball mills is considered practically and economically feasible is in the region of 30 - 45 µm (Erb et al., 2015; Jankovic, 2003). The upper feed size limit for stirred mills in hard-rock applications was initially considered for grinding feed sizes (F80) in the region of 100 µm, but recently there has been

considerable interest in the use of stirred mills in coarser applications (Erb et al., 2015; Rule, 2015), some exploring the potential to cut out tumbling mills from comminution circuits altogether (Manouchehri, 2015).

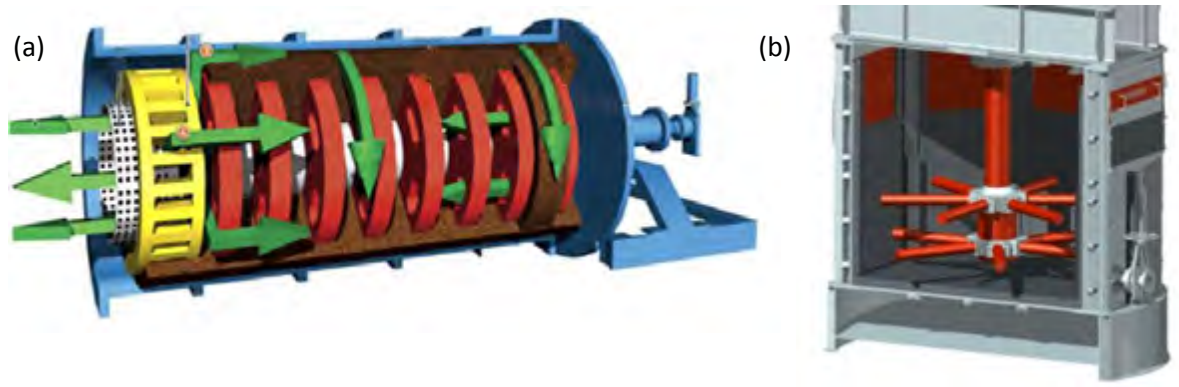

Figure 2.7: Diagrams illustrating the internals of (a) the IsaMill (Glencore Technology, 2016) and (b) the SMD (Metso, 2016).

Most breakage in stirred mills is caused by shear (Radziszewski, 2013), although inconsistencies in terminology have led to some confusion as to the understanding of the fragmentation mechanisms. It is widely accepted that the dominant breakage mechanisms in stirred mills are abrasion and attrition (Chaponda, 2011; Gao and Forssberg, 1995; Wills and Napier-Munn, 2006; Ye et al., 2010), however breakage mechanism definitions reported in the literature vary considerably.

Abrasion is sometimes defined as breakage caused by tangential shear forces (Wills and Napier-Munn, 2006), in which case, the definition is consistent with that of 'shear', and is appropriate for describing breakage in stirred mills. However most authors refer to abrasion as a gradual erosion mechanism resulting in a bimodal size distribution with fine particles being chipped off from the surfaces of parent particles due to low energy, localized stresses (Gao and Forssberg, 1995; Hogg, 1999; Kelly and Spottiswood, 1990; King, 2001; Varinot et al., 1997). Although under some conditions, both definitions could be adequate to describe the same outcome, in some operating conditions one or other of these definitions might not be applicable, which can generate confusion. For example, Resabel et al. (2014) attempted to model the mineral liberation of an ore milled in a stirred mill based on the assumption that small product particles would gradually be eroded, layer by layer, from the outside surfaces of the feed particles. This was to be simulated by the removal of fine 'particles' from the outside of two-dimensional MLA particle images. However, the experimental data obtained did not support this approach.

Table 5.1 (Chapter 5, Paper 3) and Figure 6.1 (Chapter 6, Paper 4) were compiled to clarify the author's understanding of breakage mechanisms and associated terminology. Both the table and figure clearly distinguish between terms associated with the breakage environment (i.e. impact, shear, compression), and terms associated with the fracture mechanisms (i.e. random fracture, abrasion, phase boundary fracture).

2.6 Fine grinding: how breakage mechanisms can affect particle characteristics

Particle size distribution, mineral liberation, and particle shape distribution are all particle characteristics that can be influenced by the comminution method, but these are also dependent on the ore characteristics. The degree to which the comminution method influences the progeny particle characteristics can therefore vary from ore to ore, leading to what can appear to be inconsistencies or contradictions within the literature. Findings reported in the literature for a specific ore type and grinding device are therefore not necessarily generalizable to other ore types. However, the following findings in the literature are considered of key interest for interpreting the effects of fine grinding environment on particle characteristics.

Ore texture and phase boundary fracture largely control the relationship between size reduction and liberation, as was discussed in Section 2.4. Preferential breakage (which is not the same as phase boundary fracture) refers to differences in breakage rates between minerals in an ore, and it generally leads to variation in mineral deportment to different size fractions. This is more likely to occur during particle-particle interactions such as during particle bed breakage rather than particle-media interactions (Fandrich et al., 1997).

The comminution method can impact product particle shape, which can also be linked to breakage mechanisms. Compressive or impact breakage that induces massive fracture produces angular particles, while repeated, low energy, localized stresses can lead to rounding of particles. The latter is typical in autogenous grinding and more pronounced for hard ores with long residence times (Kaya et al., 2002; Pourghahramani, 2012; Vizcarra, 2010; Vizcarra et al., 2011b). Cleavage (breakage along planes of weakness within the mineral crystal structure) can also impact shape and lead to smooth, flat surfaces (Frances et al., 2001). There have been limited studies comparing shape characteristics of fine particles after comminution in a ball mill and stirred mill, although through measurements of viscosity, Khonthu (2012) inferred that differences in shape characteristics depend on particle size and grinding time, with stirred mill products being more rounded than ball mill products after a short grinding period, and then more irregular and needle-like after a longer grinding period.

In continuous operations, the slope or shape of a product particle size distribution is determined as much by the classification method utilised (for example in an IsaMill or VertiMill

with an internal classifier) as by the breakage mechanisms themselves; but in batch laboratory mills the shape of the particle size distributions can indicate which breakage mechanisms are dominant in the system (Hennart et al., 2009; Ye et al., 2010). Abrasion is typically associated with a bimodal product size distribution, and fracture due to impact or compression with a unimodal distribution (Gao and Forssberg, 1995, 1989; Hennart et al., 2009; Kelly and Spottiswood, 1990).

Fine particles tend to be stronger than coarse particles due to a reduction in micro-flaws within the particles (Gao and Forssberg, 1995, 1989; King, 2001). Similarly, liberated mineral grains can be stronger than composite particles if inter-phase boundaries present weaknesses.

2.7 Flotation: how particle characteristics can affect grade and recovery

The two key performance indicators typically used in flotation are grade and recovery of the valuable minerals targeted in the process. The flotation literature to be reviewed was selected based on understanding the effects of physical particle characteristics on both true flotation (impacting recovery) and on entrainment (impacting grade). It is important to note that there are numerous other chemical and mechanical factors that influence flotation that are not considered within the scope of this study.

Particle size distribution has a strong impact on flotation performance. A relatively narrow/steep distribution is preferable to avoid loss of coarse composites or ultra-fines, however if there are too few fines the froth can be destabilized leading to loss of recovery (Pease et al., 2004). Different conditions are optimal for different particle size distributions (Safari et al., 2014; Schubert, 2008, 1999). For fine particle flotation – below 45 μm – high energy input is required and reagent dosages need to be adjusted to account for increases in surface area (Pease et al., 2006b, 2004). Johnson (1972) showed that the degree of entrainment was highly dependent on particle size, and this is now widely known (Wang et al., 2015).

Recovery and flotation rate are closely linked to liberation since hydrophobic minerals locked in hydrophilic minerals are unlikely to float. Improved liberation generally leads to improved recovery (as illustrated in Figure 2.8), although in cases where this does not hold, other factors such as surface chemistry need to be considered (Albijanic et al., 2014; Chapman et al., 2011; Grano et al., 1997; Solomon et al., 2011). Mineral associations can lead to the flotation of hydrophilic gangue minerals that are associated with hydrophobic minerals. These can either be naturally floatable gangue minerals such as talc, or valuable target minerals such as the base metal sulfides (Becker et al., 2009; Lotter et al., 2008).

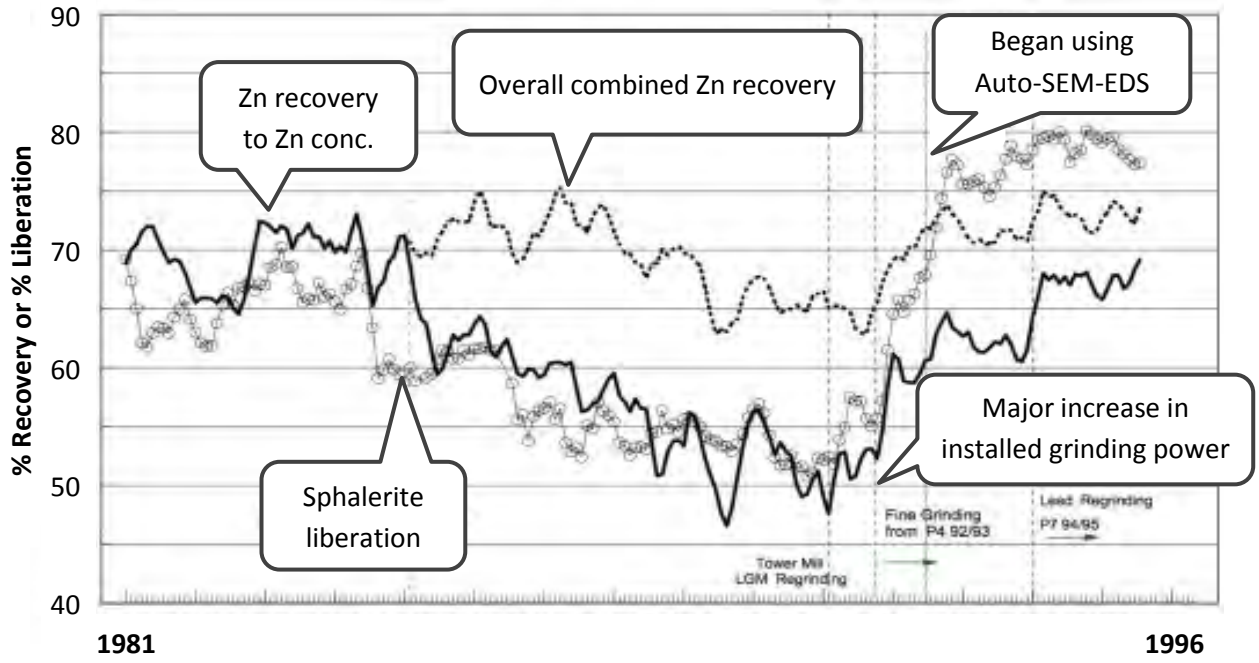

Figure 2.8: The relationship between sphalerite liberation and zinc recovery over a fifteen year period at Mt Isa in Australia. Adapted from Pease et al. (2006a).

Particle shape has a much smaller effect on flotation than particle size or hydrophobicity, but at low hydrophobicities, increased angularity or roughness can lead to faster particle-bubble attachment rates and improved flotation kinetics (Koh et al., 2009; Verrelli et al., 2012a, 2012b; Vizcarra et al., 2011a). This is illustrated in Figure 2.9, which shows the shape characteristics of chalcopyrite in concentrates 1 and 4 containing fast-floating and slow-floating particles respectively. With a collector to increase the chalcopyrite hydrophobicity, there is no difference in shape between the slow-floating and fast-floating concentrates, but with no collector added, the angular particles are recovered first (Vizcarra et al., 2011a).

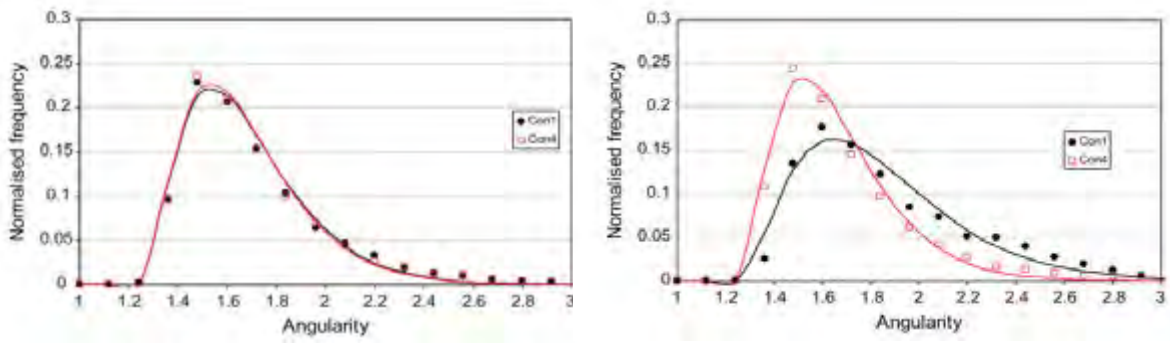

Figure 2.9: The difference in angularity distribution of the first (fast floating) and fourth (slow floating) flotation concentrates, with collector (left) and without collector (right) (Vizcarra et al., 2011a).

To date, the effect of shape on mineral particle entrainment has rarely been reported within the literature, with data from only two laboratory studies having been reported (Kirjavainen, 1992; Wiese et al., 2014). The study by Wiese et al. (2014) considered entrainment of particles in pure mineral systems in which the selected minerals had different shape characteristics. More elongated, angular mineral particles had higher rates of entrainment than rounded ones. Kirjavainen (1992) compared entrainment of mica and quartz, and the platy mica particles had the higher degree of entrainment. Comparable observations have been made in the paper industry, where longer fibres have been shown to have higher rates of entrainment than short fibres (Vashisth et al., 2011).

Wiese et al. (2014) discussed the theory of the observed effects of shape on entrainment with reference to drag coefficients of different particle shapes and hindered settling rates within plateau borders. If entrained particles within the froth are settling due to gravity within the plateau borders, they experience a drag force that will depend on their sphericity. This appeared to describe the behaviour observed by Wiese et al. (2014), however the authors acknowledged that flotation froths are typically highly unstable, with extensive coalescence between bubbles as they rise to the surface of the froth. The behaviour of the water and entrained particles within the lamellae as bubbles coalesce is not clear, and thus the overall effect of shape on the behaviour of entrained particles during these events is unpredictable.

A case study of UG2 ore

In Section 1.1, UG2 ore was selected as a case study for this work, to explore potential applications for Auto-SEM-EDS shape characterisation, towards addressing minerals processing problems. This section of the literature review is therefore focused on identifying issues specifically associated with UG2 ore processing that may benefit from an approach coupling process mineralogy and particle shape characterisation. Penberthy (2001) submitted a PhD thesis titled "The effect of mineralogical variation in the UG2 chromitite on recovery of platinum-group elements". She analysed 14 samples of UG2 ore from diverse geological locations within the Bushveld Complex. This provided an excellent foundation for the aspect of this thesis related to linking the behaviour of the ore during processing to mineralogical information. Her thesis contains detailed information on the mineralogical variation of UG2 ore as well as useful insight into its breakage, liberation and flotation performance.

2.8 UG2 ore mineralogy and processing

The 4E-PGE grade of UG2 ore typically varies between 3 and 6 g/t, with base metal sulfide (BMS) grades between 0.03 and 0.18 wt. %. The ore is predominantly composed of chromite (between 49 and 80 wt. %) and primary silicates (Penberthy, 2001). The geologically unaltered samples of UG2 typically consist of rounded chromite grains in a primary silicate matrix of pyroxene and plagioclase, with small amounts of secondary silicates such as talc and chlorite. The chromite grain size varies considerably, but of the 14 samples taken by Penberthy, the median chromite diameters varied between 164 and 177 μm (as measured by Auto-SEM-EDS). The base metal sulfides in these samples were found to mostly occur along these grain boundaries. Analysis of 4000 PGM grains showed that PGE-sulfides dominated over PGE - alloys, tellurides, arsenides and bismithotellurides, and the PGMs had a median equivalent circle diameter of 6.5 μm and were closely associated with the base metal sulfides (Penberthy, 2001).

Various mineralogical studies considering the flotation of PGMs in UG2 ore such as: Nel et al. (2004), Penberthy (2001), Chetty et al. (2009), and Rule and Schouwstra (2011) have shown that PGM floatability is largely dictated by PGM grain size, liberation and association with BMS, rather than PGM speciation (vis, PGE-sulfides, PGE-alloys, PGE-tellurides etc). Nel et al. (2004) described four categories of PGMs, with approximate distribution values in the feed: Coarse PGM (~5%), PGM associated with BMS (~40%), PGM occurring on host mineral grain boundaries (~30%) and PGM locked in silicates (~25%). The first three categories of PGMs show high recoveries, but the latter requires fine grinding to improve liberation. The understanding that losses in recovery were mostly due to inadequate PGM liberation was facilitated by Auto-SEM-EDS and is what led to the development and installation of stirred mills

for tertiary grinding in PGM concentrators. This led to a step change in PGM flotation recoveries due to improved liberation (Rule, 2011, 2010). In addition, stirred mills have been argued to provide surface cleaning of the particles, further improving recovery.

A disadvantage of fine grinding of UG2 ore is that it leads to increased entrainment of chromite to the flotation concentrate, which in turn leads to severe problems during smelting. Chrome spinel builds up in the furnace and has a freezing effect because it has a melting point about 200°C above the temperature of typical PGM furnaces. This leads to a reduction in both furnace efficiency and equipment lifespan (Bezuidenhout et al., 2013; Jones and Geldenhuys, 2011; Nel et al., 2004). Hay and Roy (2010) report the practical upper limit of chromite (based on Cr_2O_3) in furnace feed as 2.5 wt. %. The high density of the chromite relative to the silicates poses additional challenges to the comminution circuit. If a mill is operated in closed circuit with hydro-cyclones for classification, the difference in density leads to recirculation of the chromite (Becker et al., 2008; Mainza, 2006). Apart from reducing the throughput of the mills, this can lead to overgrinding of the chromite, which adversely impacts downstream processes. Fine chromite is more readily recovered by entrainment in flotation, and this in turn affects smelter performance (Hay, 2010; Jones and Geldenhuys, 2011; Wesseldijk et al., 1999).

UG2 ore processing circuits have gradually been modified to address the challenges of high chromite content and low grade, finely grained PGMs. In many plants the tumbling mills are operated in open circuit with staged flotation to avoid recirculation and overgrinding of chromite (Hay and Roy, 2010; Hay and Schroeder, 2005; Nel et al., 2004; Rule and Schouwstra, 2011). The 3-product cyclone has been developed as a means to maintain the efficiency benefits of closed circuit operation, while avoiding the overgrinding of chromite (Becker et al., 2008; Mainza et al., 2004a, 2004b; Mainza, 2006). Column flotation cells serve as cleaners at some concentrators to allow for improved froth drainage and a reduction in chromite entrainment (Hay and Roy, 2010). A typical concentrator flowsheet used for the processing of UG2 ore is provided in Figure 2.10.

As illustrated in Figure 2.10, it is typical for mainstream stirred mills in UG2 circuits to be included as optional components of the secondary grinding circuits. Whether or not the stirred mill (MIG circuit) is on or offline is likely to affect particle characteristics, having consequences for the downstream flotation performance. The influence of different fine grinding breakage mechanisms on particle shape characteristics and the subsequent effect of shape on both true flotation and entrainment have received limited attention in the public domain, and are therefore poorly understood (Khonthu, 2012).

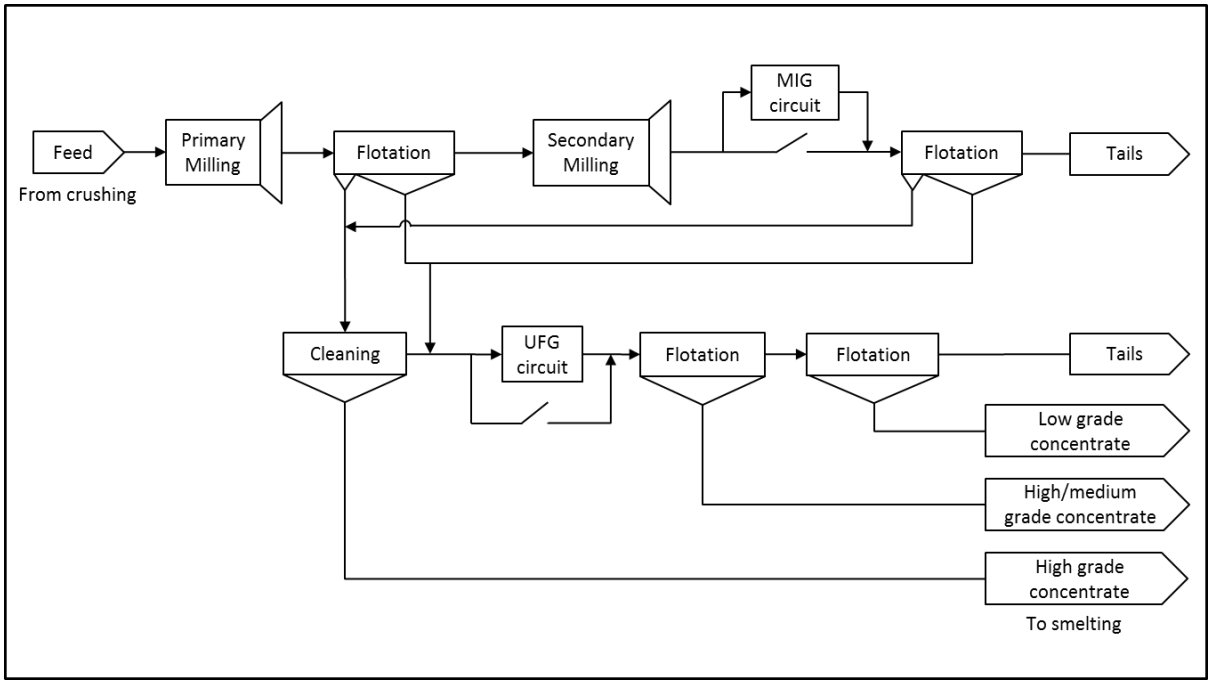

Figure 2.10: A typical concentrator flowsheet used in platinum operations adapted from Rule (2011).

2.9 UG2 ore: PGM liberation, phase boundary fracture and particle shape

There is significant evidence in the literature that indicates extensive phase boundary fracture during grinding of UG2 ore due to the 'loosely cemented' nature of the chromite silicate matrix (Hay and Roy, 2010; Leroy et al., 2011; Nel et al., 2004; Penberthy, 2001). Penberthy (2001) found a positive correlation between the occurrence of BMS and PGMs on phase boundaries in the crushed feed and the degree of liberation of these minerals after grinding. From this she concluded that the liberation characteristics of base metal sulfides and PGMs were not random, but depended on the texture of the samples prior to milling.

A link between particle shape and chromite liberation in crushed UG2 ore was observed by Leroy et al. (2011), who used image analysis to determine the roughness and translucence of particles. The translucence was used to differentiate between the chromite and silicates. She found that the chromite-silicate composite particles (examples in Figure 2.11) had higher roughness indices than liberated chromite. This was attributed to preferential breakage along phase boundaries leading to protruding chromite grains. Leroy et al. (2011) then identified roughness as a discriminant parameter to be incorporated into a real-time, on-line image analysis system to monitor the liberation and size distribution of chromite in UG2 ore grinding circuits.

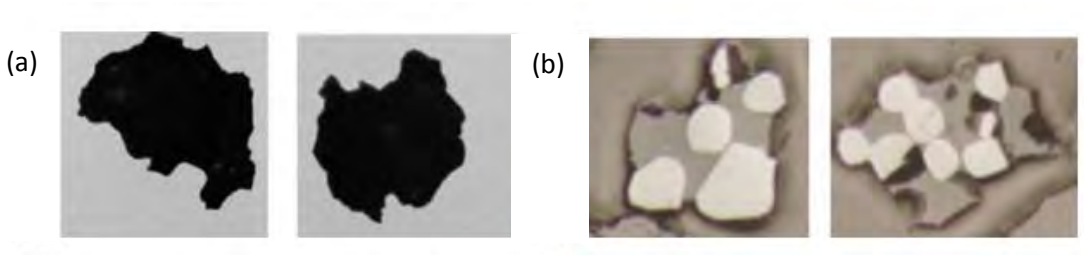

Figure 2.11: Images of UG2 ore composite particles from the -212/+150 µm fraction (a) imaged with the Nano 500, (b) as seen in reflected light microscopy (Leroy et al., 2011).

In conjunction, the findings of these two studies (Penberthy, 2001; Leroy et al., 2011) indicate that there is a possibility that particle shape characterisation can be used to quantify phase boundary fracture between chromite and silicates, which can in turn be linked to the liberation of the PGMs. This opportunity has not yet been explored.

Critical synthesis and development of hypotheses

Particle shape characterisation is widely used in many disciplines. A variety of approaches and descriptors have been developed and applied within different fields with the selection criteria depending on the characteristics of the particles being studied. Many complex shape characterisation techniques have been developed and reported in the literature, but these are rarely applied within research. Some limitations of the simpler, widely used shape characterisation approaches that have been applied in minerals processing include:

- The use of shape descriptors that are not invariant (i.e. *angularity, circularity*);
- Average values are reported rather than distributions;
- Very small differences are claimed to be significant due to perceived high confidence levels associated with large numbers of particles;
- There is a disconnection between shape and mineralogy;
- Characterisation of fine particles (-75 μm) has been scarce.

Descriptors depending on area and Feret diameters such as *roundness* and *aspect ratio* are likely to be more robust descriptors that should be appropriate for Auto-SEM-EDS shape characterisation of fine particles. Auto-SEM-EDS technology is widely used for analysis of mineral particles in process mineralogy studies and can be used for quantitative particle shape characterisation.

The application of Auto-SEM-EDS shape characterisation has potential to contribute towards the understanding of the following contentious topics or knowledge gaps within the literature:

- The relationship between phase boundary fracture and mineral liberation;
- The differences in breakage mechanisms in ball mills and stirred mills;
- The effects of particle shape on entrainment in flotation.

Hypotheses

The following hypotheses were formulated based on the literature reviewed:

1. The use of *aspect ratio* in conjunction with *roundness* will provide a quantitative, invariant shape characterisation technique that will be appropriate for the analysis of fine mineral particles (-75 μm) because neither descriptor depends on perimeter measurement.

2. During breakage of UG2 ore, phase boundary fracture between the chromite and silicates leads to enhanced liberation of the finely grained PGMs at a coarse size, because a significant portion of the PGMs occur along the weakly bonded chromite-silicate phase boundaries. The extent of this phenomenon can be inferred from the conservation of shape of the spherical chromite grains in conjunction with other techniques.

3. The significant differences in energy intensity between ball mills and stirred mills, and the dissimilar ratio of normally opposed contact forces to tangential shear forces within the two mill types will lead to significant differences in the shape characteristics between ore particles produced within the two mills.

4. Particle shape will affect the drainage rates of chromite grains entrained within the plateau borders of the flotation froth, with more rounded particles draining more readily, leaving a higher concentration of more angular particles being recovered to the froth.

Key questions

The following questions have been phrased to test each hypothesis:

- **How can Auto-SEM-EDS data best be used to characterise particle shape for minerals processing applications?**
    - How do *circularity*, *roundness* and *aspect ratio* measurements vary with image resolution?
    - Is bias introduced to the 2-D shape measurements through preferential orientation of the particles being scanned, or are they randomly orientated?
    - Are the differences observed between shape distributions statistically and practically significant?
    - How do these shape descriptors compare for different Auto-SEM-EDS systems such as the FEI QEMSCAN and Zeiss Mineralogic, and optical based systems such as the Retsch CAMSIZER XT?
    - How do the descriptors respond to differences in image processing techniques and perimeter algorithms?
- **Given the fine grain size distribution of PGMs in UG2 ore, is the liberation of PGMs typically observed at UG2 processing plants consistent with theory of random uniform isotropic fragmentation?**

  - Can differences in particle shape be related to the primary ore texture, and hence be linked to breakage along grain boundaries and liberation?
  - What descriptor or combination of descriptors will enable differentiation between the visibly liberated, spherical chromite grains and other particle types?
  - Can phase boundary fracture be quantified based on the conservation of chromite grain shape?
  - Are the findings from this method consistent with other methods for estimating phase boundary fracture?

- **How do progeny particle shape and mineral liberation characteristics compare for ball mills and stirred mills at the laboratory scale, and are these consistent with observations made at plant-scale?**

  - Do the particle shape characteristics of the major mineral components differ?
  - Do the particle shape characteristics vary with size?
  - Is there a correlation between the particle shape characteristics and grinding time in the batch mills?

- **How does the particle shape of chromite recovered to the concentrate compare to that in the feed and tails samples at laboratory and plant-scale?**

  - What is the effect of particle size on entrainment – is it a confounding variable?
  - How can the effect of shape be decoupled from the effect of size?

Chapter 3

METHODOLOGY

The FEI QEMSCAN 650F used for the mineralogical and particle shape analysis, and the laboratory SMD and ball mill that were used for the experimental test work.

Most aspects of the test work carried out for this thesis are explained later within the methodology sections of the papers presented in Chapters 4 – 6. In order to avoid repetition, this chapter provides a simple overview of the test work, referencing other sections of this thesis where the details have been documented.

3.1 Overview

The workhorse of this study was the FEI QEMSCAN 650F and associated software, iDiscover™, which was used for the initial development of the shape characterisation methodology documented in Paper 1, and for the applications of this methodology explored in Papers 3, 4 and 5. Other devices, the Zeiss Mineralogic and Retsch Camsizer XT, were tested alongside the QEMSCAN in Paper 2, which investigates the variability of different shape descriptor measurements of the same samples measured with different devices. The bulk of the samples that were analysed for this thesis were obtained through batch laboratory experiments in a ball mill, an SMD, and a modified Leeds flotation cell (8L). The remainder were sampled from UG2

ore concentrators operating in the Marikana region of the Western Limb of the Bushveld Complex.

The laboratory test work and test work associated with the plant samples are summarised in Tables 3.1 and 3.2, with reference to the sections of this thesis in which the work conducted is described, and the sections of the appendices in which the experimental details are presented.

Table 3.1: Summary of the laboratory test work.

Task	**Equipment/Materials**	**Measurements**	**Reference to details**
Sample preparation Removal of +1.18 mm fraction Blending and splitting 3 x 1 kg samples per test	UG2 ore Screen Rotary Splitter	Mass	Appendix B.1
Comminution experimentation Grinding curves 2 target grinds with each mill type	Batch ball mill Batch SMD Ceramic grinding media Fluke Power Logger Malvern Mastersizer Screens (√2 series)	Power, no-load power Specific Energy Feed PSD Product PSD P80, P50	Chapter 6.2 Appendix B.2
Flotation experimentation 3 depressant dosages 3 - 6 repeats each	8L Modified Leeds float cell Collector (SIBX) Depressant (Sendep 369) Frother (XP200/DOW200) Filter press Ovens and trays	Assays for PGE grade PGE recovery Assays for Cr grade and recovery Solids and water recoveries Degree of entrainment	Appendix B.3 Appendix E
Shape characterisation	FEI QEMSCAN 650F Retsch CAMSIZER XT Zeiss Mineralogic FEI Nova Nano-SEM	*Circularity* *Roundness* *Aspect ratio*	Chapter 4 Appendix C
Mineralogical characterisation Selected feed and concentrate samples	Assays – ICP-OES FEI QEMSCAN 650F	Modal mineralogy Grain size distribution Liberation PSIA	Chapter 5 Chapter 6.3 Appendix B.5 Appendix D.2

Table 3.2: Summary of the test work associated with the plant samples.

Task	Equipment/Materials	Measurements	Reference to details
Sampling	Automated (Vezin) sample cutters Pelican sample cutters* Stop watch Buckets	Flow rates from control system Sample mass (wet and dry)	Chapter 6.2 Chapter 6.9 Appendix B.5
Sample preparation	Filter press Ovens & trays Rotary splitter Screens (√2 series)	PSDs	Appendix B Appendix F
Shape characterisation	QEMSCAN	*Roundness* distributions	Chapter 6.3 Chapter 6.10 Appendix C.2
Mineralogical characterisation	Assays – ICP-OES QEMSCAN	Size-by-size recovery Modal mineralogy	Chapter 6.8 Appendix B.6

** A pelican sample cutter comprises a bucket with an extended 'beak' that has a narrow uniform opening designed to be passed under a vertically flowing stream to obtain a representative slurry sample, without causing severe splashing or loss of the slurry.*

Laboratory work has the advantage of allowing for a more controlled environment than is possible on site, and thus improved foundations for inference. However, effects observed in the laboratory do not always provide a realistic representation of plant behaviour, which is why the plant samples were included. Triffett et al. (2008: 833) articulated this for their example of a process mineralogy study of factors affecting the flotation of molybdenite, arguing that "there is a need for the published fundamental work to be viewed in the context of an industrial scale operation where any number of competing factors can be contributing to the behaviour of molybdenum."

The plant samples were taken from the Lonmin Eastern Platinum concentrators Eastern Platinum A (EPA) and Eastern Platinum Tailings Treatment Plant (ETTP). EPA is one of three Mill Float–Mill Float (MF2) circuits treating UG2 ore, with both primary and secondary grinding in ball mills. The tails from the three MF2 circuits are then passed through a spirals concentrator (operated by another company), which recovers some of the chromite. The tailing stream from this operation is fed to ETTP for what is effectively a tertiary Mill-Float stage. Grinding in ETTP is carried out with a ball mill and IsaMill, with a simplified flowsheet of the circuit configuration provided in Chapter 6.2.

A large number of 'exploratory' samples were taken over the plant survey period, most of which were sampled from the froth of various cells in EPA, with different methods of collection

intended to provide insight into the froth profile, and properties of the entrained particles at different levels within the froth. Analysis of the solids concentrations of these froth samples did not indicate any significant trends that would reflect the behaviour of the entrained chromite, so these samples were shelved. Instead, samples taken from the main flotation streams of EPA were selected to determine whether there were any differences in shape characteristics of the chromite recovered to the final concentrates and the chromite in the same size range of the feeds. The ETTP ball mill and IsaMill circuit did not have representative sampling points on all of the key streams, but the three samples that were selected showed highly repeatable mineralogy, and similar particle shape characteristics, indicating that they could still make a positive contribution to this thesis. The core samples from both the laboratory test work and the EPA and ETTP concentrators are listed in Table 3.3.

Table 3.3: List of key samples analysed.

Survey	Sample name	Sample ID	Purpose
Laboratory test work	Laboratory feed	Lab feed	Assessment of phase boundary fracture (Paper 3)
(Flotation feeds and concentrates at each grind)	Ball mill fine grind	BM fine	Development of shape methodology (Papers 1 & 2) Effect of grinding mechanisms on shape and mineralogy (Papers 1 & 4)
	Ball mill ultrafine grind	BM UF	
	SMD fine grind	SMD fine	
	SMD ultrafine grind	SMD UF	
ETTP concentrator	Ball mill feed	BM Feed	Effect of grinding mechanisms on shape (Paper 4)
	IsaMill feed	IM feed	
	IsaMill discharge	IM D	
EPA concentrator	Primary rougher feed	PRF	Gangue mineralogy and phase boundary fracture linked to PGM deportment and recovery (Chapter 5) Effect of shape on entrainment (Paper 5)
	Primary rougher tails	PRT	
	Secondary rougher tails	SRT	
	High grade concentrate	HGC	
	Low grade concentrate	LGC	

3.2 Experimental controls and sources of variability

Sources of error associated with shape characterisation are addressed in Chapter 4. This section provides the rationale behind some of the decisions associated with the laboratory test work that are not explicitly described in the following chapters. As no variables were manipulated for the plant samples, these are not included in this assessment, but issues associated with sampling are discussed in Chapter 6.

Random allocation for representative sampling

Initial blending and splitting of the bulk sample for the laboratory test work was intended to produce aliquots of equivalent mass and mineral composition, but a small degree of variability was still expected. For a rough estimate of this variability, each 3 kg sample was weighed before milling. There was little variation in mass, with minimum and maximum values of 3.01 kg and 3.04 kg respectively. The random uncertainty associated with measurements of grade varies depending on the abundance of the mineral or element investigated. For chromite variability within a concentrate sample (Cr grade ~10%), random uncertainty due to sampling and assaying was estimated by taking multiple aliquots from the same sample for each of the different splitters used and sending them for assays separately. The relative standard error associated with sampling and assaying together was found to vary between 0.2% and 0.5%. For PGE assays, much larger sample masses are required due to the very low grades. The 4E-PGE grade of each feed sample was back-calculated from concentrate and tails assays and solids recovery data for thirteen flotation experiments. The average grade was 4.25 g/t, with a relative standard error of 3%. This variability in PGE grade is considerably higher than the variability in chromite grade, which is expected for a trace phase where the possibility of the nugget-effect adds to the variability.

Chemistry effects: Use of ceramic grinding media and synthetic plant water

Flotation performance is known to be affected by surface chemistry (Bruckard et al., 2011; Grano, 2009; Greet et al., 2004; Vizcarra et al., 2011a). In order to reduce the differences in surface chemistry caused by different grinding environments, inert ceramic grinding media were used in both mill types. However, the substantial differences in milling times (in a stainless steel milling chamber) could still have affected the surface chemistry of the ore particles.

Figure 3.1: The ceramic grinding media used in the laboratory stirred mill (left) and ball mill (right).

Selection of target grinds and mill operating conditions

The mill operating conditions selected are provided in table 6.2. The rationale for these conditions is provided here. The range of appropriate target grind sizes was initially identified to lie between 80% passing 75 μm and 80% passing 45 μm, which represent a typical UG2 ore secondary grinding circuit product size, and the 'practical grinding limit' of ball mill circuits. This also corresponds to the mainstream inert grinding target size reported by Rule (2010). Due to the differences in slope of the PSDs of the two mill products, and inconsistencies between Malvern and screening PSDs, the grinds obtained with the two mills were neither equivalent with respect to P80 nor P50. For energy efficiency calculations, this was adjusted for by reporting size-specific energy consumption. For the study of particle shape characteristics and mineralogy, narrow size fractions were used, so the difference in size distributions was not considered a major concern with respect to shape. Finally, the proportion of fines (<10 μm) was consistent for the two mill types at both target grinds, which was considered a relatively good size control for the entrainment study and for PGM liberation.

The batch SMD used had a fixed speed drive with two choices of pin-impellor with different length pins. Initial tests showed that the short-pin impellor was not mobilising the entire charge and caking of the media and slurry was observed at the base of the mill, indicating a dead-zone. This was not observed with the long-pin impellor, so the long-pin impellor was selected for the remainder of the test work. For the stirred milling test work, zirconia-toughened alumina grinding media (s.g. = 3.83) was available in two sizes (5 mm and 3 mm), which are commonly used for mainstream inert grinding of PGMs in the platinum industry in South Africa. The 5 mm media was selected because the top size of the feed sample was coarser than that of typical mainstream inert grinding feed streams. The solids concentration used in the stirred mill (74 wt.%) was higher than is typical in industrial stirred mill applications, where materials handling issues are experienced at high solids concentrations. Most stirred mill tests are performed at solids concentrations between 45 – 65%, but for UG2 ore one can push this up because the ore is not rheologically complex (Chaponda, 2011; Khonthu, 2012; Lisso, 2013). For the test-work in this study, the higher solids concentration was selected as it allowed for the milling of 3 kg of ore per batch test, which was the mass required for the subsequent flotation tests.

The speed of the laboratory ball mill used was variable, and 70% critical speed was selected, which is fairly typical of conditions used in industry. The grinding media size was selected using Equation II proposed by Bond (1958), based on the top size of the feed, an estimate of the Bond Work Index of the ore (18 kWh/t) and the mill parameters. The top size of steel balls required was calculated to be 25.9 mm, which was adjusted for the ceramic media to 33.6 mm to account for the difference in density between steel and ceramic grinding media (s.g.~8 vs. 3.6). The

charge was then graded to simulate a worn charge based on charge distributions presented by Vermeulen and Howat (1989).

The ball mill used had a smooth lining, which is typical of laboratory ball mills as lifters can cause excessive cataracting of the mill charge at the preferred speeds of operation. No attempt was made in this work to alter the standard design of the mill used, and the operating conditions were kept as close as possible to standard practice in the laboratory where the work was performed. The conditions used for both the ball mill and stirred mill test work were neither optimised for breakage rates nor energy efficiency for the specific ore sample tested. In the ball mill, the energy intensity and perhaps the degree of impact breakage are likely to have been affected by the lower density of the ceramic grinding media (s.g. = 3.6) relative to more commonly used steel media (s.g. = 8).

(a)  (b) 

Figure 3.2: (a) The charge of the SMD during grinding, as viewed from above. Mill diameter is 22 cm. (b) the 8 L modified Leeds flotation cell showing the froth conditions during a test with no depressant added.

Sample losses

The first sample losses that occurred were of fine dust during splitting. Splitting was carried out under a vacuum hood to remove the dust. These losses were minor, and are unlikely to have affected the results in any way. Losses during the milling stage were also negligible due to careful cleaning of the mill and media into a bucket of slurry, which was carefully poured into the float cell and rinsed thoroughly. During flotation traces of concentrate were lost through splatter when bubbles burst, but these losses were unlikely to have been significant. During filtration of the flotation concentrates, the possibility of finely grained PGMs being lost through the filter paper was reduced with the use of two layers of filter paper. After drying, a small portion of the samples remained trapped within the filter paper, which was a potential source of error. This was typically 0.13 g to 0.42 g of sample (about 1 – 3%), with greater sample masses trapped in the filter paper for finer samples (see Figure 3.3). Assuming that this portion has the

same grade as that recovered for assay, this would not affect the results because recoveries were calculated based on the total mass of the concentrate. This was measured as the difference between the initial dry mass of the clean filter paper and the dry mass of the filter paper and concentrate.

Figure 3.3: Sample losses: Concentrate particles trapped in filter paper contribute to the measured mass of solids recovered, but these are not sampled for assay.

Sources of contamination

Another potential source of error in general is that of contamination from other ore samples, or between concentrates and tails. Contamination of tails and feed samples by concentrate samples was of the most concern to this study, however, various precautions were taken in the laboratory to prevent this. For example concentrate samples were dried in a separate oven to feed and tails samples. Equipment such as the rotary splitters, brushes and screens were also cleaned regularly, with particular care taken when switching between preparation of concentrate samples and tails samples.

Over-all uncertainty

A minimum of three repeats (including milling and flotation) were performed for each mill type, each grind and each depressant dosage to minimise the over-all random uncertainty for the experiments. Similarly, for the majority of the QEMSCAN analyses, three sample blocks were prepared for each fraction analysed. The QEMSCAN sample preparation procedure is outlined in Appendix B.5.

Chapter 4

AUTO-SEM-EDS SHAPE CHARACTERISATION

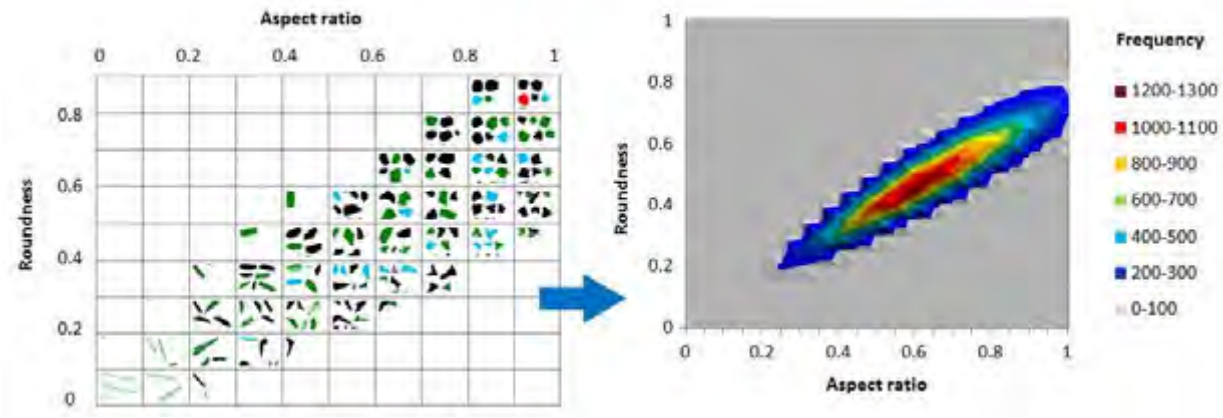

Graphical abstract for Paper 1, which illustrates the use of the descriptors roundness and aspect ratio in conjunction.

This chapter addresses the first objective of this thesis. A simple, meaningful, quantitative approach for Auto-SEM-EDS particle shape characterisation is developed, and it is suitable for characterisation of fine particles.

The hypothesis associated with this objective is:

> The use of *aspect ratio* in conjunction with *roundness* will provide a quantitative, invariant shape characterisation technique that will be appropriate for the analysis of fine mineral particles (-75 μm) because neither descriptor depends on perimeter measurement.

The bulk of the work carried out to meet the objective and test the hypothesis is presented in two papers. Paper 1 details the shape characterisation methodology as developed with the FEI QEMSCAN software iDiscover™. The research questions addressed in this paper are:

- **How can Auto-SEM-EDS data best be used to characterise particle shape for minerals processing applications?**
    - How do *circularity* and *roundness* vary with resolution?
    - Is bias introduced to the 2-D shape measurements through preferential orientation of the particles being scanned, or are they randomly orientated?
    - Are the differences observed between shape distributions statistically and practically significant?

Paper 2 tests the invariance of *circularity* and *roundness* when measured with different devices and different image processing techniques, towards addressing the following key questions:

- How do these shape descriptors compare for different Auto-SEM-EDS systems such as the FEI QEMSCAN and Zeiss Mineralogic, and optical based systems such as the Retsch CAMSIZER XT?
- How do the descriptors respond to differences in image processing techniques and perimeter algorithms?

The descriptor *aspect ratio* is not fully investigated within Papers 1 and 2, so additional sections (4.13 – 4.14) address the variability in *aspect ratio* definitions and length/width parameters. Furthermore, in Paper 1, a possible extension of the shape methodology is mentioned but not presented. This extension to the methodology is described and illustrated in Section 4.15. Finally, Sections 4.16 – 4.18 elaborate on the idea of stereological bias associated with 2-D shape measurements, and various options for weighting shape descriptor frequency distributions are discussed.

Paper 1: Auto-SEM particle shape characterisation: Investigating fine grinding of UG2 ore

Little, L., Becker, M., Wiese, J., Mainza, A.N., 2015. Minerals Engineering. 82, 92–100.

Keywords: Particle shape, QEMSCAN, UG2 ore

Abstract

For processing low grade complex ores there is a need to improve operation efficiency to maintain profitability. This may be done by introducing more efficient equipment or improving the understanding and modelling of minerals processing circuits. Particle shape can have an impact on numerous processes through its effect on drag coefficients, rheology, and particle bubble interactions. Understanding these effects in greater detail could significantly improve model capabilities. Automated scanning electron microscopy (Auto-SEM) can provide two dimensional particle shape measurements for thousands of particles, complemented by mineralogical information. These measurements are readily available from previous mineralogical studies and have the potential to be very useful.

This study shows how Quantitative Evaluation of Minerals by SCANning electron microscopy (QEMSCAN) can be used to differentiate between shape characteristics of specific mineral particles within a sample. The strengths and weaknesses of various shape descriptors were investigated including effects of image resolution and particle orientation. *Roundness* was found to be better than perimeter dependent descriptors such as *angularity*, and is recommended for studies of fine grinding that are limited by resolution. A novel approach for shape characterisation using *roundness* and *aspect ratio* in conjunction was developed and demonstrated. The potential value of the mineral specific shape characterisation enabled by Auto-SEM is demonstrated with a comparison of the major components of Upper Group 2 chromitite (UG2) platinum ore comminuted with different mill types.

4.1 Introduction

4.1.1 Particle shape in minerals processing

On a fundamental level, the shape of a mineral particle affects the basic interactions of that particle with water, air and other particles or equipment. This means that if one considers an entire minerals processing circuit, it is difficult to think of a single process that might not be affected by particle shape in some way. In crushers, the top size of the product is difficult to control as narrow plate like rocks can pass through the operating gap unbroken, even though only one dimension fits the desired size criteria. In crushers and tumbling mills, rocks/particles with certain shapes are more competent than others, which can affect the grinding outcome, and in turn, machine parameters can affect particle shape. (Bengtsson et al., 2010; Chandramohan et al., 2010; Pourghahramani, 2012; Unland and Al-Khasawneh, 2009; Vizcarra et al., 2011b). Particle shape affects classification performance of screens, cyclones and thickeners, as well as measurements of particle size distribution (Kashiwaya et al., 2012; Ozcan et al., 2000; Wills and Napier-Munn, 2006). Wills and Napier-Munn (2006: 90) discuss the latter, and suggest that "data from any size analysis should, where possible, be accompanied by some remarks which indicate the approximate shape of the particles". Downstream, shape has been shown to affect flotation performance (Koh et al., 2009; Vizcarra, 2010), and throughout a plant particle shape will affect slurry rheology and equipment wear rates (Ndlovu et al., 2011; Walker and Hambe, 2015). Particle shape is clearly important yet there is no routine analysis of particle shape distributions, and no standard methodology for particle shape analysis in minerals processing.

As quantitative analysis of particle shape could lead to improved understanding and modelling of many processes, numerous authors have tried to quantify shape and determine how comminution and mineralogy affects shape, and how shape affects various unit operations (Ahmed, 2010; Bridgwater et al., 2003; Durney and Meloy, 1986; Kaya et al., 2002; Khonthu, 2012; Koh et al., 2009; Kursun and Ulusoy, 2006; Mollon and Zhao, 2014; Ndlovu et al., 2011; Ulusoy et al., 2004; Vizcarra et al., 2011a; Yekeler et al., 2004). However measuring and quantifying shape for a sample of millions of ore particles with varying morphology is not simple, and the variety of approaches used makes it difficult to assimilate the findings from different studies.

Pirard (1989) discusses a variety of shape characterisation techniques appropriate for minerals processing applications, including parametrical analysis and harmonical analysis techniques. Parametrical analysis involves descriptors based on basic dimensions of a particle or 2D projection of a particle such as Feret diameter, *aspect ratio*, *angularity* and *roundness*.

Harmonical analysis techniques include Fourier analysis and fractal analysis, which use a function or set of coefficients to describe an object.

Pirard (1989: 206) described the following four requirements of shape analysis for minerals processing:

- "Shape parameters should be accurate (INVARIANCE);
- They should be easy to measure with automatic devices (AUTOMATION);
- They should have a clear physical meaning with respect to the process being studied (INTERPRETABILITY);
- They should be suited to statistical analysis."

The descriptor *angularity*, based on the perimeter and area of the projected image of a particle, has been most widely used in recent applications (Guven et al., 2015; Hoşten and Özbay, 1998; Kursun and Ulusoy, 2006; Pourghahramani, 2012; Vizcarra et al., 2011a; Walker and Hambe, 2015). It is easy to interpret, but it does not satisfy the invariance criterion. This was acknowledged by Pirard (1989: 207), who stated that "digital area is an unbiased estimator of true area, whereas the digital perimeter will always underestimate the true perimeter." Fourier analysis and fractal dimension techniques favoured by Pirard satisfy the invariance criterion but are more difficult to use and interpret for non-shape specialists. Other approaches to measuring particle morphology that have been used within the minerals processing industry include indirect techniques such as measurement of resistance to flow through a packed bed (Hicyilmaz et al., 2005), and rheology measurements (Khonthu, 2012). These methods are cost effective, but confounding variables such as size and surface charge (Ndlovu et al., 2011) may affect the output.

Holt (1981) reviewed the literature on the effects of comminution type on particle shape from the years 1926 to 1980. The work from this period was qualitative, and it was clearly limited by the measurement techniques available at the time. For example, in one of the studies reviewed by Holt, Heywood (1945) measured the length, breadth and width of 142 crushed sandstone particles by hand. Ahmed (2010) reviewed the literature on the topic from the following three decades focusing on the added value of modern shape measurements such as Fourier analysis and fractal dimensions. Since 2010 the increased use of automated instruments has reduced the uncertainty associated with shape measurements, as much larger numbers of particles can be scanned in relatively short time periods. For example, Vizcarra (2010) reported typical analysis of 5 000 to 10 000 particle sections per size fraction using the Mineral Liberation Analyser (MLA).

Most of the automated instruments measure cross-sections or projected areas of particles, but recently x-ray computed tomography (X-CT) and SEM micro-computed tomography (micro-CT) have been introduced to give three dimensional image data. X-CT can be used for textural characterisation of ore prior to comminution, which could also be used in conjunction with 2D shape data to further understand breakage and mineral liberation. So far, reports of micro-CT particle shape analyses have mostly been for characterisation of volcanic ash particles (Bagheri et al., 2015; Vonlanthen et al., 2015). Another recent advancement has been the development of a method to generate virtual 3D particles with realistic shapes for use in discrete element modelling of granular materials (Mollon and Zhao, 2014). It is apparent that the technology available for shape characterisation is at a stage where it can provide high quality, quantitative information. However, the technology is currently underutilized for minerals processing applications, and needs to be used more extensively for the benefits of shape characterisation to be realised.

4.1.2 Auto-SEM particle shape characterisation

Automated Scanning Electron Microscopy technology has become a useful tool for process mineralogy and has delivered significant value in numerous operations, examples of which have been described by Lotter et al. (2011); Evans et al. (2011) and Rule and Schouwstra (2011). In a paper aiming to quantify the value of automated mineralogy, Gu et al. (2014) reported that over two hundred MLA and QEMSCAN systems have been installed worldwide in the last ten years. Some examples of Auto-SEM systems are QEMSCAN, MLA, Mineralogic, TIMA and INCAMineral (FEI, 2015a, 2015b; Oxford Instruments, 2012; Tescan, 2012; Zeiss Microscopy, n.d.). The most substantial contribution of this technology so far has probably been through the use of mineral liberation analysis to determine the required grind for a target grade and recovery. The use of mineral association data has also made some significant contributions, for example to show that a hydrophilic mineral is floating due to its association with a hydrophobic mineral, or that a desired mineral is typically associated with a certain phase that should therefore be targeted (Becker et al., 2009; Lotter et al., 2008). Mineral specific particle shape data, which could be considered as a by-product of Auto-SEM, could also make a significant contribution in minerals processing, and to date there is limited information in the literature regarding the application of these data.

4.1.3 Fine grinding of UG2 ore

The Upper Group 2 Chromitite ore is a multicomponent platinum ore from the Bushveld complex in South Africa. The bulk mineralogy of the UG2 ore sample used in this study is shown in Table 4.1. Many authors have described the problems associated with the high chromite content of the ore, which ranges between 40% and 70% and leads to difficulties in processing.

These include the problem of the fine dense chromite particles being recirculated through the mill if operated in closed circuit, and also that chromite reporting to the flotation concentrate causes severe problems in the smelter (Becker et al., 2008; Hay and Roy, 2010; Hay, 2010; Jones and Geldenhuys, 2011; Mainza, 2006; Wesseldijk et al., 1999).

When considering particle shape in minerals processing, comminution is of particular interest as this is the process where the particles attain their shape, which in turn affects classification and separation stages downstream. Studying the shape characteristics of progeny particles can also be used to interpret breakage mechanisms within milling devices and in some instances, can even be related to the degree of liberation (Leroy et al., 2011). Previous work relating to shape characterisation has been done in relatively coarse size fractions, mostly greater than 150 μm, comparing breakage mechanisms in various milling devices such as the ball mill, rod mill, autogenous mill and piston-die compression unit (Ahmed, 2010; Holt, 1981; Kaya et al., 2002; Pourghahramani, 2012; Ulusoy et al., 2003; Vizcarra et al., 2011b). Although conclusions have been drawn relating abrasion or repeated impacts with increased roundness, and compression and single impacts with angularity, the findings vary with different ore types and mill operational parameters. To date there has been minimal work done on characterising the shape of particles below 75 μm, which would be of interest in many operations as fine grinding has become more prevalent with the need to process increasingly complex disseminated ores such as the UG2 ore.

Table 4.1: Bulk Mineralogy of UG2 ore sample investigated.

Mineral	**Mass %**
BMS	0.2
Olivine	1.8
Orthopyroxene	15.7
Clinopyroxene	1.2
Amphibole	1.2
Chlorite	1.6
Serpentine	0.3
Talc	0.4
Mica	0.4
Plagioclase	16. 6
Chromite	60.0
Other	0.6

4.1.4 Objectives

This paper aims to explore some of the strengths and weaknesses of various particle shape descriptors for classifying fine particle images obtained by QEMSCAN, focusing specifically on

resolution. Suitable shape descriptors are then used to compare the shape characteristics of the chromite and silicate minerals after grinding with a ball mill and vertical stirred mill.

4.2 Methodology

4.2.1 Experimental

The particle images analysed in this investigation were obtained from batch laboratory test work in which UG2 ore was ground in either a ball mill or a high speed vertical stirred mill to two target product size distributions. The feed was sampled from the primary ball mill discharge of a plant processing UG2 ore from the Western Limb of the Bushveld Complex, and the bulk sample was blended and split into smaller samples using a ten way rotary splitter.

The 300 mm diameter ball mill had a smooth lining (no lifters) and was operated at 70% critical speed, with ceramic grinding media (graded charge: top-size 32 mm). The stirred mill had a 160 mm pin-impeller with a fixed speed of 535 rpm and 5 mm round ceramic beads as grinding media. Both mills were loaded with 3 kg of ore at solids concentrations of 64% and 74% for the ball mill and stirred mill respectively. The feed had a top size of 1 mm and a F80 of 450 μm (80 % of the sample would pass through a screen with square apertures 450 μm wide). The stirred mill and ball mill product size distributions were very similar for the two mills, and parallel to the feed with P80s of 60 μm and 40 μm for the two target grinds. Due to the difference in energy intensity between the two mill types, it took roughly 14 times longer to achieve similar product size distributions in the ball mill to those produced in the stirred mill. That is to say, 6 minutes of grinding in the stirred mill would give a P80 of 60 μm, and 9 minutes of grinding would give a P80 of 40 μm, while in the ball mill this would take 83 and 133 minutes respectively.

Representative samples for different size fractions of the feed and mill products were obtained using screening, various rotary splitters and a micro-riffler. These samples were then set in blocks of resin for particle mineral analysis (PMA) with the FEG QEMSCAN 650F. The blocks were prepared as vertical sections to eliminate bias introduced by settling of the denser chromite particles relative to the silicates. Chemical assays for the major elemental components were obtained from inductively coupled plasma optical emission spectrometry (ICP-OES) for QEMSCAN data validation. For this study, the particles selected for shape analysis were liberated chromite particles, and liberated pyroxene and plagioclase particles (silicates). Particles composed of other minerals were typically excluded from the shape analysis, however these are included in the images shown in Figures 4.2 and 4.9. In these images, the minerals amphibole, chlorite, serpentine and talc constitute the alteration silicates.

Fandrich et al. (2007) gives a detailed description of the MLA. A description of QEMSCAN can be found in Goodall et al. (2005). The data investigated in this study were obtained by QEMSCAN, however similar analyses could be applied to data obtained from other systems such as the MLA. The QEMSCAN system includes accompanying software, iDiscover™, which enables the user to view and explore the data, extracting the information of interest.

4.2.2 Shape descriptors

Modern techniques such as fractal dimensions and Fourier analysis were not considered for this study because the QEMSCAN software does not currently support these methods. However at the low resolutions associated with the fine particle images obtained, it is expected that the benefits of these techniques over the simple descriptors selected for this study would be limited. The three shape descriptors that are considered in this study are defined in Table 4.2.

Table 4.2: Shape descriptors investigated – those presented in the results are in bold text.

Descriptor	Formula	Inverse
Aspect ratio	$\frac{Long\ axis}{Short\ axis}$	$\boldsymbol{\frac{Short\ axis}{Long\ axis}}$
Circularity	$\boldsymbol{\frac{4\pi \cdot Area}{Perimeter^2}}$	$Angularity = \frac{Perimeter^2}{4\pi \cdot Area}$
Roundness	$\boldsymbol{\frac{4 \cdot Area}{\pi \cdot Long\ axis^2}}$	$\frac{\pi \cdot Long\ axis^2}{4 \cdot Area}$

Initially *angularity* was investigated because it had been reported in previous work (Guven et al., 2015; Hoşten and Özbay, 1998; Pourghahramani, 2012; Vizcarra et al., 2011a, 2011b; Walker and Hambe, 2015), but *angularity* relies on perimeter measurement, which is highly dependent on resolution (Russ, 1995). As *roundness* and *aspect ratio* do not rely on perimeter measurement, these were introduced to the work and investigated in more detail. Two dimensional descriptors are generally based on comparison of a shape to a perfect circle. For example, *angularity* compares the perimeter of a shape to the perimeter of a circle with equivalent area, while *roundness* compares the area of a shape to the area of the smallest circle that would circumscribe that shape. The formulae are generally expressed as ratios, with theoretically possible values ranging from 0 to 1, or from 1 to ∞ if the ratio is inverted. One corresponds to a perfect circle in both cases, and as shapes deviate from circularity, their descriptors approach zero or infinity respectively. For example the *aspect ratio* of a circle will always be one, while that of a needle would be approximately 0.01 or 100 depending on whether it is defined as short axis/long axis or long axis/short axis. Descriptors in the 0 – 1

category tend to produce fairly normal distributions for mineral particles, and those in the 1 – ∞ category tend to produce highly skewed distributions. From a modelling perspective, the former would be advantageous, so the descriptors used in this work were all formulated to produce values in the 0 – 1 range. This determined the selection of *circularity* for this study instead of its commonly used inverse, *angularity*.

4.2.3 Data processing

The software associated with QEMSCAN, iDiscover™, was used to define categorisers to sort through particles in a sample, and classify them according to mineral composition, size, resolution and shape. The performance of these categorisers was checked through the use of an image grid, and the data were then extracted via the use of 2-D and 3-D charts, and exported to Microsoft Excel. For this work, most of the data were based on the 'particle count' or frequency of particles that fall into specific shape or area categories.

4.2.4 Effect of particle orientation

As the shape characterisation approach used is based on 2 dimensional particle images; a concern was raised that settling during QEMSCAN block preparation could introduce bias into the measured particle shape distributions. In order to determine whether particle orientation affected the particle shape measurements, one sample block (prepared in an ice-cube mould) was divided into both vertical and horizontal sections as illustrated in Figure 4.1. These sections were then remounted in round 30 mm blocks for analysis. The findings relating to particle orientation are presented in Section 4.3.3.

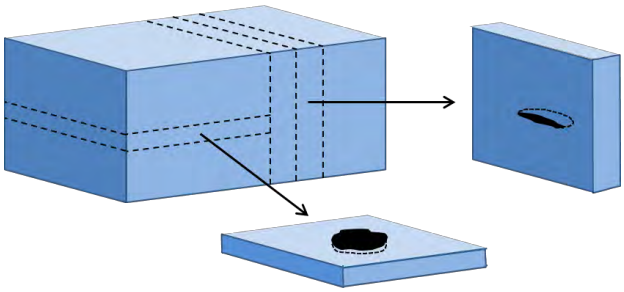

Figure 4.1: Illustration of vertical and horizontal sections prepared to investigate influence of stereology on shape measurements.

4.3 Results and Discussion

4.3.1 Circularity, roundness and resolution

Samples submitted for Auto-SEM analyses are typically wet screened into various size fractions and the scan resolution or pixel spacing is selected based on the size fraction. However particle size still varies within each size fraction, so the number of pixels per particle image can also

vary considerably. This is particularly evident for the bottom size fraction, which in this study was -10 µm. The maximum theoretical resolution/minimum pixel spacing for the FEG QEMSCAN 650 F is 0.5 µm/pixel, which is similar to that of camera based particle image analysis systems. This means that one cannot expect any detailed information for QEMSCAN images of particles finer than 1 µm, as these will typically be composed of less than 5 pixels. It is therefore necessary to establish at what size shape characteristics become meaningful, and also to understand how various shape descriptors respond to different resolutions. Furthermore, in most minerals processing applications both particle size and particle shape have significant effects, and being able to decouple these may be useful (van de Ruit et al., 2014).

Figure 4.2 is an image grid showing particles classified by *roundness* and *circularity*. This image already suggests that there is a problem with *circularity*, because it is classifying all of the very fine particles as round, and only the large particles are reporting to the correct fractions. In comparison, *roundness* can be used to distinguish between both fine and coarse particles of different shapes, independent of size or resolution. Figures 4.3 and 4.4 present a more quantitative measure of this effect, showing how the frequency distributions obtained from the two descriptors *circularity* and *roundness* vary with image resolution. In this instance, the number of pixels per particle image is used as a proxy for resolution.

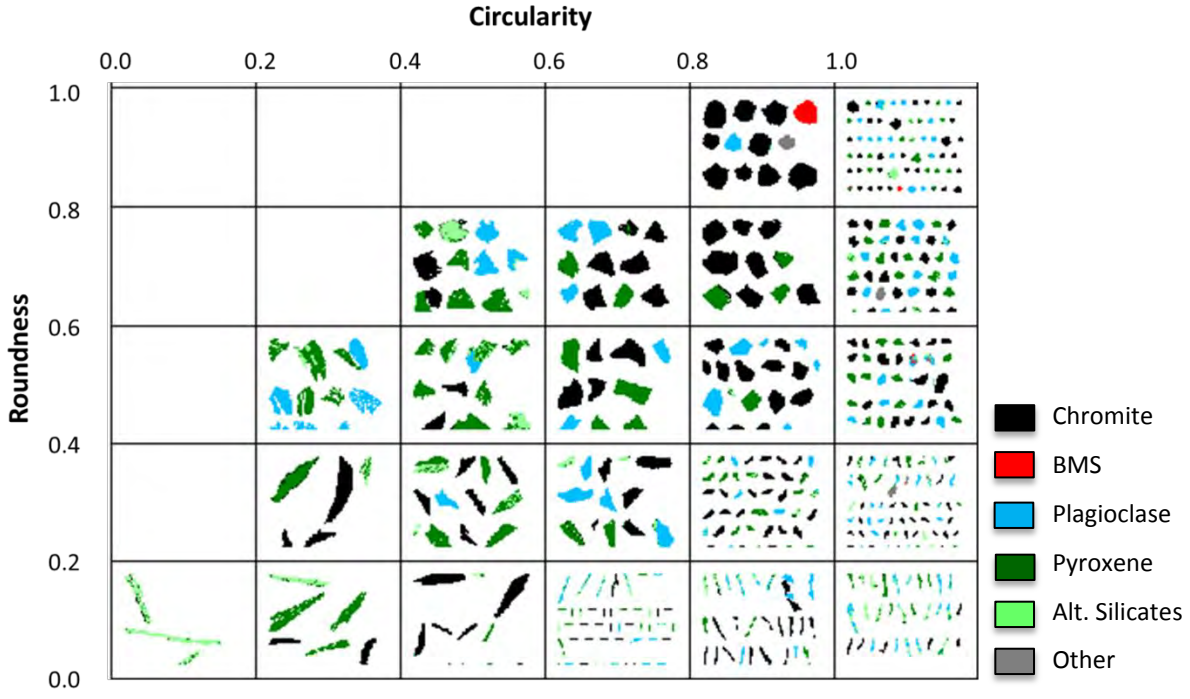

Figure 4.2: Comparison of the capabilities of roundness and circularity for categorising particles of different sizes (in the -75/+53 µm fraction of the ball mill product) measured with the same pixel spacing.

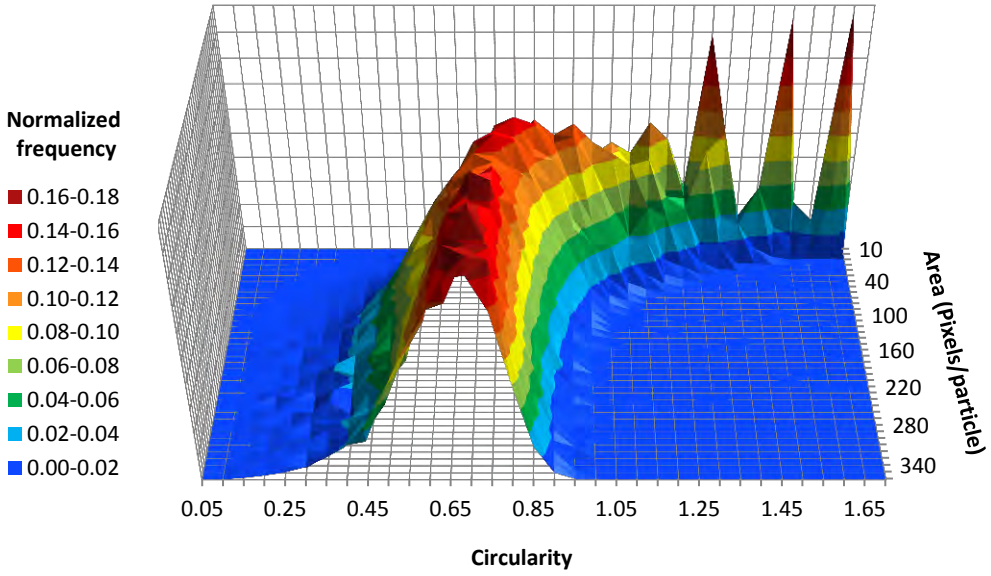

Figure 4.3: The effect of image resolution (no. pixels per particle) on circularity frequency distribution. This chart was obtained by dividing particle images in -10 µm and -25 µm fractions of both the ball mill and stirred mill products into different categories based on their area (no. pixels per particle), and then obtaining the circularity frequency distribution for each area category.

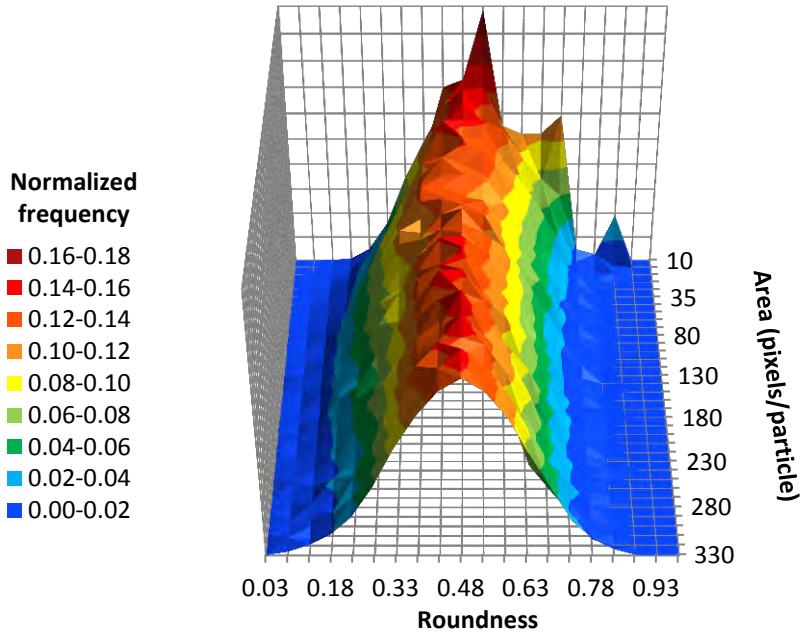

Figure 4.4: The effect of image resolution (no. pixels per particle) on roundness frequency distribution.

Circularity increases with decreasing resolution, with some particles beginning to report values greater than one at image sizes below 100 pixels, and most particles reporting circularities greater than one below 30 pixels. The three peaks around 10 pixels correspond to the limited number of common configurations of so few pixels. The values greater than the theoretical

maximum *circularity* (one) are explained by the software algorithms operating in QEMSCAN to calculate perimeter and area. The perimeter measurement is calculated as the distance around the boundary pixels, but it is measured from pixel centre to pixel centre, while the area measurement includes the full area of the boundary pixels. These results are not unexpected as perimeter measurement is known to be dependent on resolution, so descriptors that depend on perimeter measurement are also going to vary with resolution (Pirard, 1989; Russ, 1995). *Roundness* is not dependent on the measurement of perimeter, and therefore is not significantly affected by resolution, as demonstrated in Figure 4.4. It would therefore be more appropriate than *circularity* or *angularity* for comparisons of samples with different particles size distributions, or for samples that have been analysed in separate studies with different devices. Based on these results, *roundness* was selected as the best shape descriptor for investigating breakage mechanisms when fine grinding UG2 ore in the ball mill and vertical stirred mill.

4.3.2 Sample statistics

The number of particles required for statistically relevant shape parameters such as the mean, is much fewer than the number of particles that can be analysed with auto-SEM. Pons and Vivier, (1990) investigated the number of particles required for shape descriptor parameters for sugar crystals, and found that mean values stabilized around 20 particles, and standard deviation values stabilized around 100 particles. However sugar crystals are more regularly shaped than multi-component ore particles. Vizcarra (2010) did a similar analysis for the *angularity* distribution of chalcopyrite particles, and found that residuals approached 0 at around n = 400. With 10 000 to 15 000 particle images, the standard error for mean *roundness* is approximately 0.001, therefore slight differences between mean values for different samples are statistically significant. This is demonstrated in Figure 4.5, which shows the *roundness* distributions of chromite and silicates in the -75/+53 μm fraction of the stirred mill product. A statistical analysis was carried out comparing the means of the two distributions, following the approach described by Diez et al. (2012). The numerical values used for the analysis are provided in Table 4.3. Although the two sample means were found to be statistically different at the 95% confidence level, the difference between the two distributions appears practically insignificant. Simply presenting sample parameters in tables without plotting the distributions can therefore be misleading.

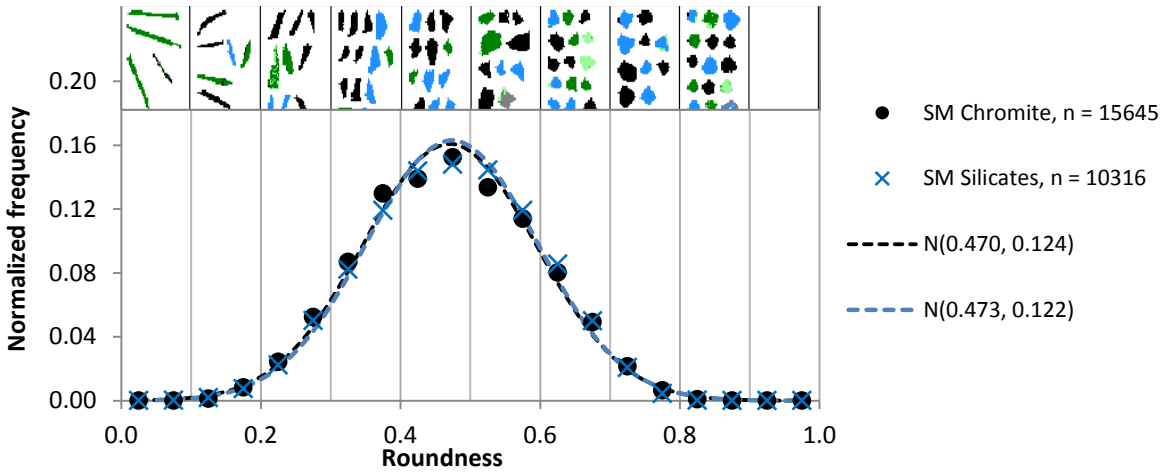

Figure 4.5: The difference between chromite and silicate distributions of the stirred mill -75/+53 µm product is statistically significant at the 95% confidence level, but practically insignificant.

Table 4.3: Statistical analysis for comparison of mean roundness of chromite and silicates in the stirred mill product (-75/+53 µm fraction).

Parameter	**Symbol**	**Chromite (subscript 'c')**	**Silicates (subscript 's')**
Sample size	n	15645	10316
Mean	$\bar{x} \approx \mu$	0.4701	0.4735
Standard deviation	$S \approx \sigma$	0.124	0.122
Standard error	SE	0.00099	0.00120
Point estimate to be tested	$\bar{x}_c - \bar{x}_s$	0.00336	
Standard error for point estimate	$SE_{\bar{x}c - \bar{x}s}$	0.00156	
Z-score		2.152	
p-value		0.0156	

4.3.3 Effect of particle orientation

In Section 4.3.2 it was shown that for analysis of the more abundant minerals within an ore, the number of particles analysed by Auto-SEM is not a limitation of the technique, however the statistics could lead to over-confidence in the quality of the data. Bias could still be introduced through sampling, during both rotary splitting and block preparation. Figure 4.6 shows a comparison of the *roundness* distributions produced for QEMSCAN blocks prepared from two vertical sections and one horizontal section of a single sample. The mean *roundness* values for the three sections were 0.4347, 0.4354 and 0.4348 respectively. The standard deviation of the mean (calculated for these three samples) is 0.0004, which is lower than that calculated based on the standard error formula which gives 0.0014. This shows the high reproducibility of the

data, irrespective of whether the samples were prepared as vertical or horizontal sections. This suggests that the orientation of the particles within the resin was random, an indication that no bias was introduced to the shape analyses through particles settling within the resin. If orientation is random and sufficient numbers of particles are measured, it follows that a sample's two dimensional shape distribution should be representative of the sample's three dimensional shape characteristics. This is in agreement with findings by Lätti and Adair (2001) who investigated stereological bias for liberation analysis of a hard-rock titanium ore.

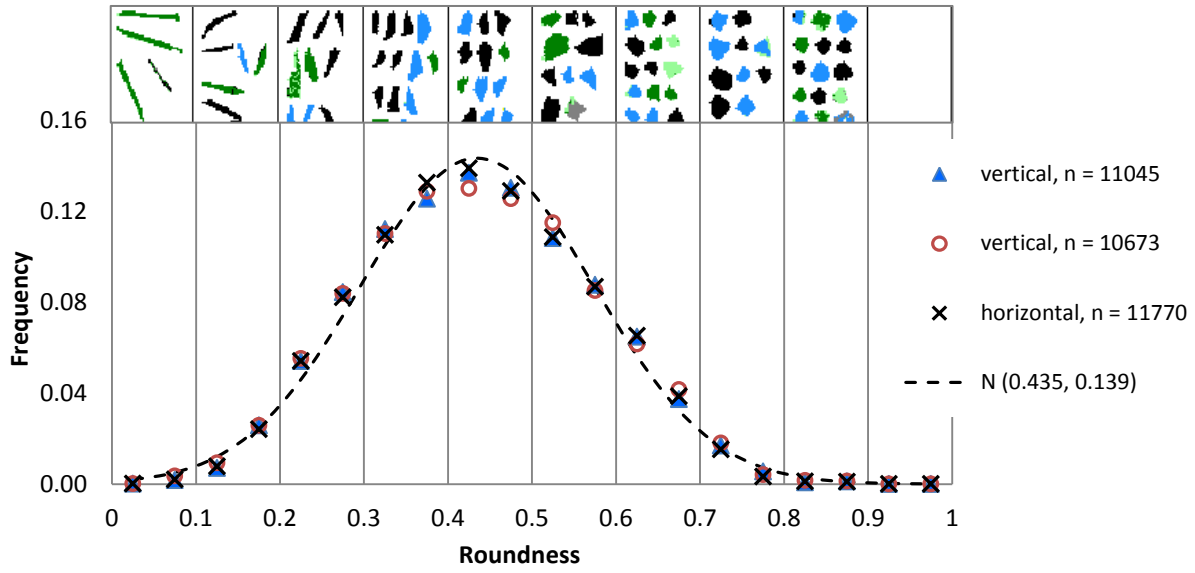

Figure 4.6: Comparison of roundness distributions from three scanned blocks prepared from vertical and horizontal sections of the same original mould (stirred mill, coarse grind, -53/+25 µm fraction).

4.3.4 Using *roundness* to interpret breakage mechanisms of UG2 ore

In comminution, breakage mechanisms are often related to the effects that they have on particle shape. Abrasion is typically associated with the chipping-off of topographical features and a polishing action that produces rounded particles with few sharp edges (Gao and Forssberg, 1995; Kaya et al., 2002; King, 2001; Pourghahramani, 2012; Vizcarra et al., 2011b). Impact and compression are typically associated with fracture patterns producing more angular particles (King, 2001; Pourghahramani, 2012; Vizcarra et al., 2011b). In general, all of the breakage mechanisms are expected to occur to some extent within both tumbling mills and stirred mills, but the extent of each varies between the mill types, and it is dependent on the grinding conditions.

The predominant breakage mechanism in ball mills is widely believed to be impact breakage, and that in stirred mills is believed to be abrasion (Chaponda, 2011; Gao and Forssberg, 1995; Wills and Napier-Munn, 2006; Ye et al., 2010). Impact is typically associated with angular

particles, and abrasion with rounded particles. However, Kaya et al. (2002) also suggested that shape is dependent on milling time or residence time, with particles becoming more rounded the longer they are exposed to the milling environment, particularly due to abrasion. It was therefore difficult to predict which mill would produce more rounded particles with the expected breakage mechanisms conflicting with the energy intensity and thus milling times. The ball mill grinding times were 83 min and 133 min compared to 6 min and 9 min grinding times in the stirred mill to achieve equivalent grinds with the same feed.

Figure 4.7 shows that in the feed, the chromite particles are more rounded than the silicates, and the image of a coarse unbroken particle suggests that this is due to the primary texture of the ore, and breakage occurring along grain boundaries of the particles. After further grinding in the ball mill and stirred mill, Figure 4.8 shows that the difference in shape between chromite and silicate particles is reduced, but the ball mill produces much more angular particles than the stirred mill in the coarse product fractions (+53 μm). It is also important to note that although the stirred mill product particles (both chromite and silicates) are mostly less elongated than those from the ball mill product, they are still angular, with a mean *roundness* below 0.5. This suggests that both the silicates and the rounded chromite particles in the feed were broken by massive fracture rather than abrasion in both mill types.

From a shape characterisation perspective, this section has shown that *roundness* is a very simple, useful descriptor, which can detect and quantify particle shape at both high and low image resolutions. However, used on its own the information that it can convey is still limited, and it is unclear whether particles with low *roundness* values are very rough with irregular shapes, or smooth but highly elongated. This was investigated further in Section 4.3.5 by using *aspect ratio* in conjunction with *roundness* to provide additional insight into particle shape.

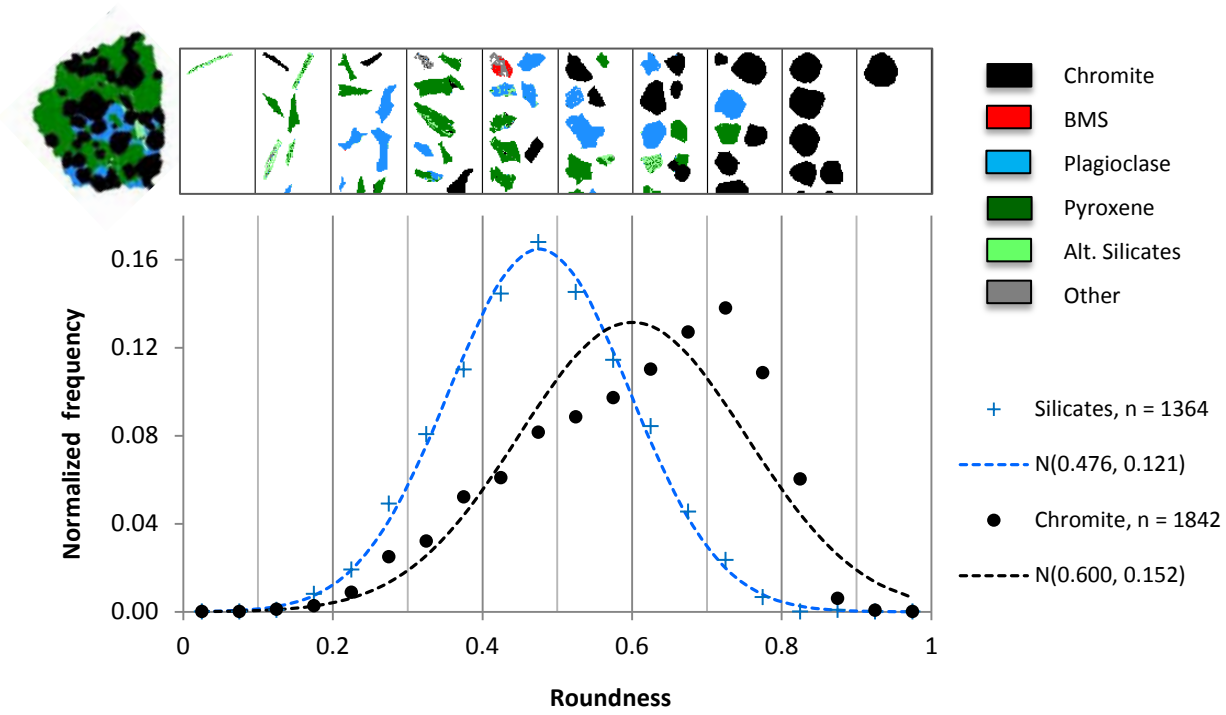

Figure 4.7: Comparison of the roundness distributions of chromite and silicates in the +150 µm fraction of the mill feed, along with a large unbroken particle (~1mm) image illustrating the initial texture of the ore.

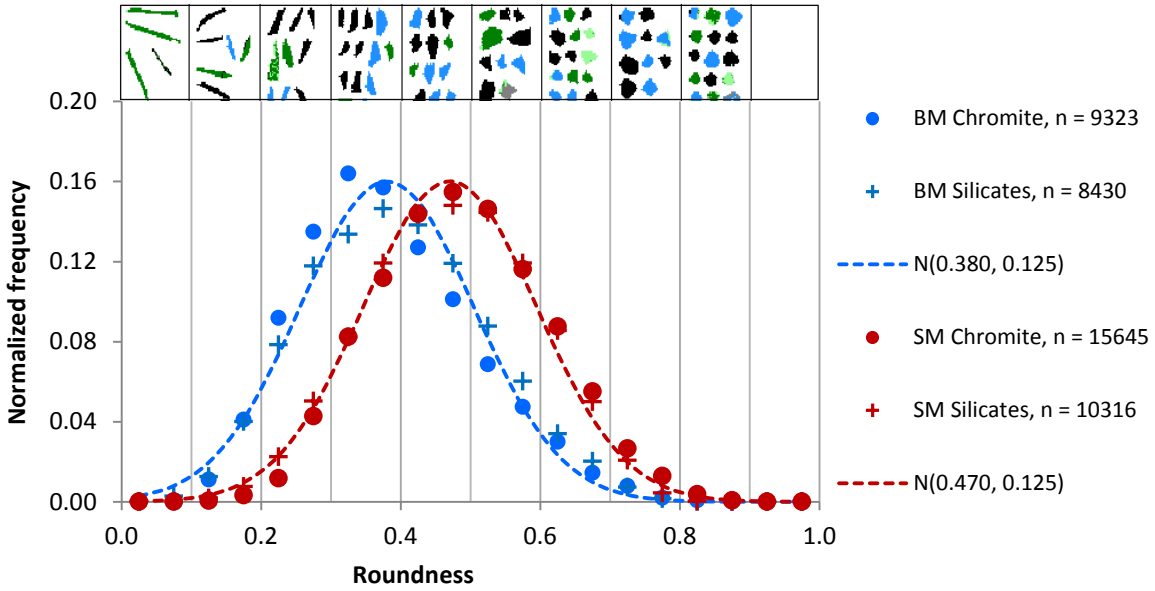

Figure 4.8: Comparison of roundness distributions of chromite and silicates in the stirred mill product to chromite and silicates in the ball mill product (-75/+53 µm size class).

4.3.5 Using aspect ratio in conjunction with roundness

The image grid in Figure 4.9 illustrates that in general, highly elongated particles report low *roundness* values, and rounded particles have *aspect ratio*s close to one. However, when used independently, *aspect ratio* does not differentiate between rounded particles and angular equant particles (i.e. categories (a) and (c)), and *roundness* does not differentiate between elongated particles and angular equant particles (i.e. categories (b) and (c)). Both descriptors are needed in order to distinguish between these particles.

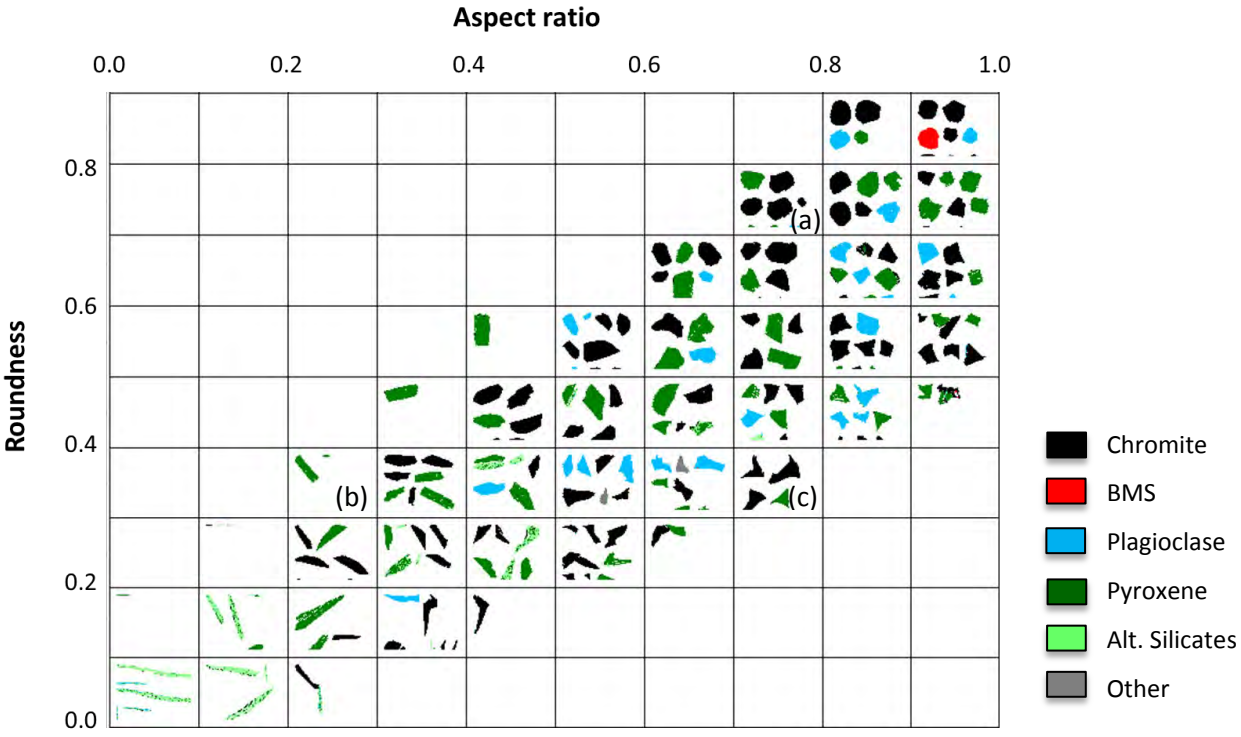

Figure 4.9: Image grid showing particles in the -75/+53 µm size class classified by both aspect ratio and roundness.

In order to use the two descriptors in conjunction quantitatively, the 'grid' was divided into much smaller intervals, and for particular samples of interest the number of particles reporting to each square in the grid was 'counted' to give the frequency distribution surface plots shown in Figure 4.10.

These frequency plots support the findings suggested by the *roundness* frequency distributions, and viewed in conjunction with Figure 4.9, give a good illustration of what the dominant shape characteristics of a sample are. However the surface frequency plots are cumbersome, and difficult to compare quantitatively, so these can rather be used to define further shape classes to draw out more quantitative data for multiple samples. In this study, shape classes defined in

this manner were defined based on the sub-divisions indicated in Figure 4.10, and these are described in Table 4.4. The ranges of *aspect ratios* and *roundness* values used in these definitions were selected based on the appearance of the categorised particles. In future studies these could be adjusted depending on the predominant shape characteristics of the sample of interest. These divisions do not have to be horizontal or vertical, for example a categoriser can also be set up for the diagonal line indicated, to determine proportions of particles that have a *roundness* value greater than 0.8 times their *aspect ratio*. This approach would be preferable to distinguish between more textural characteristics of particles, i.e. whether they are smooth or have jagged edges.

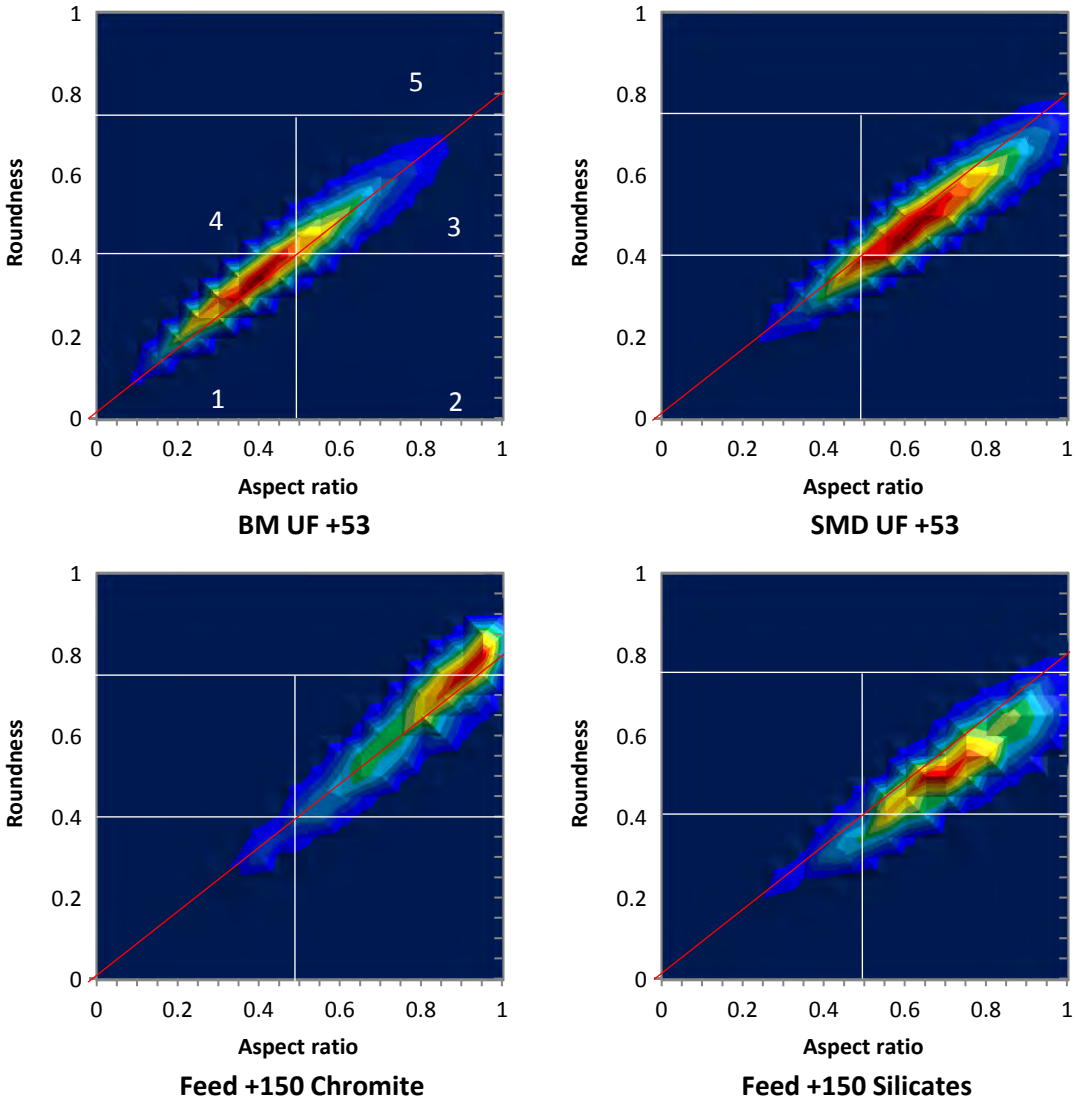

Figure 4.10: Roundness and Aspect ratio frequency surface plots for various samples of interest. These are the -75/+53 µm fractions of the ball mill and stirred mill products in the fine grind (BM UF +53 and SMD UF +53), and the liberated chromite and silicates in the -212/+150 µm fraction of the mill feed. The total number of particles in each distribution varies between 1 500 and 27 000.

Table 4.4: New shape classes defined for this study.

Shape class	**1**	**2**	**3**	**4**	**5**
Description	elongated and angular	angular	equant	elongated and smooth	round
Roundness values	0 – 0.4	0 – 0.4	0.4 – 0.75	0.4 – 0.75	0.75 - 1
Aspect ratio values	0 – 0.5	0.5 – 1	0.5 – 1	0 – 0.5	0.5 - 1
Appearance	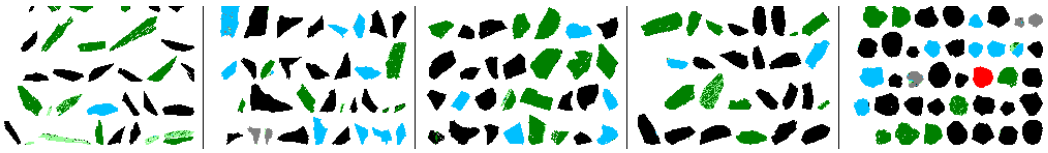				

Measuring the proportions of a sample that report to each shape class enables simple quantification based on both *roundness* and *aspect ratio*. This is demonstrated in Figure 4.11 for the same four samples of interest described previously. The large portion of round chromite particles in the mill feed has now been assigned a numerical value, 18%, while the portion of rounded particles in the silicates and mill products is less than 2%.

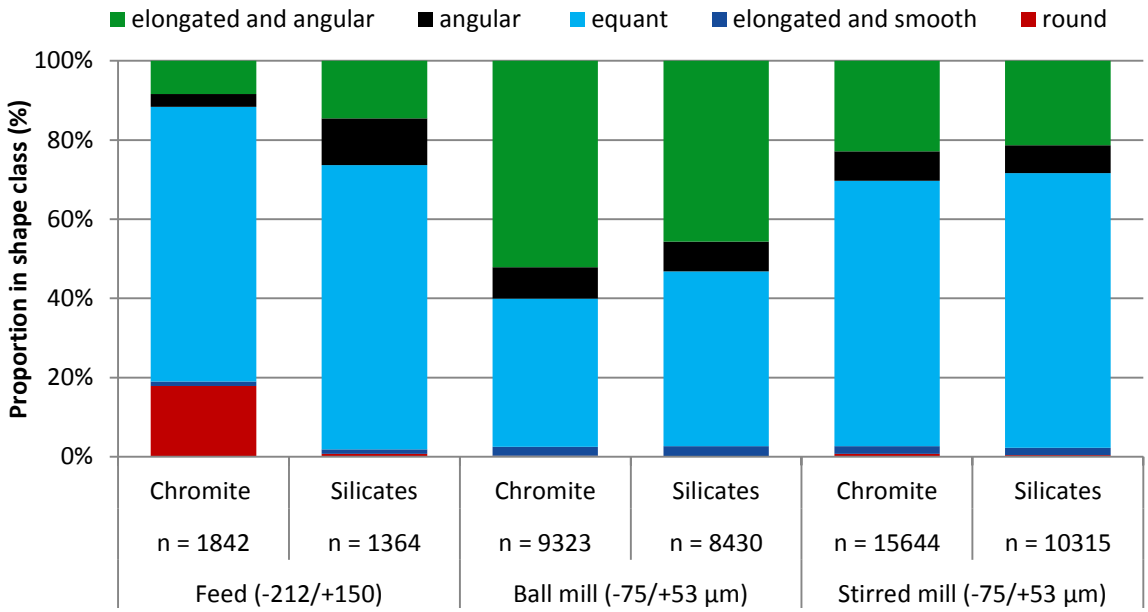

Figure 4.11: Proportions of liberated chromite and liberated silicates in selected size fractions of the feed and ball mill and stirred mill products that report to the shape classes defined in Table 4.2.

4.4 Conclusions

- The dependence of *circularity* on image resolution was clarified, demonstrating the limitations of commonly used perimeter-dependent shape descriptors for fine particle shape characterisation;
- *Roundness* is a more robust descriptor than *circularity*, but low resolution data (less than 20 pixels per particle) should be treated with caution;
- Particle orientation did not affect particle *roundness* distribution; therefore stereological bias should not be a major concern;
- Mineral specific shape data can be used to infer which breakage mechanisms are dominant within different milling devices;
- The use of *roundness* and *aspect ratio* in conjunction can provide quantitative shape characterisation for minerals processing that satisfies the triple criteria described by Pirard (1989), and which is suitable for characterisation of fine particles in which image resolution is a common limitation.

4.5 Acknowledgements

This work is based on the research supported in part by the National Research Foundation of South Africa (Grant Number 86054). Any opinions, findings and conclusions or recommendations expressed in any publication generated by the NRF supported research is that of the author(s), and that the NRF accepts no liability whatsoever in this regard.

The authors would also like to acknowledge the South African Minerals to Metals Research Institute (SAMMRI) and the South African Department of Science and Technology for funding the project. Advice and support from the SAMMRI industrial advisors for the project, Victor Ross and Anthony Anyimadu is also much appreciated.

4.6 References

Ahmed, M.M., 2010. Effect of comminution on particle shape and surface roughness and their relation to flotation process. Int. J. Miner. Process. 94, 180–191. doi:10.1016/j.minpro.2010.02.007

Bagheri, G.H., Bonadonna, C., Manzella, I., Vonlanthen, P., 2015. On the characterization of size and shape of irregular particles. Powder Technol. 270, 141–153. doi:10.1016/j.powtec.2014.10.015

Becker, M., Harris, P.J., Wiese, J.G., Bradshaw, D.J., 2009. Mineralogical characterisation of naturally floatable gangue in Merensky Reef ore flotation. Int. J. Miner. Process. 93, 246–255. doi:10.1016/j.minpro.2009.10.004

Becker, M., Mainza, A. N., Powell, M.S., Bradshaw, D.J., Knopjes, B., 2008. Quantifying the influence of classification with the 3 product cyclone on liberation and recovery of PGMs in UG2 ore. Miner. Eng. 21, 549–558. doi:10.1016/j.mineng.2007.11.001

Bengtsson, M., Lee, E., Evertsson, C.M., 2010. Influence of throw and compression ratio on particle shape – A full scale investigation and laboratory tests. Miner. Eng. 23, 549–557. doi:10.1016/j.mineng.2009.12.009

Bridgwater, J., Utsumi, R., Zhang, Z., Tuladhar, T., 2003. Particle attrition due to shearing - the effects of stress, strain and particle shape. Chem. Eng. Sci. 58, 4649–4665. doi:10.1016/j.ces.2003.07.007

Chandramohan, R., Holtham, P., Powell, M., 2010. the Influence of Particle Shape in Rock Fracture. XXV Int. Miner. Process. Congr. 3163–3171.

Chaponda, B., 2011. Effect of operating variables on IsaMill performance using Platinum bearing Ores. University of Cape Town.

Diez, D.M., Barr, C.D., Cetinkaya-Rundel, M., 2012. OpenIntro Statistics, 2nd ed. openintro.org.

Durney, T.E., Meloy, T.P., 1986. Particle shape effects due to crushing method and size. Int. J. Miner. Process. 16, 109–123.

Evans, C.L., Wightman, E.M., Manlapig, E.V., Coulter, B.L., 2011. Application of process mineralogy as a tool in sustainable processing. Miner. Eng. 24, 1242–1248. doi:10.1016/j.mineng.2011.03.017

Fandrich, R., Gu, Y., Burrows, D., Moeller, K., 2007. Modern SEM-based mineral liberation analysis. Int. J. Miner. Process. 84, 310–320. doi:10.1016/j.minpro.2006.07.018

FEI, 2015a. FEI [WWW Document]. URL http://www.fei.com/products/sem/qemscan/ (accessed 2.11.15).

FEI, 2015b. FEI [WWW Document]. URL http://www.fei.com/products/sem/mla/ (accessed 2.11.15).

Gao, M., Forssberg, E., 1995. Prediction of product size distributions for a stirred ball mill. Powder Technol. 84, 101–106.

Goodall, W.R., Scales, P.J., Butcher, A.R., 2005. The use of QEMSCAN and diagnostic leaching in the characterisation of visible gold in complex ores. Miner. Eng. 18, 877–886. doi:10.1016/j.mineng.2005.01.018

Gu, Y., Schouwstra, R.P., Rule, C., 2014. The value of automated mineralogy. Miner. Eng. 58, 100–103. doi:10.1016/j.mineng.2014.01.020

Guven, O., Ozdemir, O., Karaagaclioglu, I.E., Çelik, M.S., 2015. Surface morphologies and floatability of sand-blasted quartz particles. Miner. Eng. 70, 1–7. doi:10.1016/j.mineng.2014.08.007

Hay, M.P., 2010. A case study of optimising UG2 flotation performance part 2: Modelling improved PGM recovery and Cr2O3 rejection at Northam's UG2 concentrator. Miner. Eng. 23, 868–876. doi:10.1016/j.mineng.2010.05.015

Hay, M.P., Roy, R., 2010. A case study of optimising UG2 flotation performance. Part 1: Bench, pilot and plant scale factors which influence Cr2O3 entrainment in UG2 flotation. Miner. Eng. 23, 855–867. doi:10.1016/j.mineng.2010.05.002

Heywood, H., 1945. No Title. Trans. Inst. Min. Met. 15, 373.

Hicyilmaz, C., Ulusoy, U., Bilgen, S., Yekeler, M., 2005. Flotation responses to the morphological properties of particles measured with three-dimensional approach. Int. J. Miner. Process. 75, 229–236. doi:10.1016/j.minpro.2004.08.019

Holt, C.B., 1981. The Shape of Particles Produced by Comminution , A Review. Powder Technol. 28, 59–63.

Hoşten, Ç., Özbay, C., 1998. A comparison of particle bed breakage and rod mill grinding with regard to mineral liberation and particle shape effects. Miner. Eng. 11, 871–874. doi:10.1016/S0892-6875(98)00074-0

Jones, R.T., Geldenhuys, I.J., 2011. The pros and cons of reductive matte smelting for PGMs. Miner. Eng. 24, 495–498. doi:10.1016/j.mineng.2011.03.007

Kashiwaya, K., Noumachi, T., Hiroyoshi, N., Ito, M., Tsunekawa, M., 2012. Effect of particle shape on hydrocyclone classification. Powder Technol. 226, 147–156. doi:10.1016/j.powtec.2012.04.036

Kaya, E., Hogg, R., Kumar, S.R., 2002. Particle Shape Modification in Comminution. KONA 20, 188–195.

Khonthu, T., 2012. Investigation of the flotation behaviour of ball mill and IsaMill products. University of Cape Town.

King, R.P., 2001. Modeling & Simulation of Mineral Processing. Butterworth-Heinemann, Oxford.

Koh, P.T.L., Hao, F.P., Smith, L.K., Chau, T.T., Bruckard, W.J., 2009. The effect of particle shape and hydrophobicity in flotation. Int. J. Miner. Process. 93, 128–134. doi:10.1016/j.minpro.2009.07.007

Kursun, H., Ulusoy, U., 2006. Influence of shape characteristics of talc mineral on the column flotation behavior. Int. J. Miner. Process. 78, 262–268. doi:10.1016/j.minpro.2005.11.003

Lätti, D., Adair, B.J.I., 2001. An assessment of stereological adjustment procedures. Miner. Eng. 14, 1579–1587. doi:10.1016/S0892-6875(01)00176-5

Leroy, S., Dislaire, G., Bastin, D., Pirard, E., 2011. Optical analysis of particle size and chromite liberation from pulp samples of a UG2 ore regrinding circuit. Miner. Eng. 24, 1340–1347. doi:10.1016/j.mineng.2011.06.006

Lotter, N.O., Bradshaw, D.J., Becker, M., Parolis, L.A.S., Kormos, L.J., 2008. A discussion of the occurrence and undesirable flotation behaviour of orthopyroxene and talc in the processing of mafic deposits. Miner. Eng. 21, 905–912. doi:10.1016/j.mineng.2008.02.023

Lotter, N.O., Kormos, L.J., Oliveira, J., Fragomeni, D., Whiteman, E., 2011. Modern Process Mineralogy: Two case studies. Miner. Eng. 24, 638–650. doi:10.1016/j.mineng.2011.02.017

Mainza, A.N., 2006. Contribution to the understanding of the three-product cyclone on the classification of a dual density platinum ore. University of Cape Town.

Mollon, G., Zhao, J., 2014. 3D generation of realistic granular samples based on random fields theory and Fourier shape descriptors. Comput. Methods Appl. Mech. Eng. doi:10.1016/j.cma.2014.06.022

Ndlovu, B., Becker, M., Forbes, E., Deglon, D., Franzidis, J.-P., 2011. The influence of phyllosilicate mineralogy on the rheology of mineral slurries. Miner. Eng. 24, 1314–1322. doi:10.1016/j.mineng.2011.05.008

Oxford_Instruments, 2012. Oxford Instruments [WWW Document]. URL http://www.oxford-instruments.com/OxfordInstruments/media/nanoanalysis/brochures and thumbs/OI_EDS_INCAMineral_Brochure.pdf (accessed 2.11.15).

Ozcan, O., Ruhland, M., Stahl, W., 2000. The effect of pressure, particle size and particle shape on the shear strength of very fine mineral filter cakes. Int. J. Miner. Process. 59, 185–193. doi:10.1016/S0301-7516(99)00064-2

Pirard, E., 1989. Applications of shape analysis in ore beneficiation, in: Process Mineralogy IX: Applications to Mineral Beneficiation, Metallurgy, Gold, Diamonds. TMS, pp. 205–218.

Pons, M.-N., Vivier, H., 1990. Crystallization monitoring by quantitative image analysis. Anal. Chim. Acta 238, 243–249. doi:10.1016/S0003-2670(00)80543-7

Pourghahramani, P., 2012. Effects of ore characteristics on product shape properties and breakage mechanisms in industrial SAG mills. Miner. Eng. 32, 30–37. doi:10.1016/j.mineng.2012.03.005

Rule, C., Schouwstra, R.P., 2011. Process mineralogy delivering significant value at Anglo Platinum concentrator operations, in: 10th International Congress for Applied Mineralogy. pp. 1–5.

Russ, J.C., 1995. The Image Processing Handbook, 2nd ed. CRC Press, Raleigh, North Carolina.

Tescan, 2012. Tescan [WWW Document]. URL http://www.tescan.com/en/products/tima/tima-lm (accessed 2.11.15).

Ulusoy, U., Hiçyılmaz, C., Yekeler, M., 2004. Role of shape properties of calcite and barite particles on apparent hydrophobicity. Chem. Eng. Process. 43, 1047–1053. doi:10.1016/j.cep.2003.10.003

Ulusoy, U., Yekeler, M., Hiçyılmaz, C., 2003. Determination of the shape, morphological and wettability properties of quartz and their correlations. Miner. Eng. 16, 951–964. doi:10.1016/j.mineng.2003.07.002

Unland, G., Al-Khasawneh, Y., 2009. The influence of particle shape on parameters of impact crushing. Miner. Eng. 22, 220–228. doi:10.1016/j.mineng.2008.08.008

Van de Ruit, L., Becker, M., Wiese, J., Mainza, A., 2014. A mineralogical investigation of the effect of particle shape on chromite entrainment for a UG2 ore, in: Yianatos, J., Doll, A., Gomez, C., Kuyvenhoven, R. (Eds.), XXVII International Mineral Processing Congress, Santiago, Chile. Gecamin Ltda, Santiago, p. 226.

Vizcarra, T.G., 2010. The Effect of Comminution Mechanism on Particle Properties: Consequences for Downstream Flotation Performance. University of Queensland.

Vizcarra, T.G., Harmer, S.L., Wightman, E.M., Johnson, N.W., Manlapig, E.V., 2011a. The influence of particle shape properties and associated surface chemistry on the flotation kinetics of chalcopyrite. Miner. Eng. 24, 807–816. doi:10.1016/j.mineng.2011.02.019

Vizcarra, T.G., Wightman, E.M., Johnson, N.W., Manlapig, E.V., 2011b. The effect of breakage method on the shape properties of an iron-oxide hosted copper–gold ore. Miner. Eng. 24, 1454–1458. doi:10.1016/j.mineng.2011.07.007

Vonlanthen, P., Rausch, J., Ketcham, R.A., Putlitz, B., Baumgartner, L.P., Grobéty, B., 2015. High-resolution 3D analyses of the shape and internal constituents of small volcanic ash particles: The contribution of SEM micro-computed tomography (SEM micro-CT). J. Volcanol. Geotherm. Res. 293, 1–12. doi:10.1016/j.jvolgeores.2014.11.016

Walker, C. I., & Hambe, M., 2015. Influence of particle shape on slurry wear of white iron. Wear. doi:10.1016/j.wear.2014.12.029

Wesseldijk, Q.I., Reuter, M.A., Bradshaw, D.J., Harris, P.J., 1999. The flotation behaviour of chromite with respect to the beneficiation of UG2 ore. Miner. Eng. 12, 1177–1184.

Wills, B.A., Napier-Munn, T., 2006. Wills' Mineral Processing Technology, 7th ed. Elsevier Science & Technology Books.

Ye, X., Gredelj, S., Skinner, W., Grano, S.R., 2010. Regrinding sulphide minerals — Breakage mechanisms in milling and their influence on surface properties and flotation behaviour. Powder Technol. 203, 133–147. doi:10.1016/j.powtec.2010.05.002

Yekeler, M., Ulusoy, U., Hiçyılmaz, C., 2004. Effect of particle shape and roughness of talc mineral ground by different mills on the wettability and floatability. Powder Technol. 140, 68–78. doi:10.1016/j.powtec.2003.12.012

Zeiss_Microscopy, n.d. Zeiss Microscopy [WWW Document]. URL http://www.zeiss.co.za/microscopy/en_za/products/scanning-electron-microscopes/mineralogic-systems.html (accessed 2.11.15).

Paper 2: Shape characterisation: Can different devices produce comparable data for particulate samples?

Little, L., Becker, M., Wiese, J., Yorath, G., Mainza, A. N., Tonzetic I., Proceedings of the XXVIIIth International Mineral Processing Congress. Quebec, Canada, 2016.

Keywords: Particle shape characterisation, sphericity, circularity, roundness

Abstract

Particle shape characterisation has an important role to play in minerals processing, to clarify effects of shape on rheology, equipment wear rates, comminution, classification, sizing and flotation. However in industry, shape characterisation is not routine, and the most commonly used shape descriptor in the field (*circularity/angularity/sphericity*) is not invariant. This study aims to investigate shape measurements for a fine particulate ore sample measured with different analytical devices. Two Automated Scanning Electron Microscopy devices with Energy Dispersive X-ray Spectrometry (FEI QEMSCAN® and Zeiss Mineralogic®), and a camera based image-sizer using dynamic image analysis (Retsch CAMSIZER® XT) were compared. Each device was used to analyse the shape characteristics of specific particles in both a coarse sample (-212/+150 µm) and a fine sample (-53 µm) of UG2 platinum ore. *Circularity* and *roundness* frequency distributions obtained from the three devices were then compared. For selected individual particles, *circularity* showed higher variability than *roundness*, and the sample *circularity* distributions obtained by the three devices were completely different. It is clear that *circularity* data from different studies relying on different devices should not be compared on an absolute scale. The shape parameter *roundness* was found to be a more robust descriptor than *circularity*, and it can give a stronger indication of a particulate sample's shape characteristics on an absolute scale. However, there were still significant differences in the *roundness* measurements obtained by the CAMSIZER XT and the two Auto-SEM devices, which was attributed to the dissimilar mechanisms of image capture.

4.7 Introduction

Particle shape is known to affect slurry rheology, equipment wear rates, breakage behaviour, classification, flotation and magnetic concentration (Das and Cleary, 2010; Dworzanowski, 2014; Kashiwaya et al., 2012; Ndlovu et al., 2011; Verrelli et al., 2012b; Vizcarra et al., 2011a; Walker and Hambe, 2015). However in the field of minerals processing, particle shape is neither routinely analysed on site nor in research, unless it is the main focus of a research paper. When it is analysed, it is generally reported with mean values rather than as a distribution, and there are many different measurement techniques and shape descriptors used (Frances et al., 2001; Guven et al., 2015; Kursun and Ulusoy, 2006). The most commonly used shape descriptor reported in the minerals processing literature is *circularity*, or its inverse *angularity*, which is also described as form factor or sphericity by some authors (Guven et al., 2015; Hoşten and Özbay, 1998; Komabayashi and Spångberg, 2008; Pourghahramani, 2012; Russ, 1995; Ulusoy and Yekeler, 2005; Vizcarra et al., 2011b; Walker and Hambe, 2015). Unfortunately this descriptor is not invariant - it is dependent on the measurement of perimeter and is thus affected by image resolution. There is a wide variety of technology available for measurement of particle shape, particularly based on 2-D image analysis, and alternative, more robust descriptors than *circularity* are available (International Organisation for Standardisation, 2008; Little et al., 2015, Paper 1). If used appropriately with understanding of the possible errors, more routine measurement of shape in minerals processing operations could deliver significant value in the form of improved understanding of processing effects due to particle shape.

Process mineralogy allows for detailed characterisation of mineral particles to improve understanding of minerals processing operations. The mineral characterisation typically involves the use of Automated Scanning Electron Microscopy, coupled with Energy Dispersive X-ray Spectrometry (Auto-SEM-EDS). The QEMSCAN and Mineralogic are examples of this technology, and these have mainly been used for information of mineral abundance, associations and texture (Cropp et al., 2013; Goodall et al., 2005; Gottlieb et al., 2000; Grobler and Bosman, 2011; Hill, 2014; Tonzetic, 2015). However, the information about particle shape characteristics has hardly been used, and the extensive Auto-SEM-EDS databases could be a valuable resource to clarify the effects of particle shape in various minerals processing operations. Additionally, optical devices such as the CAMSIZER XT can provide a rapid, simple measurement, which can be applied on a routine basis (Retsch Technology, 2016; Westermann, n.d.). This work aims to determine whether the shape information obtained from different devices is comparable, an important consideration during measurement of particulate shape characteristics and the interpretation thereof.

4.8 Experimental

4.8.1 Data acquisition

Samples of UG2 ore, a platinum group mineral ore from the Bushveld Complex in South Africa, were analysed with the FEI QEMSCAN 650F, the Carl Zeiss Mineralogic v.1.3, and the Retsch CAMSIZER XT (FEI, 2015b; Retsch Technology, 2016; Westermann, n.d.; Zeiss Microscopy, n.d.). Both the QEMSCAN and Mineralogic systems were run with a Field Emission Gun (FEG) SEM platform, with Xflash 6|30 EDS detectors. Two size fractions were selected for analysis; a coarse fraction (-212/+150 µm) and a fine fraction (-53 µm). For the coarse fraction, no resolution limitations were expected, while the fine fraction was selected to test the limits of the two Auto-SEM-EDS devices. The CAMSIZER XT was not used for the fine fraction at this stage.

For the Auto-SEM-EDS devices, the samples were mounted in resin, sliced into vertical sections, and then remounted into three blocks: A, B and C, each of which was run in both Auto-SEM-EDS machines. For the coarse fraction, the QEMSCAN mesh resolution was set at 5 µm per pixel, applicable for both the BSE and X-ray map image obtained, resulting in image resolutions within the region of 400 pixels per particle. Mineralogic image resolutions are based on the back scattered electron detector (BSD) pixel size with a resolution of 2 µm per pixel (2500 pixels per particle). For the fine fraction, resolutions of 0.475 µm/pixel and 0.44 µm/pixel were used for the Mineralogic and QEMSCAN respectively.

Mineralogic uses an image processing add-in supplied by Matrox (Matrox, 2016). In order to investigate the possible effects of variations in the image processing approach on *roundness* and *circularity* measurements, three different image processing functions were applied to the Mineralogic images. These were a basic threshold, a delineated setup and a smoothed setup. The threshold function is used to differentiate particles from background, the delineate function sharpens the edges of particles to remove blurry halos, and the smoothed function adjusts image-boundary grey levels to smoothen particle edges and remove noisy artefacts. Effects of these image processing functions are discussed in Section 4.9.3.

The CAMSIZER XT is completely different to the Auto-SEM-EDS devices. It uses two cameras, a CCD basic camera and a CCD zoom camera, to capture images of particles as they move through an aperture between the two lenses. An important difference to consider is that although all three devices are using 2-D image analysis, the CAMSIZER XT is capturing an image representing the projected area of each particle as it moves past the camera lenses, while the Auto-SEM-EDS devices are measuring the flat, polished cross-sections of stationary particles. The CAMSIZER XT has different modules that have various mechanisms of transporting the particles between the two lenses, the selection of which will depend on the sample

characteristics (Westermann, n.d.). For the CAMSIZER XT measurements, the coarse sample was analysed as a dry powder using the gravity feeder. Multiple repeats were carried out to reduce the random uncertainty associated with sampling. Measurements were also carried out using the X-Flow module in which the particles were suspended in water, but these results are not presented.

A raw image obtained with the CAMSIZER XT CCD basic camera is provided in Figure 4.12(a), along with an enlarged section of this in Figures 4.12(b) and 4.12(c), to illustrate the particle contours on which the shape parameter measurements are based. Figure 4.12(d) shows a raw image from the zoom camera. The software uses the data from both cameras depending on the particle size range. Although the unprocessed images appear fuzzier than those obtained with the SEM devices, millions of particle images are obtained within a few minutes, and these can be filtered so that only images that have a sharpness above a selected threshold are included in the particle shape measurements. For the analysis presented in this work, only images from the basic camera were considered, with a sharpness threshold of 20.

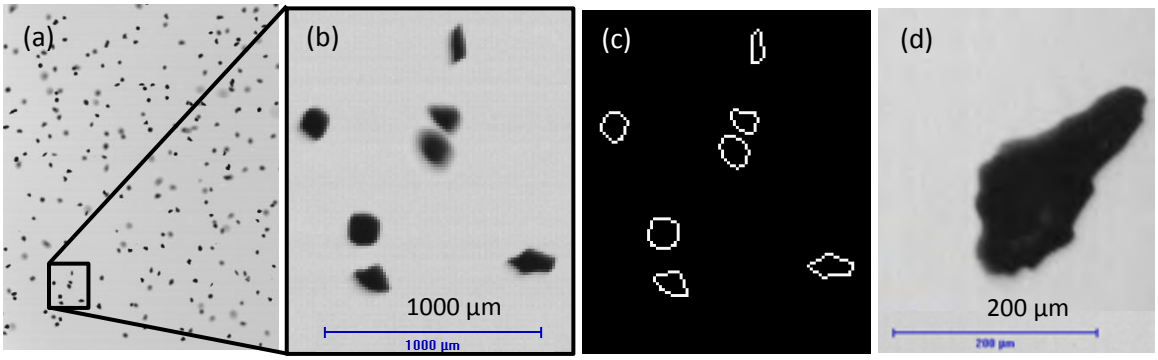

Figure 4.12: CAMSIZER XT images of particles in the coarse fraction (-212/+150µm) obtained with the basic camera (a,b,c), and the zoom camera (d).

4.8.2 Shape characterisation

The shape characterisation referred to in this paper is based on 2-D image analysis, where cross-sections or projected images of thousands of randomly orientated particles are obtained using SEM or dynamic image analysis. Image processing software is then used to calculate shape parameters for each particle, which are combined to produce a shape distribution for the sample. For individual particles these 2-D shape descriptors might not be adequate to explain three dimensional particle properties, however sample distributions based on thousands of particles should directly relate to properties of the particulate sample. Although the 2-D data are well suited to provide a random, statistically significant, quantitative assessment of shape, it is useful to couple this with a qualitative assessment of the 3D morphology, using X-CT or SEM images of 3-D non-polished particles. If there is a high portion of flat, flaky particles, this should

be taken into consideration during interpretation of the 2-D results. For this reason, secondary electron images of UG2 ore particles from the two size fractions are provided in Figure 4.13, taken with an FEI Nova Nano-SEM. Neither sample is highly flaky, and the coarse sample appears to contain more rounded and smooth particles than the fine sample.

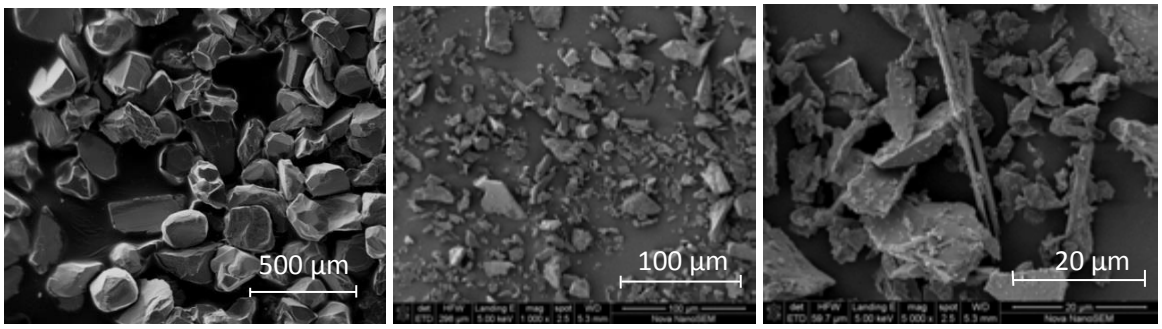

Figure 4.13: SEM Secondary electron images of UG2 ore particles from the coarse size fraction (left) and fine size fraction (center, right).

The only shape parameter that can readily be extracted as a distribution using the software of all three devices in this study is *circularity,* as defined in Equation 4.1. This is obtained from the QEMSCAN using the 'shape factor', from the Mineralogic as the inverse of 'compactness', and from the CAMSIZER XT as 'sphericity'. This is the descriptor that, under a variety of different names, has been most widely reported for minerals processing applications. It is described as a meso-shape descriptor, and the use of perimeter is intended to provide an indication of surface roughness. However, in previous work using QEMSCAN, Little et al. (2015, Paper 1) highlighted some of the weaknesses of the descriptor, and suggested the parameter *roundness* as an appropriate alternative for characterisation of fine particulates. The descriptor *roundness* is defined in the ISO Standard for 'descriptive and quantitative representation of particle shape and morphology', classified as a macro-shape descriptor in the proportion descriptors category. It is presented in Equation 4.2 where Fe_{max} represents the maximum Feret diameter of the particle, which is its longest axis. The ISO standard also mentions that for descriptors depending on perimeter, a minimum resolution of 5000 pixels per particle is required, while for more robust alternatives such as *roundness*, 100 - 200 pixels per particle is adequate. For measurement of fine particulate samples containing particles below 10 µm, resolutions in the latter range are likely. The software for the three devices does not currently include a calculation for *roundness*, although measurements of cross-sectional or projected area, maximum Feret diameter and perimeter data for each particle can be readily extracted. In the case of the Mineralogic and CAMSIZER XT, these data were exported to Microsoft Excel with which *roundness* was calculated for each particle. In the case of the QEMSCAN, the software

iDiscover enables the user to formulate categorisers based on a wide variety of particle properties, which allowed for the determination of *roundness* distributions directly.

$$Circularity = \frac{4\pi \cdot Area}{Perimeter^2} \quad 4.1$$

$$Roundness = \frac{4 \cdot Area}{\pi \cdot Fe_{max}{}^2} \quad 4.2$$

4.9 Results and Discussion

4.9.1 Comparison of shape descriptors for individual particles

In this section, the shape characteristics of individual particles analysed by both Auto-SEM-EDS devices are identified and compared using the two shape descriptors; *roundness* and *circularity*. Some particle images obtained with the CAMSIZER XT for the coarse fraction are also identified, three of which have similar shape to particles selected for the two Auto-SEM-EDS devices. Particles A – F in Figure 4.14 are particles from the coarse fraction, measured with the QEMSCAN and Mineralogic. Particles G – L in Figure 4.15 are also from the coarse fraction, measured with the CAMSIZER XT. Particles M – Q in Figure 4.16 are from the fine fraction, measured with the QEMSCAN and Mineralogic only. The CAMSIZER XT was not included in the comparison for the fine sample measurement as the size range is below the practical limit for shape characterisation with the device. The area, perimeter and length (Fe_{max}) measurements of these specific particles were obtained using the device software for each instrument, and these were used to calculate the *roundness* and *circularity* values using Equations 4.1 and 4.2. The Mineralogic measurements were obtained using three different image processing techniques, a basic threshold, a delineate function and a smoothing function. The Auto-SEM-EDS *circularity* and *roundness* measurements obtained with the two instruments and three image processing functions is presented in Table 4.5.

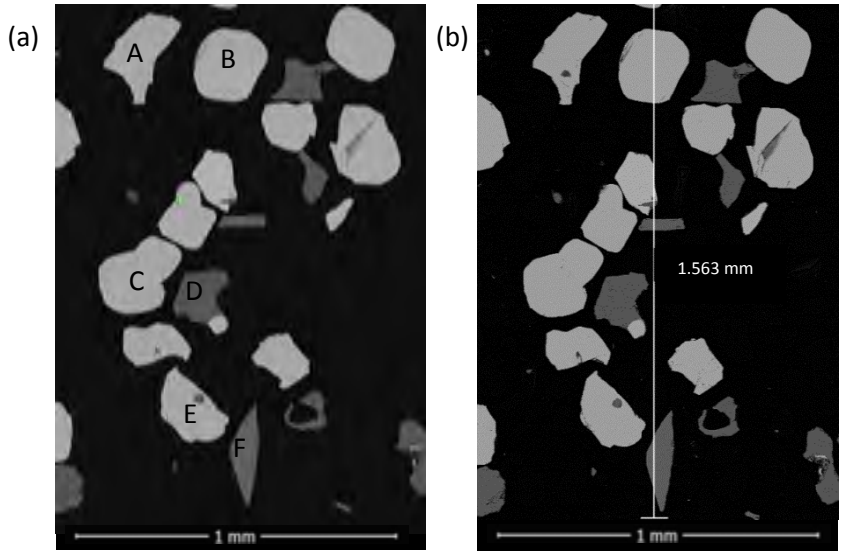

Figure 4.14: BSE image taken from the same field of a coarse sample block with the QEMSCAN (a) and Mineralogic (b).

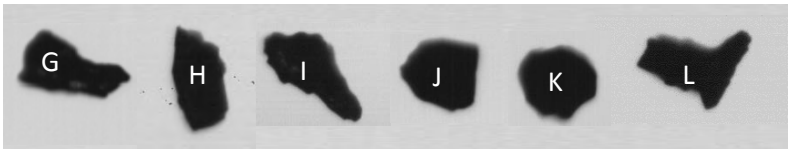

Figure 4.15: CAMSIZER XT images of particles from the coarse fraction, obtained with the zoom camera.

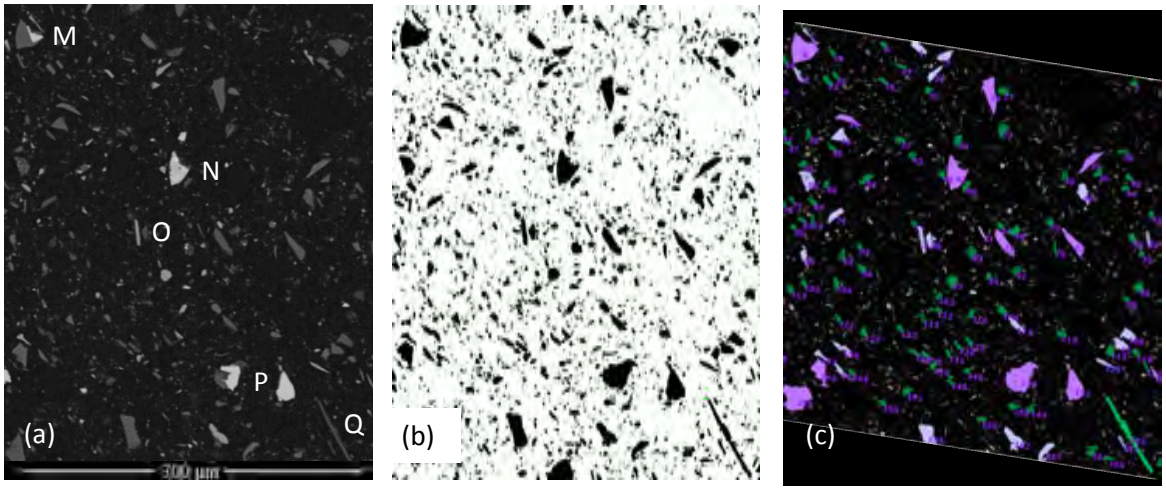

Figure 4.16: BSE image from the QEMSCAN SEM (a), and scanned/processed images of the same field from the QEMSCAN (b) and Mineralogic (c) for the fine fraction analysed.

Table 4.5: Comparison of circularity and roundness values for individual particles A-F (coarse) & M-Q (fine), measured with the QEMSCAN (QS) and Mineralogic: Threshold (T), Delineate (D), and Smoothed (S). Standard deviation (S.D.) of the four measurements of each particle is provided.

I.D.	***Circularity***					***Roundness***				
	QS	**Mineralogic**			**S.D.**	**QS**	**Mineralogic**			**S.D.**
		T	**D**	**S**			**T**	**D**	**S**	
A	0.59	0.54	0.53	0.55	0.027	0.47	0.45	0.45	0.46	0.009
B	0.88	0.82	0.80	0.84	0.034	0.82	0.82	0.81	0.82	0.003
C	0.77	0.68	0.71	0.74	0.038	0.66	0.66	0.66	0.67	0.004
D	0.59	0.39	0.35	0.54	0.117	0.61	0.59	0.58	0.60	0.011
E	0.70	0.66	0.65	0.68	0.021	0.56	0.56	0.55	0.56	0.004
F	0.43	0.36	0.34	0.40	0.041	0.22	0.20	0.20	0.21	0.008
M	0.63	0.58	0.51	0.63	0.055	0.69	0.65	0.64	0.66	0.022
N	0.53	0.44	0.31	0.49	0.097	0.46	0.43	0.40	0.43	0.023
O	0.34	0.22	0.09	0.28	0.106	0.19	0.16	0.13	0.17	0.026
P	0.48	0.32	0.21	0.46	0.128	0.54	0.54	0.51	0.55	0.019
Q	0.09	0.03	0.02	0.08	0.034	0.06	0.05	0.05	0.05	0.006

For the same individual particles identified and analysed using the two different devices and three image processing setups, Table 4.5 shows the high variability in *circularity* measurements with standard deviations ranging between 0.021 and 0.128 (absolute). Comparatively, the standard deviations for *roundness* are on average six times lower, ranging between 0.003 and 0.026. The higher variability in *circularity* measurements for each particle is due to the significant variation in perimeter measurement used to calculate *circularity* as compared to the close agreement between maximum Feret diameter and area measurements used to calculate *roundness*. This indicates that the descriptor *roundness* is more robust than *circularity*.

The different measurement approach for the CAMSIZER XT makes it impossible to compare shape parameters for identical particles. Table 4.6 is therefore intended to provide some CAMSIZER XT particle measurements with an indication of how these compare to Auto-SEM-EDS measurements. It appears that similar shape characteristics are obtained from similar particle images. However, when large numbers of particle images are qualitatively assessed, it is apparent that fewer images of angular or elongated particles are obtained with the CAMSIZER XT than with the Auto-SEM-EDS devices. For example, with the latter it was possible to identify many particles with *circularity* values below 0.5, however it was difficult to do so with the CAMSIZER XT. This is likely due to the difference in image acquisition, which is discussed further in Section 4.9.3.

Table 4.6: Circularity and roundness values for individual particles G - L, measured with the CAMSIZER XT, as compared to QEMSCAN measurements of three similar particles.

	Particle ID	**G**	**H**	**I**	**J**	**K**	**L**
CAMSIZER XT	Image						
	Circularity	0.64	0.74	0.64	0.92	0.93	0.59
	Roundness	0.43	0.49	0.38	0.83	0.86	0.46
	Particle ID		**E**			**B**	**A**
QEMSCAN	Image						
	Circularity		0.70			0.88	0.59
	Roundness		0.56			0.82	0.47

4.9.2 Comparison of circularity and roundness distributions

Comparisons of the *circularity* and *roundness* distributions obtained by the devices for the coarse and fine sample are provided in Figures 4.17 and 4.18 respectively. The uncertainty associated with sampling (random error) was estimated through measurements of different blocks/samples with each device, and is indicated by the error bars showing 95% confidence limits. The variability between measurements with different devices is seen to be much greater than the random error for the descriptor *circularity*, and for comparison between the Auto-SEM-EDS devices and the CAMSIZER XT. For the descriptor *roundness*, the difference between the two Auto-SEM-EDS devices is of a similar magnitude to the random error.

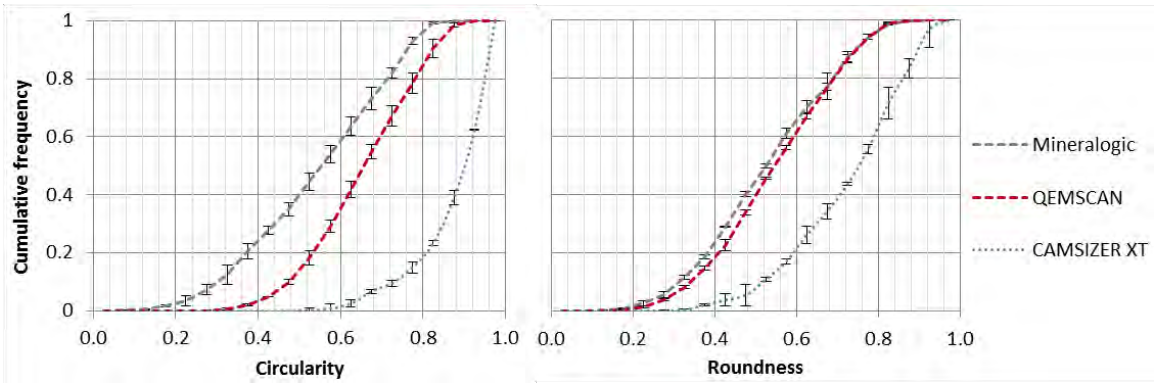

Figure 4.17: Circularity and roundness distributions for the coarse sample (-212/+150 µm), as measured with the QEMSCAN, Mineralogic, and CAMSIZER XT. The average distributions from two or three measurements are indicated, with error bars showing 95% confidence intervals based on these repeats. The number of particles analysed per measurement ranged from 235 to 1538.

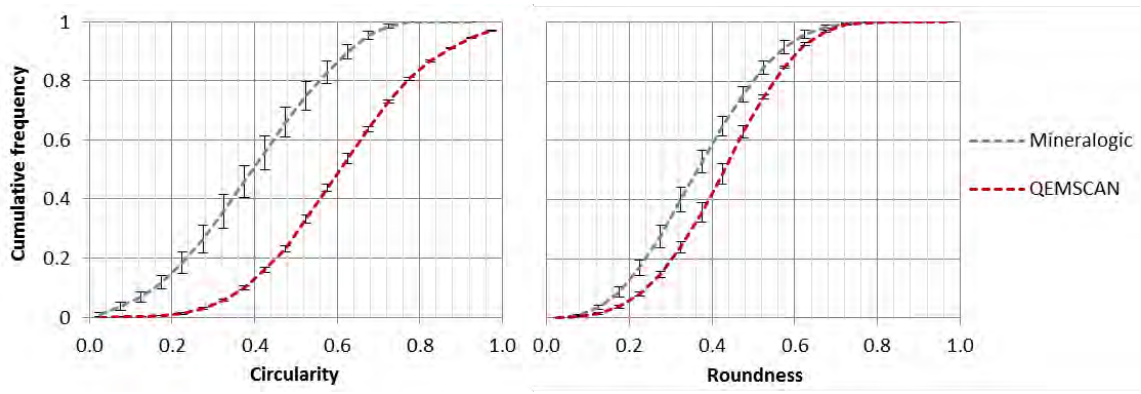

Figure 4.18: Circularity and roundness distributions for the fine sample (-53 µm), as measured with the QEMSCAN and Mineralogic. The average distributions from three measurements are indicated, with error bars showing 95% confidence intervals based on these repeats. The number of particles analysed per measurement ranged from 11500 to 40652.

It is apparent that *circularity* measurements obtained from different devices are currently incomparable, which was expected due to the weaknesses of the descriptor that have been highlighted in the literature (International Organisation for Standardisation, 2008; Little et al., 2015, Paper 1; Pirard, 1989; Russ, 1995). The differences between measurements of shape distribution between the Auto-SEM-EDS devices and the CAMSIZER XT are significant for both descriptors, which is likely due to the dissimilar mechanisms of image capture.

4.9.3 Major factors affecting shape characterisation

This section explores possible reasons for the inconsistencies observed in Sections 4.9.1 and 4.9.2, such as the dissimilar mechanisms of image capture, perimeter algorithms, and effects of image processing. Effects of image resolution on *circularity* and *roundness* measurements were investigated by Little et al. (2015, Paper 1) and are not addressed here.

Image capture: Projected area vs cross-sectional area

The Auto-SEM-EDS images are of particle cross-sections obtained from the polished surfaces of randomly orientated particles in a fixed position. The CAMSIZER XT relies on images of whole particles, captured as they move freely – either falling in air or suspended in water. The shape measurements based on 2-D projected images of particles were found to differ to those based on 2-D cross-sectional images, which are in turn likely to differ to those based on 3-D measurements. This is illustrated qualitatively by the example of an irregular UG2 particle in Figure 4.19. A SEM image of the 3-D (non-polished) particle (a), is compared to a plausible cross-sectional view (b), and a plausible projected view (c), which are very different in shape. This does not necessarily mean that one or other of the measurement methods is wrong, just that they are not directly comparable. It should be noted that the primary function of all of these

devices is not shape characterisation. The CAMSIZER XT is primarily intended for particle size analysis, and for this purpose projected area is more appropriate than cross-sectional area, which will lead to an underestimate of size relative to 3-D techniques. The Auto-SEM-EDS devices are intended for various mineralogical analyses, for which the flat, polished surface and high image resolution are necessary to enable accurate mineral identification and analysis of finely grained minerals.

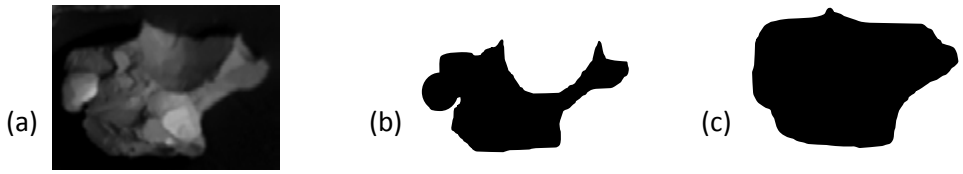

Figure 4.19: A 3-D SEM image of a coarse UG2 particle (a), along with a plausible cross-sectional image of the particle (b), and a plausible projected area image (c), illustrating how shape information based on projected area can provide a more rounded representation of particulates than that based on 2-D cross-sections.

Perimeter algorithms

Another factor contributing to the differences between the device outputs is the perimeter algorithms that the devices use. As illustrated in Figure 4.20, the QEMSCAN perimeter is taken as the distance around the particle from centre to centre of the external pixels (which are considered as squares rather than points), while the Mineralogic perimeter is taken along the border of external pixels, with a smoothening correction for pixels occurring on the diagonal. In both cases the area is taken as the total area of the image pixels. At low resolutions this difference would lead to the Mineralogic reporting lower *circularity* values than the QEMSCAN as was observed in Table 4.5, Figure 4.17 and Figure 4.18. For the QEMSCAN, the treatment of exterior pixels in the area and perimeter algorithms leads to particle images composed of fewer than 40 pixels typically reporting circularities greater than the theoretical maximum of 1(Little et al., 2015, Paper 1). Pirard (2004) discusses perimeter algorithms, defining inner and outer perimeter measurements, with four- or eight-connectivity depending on how many of the surrounding pixels are taken into consideration when connecting the boundary pixels. Both examples provided in Figure 4.20 have eight-connectivity (diagonal boundary lines). The QEMSCAN example would be considered an inner perimeter, and the Mineralogic example falls between the inner and outer perimeters described by Pirard. Use of the Cauchy-Crofton formula is an alternative to these approaches, which, although poorly known is considered mathematically indisputable, and it is the approach recommended in ISO 9276-6 (International Organisation for Standardisation, 2008; Pirard, 2004). It should also be noted that there is another entirely different algorithm for perimeter measurement that is used by some systems.

It is based on the length and width parameters, with the assumption that each particle can be represented by an ellipse (Roufail, 2011; Ulusoy, Hiçyılmaz, & Yekeler, 2004).

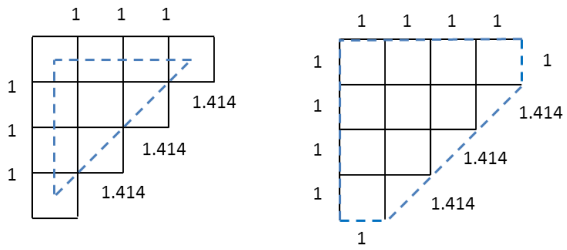

Figure 4.20: The perimeter algorithms indicated by the blue dashed line, for the QEMSCAN (left) and Mineralogic (right), would lead to circularity measurements for the two identical 'images' of 1.20 and 0.62 respectively.

Image processing and separation of touching particles

Image processing plays an important role in automatically extracting meaningful, quantitative information from raw images. Different image processing tools directly affect measurements of individual particle shape characteristics, as was observed in Section 4.9.1 where Mineralogic measurements with a basic threshold, a delineate setup and a smoothening setup were compared. This was found to be due to variation in the perimeter measurement which is illustrated in Figure 4.21 (a) for the fine particle Q. The EDS information indicates that particle Q is muscovite (mica), which means that it is likely a thin plate rather than a needle shaped particle. The layers are detected with the application of a basic threshold, which leads to a large measurement of perimeter with inclusion of the 'boundary' pixels between the layers. The delineate function (added to the basic threshold) enhances this effect, leading to an even larger perimeter measurement. The smoothing function does the opposite, blurring the mineral layers to produce a perimeter measurement corresponding only to the exterior surface of the particle.

The image processing functions can also indirectly impact both *circularity* and *roundness* frequency distributions through an effect on the algorithms for automatic separation of touching particles. Examples are highlighted in Figure 4.21 (b), where the initial identification of particles as separate or touching varies for all three image processing functions. In post-measurement processing stages with either of the Auto-SEM-EDS devices, even if initially classified as touching particles, these examples would likely be identified as candidates for automatic separation. However, in a large sample of fine particles there are likely to be many touching particle boundaries that are less distinct, which will either be automatically separated, or identified as single irregularly shaped particles, depending on the image processing functions applied. Device manufacturers, or different users of the same device, are likely to use a variety

of image processing combinations, which will impact the shape parameter measurements obtained for any given sample.

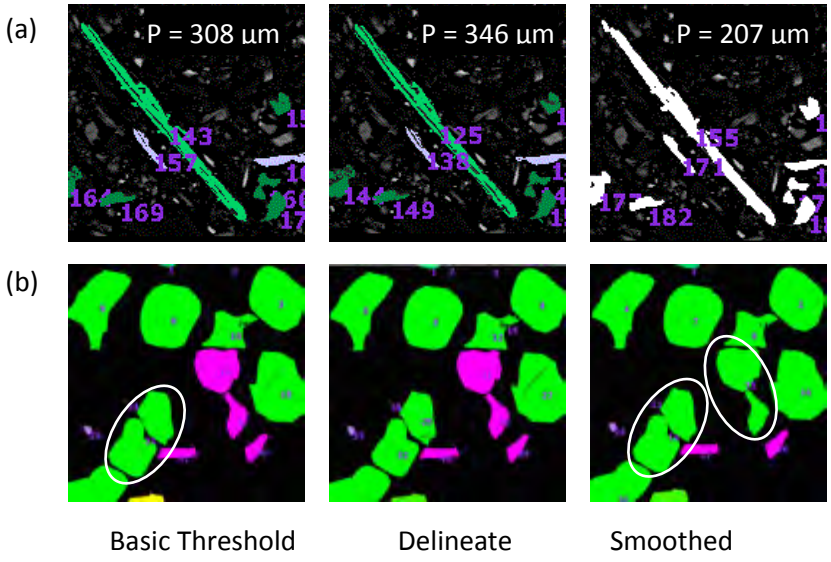

Figure 4.21: The effects of image processing on: (a) the appearance and perimeter measurement of particle Q and (b) the separation of touching particles. Pairs of particles that are not identified as separate particles are circled in white.

4.10 Conclusions

The three devices assessed do not give comparable shape information for particulate samples. Currently, the only shape descriptor that the three devices have in common (included in the software for each device) is *circularity*. Each device has a different name for the descriptor, and the variation in image processing and perimeter measurement algorithms leads to considerable differences in the *circularity* measurements obtained with the three devices for the same samples. However, it is possible to indirectly obtain *roundness* distributions for the three devices, and *roundness* is a more robust descriptor. When selecting a shape descriptor, *circularity* may initially appear preferable to *roundness* because it is a meso-shape descriptor rather than a macro-shape descriptor, and thus should theoretically give a better indication of surface roughness. Unfortunately, the subtle differences in roughness between fine particulate mineral samples are not likely to be accurately quantifiable using a descriptor such as *circularity* due to the high variability in perimeter measurements with factors such as image resolution. In these instances, *roundness* is likely to give a better indication of the morphology of the particulate sample. Measurements from devices that are fundamentally different in nature (i.e. projected image vs cross-sectional image) should not be compared directly. Further work is required in this field in order to achieve a higher level of confidence in particulate shape characterisation data.

4.11 Acknowledgements

The authors would like to acknowledge the South African Minerals to Metals Research Institute (SAMMRI) and the South African Department of Science and Technology for funding the work. The assistance we received from representatives from Carl Zeiss, Retsch and FEI is much appreciated. Thanks in particular to Shaun Graham for performing the Mineralogic measurements. This work is based on research supported in part by the National Research Foundation of South Africa (Grant Numbers 86054 & 93189). Any opinions, findings and conclusions or recommendations expressed in any publication generated by the NRF supported research is that of the author(s), and the NRF accepts no liability whatsoever in this regard.

4.12 References

Cropp, A. F., Goodall, W. R., & Bradshaw, D. J. (2013). The Influence of Textural Variation and Gangue Mineralogy on Recovery of Copper by Flotation from Porphyry Ore – A Review. AusIMM GeoMet 2013 Proceedings, (October), 279–291.

Das, R., & Cleary, P. W. (2010). Effect of rock shapes on brittle fracture using Smoothed Particle Hydrodynamics. Theoretical and Applied Fracture Mechanics, 53(1), 47–60. doi:10.1016/j.tafmec.2009.12.004

Dworzanowski, N. I. (2014). Maximizing haematite recovery within a fine and wide particle-size distribution using wet high-intensity magnetic separation. The Journal of The South African Institute of Mining and Metallurgy, 114, 559–567.

FEI. (2015b). FEI. Retrieved February 11, 2015, from http://www.fei.com/products/sem/qemscan/

Frances, C., Le Bolay, N., Belaroui, K., & Pons, M.-N. (2001). Particle morphology of ground gibbsite in different grinding environments. International Journal of Mineral Processing, 61(1), 41–56. doi:10.1016/S0301-7516(00)00025-9

Goodall, W. R., Scales, P. J., & Butcher, A. R. (2005). The use of QEMSCAN and diagnostic leaching in the characterisation of visible gold in complex ores. Minerals Engineering, 18(8), 877–886. doi:10.1016/j.mineng.2005.01.018

Gottlieb, P., Wilkie, G., Sutherland, D., Ho-Tun, E., Suthers, S., Perera, K., … Rayner, J. (2000). Using quantitative electron microscopy for process mineralogy applications. Journal of Mineralogy, 52(4), 24 – 25.

Grobler, J. D., & Bosman, J. B. (2011). Gravity separator performance evaluation using Qemscan® particle mineral analysis. Journal of the Southern African Institute of Mining and Metallurgy, 111(September 2009), 401–408.

Guven, O., Ozdemir, O., Karaagaclioglu, I. E., & Çelik, M. S. (2015). Surface morphologies and floatability of sand-blasted quartz particles. Minerals Engineering, 70, 1–7. doi:10.1016/j.mineng.2014.08.007

Hill, E. (2014). Zeiss Mineralogic Mining - Ore Process Optimization. Carl Zeiss White Paper.

Hoşten, Ç., & Özbay, C. (1998). A comparison of particle bed breakage and rod mill grinding with regard to mineral liberation and particle shape effects. Minerals Engineering, 11(9), 871–874. doi:10.1016/S0892-6875(98)00074-0

International Organisation for Standardisation. (2008). Representation of results of particle size analysis - Part 6: Descriptive and quantitative representation of particle shape and morphology. ISO 9276 - 6 (Vol. 2008). Geneva.

Kashiwaya, K., Noumachi, T., Hiroyoshi, N., Ito, M., & Tsunekawa, M. (2012). Effect of particle shape on hydrocyclone classification. Powder Technology, 226, 147–156. doi:10.1016/j.powtec.2012.04.036

Komabayashi, T., & Spångberg, L. S. W. (2008). Comparative analysis of the particle size and shape of commercially available mineral trioxide aggregates and Portland cement: a study with a flow particle image analyzer. Journal of Endodontics, 34(1), 94–8. doi:10.1016/j.joen.2007.10.013

Kursun, H., & Ulusoy, U. (2006). Influence of shape characteristics of talc mineral on the column flotation behavior. International Journal of Mineral Processing, 78(4), 262–268. doi:10.1016/j.minpro.2005.11.003

Little, L., Becker, M., Wiese, J., & Mainza, A. N. (2015). Auto-SEM particle shape characterisation: Investigating fine grinding of UG2 ore. Minerals Engineering, 82, 92–100. doi:10.1016/j.mineng.2015.03.021

Matrox. (2016). Matrox Imaging Library Overview. Retrieved May 17, 2016, from http://www.matrox.com/imaging/en/products/software/mil/

Ndlovu, B., Becker, M., Forbes, E., Deglon, D., & Franzidis, J.-P. (2011). The influence of phyllosilicate mineralogy on the rheology of mineral slurries. Minerals Engineering, 24(12), 1314–1322. doi:10.1016/j.mineng.2011.05.008

Pirard, E. (1989). Applications of shape analysis in ore beneficiation. In Process Mineralogy IX: Applications to Mineral Beneficiation, Metallurgy, Gold, Diamonds (pp. 205–218). TMS.

Pourghahramani, P. (2012). Effects of ore characteristics on product shape properties and breakage mechanisms in industrial SAG mills. Minerals Engineering, 32, 30–37. doi:10.1016/j.mineng.2012.03.005

Retsch Technology. (2016). Camsizer XT. Retrieved January 13, 2016, from http://www.retsch-technology.com/rt/products/dynamic-image-analysis/camsizer-xt/function-features/?

Roufail, R. A. (2011). The effect of stirred mill operation on particles breakage mechanism and their morphological features. The University of British Columbia.

Russ, J. C. (1995). The Image Processing Handbook (2nd ed.). Raleigh, North Carolina: CRC Press.

Tonzetic, I. (2015). Quantitative analysis of iron ore using SEM based technologies. In Iron ore: Mineralogy, Processing and Environmental Issues.

Ulusoy, U., Hiçyılmaz, C., & Yekeler, M. (2004). Role of shape properties of calcite and barite particles on apparent hydrophobicity. Chemical Engineering and Processing, 43(8), 1047–1053. doi:10.1016/j.cep.2003.10.003

Ulusoy, U., & Yekeler, M. (2005). Correlation of the surface roughness of some industrial minerals with their wettability parameters. Chemical Engineering and Processing: Process Intensification, 44(5), 555–563. doi:10.1016/j.cep.2004.08.001

Verrelli, D. I., Koh, P. T. L., Bruckard, W. J., & Schwarz, M. P. (2012b). Variations in the induction period for particle–bubble attachment. Minerals Engineering, 36-38, 219–230. doi:10.1016/j.mineng.2012.03.034

Vizcarra, T. G., Harmer, S. L., Wightman, E. M., Johnson, N. W., & Manlapig, E. V. (2011). The influence of particle shape properties and associated surface chemistry on the flotation kinetics of chalcopyrite. Minerals Engineering, 24(8), 807–816. doi:10.1016/j.mineng.2011.02.019

Vizcarra, T. G., Wightman, E. M., Johnson, N. W., & Manlapig, E. V. (2011). The effect of breakage method on the shape properties of an iron-oxide hosted copper–gold ore. Minerals Engineering, 24(13), 1454–1458. doi:10.1016/j.mineng.2011.07.007

Walker, C. I., & Hambe, M. (2015). Influence of particle shape on slurry wear of white iron. Wear. doi:10.1016/j.wear.2014.12.029

Westermann, J. (n.d.). Particle Characterization with Dynamic Image Analysis. Retsch Technology Whitepaper, 1–8.

Zeiss_Microscopy. (n.d.). Zeiss Microscopy. Retrieved February 11, 2015, from http://www.zeiss.co.za/microscopy/en_za/products/scanning-electron-microscopes/mineralogic-systems.

More about aspect ratio and roughness

In Papers 1 and 2, the shape factors *circularity* and *roundness* were interrogated thoroughly. A shape characterisation methodology was developed based on using *roundness* in conjunction with *aspect ratio* to distinguish between rough, equant particles, and smooth, elongated particles. In this section *aspect ratio* is interrogated in the same manner as the other two descriptors were in Papers 1 and 2, and the potential of the methodology to distinguish between rough and smooth particles is explored.

4.13 Effects of image resolution on aspect ratio

In Section 4.3.1, the sensitivity of *circularity* and *roundness* to resolution limitations was tested by plotting the normalized frequency distribution of each descriptor against resolution, expressed as the number of pixels per particle. The equivalent analysis for *aspect ratio* is presented in Figure 4.22. The plot is seen to be more similar to that of *roundness* (Figure 4.4) than *circularity* (Figure 4.3), with minimal variation in *aspect ratio* distribution in the resolution range from 40 to 100 pixels per particle. Below 40 pixels per particle, the distribution narrows and splits into peaks. As these peaks lie within the modal range of the distribution, if a small proportion of particles falls within this range, it will not cause significant bias to *aspect ratio* distribution measurements. In terms of image resolution, *aspect ratio* is indeed a robust descriptor, as was inferred based on the literature (International Organisation for Standardisation, 2008).

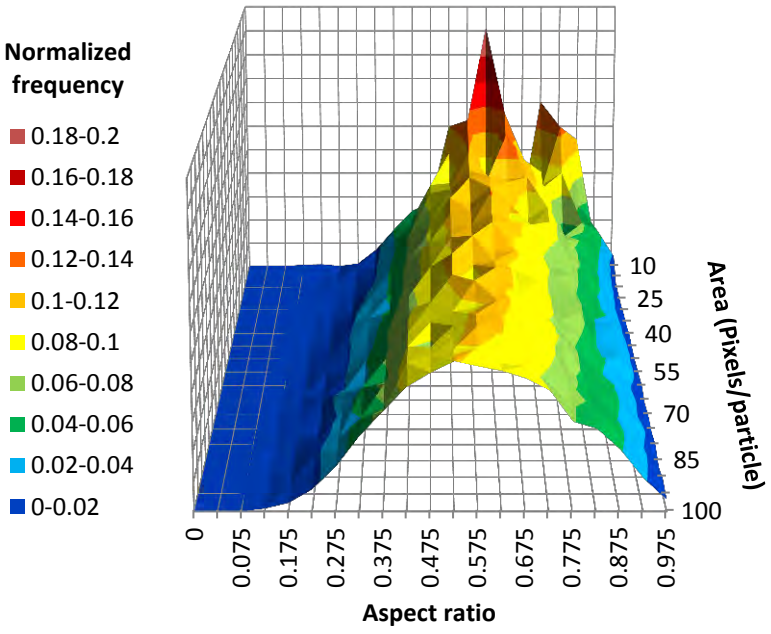

Figure 4.22: The effect of image resolution (no. pixels per particle) on aspect ratio frequency distribution. n = 325 587.

4.14 Aspect ratio – variation in definitions and algorithms

In Chapter 2.2, Table 2.2, various definitions of aspect ratio that have been reported in the literature were presented, all of which could be loosely described as the ratio of width to length. The intention of this section is to illustrate that loosely defining aspect ratio as width over length is insufficient and the exact measurements used need to be clearly indicated. Figure 4.23 shows the variability that can occur in aspect ratio measurements due to the use of dissimilar length and width parameters. Aspect ratios are presented for the particles A-F (-212/+150 μm) and M-P (-53 μm), which were analysed by QEMSCAN and Mineralogic and identified for comparison in Section 4.9.1. The *aspect ratio* reported for QEMSCAN was based on the parameters Long Axis and Short Axis, which are used as measurements of length and width in the iDiscover software, and are consistent with the ASTM standard (ASTM International, 2010). Long Axis is equivalent to the maximum Feret diameter, and Short Axis is the maximum width of the particle cross-section measured perpendicular to the Long Axis.

The image processing package used by the Mineralogic (supplied by Matrox), has a wide variety of shape parameters available. In the first version of the Mineralogic software that was used for this analysis, the only width parameter included was 'breadth', which is recommended for long thin particles, and is actually obtained indirectly based on area and perimeter measurements. Each particle is modeled as a rectangle with equivalent area and perimeter, and the length and breadth parameters are obtained from this. The values obtained in Figure 4.23 are therefore based on breadth/maximum Feret diameter for the Mineralogic. As particles A, D and P have high perimeter measurements relative to area, they report as narrow, elongated rectangles for this measurement.

The differences between the measurements obtained for slight variations of the aspect ratio definition (i.e. short axis vs. breadth) are seen to be substantial. Consideration of the exact definition of aspect ratio as well as the definitions of the length and width parameters used will clearly be important for comparison of aspect ratio across studies in which different measurement devices are used. The latest version of the Mineralogic software includes minimum Feret diameter as an alternative measurement for width, which would be expected to give more similar aspect ratio measurements to those based on Short Axis.

In addition to the differences in definition for descriptors such as aspect ratio, an additional level of variation to all shape measurements can be introduced through differences in the algorithms used to determine the fundamental parameters such as the Maximum Feret diameter.

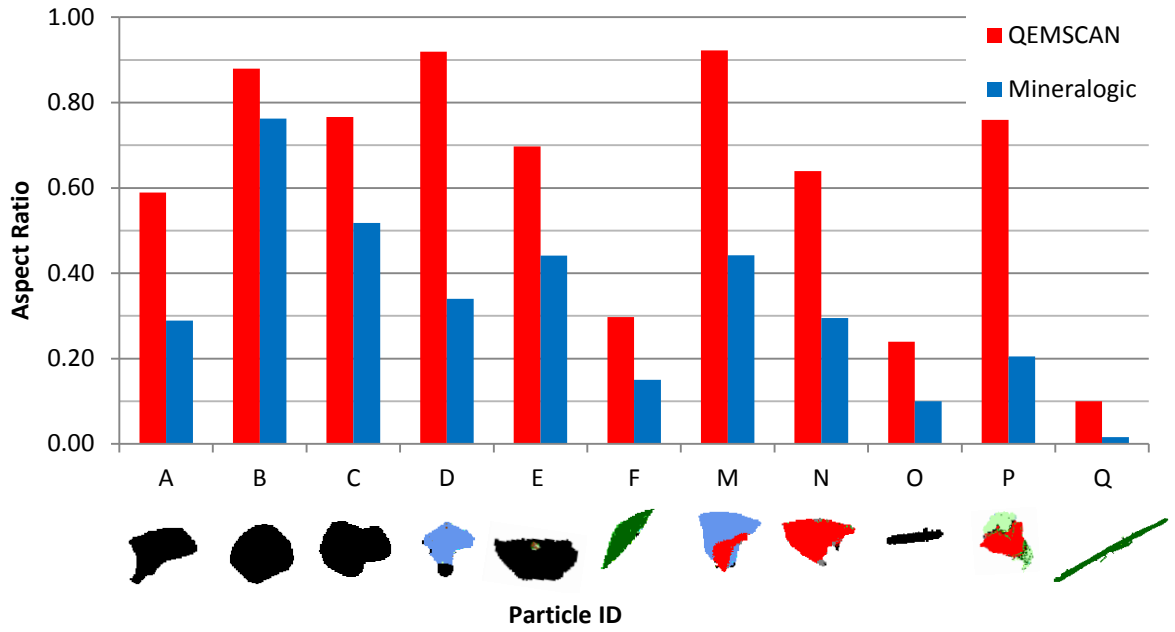

Figure 4.23: Comparison of the output of two different aspect ratio measurements for the same particles; each bar corresponds to a single particle measurement, with the associated particle images displayed below the chart. 'Width' for QEMSCAN is maximum width measured perpendicular to max Feret diameter. For the Mineralogic measurements 'breadth' was used, which is based on an ellipse with equivalent perimeter and area to the particle.

4.15 Using aspect ratio and roundness to describe roughness

In Section 4.3.5 it was acknowledged that shape class definitions, based on the use of *aspect ratio* and *roundness* in conjunction, could be adjusted depending on the shape characteristics of interest in a particular investigation. The possibility of using a 'diagonal' division on the *roundness* - *aspect ratio* matrix was suggested, to determine the proportions of particles that have a *roundness* value greater than 0.8 times their *aspect ratio*. This approach would be more suitable for distinguishing the textural characteristics of particles over the full range of *aspect ratios*. In order to demonstrate this, a roughness categoriser termed 'jaggedness' was made using two parallel diagonal divisions to give three shape classes. Representing the *roundness*/*aspect ratio* matrix in the Cartesian plane, these can be described as y = mx + C1 and y = mx + C2, where y is *roundness*, and x is *aspect ratio*. The gradient m, and constants C1 and C2, were selected based on qualitative assessment of the particles categorised using these divisions. The 'smooth' category was then set to select all particles for which *roundness* was greater than 0.75 times the *aspect ratio* plus 0.05, and the 'jagged' category was set to select all particles for which *roundness* was less than 0.75 times the *aspect ratio* (C2 = 0). This is illustrated in Figure

4.24. The resulting particle shape classes can be assessed qualitatively with the image grid presented in Figure 4.25.

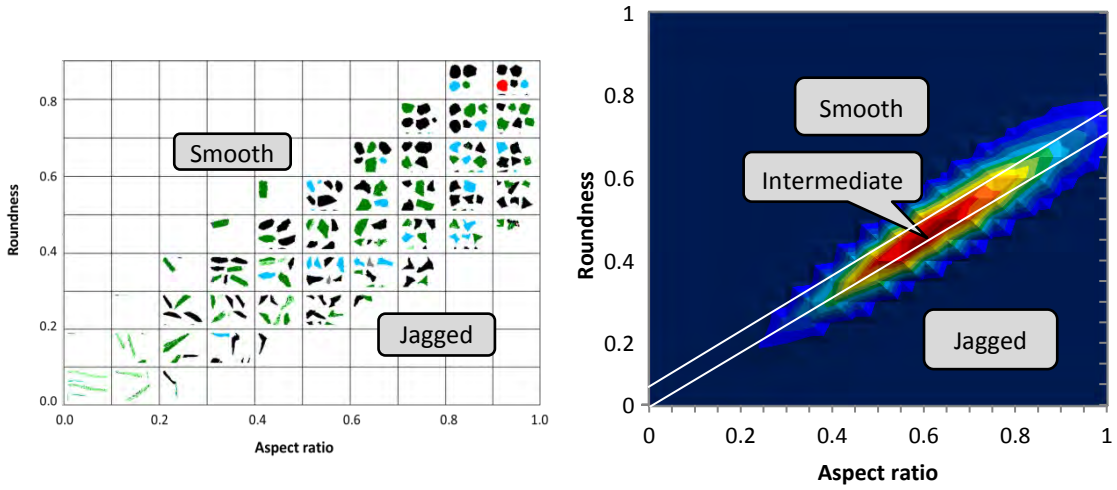

Figure 4.24: Illustration of 'jaggedness' categories from the roundness – aspect ratio matrix. Refer to Figures 4.9 and 4.10 for more details.

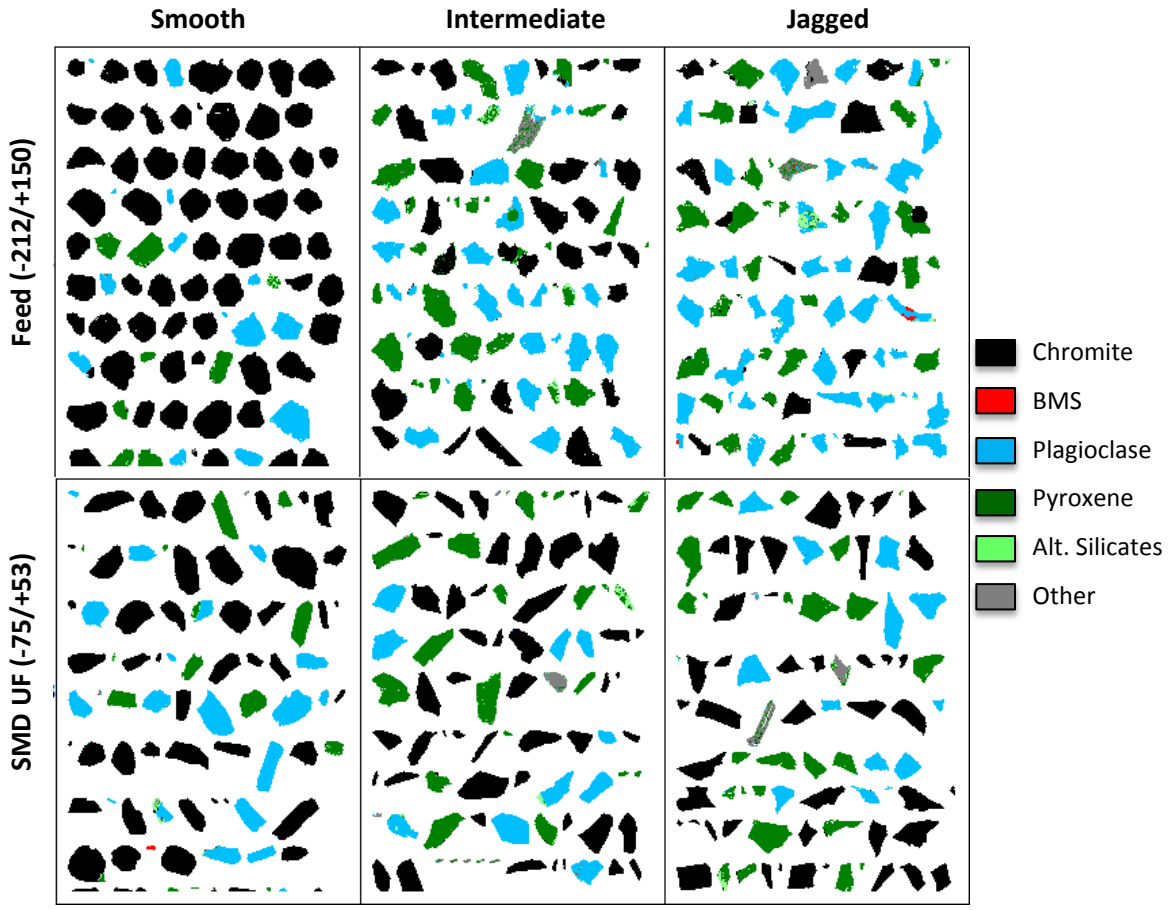

Figure 4.25: Image grid showing performance of the jaggedness categoriser.

The UG2 ore samples from the laboratory fine grinding test work were classified using the jaggedness categoriser, and the results are presented in Figure 4.26. There is very little variation in particle roughness between the fine feed and fine grinding products. However, there is a significant difference between the chromite and silicates in the coarse feed fraction. The smooth chromite and angular silicates in the coarse fraction are an indication of phase boundary fracture, which is discussed in more detail in Chapter 5. The minimal differences between the angularity of the remaining samples suggests that after grinding below the grain size distribution of chromite, the chromite, pyroxene and plagioclase break into particles with similar roughness that is not severely affected by grinding time, mill type or cleavage.

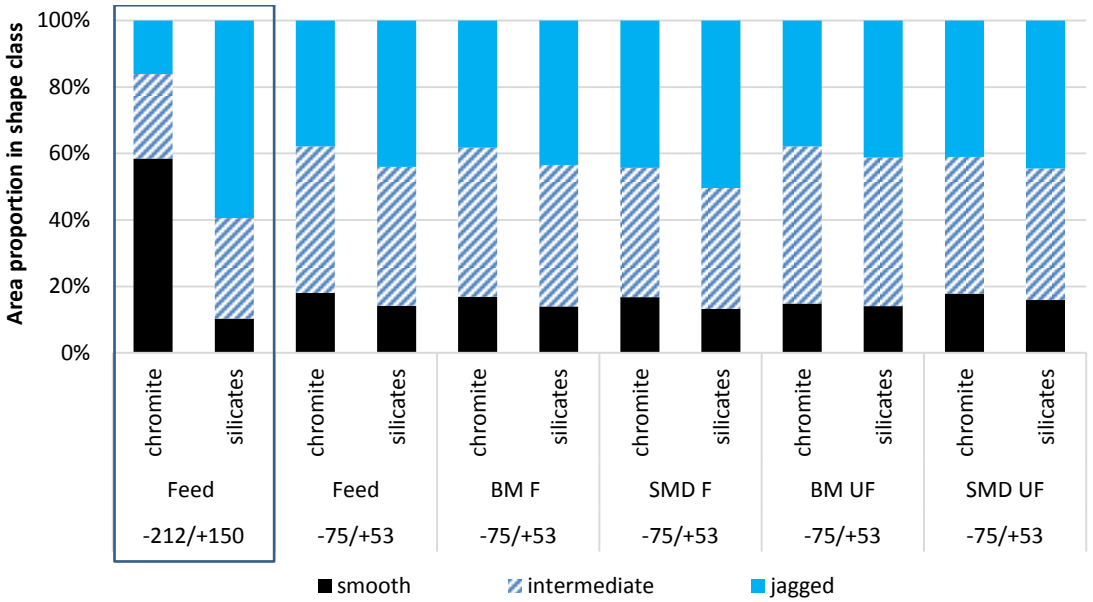

Figure 4.26: Application of the jaggedness categoriser to the laboratory fine grinding feed and product samples in the -212/+150 and -75/+53 µm fractions respectively. Refer to Table 3.3 for definition of the abbreviations used.

The jaggedness categoriser defined here was intended to serve as a simple measurement of roughness that did not depend on image resolution (or perimeter measurement), and that could be computed with the parameters currently available in the iDiscover software. When characterising other ore types and/or coarser particles, roughness may be a more important parameter to consider, and in these instances more advanced meso-shape descriptors would likely be useful. Some of these descriptors are defined in Chapter 2, Table 2.3.

Stereology, size, and weighting of shape distributions

4.16 Stereology for size and liberation

In particle characterisation, particle shape has long been recognised as an important factor relevant to stereology. However, generally assumptions are made about shape to enable the development of correction procedures for other 2-D measurements such as grain size distribution or mineral liberation. Comparatively little has been reported about stereological considerations for 2-D particle shape characterisation.

The early work on stereology that was applicable to minerals processing focused on stereological correction procedures for the determination of particle or grain size distributions from 2-D or 1-D measurements. These needed to be weighted by volume for compatibility with alternative sizing methods such as screening (Barbery, 1974; King, 1984, 1982, 1978). Initial derivations were based on relationships for spheres or homothetic samples (comprising particles of similar shape), and later adjustments allowed for irregularly shaped particles, provided that the shape characteristics of the particles of interest did not change significantly with size (King, 1982). Mean intercept length (1-D) was initially preferred as a size parameter because the mathematics of random intercepts was more highly developed than that of random sections (Barbery, 1974). This has ultimately led to the use of 1-D measurements rather than 2-D measurements for the 'stereologically correct' parameters incorporated in Auto-SEM-EDS software such as iDiscover™ (Spencer and Sutherland, 2000). An example of this is the parameter phase specific surface area (PSSA) which, based on mean intercept length, was proposed as an unbiased parameter for estimation of grain size using automated mineralogy (Sutherland, 2007). Sutherland (2007) observed a correlation between PSSA and concentrate P80s for a number of industrial concentrators, concluding that this 'strongly supported' the use of PSSA as an indicator of grain size. However the evidence on which this claim was based is weak as an inverse relationship between PSSA and particle size is inherent in the definition of PSSA.

In spite of the more highly developed mathematics for random intercepts, areal based measurements have been considered 'inherently more accurate' than 1-D measurements (Leigh et al., 1996). Furthermore, Ralph and Kurzydłowski (1997) observed that it is often better to compare 2-D data, which have a higher built-in statistical confidence, than to compare these data after stereological transformation to 3-D. These arguments are supported by the image grid in Figure 4.27, which compares the classification of particles by the QEMSCAN ESD parameter (stereologically correct, based on 1-D measurement in x-direction), to the equivalent circle diameter (ECD, calculated directly from the 2-D cross-sectional area). The size ranking

presented by the columns in the grid (ECD, increasing from left to right) is more intuitive than that presented by the rows (ESD, increasing from bottom to top).

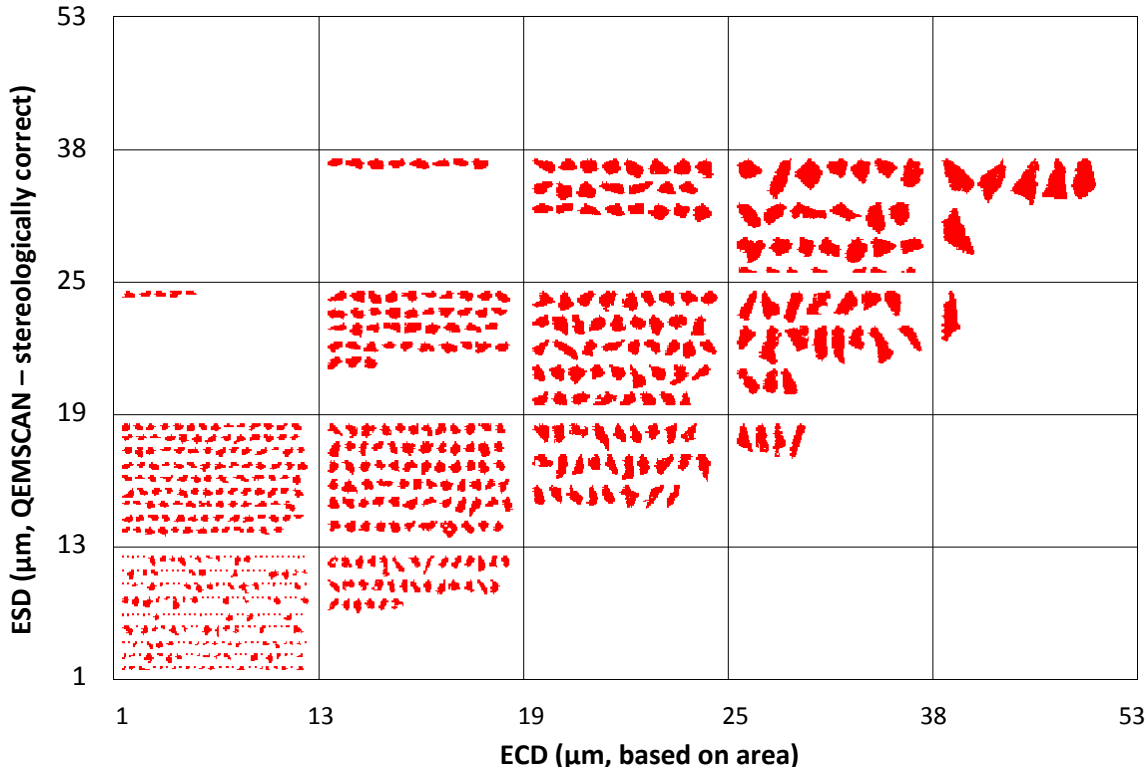

Figure 4.27: Image grid showing classification of liberated base metal sulfide grains by size parameters based on 1D (ESD) and 2D (ECD).

The next widely investigated application of stereology in minerals processing was related to the measurement of liberation, and the bias introduced to liberation and abundance measurements through sections that do not cut through all mineral phases of a particle (Barbery, 1987; Lätti and Adair, 2001; Leigh et al., 1996). However Lätti and Adair (2001) observed minimal differences in liberation data from 2-D measurements and reconstructed 3-D data based on multiple thin sections of the same ore particles. This led them to question whether stereological corrections for liberation measurements are necessary for real ores with complex textures and associations as opposed to the simple binary systems for which most theoretical stereological relationships are typically derived. Note that the average grade, modal mineralogy or bulk mineralogy measurements based on areal sections of sufficient numbers of particles are not considered biased. This is because as the number of particle cross-sections analysed becomes large (i.e > 10 000), the area-based measurement becomes equivalent to an integration over the volume of a small number of representative particles.

An additional factor relating to stereology for Auto-SEM-EDS measurements is that sectional mineralogy measurements are not strictly 2-D, and the image obtained is affected by the interaction volume of the electron beam, which penetrates the surface of the block, and thus can significantly affect the perceived cross-sectional area of a given particle (Payton and Mills, 2011).

4.17 Stereology and shape

In comparison to the applications of stereology to measurements of grain size and mineral liberation, only minimal attention has been paid to the application of stereology to 2-D measurements of shape distributions. Comparisons have been made between 2-D and 3-D shape measurements, which could perhaps be classified as stereological research, however stereology was not mentioned explicitly in these texts (Bagheri et al., 2015; Garboczi et al., 2012; Rickman et al., 2016). Bagheri et al. (2015) and Garboczi et al. (2012) used 3-D X-CT to investigate 2-D and 3-D shape characteristics of volcanic ash particles and crushed gravel respectively. Bagheri et al. (2015) investigated the correlations between a wide variety of shape descriptors and found that descriptors based on 2-D variables (i.e. area, perimeter) could be more closely correlated with sphericity than those based on 1-D variables (i.e. length, breadth, width). Garboczi et al. (2012) compared 3-D parameters with the equivalent 2-D parameters obtained from the same X-CT images. However the '2-D' parameters reported were all calculated as the average of three orthogonal projections, so these were not strictly 2-D measurements and were likely much more representative of the 3-D particles than measurements from single projections would be. Shape factor frequency distributions (weighted by volume) were presented for the 3-D data but the 2-D vs 3-D comparisons were based on equivalent sphere/circle diameter (3-D: ESD; 2-D: ECD), width and surface area. Of these, the closest correlation was for ECD and ESD, which had standard deviations in the range of 3-5% for three size classes measured. The other parameters had standard deviations in the range of 8-12% (Garboczi et al., 2012). This finding also supports the selection of ECD as a size parameter (Section 4.16).

In Section 4.3.3 in Paper 1, it was postulated that provided sufficient numbers of randomly orientated particles are measured, 2-D *roundness* frequency distributions will be indicative of a particulate sample's 3-D shape properties. The excellent reproducibility of roundness distributions obtained from orthogonal sections of a single sample block supported this theory. More recently, Rickman et al. (2016) presented 2-D shape frequency distributions obtained from thousands of projections and cross-sections of single 3-D geometric shapes. The authors used a similar characterisation method to that presented in Paper 1, presenting combined *circularity-aspect ratio* probability distributions from multiple sections of individual geometric

solids rather than *roundness-aspect ratio* frequency distributions for single cross-sections of multiple irregularly shaped particles. Rickman et al. (2016) concluded that unique probability density distributions existed for each convex solid investigated, and that the probability density surface (PDS) of a mixture of solids is the proportional combination of the individual solid's PDS. This further corroborates the theory postulated in Section 4.3.3.

Ulusoy and co-authors (Ulusoy and Igathinathane, 2014; Ulusoy and Yekeler, 2014) agree that a sufficient number of 2-D measurements of randomly orientated particles can provide a true representation of a particulate sample's 3-D characteristics. They go so far as to classify dynamic image analysis as a 3-D shape characterisation technique, based on the instrument manufacturer's claim that particles suspended in the carrier fluid are randomly orientated and recirculated (Micromeritics, 2016).

4.18 Weighting of shape frequency distributions

Apart from the question of whether 2-D shape measurements can be used to describe 3-D shape properties, the question of how to weight shape descriptor frequency distributions could also be linked to stereology. In the case of size measurements based on 2-D image analysis, stereology is required to obtain volume-weighted size distributions for comparison to mass-weighted size distributions obtained by physical separation techniques. However the question of whether shape distributions should be weighted by particle number, area, or volume has not been clearly addressed within the literature.

In Paper 1, the frequency distributions were weighted based on the number of particles reporting to each shape class. This was following the approach assumed to have been applied by Vizcarra (2010), with the intention of ensuring that more rounded particles were not weighted more heavily than plate-like particles or needle-shaped particles. Examples of shape descriptor distributions provided in ISO 9276-6 are also weighted by particle count, and this has been widely used as the basis for the weighting of frequency distributions as well as for the estimation of the mean and standard deviation of shape parameters (International Organisation for Standardisation, 2008; Kaya et al., 2002; Pons et al., 2002; Pourghahramani, 2012; Triffett and Bradshaw, 2008; Walker and Hambe, 2015). In the past when shape measurements were limited to a small number of particles in a sample, this approach was perhaps the obvious choice. Now, with the ability to measure tens of thousands of particles for a particular sample, it is perhaps not ideal. If there is variation in shape characteristics with size (or resolution), shape distributions weighted by number will be dominated by the finer particles in a sample, which will be much more numerous than is reflected by their mass or volume proportion of the

sample. Artefacts of poor image resolution that affect the shape measurements of fine particles would then be exaggerated rather than reduced.

An alternative approach that is typically used with dynamic image analysis systems is to weight shape distributions by volume (Garboczi et al., 2012). Califice et al. (2013) studied the influence of shape on size distribution measurements based on both 2-D and 3-D image analysis methods. He simply used the assumption that the volume of a particle could be approximated by $A^{3/2}$, where A is projected area. The samples that were measured comprised spherical particles and fibres, so this assumption was only appropriate for the spherical particles. It led to an overestimate of the proportion of fibres by volume in the mixed sample. Systems such as the CAMSIZER XT estimate the volume of individual particles by representing the projected particle image with an ellipse of equivalent area and long axis, and rotating this ellipse around its long axis. This approach relies on the assumption that the projected image captures the longest axis of the 3-D particle, so although it would be more appropriate for the fibres studied by Califice et al. (2013), it would not be appropriate for sectional images. In sectional images, an elongated image is more likely to represent the cross-section of a disk or flake than a needle-shaped particle, as a needle-shaped particle would have a low probability of being orientated with the long axis in the direction of the sectional plane.

When considering the selection of a weighting parameter, the size boundaries of the sample being measured play a significant role. If the fraction being measured was prepared with a physical separation such as screening, this is likely to affect the shape characteristics of the particles in the near-size regions. However, if the particles are first separated by screening, and then filtered virtually by selecting upper and lower ECD boundaries, the largest rounded particle images will have equivalent cross-sectional area to the largest elongated particle images. This is illustrated in Figure 4.28, which shows particles in a narrow ECD interval that have been classified by *roundness*. With particles filtered by ECD, the difference between weighting by number of particles, cross-sectional area, or volume (with the assumption $V = A^{3/2}$) would then only lie in the proportional contributions of particle images with larger cross-sectional area relative to images with smaller area. To test this, Figure 4.29 shows cumulative roundness frequency distributions weighted by particle count, image area and volume (using assumption $V = A^{3/2}$). Data obtained with the Mineralogic for the coarse size fraction (-212/+150 μm) are reported for this analysis.

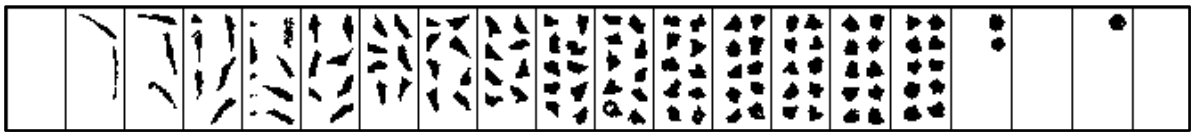

Figure 4.28: Image grid showing particle cross-sections from a narrow ECD interval (-10/+8 µm), classified by roundness.

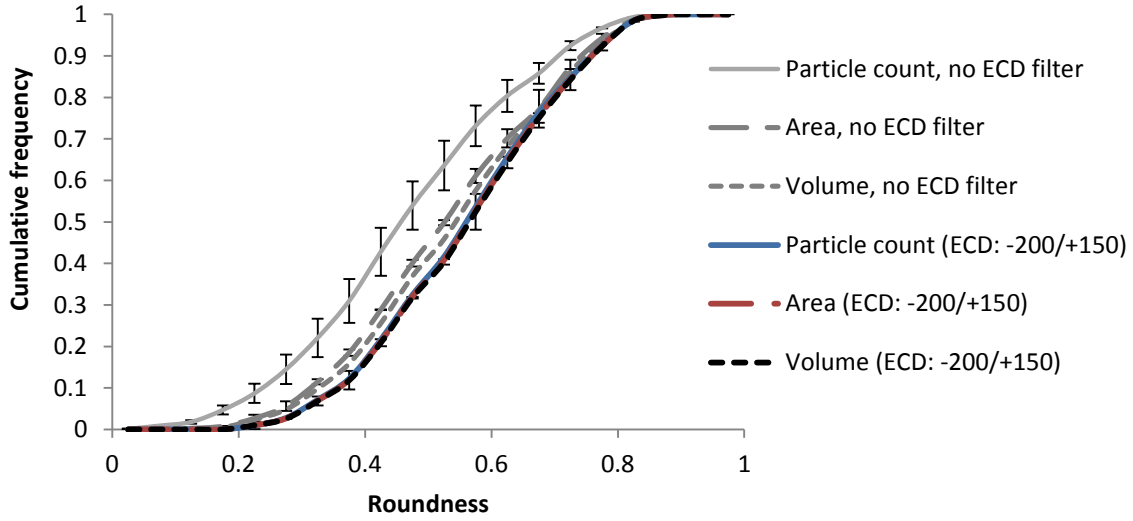

Figure 4.29: Comparison of Mineralogic roundness frequency distributions weighted by particle count, area and volume for a -212/+150 µm fraction with and without filtering by ECD.

The area-weighted distribution with no ECD filter is that which was presented in Paper 2 for comparison with QEMSCAN. With no ECD filter there are significant differences between the distributions weighted by particle count and area. With ECD filters at 150 and 200 µm, the particle count, area and volume distributions converge to the same line, which is much closer to the distribution reported for the QEMSCAN in Figure 4.17, Paper 2.

From this analysis, it is recommended that after separation into narrow fractions for Auto-SEM-EDS analysis, measurements for each fraction should be further virtually filtered by ECD or area, before determining particle shape distributions. This will reduce the influence of the separation method on the shape characteristics of the near size particles, and will also ensure that particles can be weighted by cross-sectional area without concern that this will favour particles of a particular shape. Weighting by area is considered preferable to weighting by particle count, because the finest particles in a sample will constitute a much larger proportion of the sample by number than by mass. This may be undesirable as it is the finer particles within a size fraction that are more likely to be impacted by effects of resolution. Weighting by area is also considered preferable to weighting by volume as it constitutes a direct 2-D measurement, which "has a higher, built-in statistical confidence" than data which have undergone stereological

transformation to 3-D (Ralph and Kurzydłowski, 1997: 219). However, with Auto-SEM-EDS data there is a fourth option to consider. With automated identification of minerals, it is possible to incorporate estimates of the density of each mineral phase measured, which can be multiplied by the areal proportion of each mineral phase in a sample to estimate mass proportion. This is done automatically by the iDiscover software. For ores in which the major mineral components have similar densities this would not affect measured roundness distributions significantly, nor would it have an effect on roundness distributions of single mineral components. However, the distribution of the -212/+150 μm feed sample measured in Paper 2 would be more skewed, i.e. have a higher modal roundness when weighted by mass than by area due to a higher weighting of the rounded chromite particles, which have a higher density than the silicates.

In Paper 1, distributions were weighted by particle count because that appeared to be the most common method used in the literature. For the analysis in Paper 2, distributions were weighted by particle count and area, but those based on area were selected for presentation. This was because particle count allocates a higher weighting to the fine particles in a sample fraction, which are considered more likely to be impacted by resolution. Weighting by mass was not an option for Paper 2 as the devices tested did not all incorporate mineralogy measurements. In the following chapters, which all rely on QEMSCAN analysis, distributions were weighted by mass. In Paper 3, weighting by mass was preferred because the analysis incorporated particle size, mineralogy, and particle shape (e.g. Figure 5.3), and size and mineralogy distributions are typically weighted by mass. In the fine grinding study in Paper 4, weighting by mass or area would produce very similar results because there were no significant differences between the shape characteristics of the major mineral components (Paper 1). In Paper 5 weighting by mass or area would have produced identical distributions because only a single mineral component was considered.

Chapter 5

PHASE BOUNDARY FRACTURE ANALYSIS

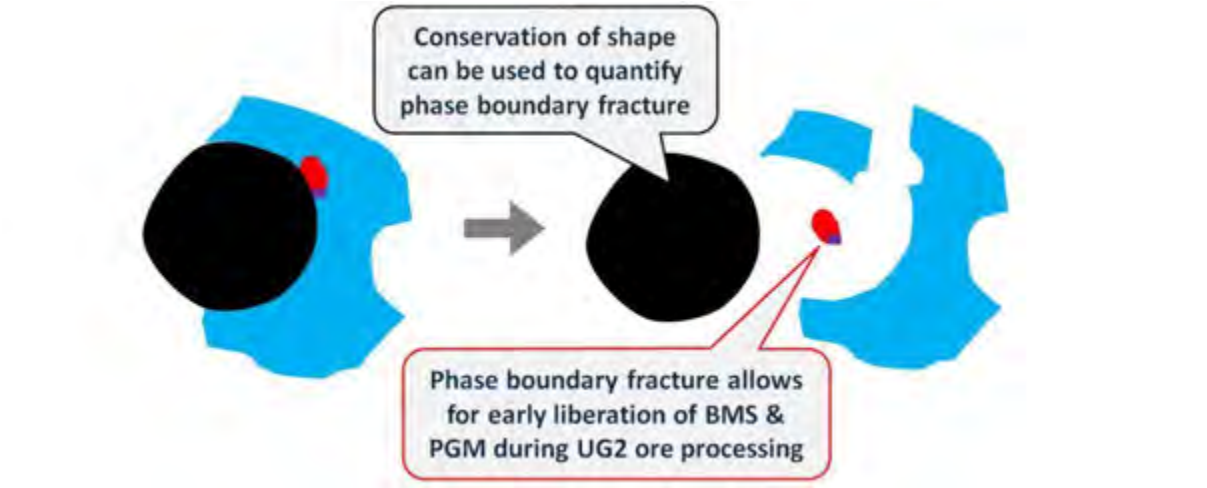

Graphical abstract for Paper 3, illustrating how phase boundary fracture between the major gangue minerals in UG2 ore leads to enhanced liberation of the platinum group minerals.

This chapter addresses the first part of the second objective of this thesis, demonstrating how the shape characterisation methodology can contribute towards the understanding of fracture mechanisms and the link between phase boundary fracture and liberation. Various methodologies for quantifying phase boundary fracture are explored, and a new methodology is proposed based on the conservation of grain shape.

The hypothesis addressed in this chapter is:

> During breakage of UG2 ore, phase boundary fracture between the chromite and silicates leads to enhanced liberation of the finely grained PGMs at a coarse size, because a significant portion of the PGMs occur along the weakly bonded chromite-silicate phase boundaries. The extent of this phenomenon can be inferred from the conservation of shape of the spherical chromite grains in conjunction with other techniques.

The work carried out to meet this objective and test this hypothesis is presented in Paper 3. The key-questions that drove this research were:

- **Given the fine grain size distribution of PGMs in UG2 ore, is the liberation of PGMs typically observed at UG2 processing plants consistent with theory of random uniform isotropic fragmentation?**
    - Can differences in particle shape in comminution products be related to the primary ore texture, and hence be linked to breakage along grain boundaries and liberation?
    - What descriptor or combination of descriptors will enable differentiation between the visibly liberated, spherical chromite grains and other particle types?
    - Can phase boundary fracture be quantified based on the conservation of chromite grain shape?
    - Are the findings from this method consistent with other methods for estimating phase boundary fracture?

To complement the conclusions drawn in Paper 3, the platinum concentrator samples taken for this thesis were analysed to determine PGM deportment and size-by-size recovery, which are presented and discussed in Section 5.8. These data support the conclusions drawn in Paper 3, which were partially based on an assessment of the literature.

Paper 3: Using mineralogical and particle shape analysis to investigate enhanced mineral liberation through phase boundary fracture

Little, L., Mainza, A. N., Becker, M., Wiese, J. 2016. Powder Technology. 301, 794-804.

Keywords: Phase boundary fracture, breakage mechanisms, liberation, UG2 ore

Abstract

In comminution, liberation has been recognised as a more important performance indicator than size reduction because the degree of liberation of valuable minerals dictates the theoretically achievable grade-recovery curve for downstream separation processes. The degree of liberation of a certain mineral within an ore, ground to a specific particle size distribution, will be dependent on the primary ore texture, the mineral grade and grain size distribution, and the degree and nature of phase boundary fracture, which can, allegedly, be linked to the breakage mechanisms employed within the comminution device. The occurrence of enhanced liberation through phase boundary fracture is desirable, and in recent years, studies have focused on whether or not certain comminution devices enhance this phenomenon. However, comparatively little attention has been paid to quantifying phase boundary fracture in typical minerals processing operations.

In this study, a novel approach to quantify phase boundary fracture is proposed that is based on the conservation of grain shape. The approach is demonstrated through a mineralogical analysis of UG2 ore sampled from the discharge of a primary ball mill. Phase boundary fracture was found to be the mechanism responsible for producing 50% PGM liberation at a grind of 40% passing 75 μm, rather than a grind of 50% passing 3 μm which would be required under theoretical random breakage assumptions.

5.1 Introduction

5.1.1 Introduction and Objectives

In minerals processing applications, the purpose of comminution is typically to liberate the valuable minerals in an ore so that they can be separated from the gangue minerals in subsequent separation processes such as flotation. However, the performance of a comminution circuit is typically modelled, designed or assessed based on product size distribution rather than liberation. Powell and Morrison (2007) describe the incorporation of liberation as the 'holy grail' of comminution modelling. King (1993), as quoted by Powell and Morrison (2007: 228), stated that "…significant advances in comminution technology will only come from the exploitation of basic fundamental understanding of the fracture process".

The ability to measure phase boundary fracture is critical to the development of understanding of how liberation changes during size reduction. Some progress has been made towards quantifying phase boundary fracture in fundamental research studies, typically incorporating different grinding devices. It is however a challenging task, and there have been no industrial case studies that convincingly demonstrate the significant impact that phase boundary fracture can have on liberation in a typical comminution circuit. The first objective of this study is to present a new approach for quantifying the occurrence of phase boundary fracture based on the conservation of grain shape. The technique is used here to determine the extent to which the rounded chromite grains in UG2 ore are liberated by detachment. This is then compared to the traditional approach based on conservation of phase specific interfacial area (PSIA). The second objective of the study is to demonstrate the key role of phase boundary fracture in the liberation of finely grained platinum group minerals (PGMs) during UG2 ore processing.

5.1.2 Breakage mechanisms and liberation

For discussion of fracture mechanisms, two broad terms are commonly used to describe fracture: *random* and *non-random*, although these vary depending on the underlying assumptions and the application. When using the population balance model, the term random is used to describe breakage in which particles from a single size class will be broken into a predictable unimodal distribution of finer particles. Liberation and mineralogy is not taken into consideration, so whether phase boundary fracture occurs or not does not necessarily influence the applicability of this modelling approach to a given ore type. However, when liberation is of interest, the definition of random breakage is extended to include liberation effects, and Barbery (1991) describes this as random uniform isotropic fragmentation (RUIF). Key assumptions are that interfacial area is conserved during breakage and that grade does not vary with particle size. Any breakage in which these criteria are not satisfied is then classified as non-random fracture. This is discussed in more detail in Section 5.3.1.

King and Schneider (1998) described several mechanisms of non-random fracture, including selective breakage, differential breakage, preferential breakage, phase boundary breakage, liberation by detachment and boundary region fracture. However, it is not typical to differentiate between all of these mechanisms; the first three mechanisms can be referred to as preferential breakage, and the latter three as phase boundary breakage. A phase boundary is defined as the interface between two different minerals within a multi-component ore. A schematic illustrating these fracture mechanisms, along with definitions related to how energy is imparted to a particle is provided in Table 5.1 (Frances et al., 2001; Gao and Forssberg, 1995; Kawatra, 2006; King, 2001, 1992; Pourghahramani, 2012; Radziszewski, 2013; Tavares, 2009; Varinot et al., 1997; Vizcarra, 2010).

Table 5.1: Definitions of breakage mechanisms - circles represent grinding media, shaded and not-shaded represent different mineral phases. A mineral grain is defined as a 3-dimensional entity consisting of only one mineral phase: particles consisting of one, two, or more grains are defined as liberated, binary and composite particles respectively.

Grinding action	**Other factors affecting outcome**	**Grinding outcome**
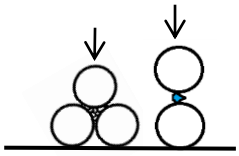 Compression	**Contact energy** (Repeated, low energy contacts vs single high energy contacts) **Ore characteristics** (Strength of independent mineral components and grain boundaries) 	 Inter-granular fracture Phase boundary fracture Grain-boundary fracture
Impact 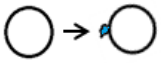		 Preferential fracture Selective breakage
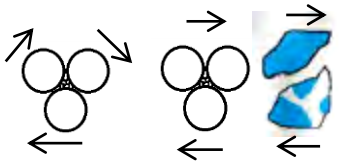 Shear		 Massive fracture Random fracture
		 Abrasion Attrition Chipping

In the late 1980s and early 1990s, various authors attempted to develop approaches for modelling and simulation of random and non-random fracture, and the subsequent liberation response (Barbery, 1991, 1987; King, 1994, 1992). However the majority of the work was theoretical, and mostly involved predicting the liberation response under random breakage assumptions, and then showing whether or not this matched experimental data. In recent years, the topic has received much less attention, which is surprising as there has been an increase in the use of Automated Scanning Electron Microscopy coupled with Energy Dispersive X-ray

Spectroscopy (Auto-SEM-EDS). This technology is widely used for analysis of liberation, providing valuable insight into minerals processing operations, but the liberation data produced is seldom being linked back to fracture mechanisms. Of the more recent work that has been done in the field, most studies have focused on whether or not grinding devices utilising compression breakage give enhanced liberation relative to traditional tumbling mills (Apling and Bwalya, 1997; Fandrich et al., 1997; Garcia et al., 2009; Solomon et al., 2011; Vizcarra et al., 2010; Xu et al., 2013). The conclusions of these studies, based on comparison of liberation, are not always in agreement. From a statistical analysis of Auto-SEM-EDS liberation data, Vizcarra (2010) suggested that most of the differences reported in literature may not be statistically significant at a high confidence level. Qualitative research has also been carried out into phase boundary fracture during electric pulse breakage (SELF-RAG) and microwave pre-treatment (Cabri et al., 2008; Charikinya, 2015; Dal Martello et al., 2012; Omran et al., 2015; Song et al., 2013).

The occurrence of phase boundary fracture and the implications for liberation will vary from ore to ore, so findings relating to phase boundary fracture will not usually be generalizable between studies considering different ore types and different grinding devices. The main approach that has been used to quantify phase boundary fracture to date has been the measurement of PSIA before and after breakage (Charikinya, 2015; Fandrich et al., 1997; Garcia et al., 2009; King, 1992; Vizcarra, 2010; Xu et al., 2013). A decrease in PSIA during breakage indicates the occurrence of phase boundary fracture. With 3-D data from micro X-CT, this technique has great potential for research in this area (Garcia et al., 2009; Xu et al., 2013). However, when based on 2-D data from the more widely used Auto-SEM-EDS devices; it relies on a number of assumptions, stereological correction procedures and correction factors, which result in an indirect measurement. After developing and demonstrating this technique, King (1992) observed that other, more direct measurements of phase boundary fracture would be required to supplement this approach.

5.1.3 UG2 ore mineralogy and processing

The UG2 ore is a multi-component platinum group element (PGE) ore from the Bushveld Complex in South Africa, contributing an estimated 40% to global PGE resources (Mudd, 2012). Typically, the UG2 chromitite layer consists of rounded chromite grains in a primary silicate matrix of pyroxene and plagioclase, with small amounts of secondary silicates such as talc and chlorite. Chromite content in the mined ore varies between 50 and 90 wt. %, and PGE grades are generally in the range of 3 – 6 g/t. Base metal sulfide (BMS) grades vary between 0.03 and 0.2 wt. % (Becker et al., 2013, 2008; Chetty et al., 2009; Hay and Roy, 2010; Leroy et al., 2011; McFadzean et al., 2015; Mudd, 2012; Nel et al., 2004; Penberthy, 2001; Solomon et al., 2011).

The bulk mineralogy of an ore sample from the southern portion of the Western Limb of the Bushveld complex is shown in Table 5.2.

Table 5.2: Bulk Mineralogy of the UG2 ore sample investigated.

Mineral	**Mass %**
Base metal sulfides	0.2
Olivine	1.8
Orthopyroxene	15.7
Clinopyroxene	1.2
Amphibole	1.2
Chlorite	1.6
Serpentine	0.3
Talc	0.4
Mica	0.4
Plagioclase	16. 6
Chromite	60.0
Other	0.6

The chromitite layer is friable due to the loosely cemented nature of the chromite within the silicate matrix. The occurrence of breakage along the chromite-silicate phase boundaries has been inferred qualitatively through observations of liberated, rounded chromite grains (Leroy et al., 2011; Penberthy, 2001). The PGMs are finely grained, with a median grain size (by mass) in the region of 6.5 μm (Chetty et al., 2009; Penberthy, 2001; Solomon et al., 2011). In comparison, the median chromite grain size is much coarser, in the region of 160 μm (Penberthy, 2001). There is typically a high degree of association between PGMs and BMS, and both PGM and BMS grains commonly occur along chromite silicate grain boundaries (Penberthy, 2001). This is illustrated in Figure 5.1, which shows rounded chromite grains in a silicate matrix, with a composite BMS grain associated with a PGM occurring on a chromite-silicate phase boundary. There is significant variation within the ore that is not captured by this simple description – for example there are regions where there is little to no association of PGMs with BMS, and regions where annealing of chromite grains has led to the formation of much coarser super-grains.

UG2 ore processing circuits typically incorporate staged grinding and flotation (Becker et al., 2008; Hay and Roy, 2010; Rule, 2010). After the relatively coarse primary grind (typically in a ball mill circuit), the primary rougher concentrates constitute the majority of the PGE recovery (~70%). The following main stream grinding stages, which may incorporate stirred mills, target

PGMs that remain locked in silicates after the primary grind, and account for an additional 10 - 20% recovery. Stirred mills are also used for regrinding concentrates to improve final concentrate grades (Chetty et al., 2009; Hay and Roy, 2010; Nel et al., 2004; Rule, 2010).

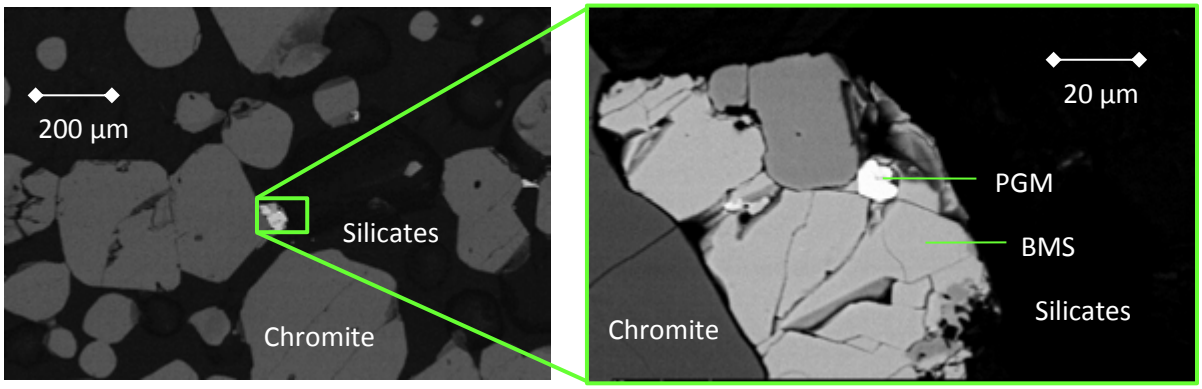

Figure 5.1: Back scattered electron images of UG2 illustrating the texture of the ore (Becker, unpublished).

5.2 Materials and Methods

The test work carried out involved preparation and analysis of a UG2 ore sample using quantitative evaluation of minerals by scanning electron microscopy (QEMSCAN). The ore was sampled from the primary ball mill discharge of a concentrator on the Western Limb of the Bushveld Complex. Ore preparation involved blending and representative splitting down to 200 g aliquots using a rotary splitter. A 200 g sample was then split into five size fractions using a combination of wet and dry screening. The mass retained in each size fraction was then further split, using a small rotary splitter and a micro-riffler, into 4 g aliquots which were mounted in resin. The resulting blocks were then cut into vertical sections; each of which was reset to form a new block which was then polished and carbon-coated for QEMSCAN analysis on an FEI QEMSCAN 650F. The reason for preparing the blocks as vertical sections was to prevent bias caused by settling of the dense chromite particles within the ore relative to the silicates. Fire assays, followed by inductively coupled plasma-optical emission spectroscopy, were also performed for QEMSCAN data validation.

The QEMSCAN analyses performed included bulk mineral analysis, particle mineral analysis and a trace mineral search for base metal sulfides (BMS). Categorisers and filters (formulated with the iDiscover™ software), were then used to extract the information of interest relating to shape, grain size, liberation, PSIA, and association data for each fraction. In combining the data from the different fractions, distributions for each fraction were normalized, and then weighted based on particle size distribution (PSD), chromite deportment or BMS deportment accordingly.

The QEMSCAN data obtained allowed for investigation of the breakage and liberation response of the chromite and BMS phases, however the PGM data examined was taken from a detailed review of the literature. The work considered in the review included data from some major UG2 concentrators, as well as that from pilot scale and laboratory scale test work (Becker et al., 2008; Chetty et al., 2009; Nel et al., 2004; Penberthy, 2001; Rule and Schouwstra, 2011; Solomon et al., 2010). The datasets that are considered most robust are those of Penberthy (2001) from a laboratory based PhD study on UG2 ore, and Chetty et al. (2009) from a concentrator survey. In each of these studies, over 4000 PGM grains were analysed using Auto-SEM-EDS, whereas in most of the other studies only 100 PGM grains were analysed or some details were not presented. Factors deemed of key interest for this paper were the PGM grain size distributions reported, and the degree of PGM liberation at the particle size distributions investigated.

5.3 Theory

5.3.1 Random uniform isotropic fragmentation and phase boundary fracture

Random uniform isotropic fragmentation (RUIF) was a term coined by Barbery (1991), to describe what was previously referred to as pure trans-granular breakage, random breakage, or interfacial area conservation (IAC). Modelling of this type of breakage enables comparison of real fragmentation to the limiting case, as any degree of phase boundary fracture will lead to greater liberation than that predicted under RUIF assumptions. Barbery observed that identifying regularities in the differences between observed fragmentation and simulated RUIF would be useful for process assessment, modelling and simulation. One of the key theoretical observations for RUIF is that phase specific interfacial area (PSIA) is always conserved, which has been the topic of many papers, but has been traced back to Gaudin (1939). This led to the development of the technique of quantifying phase boundary fracture through measurement of PSIA. Apart from PSIA, other properties that should theoretically be conserved during RUIF include mineral content within a given size fraction, and the percentage of mineral exposed on particle surfaces (Laslett et al., 1990). Variation in deportment of certain minerals to different size fractions can therefore also provide a good indication of whether non-random breakage is occurring, although this does not independently show whether this is due to preferential breakage or phase boundary fracture.

Auto-SEM-EDS systems such as the QEMSCAN have algorithms built into the software to measure phase specific surface area (PSSA) and mineral associations. These two functions can be used in conjunction to estimate PSIA. The PSSA measurement is not based on perimeter to area ratio, but rather the mean intercept length measurement and geometric relationships that correct for stereology (Sutherland, 2007). In this way, error related to image resolution is

avoided, but the geometric relationships used depend on assumptions such as that grain shape does not change with size, which means that the measurement is still an indirect estimate of the true quantity.

5.3.2 Shape characterisation

In a previous study, Little et al. (2015, Paper 1) investigated various shape descriptors for analysis of shape using Auto-SEM-EDS. The descriptor, *roundness* (presented in Equation 5.1), was found to be a more robust descriptor than the commonly used c*ircularity,* which is dependent on image resolution. A method for characterising shape using roundness and *aspect ratio* in conjunction was developed, and this was the approach used in this study for the initial shape characterisation of different particle types. However for the majority of the analyses, a *roundness* value of 0.7 was deemed appropriate for differentiating between the shape of the rounded chromite grains (*roundness* > 0.7) and all other particle shapes (*roundness* < 0.7).

$$Roundness = 4 \cdot Area/(\pi \cdot {Fe_{max}}^2) \quad 5.1$$

*Fe_{max} is the maximum Feret diameter, or the long axis of the particle.

5.3.3 Quantifying liberation

Liberation is a measure of the percentage of a certain mineral within a particle, and is typically presented as a composition distribution, showing proportions of particles with a range of compositions (Fandrich et al., 2007; King and Schneider, 1998; Laslett et al., 1990; Vizcarra et al., 2010). However, in many cases a combination of variables is thought to best describe the liberation characteristics of a desired mineral. For example, in the case of PGMs, common categorical variables include: liberated PGMs, PGM associated with BMS, PGM enclosed within silicate or oxide gangue, or PGM attached to silicate or oxide gangue particles (Chetty et al., 2009; Nel et al., 2004; Penberthy, 2001; Rule and Schouwstra, 2011). This approach was used in the majority of the work reviewed relating to PGM liberation.

Liberation is most commonly analysed using Auto-SEM-EDS, with which thousands of 2-D cross-sectional images of particles are obtained and the associated EDS information and accompanying software allows for detailed mineralogical analysis of the particles within the sample. As these images are 2-D, liberation measurements derived from them are typically reported as area percent rather than volume percent, which initially led to considerable investigations into the requirement for stereological corrections (Spencer and Sutherland, 2000). Lätti and Adair (2001) showed that analysis of a sufficient number of random particle cross-sections (from a large number of randomly orientated particles), was effectively

equivalent to taking multiple cross-sections of a few particles and integrating over the volume of those particles, effectively limiting the stereological bias of area based analysis of mineral abundance. Mineral liberation is still affected by stereological bias, particularly with simple textures leading to 2-D measurements presenting higher liberation than is observed in 3-D.

Particle and grain size distributions, based on equivalent circle diameter of 2-D cross-sections, will give an underestimate of size relative to other sizing techniques such as screening, because many grains will not be sliced through their maximum dimension along the z axis. In early work, mean intercept length was typically used for quantifying texture because it eliminates stereological bias (Sutherland, 2007). The disadvantage of this measure is that it gives no indication of the spread of a grain size distribution. The equivalent sphere diameter (ESD) incorporated in the QEMSCAN software, iDiscover, is based on the mean intercept length and incorporates stereological corrections, but it gives a very similar grain size distribution to that obtained using equivalent circle diameter (ECD), calculated based on grain cross-sectional area. ECD is therefore thought to provide a reliable, transparent measure of size, provided that the fact that it underestimates particle size relative to other 3-D sizing techniques is acknowledged.

5.4 Results and Discussion

5.4.1 Characterisation of gangue in UG2 ore sample

The intention of this section is to describe the bulk of the particles which make up the ore sample. 99.8% of the ore sample is gangue minerals (Table 5.2), so the nature and behaviour of the ore in minerals processing operations is likely to be highly dependent on the character and behaviour of the gangue particles.

The roundness - *aspect ratio* frequency distributions in Figure 5.2 provide an indication of the shape characteristics of chromite-silicate composites, liberated chromite, and silicates. This methodology for shape characterisation is described in more detail by Little et al. (2015, Paper 1). There is a clear difference in roundness between the liberated chromite and other particle categories, with the former having a peak above 0.7. It was therefore deemed appropriate to simplify the shape characterisation for the remainder of the study by classifying all particles into two categories: ‘round’ (roundness ≥ 0.7) and ‘not round’ (roundness < 0.7). Note that the descriptor *aspect ratio* (considering the distribution from the x-direction only) does not show as distinct a difference as roundness, due to the presence of equant non-rounded particles in all particle categories.

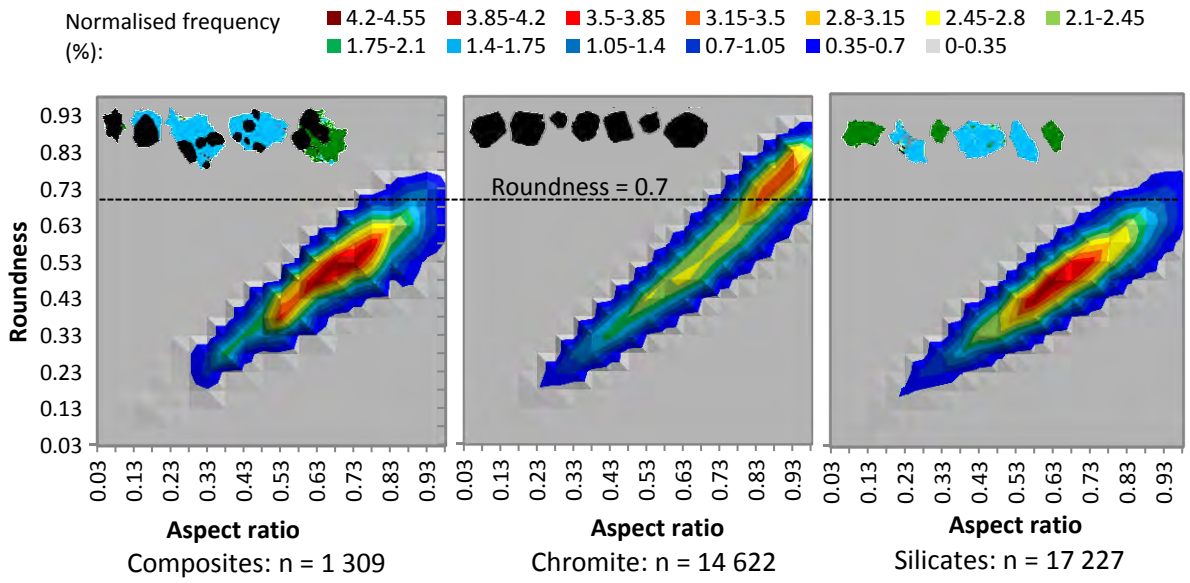

Figure 5.2: Roundness - aspect ratio frequency distributions showing the difference in shape characteristics between particle types. n = number of particles analysed.

Sized fractions of the ore sample were categorised based on both mineral composition and roundness, and the mass frequency distribution of particles within each category was plotted in Figure 5.3 to give a general description of the sample's gangue mineralogy.

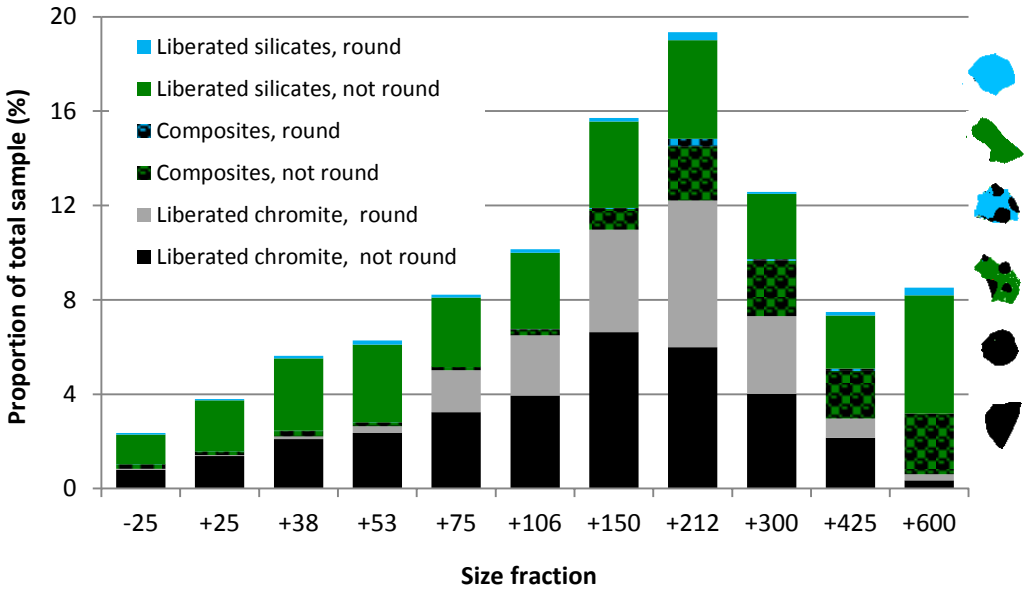

Figure 5.3: Particle distribution (by mass) - incorporating particle size, shape and mineralogy. Liberated silicates: <10% chromite; Composites: 10 - 90% chromite; Liberated chromite: >90% chromite (by area). Round: Roundness > 0.7; not round: Roundness < 0.7.

Figure 5.3 indicates that the sample PSD follows the chromite grain size distribution closely. It also shows that in the fractions above 75 µm, a large portion of the liberated chromite grains are rounded, while in the finer size fractions the chromite is mostly angular. The composite and silicate particles in all size classes are mostly angular.

5.4.2 Assessment of phase boundary fracture of a major phase (chromite)

In this section, the liberation of chromite by phase boundary fracture is assessed by a variety of approaches including; a simple qualitative illustration, the conservation of shape approach developed in this study, and other methods reported in the literature.

The qualitative approach

The Auto-SEM-EDS false-colour images and the SEM BSE images of coarse UG2 particles in Figure 5.4, qualitatively illustrate the occurrence of fracture along the phase boundaries between chromite grains and the silicate matrix. This is not a new observation, Leroy et al. (2011) correlated chromite shape with chromite liberation for an online image-analysis system, recognising that particles with rough edges were more likely to be composites than smooth particles. Penberthy (2001) was also aware of this phenomenon. Qualitative assessments based on particle images have been used to make valuable contributions and these play an important role in the understanding of fracture mechanisms (Cabri et al., 2008; Omran et al., 2015; Song et al., 2013). Disadvantages of qualitative work are that it may be subjective, and observations are difficult to translate into parameters to be used for the development of models.

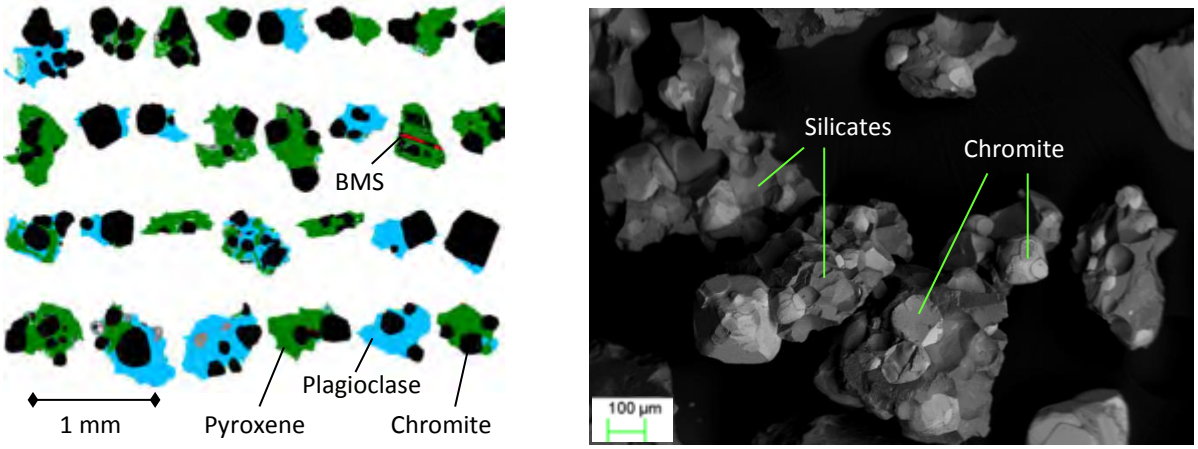

Figure 5.4: Coarse composite particles of UG2 ore. Left: QEMSCAN false colour images of polished sections; Right: SEM BSE images showing 3-D appearance (FEI Nova Nano SEM).

The conservation-of-shape approach

This approach is a simple, direct, quantitative method for assessing phase boundary fracture, developed based on the observations highlighted in Section 5.4.1. It is based on knowledge of

the ore texture, and mineral specific shape characterisation of liberated and locked grains in the comminuted sample, which is enabled by Auto-SEM-EDS. For this example, QEMSCAN analysis of the UG2 ore primary mill discharge sample was used in conjunction with the FEI software, iDiscover™.

Firstly, the proportion of chromite grains in coarse composites that are rounded was determined using a filter that selected composites, followed by a granulator filter and a roundness categoriser. This was found to be 72% (by mass). The proportion of liberated chromite particles that are rounded was similarly calculated, and found to be 41%. After grinding below 75 microns, i.e. below the chromite grain size P20, the proportion of rounded grains in the sample is negligible (<3%). Furthermore, if other particle types are considered, the proportion of rounded particles or grains is similarly low. The assumption is therefore made that the predominant mechanism for production of rounded particles is through phase boundary fracture or detachment of rounded grains.

The proportion of chromite grains produced through phase boundary fracture is therefore at least 41%. However, this does not account for the 28% of the chromite grains in the initial matrix that are not rounded initially. Taking this into account, the proportion of rounded grains liberated by phase boundary fracture is 57% (57% x 72 = 41%). Assuming that a similar proportion of the chromite grains that are not rounded to start with are also liberated by complete phase boundary fracture, the estimate of 57% will hold for the entire sample. This is a quantitative measure of phase boundary fracture, which is illustrated in Table 5.3.

Table 5.3: Conservation of shape approach to quantify phase boundary fracture.

Category	***Roundness* > 0.7**	***Roundness* < 0.7**
Chromite grains locked in composites (*roundness* of the chromite grains, not the host particles) n > 1000	**72 wt.%** 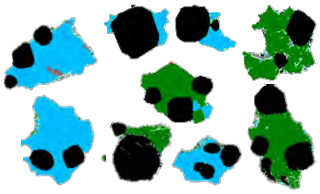	**28 wt.%** 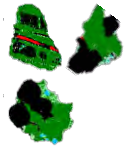
Liberated chromite grains in size range of chromite GSD (-1000 µm /+75 µm) n > 15 000	**41 wt.%** 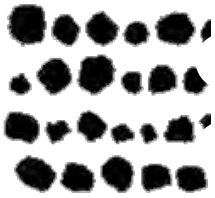	**59 wt.%** 
Liberated chromite grains below chromite GSD (-75 µm) n > 15 000	**~3 wt.%** 	**~97 wt.%** 
Other particle types n > 15 000	**~3 wt.%** 	**~97 wt.%** 

This approach to quantify phase boundary fracture will now be compared to previous approaches reported in the literature such as comparison to random fracture and the conservation of PSIA approach.

The comparison-to-random-fracture approach

There have been numerous models proposed for predicting liberation under assumptions of random fracture, but that described by Gay (2004) was deemed most appropriate for this study. Gay's model applied to a similar ore texture, as shown in Figure 5.5, which made a direct comparison possible. The change in liberation of the spherical phase with size, as modelled by Gay, was directly compared to the chromite liberation observed for the UG2 ore sample in Figure 5.6. In both cases the 'particle size' was divided by the median grain size to provide a normalised 'relative size' for comparison.

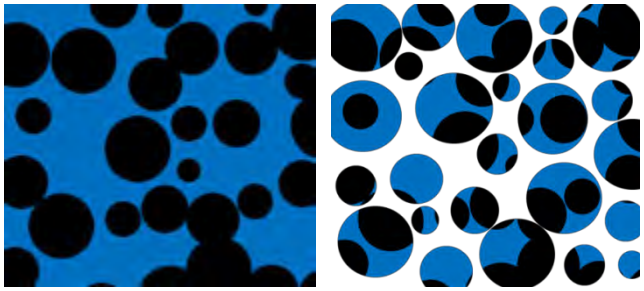

Figure 5.5: Illustration of the method used by Gay (2004) to predict liberation for an ore with a Boolean texture under random breakage assumptions.

Gay's random breakage model predicts only 14% liberation for the mineral occurring as spherical grains (i.e. chromite) at a particle size distribution close to the mineral grain size distribution (relative size = 1). On the other hand, for the UG2 ore sample investigated (all fractions combined), the portion of liberated chromite is 52.6 wt.%, with a median particle size (200 µm), close to the median chromite grain size (170 µm). This accounts for over 90 wt.% of the chromite in the sample. It is therefore evident that the degree of liberation of chromite for the UG2 sample is much higher than that predicted under random breakage assumptions, indicating a high degree of phase boundary fracture. The difference between the observed and predicted values could be used as a relative measure of the degree of phase boundary fracture for comparison across samples – perhaps to be calibrated using the conservation of shape approach.

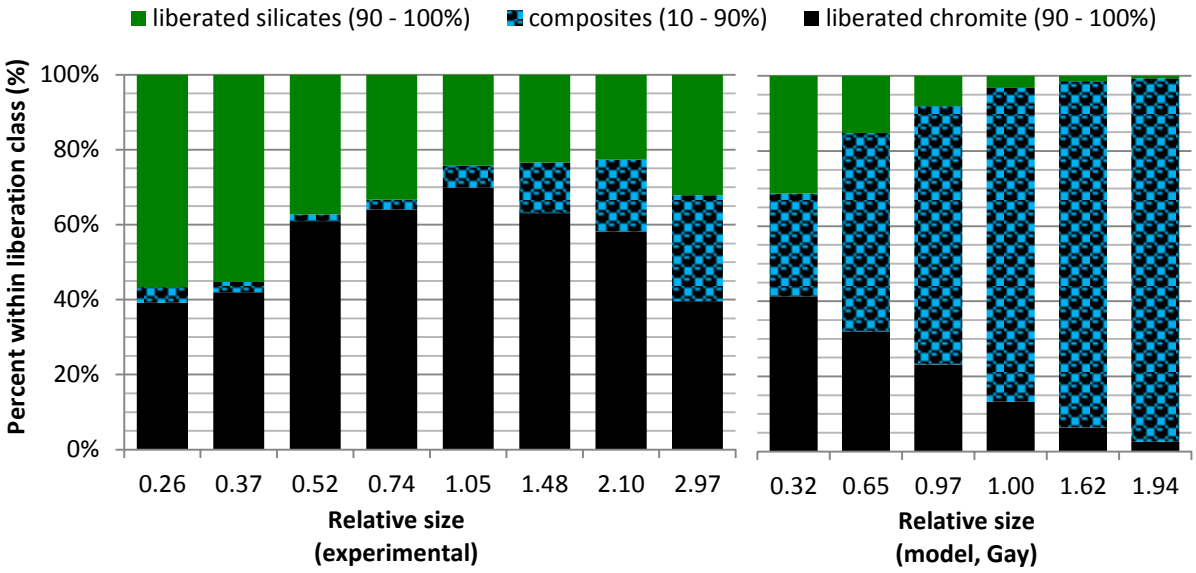

Figure 5.6: The liberation characteristics of the milled UG2 ore sample, as compared to liberation characteristics predicted by the random breakage model developed by Gay (2004).

The conservation-of-PSIA approach

This is the technique that has been used most widely for quantifying phase boundary fracture. Although it is a relative technique, it has wider applicability than the conservation of shape approach, and it is therefore proposed that the two methods be used in conjunction.

Before blasting, the phase specific interfacial area (PSIA) of the in-situ chromite is equivalent to the phase specific surface area (PSSA), assuming that the pore space along chromite phase boundaries is negligible. The PSIA before breakage can therefore be calculated from an estimate of the chromite grain size distribution. Figure 5.7 shows estimates of the chromite grain size distribution (as measured for the milled UG2 ore sample analysed) based on ECD measurements of different categories of chromite grains. All four distributions are probably underestimates of the 3-D distributions, both due to stereological limitations, and the fact that they are based on a sample that has been ground to some extent so any chromite super-grains (formed through post crystallization annealing) will have been broken. However, the distributions obtained for 'only rounded chromite grains' and 'all chromite grains' (median diameter of 170 µm), are in close agreement with chromite grain size distributions reported by Penberthy (median diameters of 160 - 174 µm) for various crushed ore samples, and these were therefore deemed appropriate to estimate the PSIA of chromite in the unbroken feed. The category 'only chromite within composites' has a finer grain size distribution, as most of the coarse chromite grains are fully liberated.

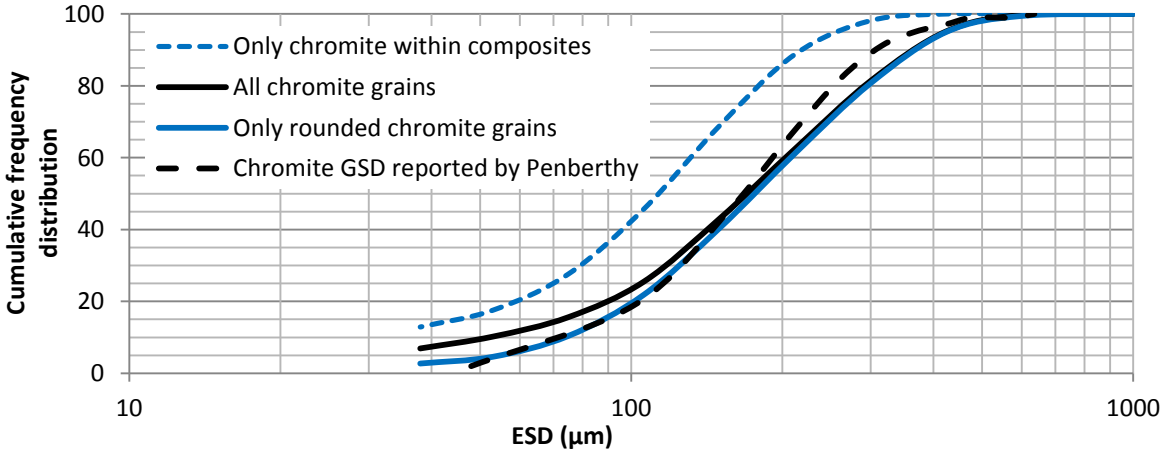

Figure 5.7: Chromite grain size distributions – considering all grains, only rounded chromite grains, and only grains locked within composites.

With an estimate for the grain size distribution, it is possible to calculate the PSSA for chromite and thus PSIA of chromite in the unbroken feed based on the relationship for spheres: PSSA = 6/D where D is the grain size. This was done, and was found to be comparable to the QEMSCAN 'stereologically correct' PSSA measurement, as well as PSSA calculated from QEMSCAN

perimeter and area measurements (Figure 5.8). The PSSA of chromite in composites is higher than this, which corresponds to the finer grain size distribution, as shown in Figure 5.7. The PSIA of the milled ore sample was estimated as the proportion of chromite grain boundaries associated with other minerals as opposed to background, multiplied by the QEMSCAN PSSA estimate. The PSIA distribution obtained is remarkably similar to that reported by Fandrich et al. (1997) for hematite/magnetite in an iron ore.

In terms of evidence of phase boundary fracture, the bulk of the chromite in the milled sample has a PSIA less than 0.01 μm^{-1}, which is significantly lower than the estimated PSIA for these chromite grains in-situ (0.045 μm^{-1}), based on the chromite grain size distribution. The weighted average PSIA for chromite for the entire sample after grinding was calculated to be 0.0064 μm^{-1}. These estimates indicate that the PSIA decreases by 85%, which implies that 85% of the chromite-silicate phase boundaries are broken apart during blasting, crushing and grinding. This seems greater than the estimate based on conservation of shape, but it is plausible that 85% of chromite-silicate phase boundaries are broken, with only 57% of the liberated chromite grains having been produced by complete phase boundary fracture or liberation by detachment.

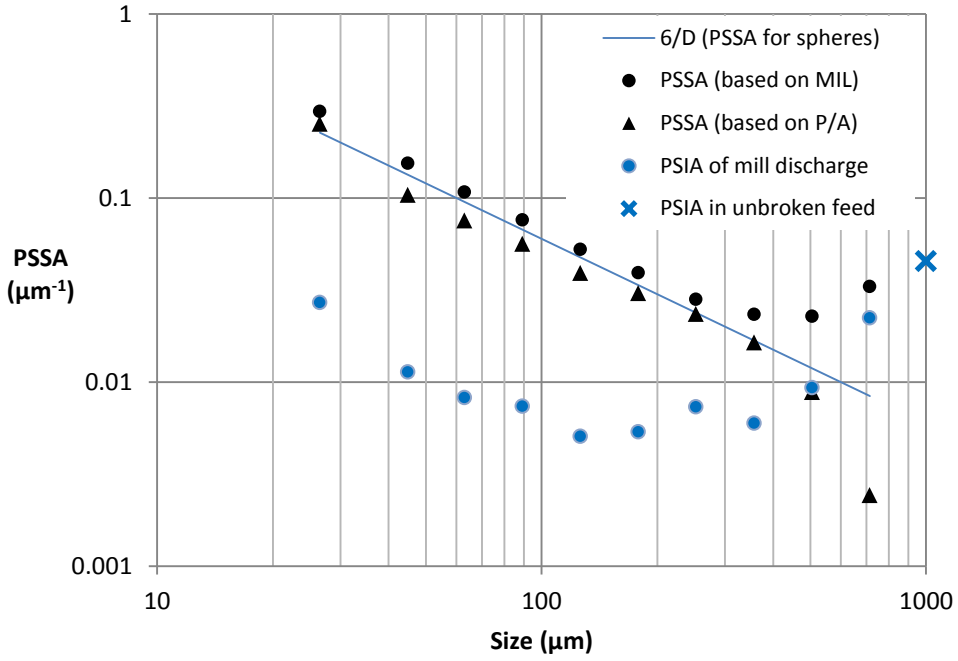

Figure 5.8: PSSA of chromite based on different methods - used to estimate PSIA of chromite in-situ (before blasting or grinding) for comparison with the measured PSIA of the milled ore. MIL: Mean Intercept Length; P/A: Perimeter/Area.

5.4.3 Phase boundary fracture: Implications for liberation of a minor phase (BMS)

The grain size distributions of chromite and BMS along with the PSD of the ore sample analysed are provided in Figure 5.9. The deportment of these minerals to different size fractions, and their liberation characteristics are shown in Figure 5.10. The BMS are mostly concentrated in the -75 µm fraction, and are over 50% liberated, in spite of the fine BMS grain size relative to the coarse grind. This is an indication of liberation by detachment, perhaps caused by chromite-silicate phase boundary fracture. Considering fine BMS grains in coarse particles, only 6% are completely enclosed in gangue, while the majority are exposed to the surface. This is another indication of phase boundary fracture leading to enhanced liberation, which is relevant for flotation and PGM recovery because of the high association of PGMs with BMS. In flotation, a small amount of exposed surface area can lead to sufficient hydrophobicity for recovery.

For a low grade mineral i.e. BMS or PGM, with grain size an order of magnitude lower than particle size, random breakage assumptions would predict much lower than 14% of the mineral to be fully liberated (Barbery, 1991). However, in this study 53% of BMS was fully liberated (Figure 5.10), and PGM processing plants are able to achieve over 70% recovery in the primary roughers after a grind of only 40% passing 75 µm (Chetty et al., 2009). This is an indication that phase boundary fracture does not only have a significant effect on the liberation properties of the major phases i.e. chromite, but also on the finely grained valuable minerals.

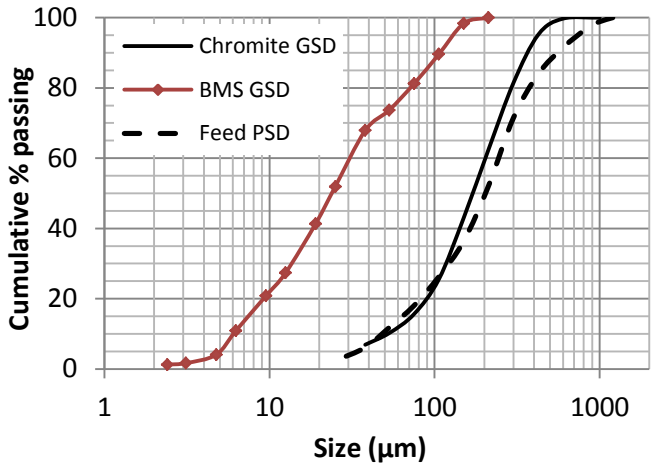

Figure 5.9: PSD of the feed sample; and BMS and Chromite ECD grain size distributions as measured by QEMSCAN.

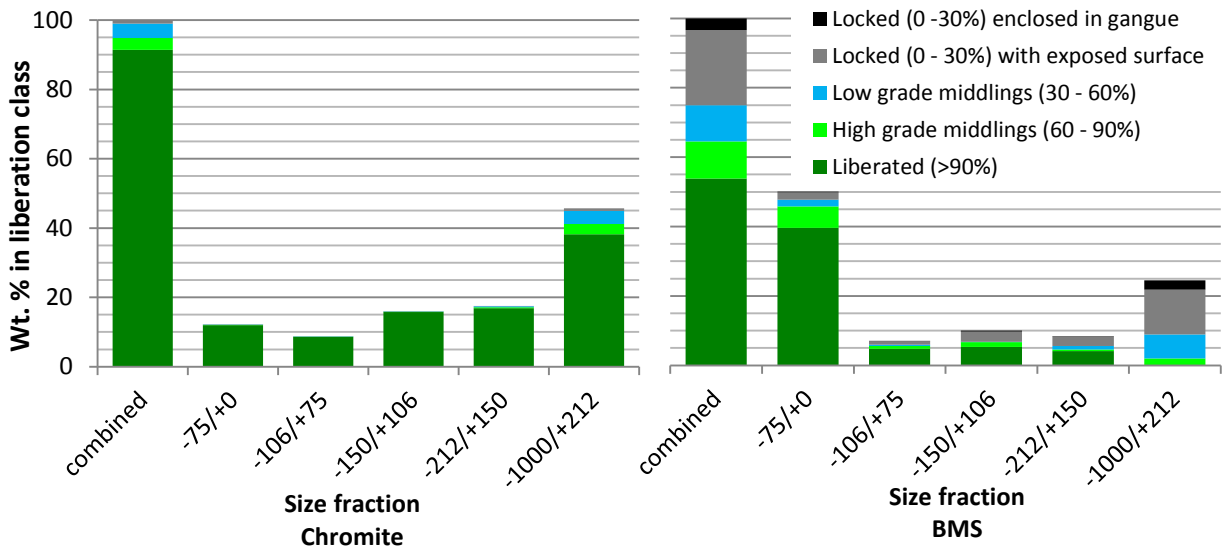

Figure 5.10: Comparison of the deportment and liberation distributions of chromite and BMS. 90% of the chromite is liberated, relative to 56% of the BMS.

The PSIA profiles of both chromite and BMS are provided in Figure 5.11. The PSIA of the BMS is an order of magnitude higher than that of the chromite, which is expected due to the finer grain sizes. Furthermore, the reduction in PSIA of the BMS with decreasing size is similar to that of the chromite, which indicates that the effect of phase boundary fracture on BMS liberation is highly significant. In Section 5.4.1, a reduction in PSIA of 85% was estimated for chromite. Similarly, the weighted average PSIA for BMS after grinding was estimated to be 0.13, indicating a 68% reduction in PSIA for BMS – a substantial amount of phase boundary fracture.

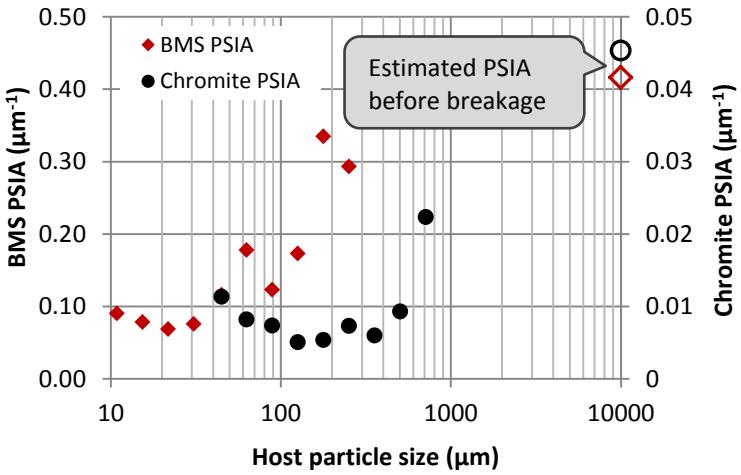

Figure 5.11: PSIA of BMS (as compared to chromite). The PSIA of the BMS is an order of magnitude greater than that of the chromite, as the grains are approximately an order of magnitude finer.

5.4.4 Phase boundary fracture: Implications for liberation of a trace phase (PGM)

The breakage and liberation of a major phase (chromite), and minor phase (BMS) have now been assessed using conservation of shape, comparison to random breakage, and estimates of PSIA. For the assessment of liberation of a trace phase, data obtained from a literature survey was used, so the only applicable method was comparison to random breakage. For this, an estimate of the PGM grain size distribution is required, as well as measurements of liberation at a specific particle size distribution. Various theses, papers and reports were reviewed and the relevant information is summarised in Table 5.4. The PGM grain size distribution reported by Penberthy (2001) for a coarsely crushed UG2 sample is presented in Figure 5.12, along with the particle size distribution from this work as a relative comparison.

The main findings from this review are that the PGM grain size distribution is typically very fine, and that significant PGM liberation is achieved at a grind much coarser than the PGM grain size. The industry is already aware of the early liberation of PGMs, and has taken advantage of it to some extent through concentrator flow-sheets incorporating staged grinding and flotation, and incorporating natural fines circuits (Nel et al., 2004). However, little attention has been paid to understanding the extent to which phase boundary fracture is responsible for this phenomenon, which in this case is investigated through comparison to random uniform isotropic fragmentation (RUIF).

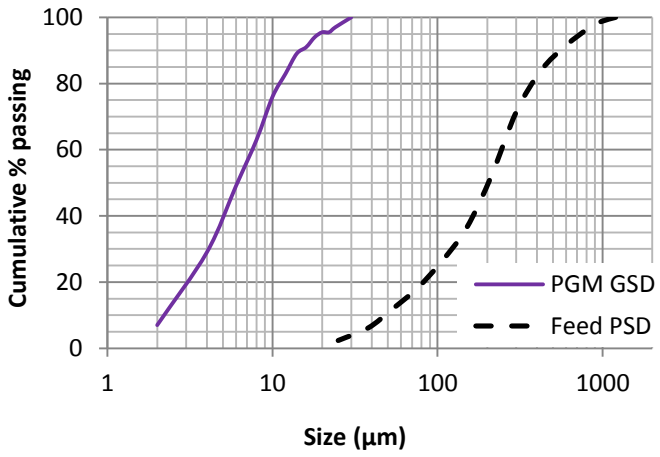

Figure 5.12: PSD of the feed sample in this study measured by screening, and PGM ECD grain size distribution as reported by Penberthy (2001).

Table 5.4: PGM grain size distributions, and associated liberation data for UG2 ore, ground in a variety of devices to different product size distributions.

Paper	Ore prep.	No. of PGM grains analysed	PGM grain size ECD (area %/µm)	Grind (µm)	% liberated PGMs (area)	% PGMs assoc. with liberated BMS	% PGMs attached to silicates	% Recovery (flotation)
Penberthy (2001) pp. 113 – 115 Average of 14 samples from Western Limb (Marikana – Brits area)	Lab. crushed	4392	95% <25 80% <12.4 **50% < 6.3** 20% < 3.2	100% < 2000 **10% < 75**	40 – 70*			-
	Lab. rod mill	2636	100% <18 80% < 9 **50% <4.8** 20% <2.6	98% <106 **78% < 75** 45% < 38	60	18	7	90
Chetty et al. (2009) Primary rougher circuit, Western Limb Concentrator	Primary mill	4513	95% <25 78% <12 **50% < 8**	**40% < 75**	50	10	25	70
Nel et al. (2004) Impala Platinum, plant data, primary high grade rougher	Primary mill (AG)	-	**~50% < 10**	100% < 600 **30% < 75**	~30**	~40**	-	52
Rule & Schouwstra (2011), Rule (2010) Anglo Platinum, Amandelbult UG2 plant data	Monthly composite plant data – feed	-	100 < 19 80% < 12 50% < 8 20% < 4.2	-	49.2	32	6.2	-
Becker et al. (2008) Pilot-scale classification study	Ball mill with 3-product cyclone circuit	100	-	90% < 90 14% < 11	34	25	14	~88
	Pilot ball mill with conventional cyclone	100	-	80% < 90 14% < 11	21	13	20	~82
Solomon et al. (2010, 2011) Lonmin ore	HPGR 1.5mm operating gap	100	-	90% < 400 **42% < 75** 30% < 38	~45	~20	-	~60
	Ball mill	100	-	90% < 200 **35% < 75** 20% < 38	~45	~30	-	~70

* Liberated PGM and PGM at grain boundaries - variation between samples
** PGM mode of occurrence described as: 5% coarse PGM, 40% PGM associated with base metal and iron sulfides, 30% PGM occurring on host mineral grain boundaries, 25% PGM locked in silicates

As was discussed in Section 5.3.1, Barbery (1991) calculated theoretical liberation profiles under RUIF. He showed that the degree of liberation of a sparse phase (present in grains described by Poisson polyhedral with a Boolean texture) only becomes significant at a particle size of similar dimensions to the mean grain size of that phase. For instance, for liberation measured in two dimensions (as done in Auto-SEM EDS), 50% liberation is only attained at a

particle size less than one third of that of the texture scale/grain size. Based on the median PGM grain size of 8 μm reported by Chetty et al. (2009), the median particle size required to produce 50% liberation, predicted under the assumption of random uniform isotropic fragmentation, would be less than 3 μm. With the high costs associated with fine grinding, if a product size of 3 μm was required to liberate the PGMs, such operations would not be economically feasible. However, in the same study, Chetty et al. (2009) reported 50% of the PGM was liberated for a particle size distribution with only 40% passing 75 μm. Selective breakage (as defined in Table 5.1) does not explain this phenomenon, as the PGM grain size is much finer than the product size, and does not change much during grinding (Penberthy, 2001). Phase boundary fracture and liberation by detachment provide the only logical explanation. The extent to which phase boundary fracture can affect the relationship between liberation and size (highlighted by this example of UG2 ore) makes a strong case for the need for liberation analysis to be considered in the design of minerals processing circuits – and not just at one or two grinds.

Penberthy's observations also support the conclusion that phase boundary fracture and liberation by detachment are the dominant mechanisms that allow for the liberation and recovery of finely grained platinum group minerals at target grinds that are economically feasible. Penberthy hypothesised that BMS grains occurring on phase boundaries would be more readily liberated than those occurring as inclusions in silicates or chromite. From this, she attempted to predict BMS liberation after grinding, based on the associations of BMS in the crushed feed. She found that a correlation did exist, however "the measured apparent degree of liberation was higher than predicted liberation in all but two samples" (Penberthy, 2001: 181). Her observations were similar for the PGMs; predictions of PGM liberation based on their occurrence on chromite-silicate grain boundaries led to an underestimate of liberation. This implies that it is not only phase boundary fracture between chromite and silicates affecting PGM liberation, but that there is also preferential fracture around phase boundaries of PGMs occurring as inclusions within these minerals.

This work illustrates the indirect relationship that can occur between liberation, grain size distribution and particle size distribution for an ore showing a high level of phase boundary fracture. This means that the target grind required to provide the desired liberation for a process should not be predicted or assessed based on particle size distribution alone. Texture and grain size distribution help, but understanding of phase boundary fracture is also required. In cases where phase boundary fracture is extensive, liberation is not a continuous function of size, but discrete step changes can occur. For example, in comminution of UG2 ore, the first step change for BMS and PGM liberation occurs when the chromite grains are liberated from the silicate matrix (at a PSD near the chromite grain size distribution). Thus breakage and liberation

of the gangue is critical to understanding the liberation behaviour of the target minerals. This has implications for circuit design and optimisation in which a holistic approach to comminution and flotation is used.

5.5 Conclusions

The conservation of shape approach developed is a simple, direct, quantitative measure of phase boundary fracture. It has limited applicability to particular ore textures, but it can be used in conjunction with other techniques to facilitate their interpretation. For example, coupled with PSIA, the approach could be useful in the assessment of phase boundary fracture in different grinding devices, using abundant gangue mineralogy data (with low associated uncertainty), to support findings based on data for minor or trace phases (with high associated uncertainty). This type of analysis based on 2-D Auto-SEM-EDS data would also complement similar work carried out with 3-D X-ray computed micro-tomography (Charikinya, 2015; Garcia et al., 2009; Xu et al., 2013).

The high degree of liberated PGMs attainable at a relatively coarse grind (up to ten times the grain size of the PGMs) can only be explained by phase boundary fracture leading to enhanced liberation of these minerals. The consequences of phase boundary fracture for liberation are such that understanding it and quantifying it should be an imperative in circuit design and liberation modelling.

There is a tendency to associate the breakage mechanisms in ball mills with non-selective, random breakage, which leads to the outlook that the benefits of phase boundary fracture can only be appreciated through the use of alternative technologies. This work shows that UG2 ore is an example of an ore for which a very high degree of liberation by phase boundary fracture does occur in traditional ball mills.

5.6 Acknowledgements

This work is based on research supported in part by the National Research Foundation of South Africa (Grant Number 86054). Any opinions, findings and conclusions or recommendations expressed in any publication generated by the NRF supported research is that of the author(s), and the NRF accepts no liability whatsoever in this regard. The authors would also like to acknowledge the South African Minerals to Metals Research Institute (SAMMRI) and the South African Department of Science and Technology for funding the work. Thanks also to Dr Robert Schouwstra for useful discussions on this study.

5.7 References

Apling, A., Bwalya, M., 1997. Evaluating high pressure milling for liberation enhancement and energy saving. Miner. Eng. 10, 1013–1022. doi:10.1016/S0892-6875(97)00080-0

Barbery, G., 1987. Random sets and integral geometry in comminution and liberation of minerals, in: AIME Transactions. Soc. Min. Eng., pp. 96–102.

Barbery, G., 1991. Mineral liberation: measurement, simulation and practical use in mineral processing. Les Editions GB, Quebec.

Becker, M., Mainza, A.N., Powell, M.S., Bradshaw, D.J., Knopjes, B., 2008. Quantifying the influence of classification with the 3 product cyclone on liberation and recovery of PGMs in UG2 ore. Miner. Eng. 21, 549–558. doi:10.1016/j.mineng.2007.11.001

Becker, M., Yorath, G., Ndlovu, B., Harris, M., Deglon, D., Franzidis, J.-P., 2013. A rheological investigation of the behaviour of two Southern African platinum ores. Miner. Eng. 49, 92–97. doi:10.1016/j.mineng.2013.05.007

Cabri, L.J., Rudashevsky, N.S., Rudashevsky, V.N., Gorkovetz, V.Y., 2008. Study of native gold from the Luopensulo deposit (Kostomuksha area, Karelia, Russia) using a combination of electric pulse disaggregation (EPD) and hydroseparation (HS). Miner. Eng. 21, 463–470. doi:10.1016/j.mineng.2008.02.006

Charikinya, E., 2015. Characterising the effect of microwave treatment on bio-leaching of coarse, massive sulphide ore particles. Stellenbosch University.

Chetty, D., Gryffenberg, L., Lekgetho, T.B., Molebale, I.J., 2009. Automated SEM study of PGM distribution across a UG2 flotation concentrate bank: Implications for understanding PGM floatability. J. South. African Inst. Min. Metall. 109, 587–593.

Dal Martello, E., Bernardis, S., Larsen, R.B., Tranell, G., Di Sabatino, M., Arnberg, L., 2012. Electrical fragmentation as a novel route for the refinement of quartz raw materials for trace mineral impurities. Powder Technol. 224, 209–216. doi:10.1016/j.powtec.2012.02.055

Fandrich, R., Gu, Y., Burrows, D., Moeller, K., 2007. Modern SEM-based mineral liberation analysis. Int. J. Miner. Process. 84, 310–320. doi:10.1016/j.minpro.2006.07.018

Fandrich, R.G., Bearman, R.A., Boland, J., Lim, W., 1997. Mineral liberation by particle bed breakage. Miner. Eng. 10, 175–187.

Frances, C., Le Bolay, N., Belaroui, K., Pons, M.-N., 2001. Particle morphology of ground gibbsite in different grinding environments. Int. J. Miner. Process. 61, 41–56. doi:10.1016/S0301-7516(00)00025-9

Gao, M., Forssberg, E., 1995. Prediction of product size distributions for a stirred ball mill. Powder Technol. 84, 101–106.

Garcia, D., Lin, C.L., Miller, J.D., 2009. Quantitative analysis of grain boundary fracture in the breakage of single multiphase particles using X-ray microtomography procedures. Miner. Eng. 22, 236–243. doi:10.1016/j.mineng.2008.07.005

Gaudin, A.M., 1939. Principles of Mineral Dressing. McGraw-Hill Book Company, Inc., New York.

Gay, S.L., 2004. Simple texture-based liberation modelling of ores. Miner. Eng. 17, 1209–1216. doi:10.1016/j.mineng.2004.06.032

Hay, M.P., Roy, R., 2010. A case study of optimising UG2 flotation performance. Part 1: Bench, pilot and plant scale factors which influence Cr2O3 entrainment in UG2 flotation. Miner. Eng. 23, 855–867. doi:10.1016/j.mineng.2010.05.002

Kawatra, K., 2006. Advances in Comminution, 1st ed. Society for Mining, Metallurgy and Exploration, Inc., Littleton, Colorado.

King, R.P., 1992. Techniques for estimating the amount of grain-boundary fracture during comminution of mineralogical materials, in: Kawatra, K. (Ed.), Comminution - Theory and Practice. Soc. Min. Eng., pp. 1–16. doi:10.1016/B978-0-7020-2797-0.00001-1

King, R.P., 1993. Comminution research - a success story that has not yet ended., in: Proceedings XVIII International Mineral Processing Congress. pp. 39–45.

King, R.P., 1994. Linear stochastic models for mineral liberation. Powder Technol. 81, 217–234. doi:10.1016/0032-5910(94)02886-9

King, R.P., 2001. Modeling & Simulation of Mineral Processing. Butterworth-Heinemann, Oxford.

King, R.P., Schneider, C.L., 1998. Mineral liberation and the batch comminution equation. Miner. Eng. 11, 1143–1160. doi:10.1016/S0892-6875(98)00102-2

Laslett, G.M., Sutherland, D.N., Gottlieb, P., Allen, N.R., 1990. Graphical assessment of a random breakage model for mineral liberation. Powder Technol. 60, 83–97. doi:10.1016/0032-5910(90)80135-L

Lätti, D., Adair, B.J.I., 2001. An assessment of stereological adjustment procedures. Miner. Eng. 14, 1579–1587. doi:10.1016/S0892-6875(01)00176-5

Leroy, S., Dislaire, G., Bastin, D., Pirard, E., 2011. Optical analysis of particle size and chromite liberation from pulp samples of a UG2 ore regrinding circuit. Miner. Eng. 24, 1340–1347. doi:10.1016/j.mineng.2011.06.006

Little, L., Becker, M., Wiese, J., Mainza, A.N., 2015. Auto-SEM particle shape characterisation: Investigating fine grinding of UG2 ore. Miner. Eng. 82, 92–100. doi:10.1016/j.mineng.2015.03.021

McFadzean, B., Pani, S., Wiese, J., O'Connor, C.T., 2015. The interactive effects of chemical and process parameters on the flotation performance of a UG2 ore. Miner. Eng. 70, 92–98. doi:10.1016/j.mineng.2014.08.016

Mudd, G.M., 2012. Key trends in the resource sustainability of platinum group elements. Ore Geol. Rev. 46, 106–117. doi:10.1016/j.oregeorev.2012.02.005

Nel, E., Theron, J., Martin, C., Raabe, H., 2004. PGM Ore Processing at Impala's UG-2 Concentrator in Rustenburg, South Africa. SGS Mineral Services.

Omran, M., Fabritius, T., Mattila, R., 2015. Thermally assisted liberation of high phosphorus oolitic iron ore: A comparison between microwave and conventional furnaces. Powder Technol. 269, 7–14. doi:10.1016/j.powtec.2014.08.073

Penberthy, C.J., 2001. The effect of mineralogical variation in the UG2 chromitite on recovery of platinum-group elements. University of Pretoria.

Pourghahramani, P., 2012. Effects of ore characteristics on product shape properties and breakage mechanisms in industrial SAG mills. Miner. Eng. 32, 30–37. doi:10.1016/j.mineng.2012.03.005

Powell, M.S., Morrison, R.D., 2007. The future of comminution modelling. Int. J. Miner. Process. 84, 228–239. doi:10.1016/j.minpro.2006.08.003

Radziszewski, P., 2013. Assessing the stirred mill design space. Miner. Eng. 41, 9–16. doi:10.1016/j.mineng.2012.10.012

Rule, C., 2010. Stirred milling — new comminution technology in the PGM industry, in: The 4th International Platinum Conference, Platinum in Transition "Boom or Bust." pp. 71–78.

Rule, C., Schouwstra, R.P., 2011. Process mineralogy delivering significant value at Anglo Platinum concentrator operations, in: 10th International Congress for Applied Mineralogy. Trondheim, pp. 1–5.

Solomon, N., Becker, M., Mainza, A., Petersen, J., Franzidis, J.-P., 2011. Understanding the influence of HPGR on PGM flotation behavior using mineralogy. Miner. Eng. 24, 1370–1377. doi:10.1016/j.mineng.2011.07.015

Solomon, N., Mainza, A., Becker, M., Petersen, J., Ross, V., Franzidis, J.-P., 2010. Effects of high pressure grinding rolls on platinum-bearing ores and the flotation response as compared to the conventional ball mill, in: XXV International Mineral Processing Congress (IMPC) 2010 Proceedings. Brisbane, Australia, pp. 1249–1263.

Song, S., Campos-Toro, E.F., López-Valdivieso, A., 2013. Formation of micro-fractures on an oolitic iron ore under microwave treatment and its effect on selective fragmentation. Powder Technol. 243, 155–160. doi:10.1016/j.powtec.2013.03.049

Spencer, S., Sutherland, D., 2000. Stereological Correction of Mineral Liberation Grade Distributions Estimated By Single Sectioning of Particles. Image Anal. Stereol. 19, 175–182. doi:10.5566/ias.v19.p175-182

Sutherland, D., 2007. Estimation of mineral grain size using automated mineralogy. Miner. Eng. 20, 452–460. doi:10.1016/j.mineng.2006.12.011

Tavares, L.M., 2009. Analysis of particle fracture by repeated stressing as damage accumulation. Powder Technol. 190, 327–339. doi:10.1016/j.powtec.2008.08.011

Varinot, C., Hiltgun, S., Pons, M.-N., Dodds, J., 1997. Identification of the fragmentation mechanisms in wet-phase fine grinding in a stirred bead mill. Chem. Eng. Sci. 52, 3605–3612.

Vizcarra, T.G., 2010. The Effect of Comminution Mechanism on Particle Properties: Consequences for Downstream Flotation Performance. University of Queensland.

Vizcarra, T.G., Wightman, E.M., Johnson, N.W., Manlapig, E.V., 2010. The effect of breakage mechanism on the mineral liberation properties of sulphide ores. Miner. Eng. 23, 374–382. doi:10.1016/j.mineng.2009.11.012

Xu, W., Dhawan, N., Lin, C.L., Miller, J.D., 2013. Further study of grain boundary fracture in the breakage of single multiphase particles using X-ray microtomography procedures. Miner. Eng. 46-47, 89–94. doi:10.1016/j.mineng.2013.03.016

5.8 PGM deportment in EPA plant samples

In Paper 3, the link between phase boundary fracture and flotation recovery was inferred through the assessment of PGM liberation and flotation recovery data that have been reported in the literature. The plant samples taken from Lonmin's EPA concentrator provide additional evidence that supports the conclusions drawn based on the literature. The analysis used in Section 5.4 to describe the gangue mineralogy in terms of liberation, size distribution, and shape is applied here to the primary rougher feed (PRF) from the Lonmin EPA flotation circuit. The shape and composition distributions for the gangue presented in Figure 5.13 are very similar to those presented in Figure 5.3, with the main difference being that the PRF sample is considerably finer than the primary mill discharge sample analysed previously. Again, the high proportion of rounded chromite grains and low proportion of composites indicate a high degree of phase boundary fracture between the gangue minerals. The impact of this on the PGM liberation can be inferred through assessment of the PGE deportment and size-by-size recovery.

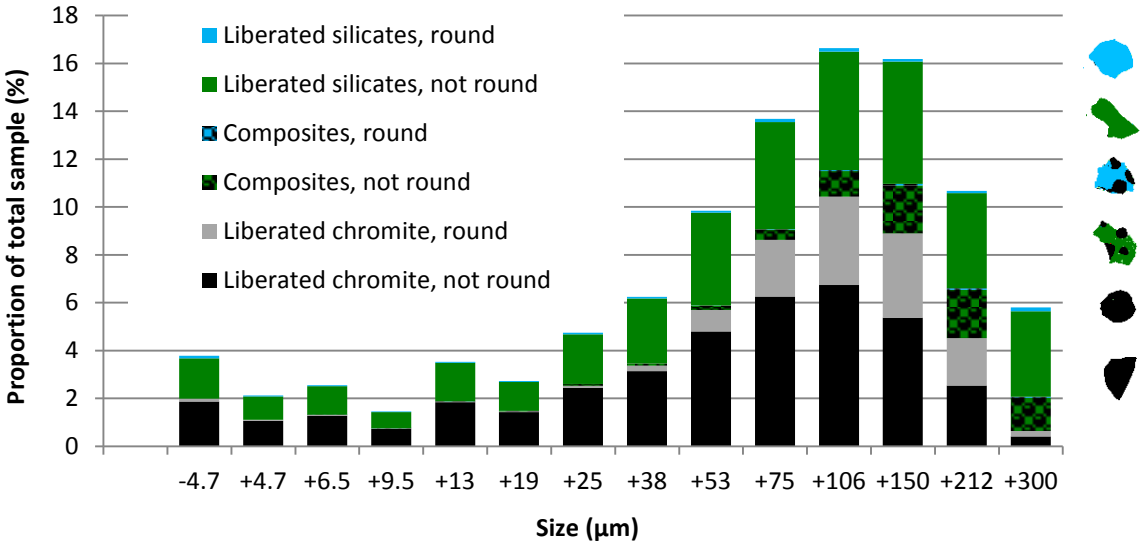

Figure 5.13: Description of Lonmin EPA primary rougher feed sample gangue mineralogy incorporating shape, liberation and particle size distribution.

The fractional 4-E-PGE assay data from the PRF, primary rougher tails (PRT) and secondary rougher tails (SRT) of the Lonmin EPA flotation circuit were used to estimate PGE size-by-size recovery. The particle size distribution based on four size fractions of the three samples (PRF, PRT, SRT) is presented in Figure 5.14. This is complemented by Figure 5.15 which shows the PGE distribution to the same four fractions in each sample.

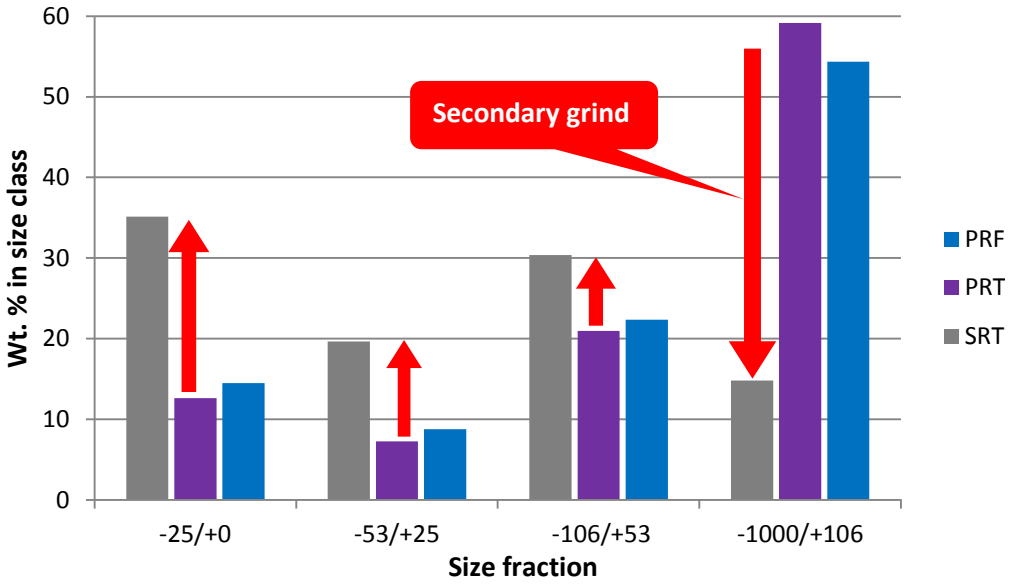

Figure 5.14: The particle size distributions before (PRF, PRT) and after secondary grinding (SRT) at the Lonmin EPA concentrator.

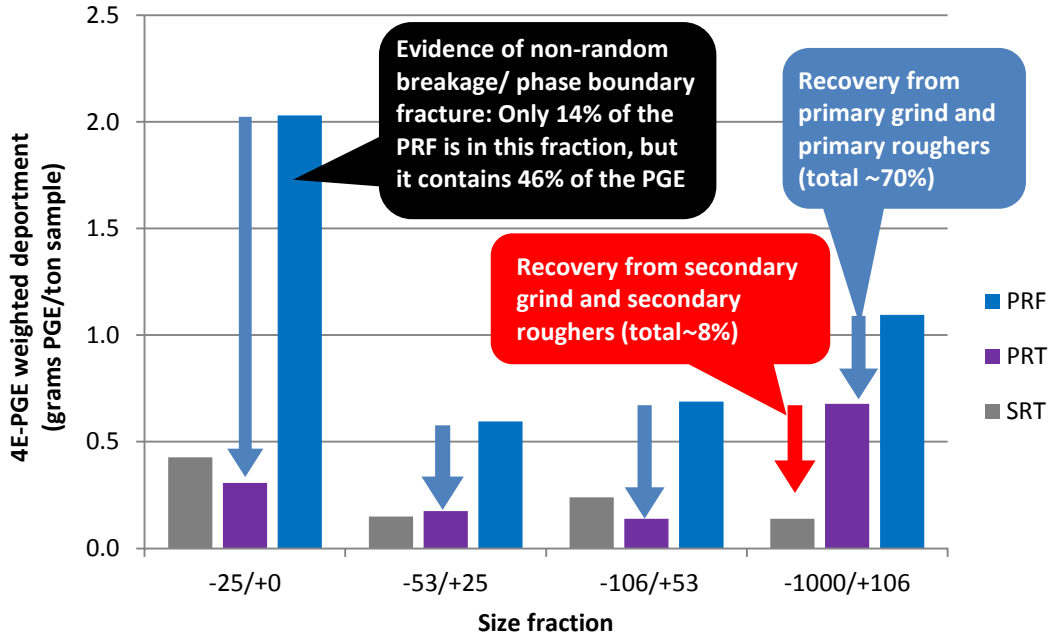

Figure 5.15: The 4E-PGE deportment (i.e. grams PGE in size fraction/ton of sample) before and after primary rougher flotation (PRF, PRT), and after secondary rougher flotation (SRT) for the Lonmin EPA concentrator.

After the primary grind, i.e. in the primary rougher feed, most of the ore (>50%) is coarser than 106 µm, and less than 15% is in the -25 µm fraction (blue bars in Figure 5.14). However, most of the PGE (46%) has deported to the -25 µm size fraction (blue bars in Figure 5.15). The difference in PGE deportment between the primary rougher feed and primary rougher tails in

each size class represents the size-by-size PGE recovery in the primary rougher circuit (blue arrows in Figure 5.15), which adds up to approximately 70%. The majority of the PGEs deported to the three finer size classes are recovered in the primary roughers, but less than half of the PGEs in the coarse (+106 μm) fraction are recovered.

The effect of secondary grinding on particle size distributions and PGE recovery are illustrated by the red arrows in Figures 5.14 and 5.15 respectively. The size-by-size recovery of the secondary roughers cannot be deduced without the secondary rougher feed, however the overall contribution of the secondary grind and secondary roughers can be estimated as an additional ~8% in recovery, most of which can likely be attributed to a reduction in the proportion of unliberated PGMs in the coarse size fraction. After primary grinding, the -25 μm fraction accounts for the highest PGE recovery, however after secondary grinding and flotation, this fraction also accounts for the biggest losses to the tails, which is perhaps due to overgrinding of the fines. However, the PGE deportment to the -10/+0 and -25/+10 μm fractions in the secondary rougher tails is split evenly with 0.22 grams PGE deported to the -10/+0 μm size fraction per ton of secondary rougher tails, and 0.21 grams PGE deported to the -25/+10 μm fraction (calculated from the assay data). This suggests that overgrinding of fines is not the only problem, and other factors such as mineral speciation are likely contributing to the main PGE losses.

The initial 70% recovery at a coarse grind can be attributed to early liberation of PGMs due to phase boundary fracture, as was concluded in Section 5.4.4 through an in depth study of the literature on phase boundary fracture and PGE flotation. The additional 8% after secondary grinding can mostly be attributed to the liberation of locked BMS/PGM from the +106 μm size class, which likely also involves phase boundary fracture. The BSE image and corresponding false colour image provided in Figure 5.16 illustrate the occurrence of phase boundary fracture around one side of a PGM grain which remains partially attached to a silicate particle.

When processing precious metal ores, small increments in overall recovery have a large impact on profitability, and thus the economic viability of fine grinding. For a fine grinding study, it would therefore be preferable to examine improved liberation afforded by fine grinding of primary or secondary rougher tails. However, as fractional PGE grades decrease below 0.4 g/t (as illustrated in Figure 5.15 for the SRT), the feasibility of obtaining representative PGM liberation data, and the attainable confidence levels associated with such data decreases. It was concerns such as these that contributed to the selection of a primary mill discharge sample (rather than a primary rougher tails sample) for the laboratory fine-grinding and flotation test work comparing ball mills and stirred mills presented in Chapter 6, Paper 4.

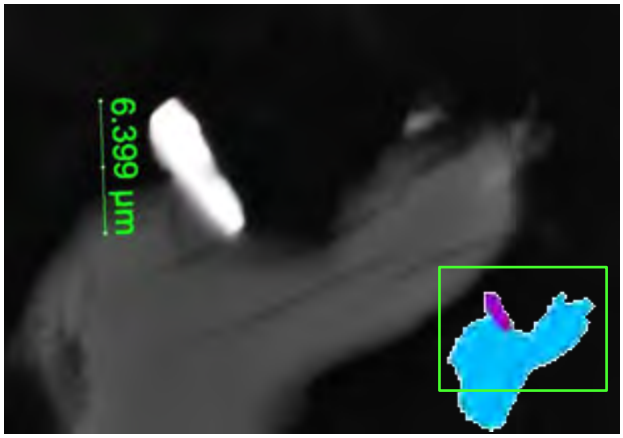

Figure 5.16: BSE and false colour images of a platinum group mineral grain attached to a plagioclase particle – from an SMD ultrafine grinding product sample.

Chapter 6

FINE GRINDING AND FLOTATION

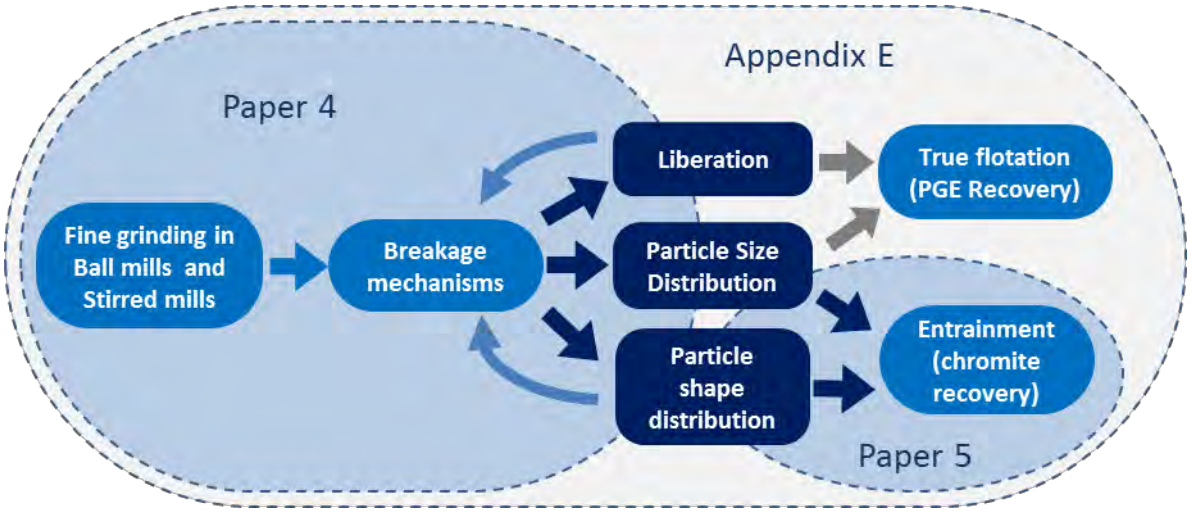

Chapter 6 comprises Paper 4 and Paper 5, which document the application of the shape characterisation methodology to the study of fine grinding and entrainment respectively. Additional flotation data associated with the test work which does not relate to shape characterisation is presented in Appendix E.

The second objective of this thesis was to demonstrate how the shape characterisation methodology can contribute towards the understanding of:

(a) Fracture mechanisms and the link between phase boundary fracture and liberation;
(b) The modification of shape during fine grinding in ball mills and stirred mills;
(c) The effects of particle shape on entrainment during flotation.

In Chapter 5, part (a) was addressed, and this chapter addresses parts (b) and (c).

The hypotheses addressed in this chapter are:

The significant differences in energy intensity between ball mills and stirred mills, and the dissimilar ratio of normally opposed contact forces to tangential shear forces within the two mill types, will lead to significant differences in the shape characteristics between ore particles produced within the two mills.

The work carried out to test this hypothesis is presented in Paper 4. The key-questions addressed in this paper are:

- **How do progeny particle shape and mineral liberation characteristics compare for ball mills and stirred mills at the laboratory scale, and are these consistent with observations made at plant scale?**
    - Do the particle shape characteristics of the major mineral components differ?
    - Do the particle shape characteristics vary with size?
    - Is there a correlation between the particle shape characteristics and grinding time in the batch mills?

Particle shape will affect the drainage rates of chromite grains entrained within the plateau borders of the flotation froth, with more rounded particles draining more readily, leaving a higher concentration of more angular particles being recovered to the froth.

The work carried out to test this hypothesis is presented in Paper 5. The key-questions addressed in this paper are:

- **How does the particle shape of chromite recovered to the concentrate compare to that in the feed and tails samples at laboratory and plant-scale?**
    - What is the effect of particle size on entrainment – is it a confounding variable?
    - How can the effect of shape be decoupled from the effect of size?

Paper 4: Fine grinding: how mill type affects particle shape characteristics and mineral liberation

Little, L., Mainza, A.N., Becker, M., Wiese, J. Minerals Engineering. Under review.

Keywords: Particle shape, fine grinding, breakage mechanisms, liberation, UG2 ore

Abstract

In minerals beneficiation applications, the main function of comminution circuits is to liberate valuable minerals to facilitate downstream separation processes such as flotation. Traditionally, design and optimisation of comminution circuits was based on the production of a target particle size distribution at an optimised throughput with consideration of energy efficiency and equipment wear rates. However, research in flotation and process mineralogy is leading to queries as to whether more should be demanded from the comminution circuit in terms of particle preparation. For example – if particle shape affects hydrophobicity, can mill operating conditions be adjusted to produce particles with shape characteristics which are more amenable to flotation? For this work UG2 ore (a South African platinum group mineral ore) was milled in a laboratory ball mill and stirred mill. To supplement the laboratory study, samples were taken from the fine grinding circuit of an operational UG2 concentrator. Automated Scanning Electron Microscopy with Energy Dispersive X-ray Spectroscopy (Auto-SEM-EDS) was used for mineralogical and particle shape analysis of feed and product samples. Although the laboratory test work indicated a significant difference in product particle shape characteristics for the two mill types, the difference was not evident in the plant data.

6.1 Introduction

6.1.1 Background

With the continual depletion of high grade simple ore bodies, more complex, finely disseminated ore bodies are being processed, which has led to an increase in the prevalence of fine-grinding (Sinnott et al., 2006). This has been evident in the platinum group element (PGE) industry in South Africa, where the Bushveld Complex hosts 70% of global PGE reserves. Since 1995, average feed grades of PGE ores being processed have dropped from around 6 g/t to less than 4 g/t (Mudd, 2012). From the early 2000's the industry invested in technology for fine grinding (Rule, 2011, 2010), simultaneously investing in technology for quantitative mineralogy to better understand the potential benefits associated with fine grinding (Gu et al., 2014; Rule and Schouwstra, 2011).

The first stirred mill was installed in the platinum industry in 2002, and by the year 2010, forty stirred mills had been installed at various platinum operations in South Africa, and these led to a step change in flotation recoveries (Rule, 2011, 2010). Over the last decade, approximately 200 Automated Scanning Electron Microscopy (Auto-SEM-EDS) systems have been installed worldwide. The contribution of these devices in facilitating the introduction of stirred mills at Anglo Platinum is used as a case study illustrating the value of process mineralogy (Gu et al., 2014; Rule and Schouwstra, 2011). It is apparent that both stirred milling and Auto-SEM-EDS technology have already made a valuable contribution in numerous minerals processing applications. However the industry still faces continual challenges, and improved understanding of fine grinding mechanisms, liberation response, and the role of particle shape has the potential to lead to further opportunities for optimisation. In minerals processing it is typical for significant process fluctuations, due to ore variability, to affect mill throughput and/or flotation grade and recovery. When these fluctuations cannot be explained by operational factors, they are typically ascribed to mineralogy or poorly understood factors such as particle shape. There is also currently increased interest in the effects of particle morphology on flotation performance, and questions being raised as to whether the shape characteristics of particles can be selectively modified using particular grinding conditions or different mill types (Guven and Çelik, 2015).

In a previous paper (Little et al., 2015, Paper 1), the authors developed a methodology for Auto-SEM-EDS shape characterisation, which was applied to data from laboratory fine-grinding experiments with UG2 ore. The data presented indicated significant differences in shape characteristics between the major mineral components of the mill feed, with a high proportion of rounded chromite grains relative to the more angular silicates. After fine grinding, the chromite had very similar shape characteristics to the silicates, although significant differences

were observed between the progeny of the two mill types (Little et al., 2015, Paper 1). This paper aims to explore these observations further, focusing on the two fine grinding devices and the breakage mechanisms there-in, size-by-size shape characteristics and valuable mineral liberation. Shape characteristics of samples taken from a UG2 ore concentrator are also analysed for comparison.

6.1.2 Fine grinding

As specific energy required for grinding increases exponentially with product fineness, energy efficiency is always a concern in fine grinding operations. Energy efficiency is probably the most significant advantage of stirred mills over traditionally used tumbling mills for fine grinding, and is likely to remain one of the dominant factors affecting decisions relating to mill design and operation. Whereas the energy intensity of ball mills is limited by the requirement for gravity to cause breakage, in stirred mills energy is imparted to the charge with an impeller, which allows for much higher energy intensities (Jankovic, 2003). In platinum group mineral (PGM) ore processing, stirred mills are used for both mainstream grinding applications at high throughputs, and concentrate regrind applications at low throughputs. In mainstream applications, an IsaMill (horizontally orientated mill) is typically installed as an optional tertiary grinding stage after primary and secondary ball mills. Vertical stirred mills such as the Stirred Media Detritor (SMD) or Vertimill are mostly used for concentrate regrind applications in the South African PGM industry (Rule, 2010).

The breakage mechanisms in stirred mills – regardless of the mill orientation – are typically described as abrasion and attrition (Gao and Forssberg, 1995; Sinnott et al., 2006; Wills and Napier-Munn, 2006; Ye et al., 2010), or more simply 'shear' breakage (Radziszewski, 2013). The dominant breakage mechanism in ball mills is generally considered to be impact breakage in the toe of the mill, although recent Discrete Element Method (DEM) work has led to observations that low energy, repeated contacts in the bulk of the charge are dominant, causing damage accumulation and incremental breakage (Tavares, 2009; Weerasekara et al., 2013). Figure 6.1 illustrates the various breakage mechanisms and associated terminology, drawing attention to the manner in which breakage mechanisms can affect liberation and shape. Understanding of these breakage mechanisms (which are dependent on ore characteristics), is important for modelling and simulation of comminution circuits for design and optimisation – particularly if effects on liberation are to be predicted. Approaches to studying these breakage mechanisms include computational methods such as DEM and Computational Fluid Dynamics (CFD) (Cleary et al., 2006; Sinnott et al., 2006; Weerasekara et al., 2013), as well as experimental methods where progeny size distribution, particle shape, and liberation characteristics are used to provide insight into the mechanisms (Frances et al., 2001; Gao and Forssberg, 1995; Hoşten and

Özbay, 1998; Kaya et al., 2002; Palaniandy et al., 2008; Roufail, 2011; Varinot et al., 1997; Vizcarra et al., 2011b; Ye et al., 2010). Most of this work has focused on relatively coarse grinding (>150 μm), so understanding of breakage mechanisms in the fine grinding region relevant to PGM processing remains limited.

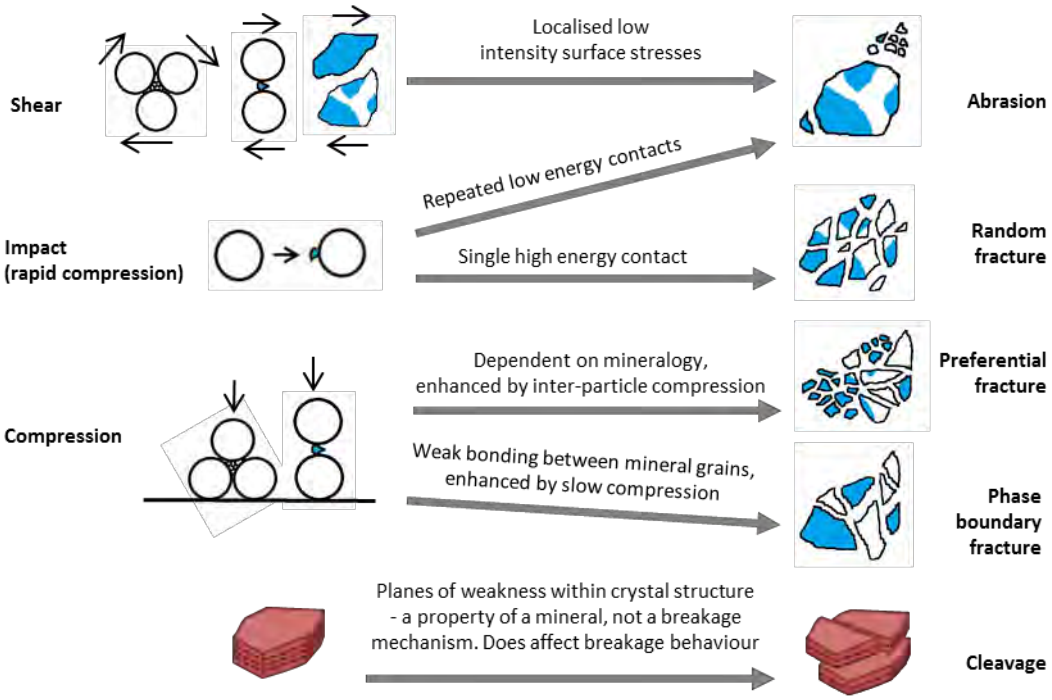

Figure 6.1: Breakage mechanisms - definitions and terminology highlighting suggested linkages between contact events (force application) and breakage outcome (adapted from Little et al., 2016, Paper 3). Circles represent grinding media, shaded and not-shaded represent different mineral phases. A mineral grain is defined as a 3-dimensional entity consisting of only one mineral phase: particles consisting of one, two, or more grains are defined as liberated, binary and composite particles respectively.

Cleavage is also sometimes classified as a breakage mechanism, although the term has different connotations in different fields. A generic description provided by King (2001) is that cleavage results when the original solid has some preferred surfaces along which fracture is likely to occur. In mineralogy, these preferred surfaces are planes of weakness within a crystal structure dictated by the atomic arrangement. The number and orientation of cleavage planes within a mineral are used as a diagnostic property for mineral identification. In mineralogy, fracture and cleavage are mutually exclusive – irregular breakage is considered fracture; breakage along regular surfaces related to the crystal structure is termed cleavage. Of the major gangue minerals in UG2 ore, chromite has no cleavage and orthopyroxene and plagioclase have prismatic cleavage.

Although understanding of breakage mechanisms is important for design and optimisation of comminution circuits, the progeny particle characteristics such as size distribution, shape distribution, and liberation characteristics play a fundamental role in downstream processing operations such as flotation. Understanding the possible effects of the breakage mechanisms in different mill types on these properties can therefore also make a valuable contribution.

6.1.3 Auto-SEM-EDS particle shape characterisation

At the particle sizes typically associated with fine grinding in minerals processing (<75 µm), viable options for quantitative particle shape characterisation are limited, and effects of image resolution are of particular concern (Little et al., 2015; Varinot et al., 1997). Scanning electron microscopes provide higher resolution than optical dynamic image analysis devices, which enables analysis of finer particles. As the ore texture and mineral structure affect particle shape, the associated mineralogical information obtained with Auto-SEM-EDS is an added benefit of the technology.

Measurement and analysis of the full particle size distribution of a sample is necessary to understand and interpret effects of particle size, and being able to measure and represent particle shape with a distribution is similarly important. This is possible with the thousands of particle images obtained from Auto-SEM-EDS, using simple geometric descriptors (that do not rely on perimeter measurements), to assign a numerical value to each particle. *Roundness* is such a descriptor, which is the ratio of the cross-sectional area of the particle, to that of a circle/ sphere with a diameter equivalent to the maximum Feret diameter (Fe_{Max}) of the particle. The roundness descriptor used in this work is presented in Equation 6.1. It should be noted that some authors use the same name for other descriptors (Rahimi et al., 2012; Ulusoy et al., 2003). Issues relating to resolution, stereology, random orientation and uncertainty associated with Auto-SEM EDS shape characterisation were addressed by Little et al. (2015, Paper 1).

$$Roundness = \frac{4 \cdot Area}{\pi \cdot {Fe_{max}}^2} \qquad 6.1$$

6.1.4 Objectives

The objective of this work is to assess the influence of fine grinding in ball mills and stirred mills on valuable mineral liberation and particle shape characteristics of UG2 ore, a South African PGM ore. The work demonstrates how process mineralogy tools can be applied in a comminution context to provide insight into fine grinding breakage mechanisms in ball mills and stirred mills.

6.2 Methodology

6.2.1 Overview

The bulk of the work for this study was done at the laboratory scale, which involved batch grinding of UG2 ore in a ball mill and in a stirred mill. These experiments were effectively conducted in parallel, with representative samples of the same feed being milled in each device to two target grinds: 'fine' (28% passing 10 μm) and 'ultra-fine' (40% passing 10 μm). Mineralogical analysis of product samples was carried out using QEMSCAN, investigating bulk mineralogy, particle shape, base metal sulfide (BMS) liberation and platinum group mineral (PGM) liberation. To complement the laboratory data on shape, samples were taken from a plant-scale UG2 fine-grinding circuit with a ball mill and IsaMill operating in series. This was to determine whether the findings relating to particle shape from the batch laboratory grinding data would be consistent with plant-scale operations. It should be noted that the laboratory work, carried out under repeatable, controlled conditions forms the back-bone of this study, while the plant data are considered supplementary. The plant data represent grinding at a completely different scale to the laboratory mills with continuous operation, the ball mill and stirred mill in series rather than parallel, and a horizontal IsaMill with internal classification as opposed to a vertical SMD. Nevertheless, in both cases grinding in a ball mill is being compared to grinding in the high shear environment of a stirred mill. Table 6.1 summarises the samples analysed in the study along with their P80's (as measured by screening), and associated acronyms.

Table 6.1: Sample list and P80s.

	Sample ID	**Grind (P80, μm)**
Laboratory	Laboratory feed (Lab Feed)	380
	Ball mill, fine grind (BM Fine)	50
	Ball mill, ultrafine grind (BM UF)	33
	SMD, fine grind (SMD Fine)	62
	SMD, ultrafine grind (SMD UF)	41
Plant	Ball mill feed (BM Feed)	110
	IsaMill Feed	90
	IsaMill Discharge	70

6.2.2 Details of laboratory test work

The procedure for the laboratory test work and some of the findings were reported by Little et al. (2015, Paper 1). The laboratory mill feed was sampled from the primary ball mill discharge of a different UG2 concentrator to that from which the plant samples were taken. The mill

specifications and operating conditions for the laboratory test work are presented in Table 6.2. Ceramic grinding media was used in both mill types. A Fluke Power Logger was used to determine the power drawn by the mills, based on measurements of current and potential difference. The no-load power and the power drawn over the entire grinding period were then used to estimate the energy efficiency of the two mill types, as illustrated in Figure 6.2.

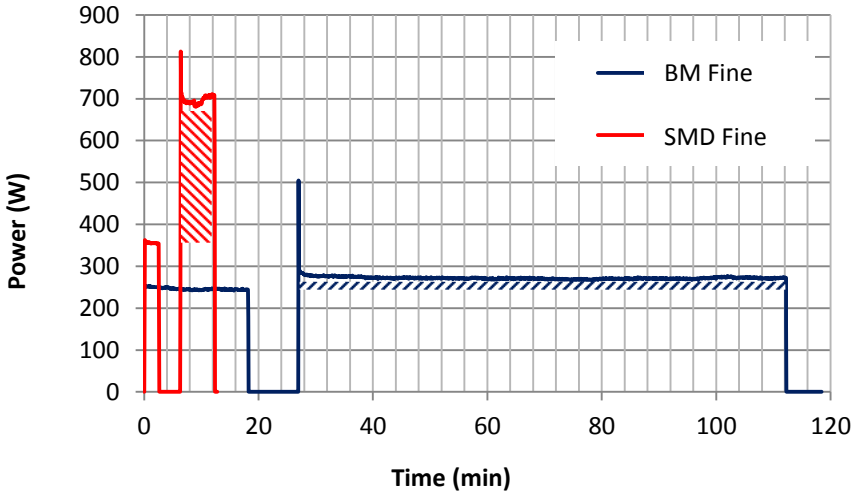

Figure 6.2: Fluke Power Logger measurements for the two laboratory mill types illustrating the difference in energy intensity between them.

Table 6.2: Laboratory mill operating specifications.

Specification	Units	SMD	Ball mill
Mill diameter	mm	219	300
Media size (graded charge)	mm	5	(12, 19, 25, 32)
Mass of media	kg	8.35	11.87
Media density (ceramic)	kg/m^3	3.83	3.6
Mass of ore sample	kg	3.0	3.0
Slurry density (% solids by mass)	%	74	64
Impeller speed	rpm	535	NA
Mill speed	% critical	NA	70
Impeller diameter	mm	161	NA
Power draw under these conditions	W	702	275
No-load power (no media or slurry)	W	354	245
Net power	W	348	30
Milling time – fine grind	min	6	85
Milling time – UF grind	min	9.2	133
Size specific energy intensity (-53µm) fine grind	kWh/t-53	19.6	19.9
Size specific energy intensity (-53 µm) UF grind	kWh/t-53	22.1	26.0

In Figure 6.2, the initial period for each curve indicates the no-load power, after which the mill is stopped and the media and slurry added, and then the mill is started for the duration of the grinding period. The net power drawn by the stirred mill is much higher than that of the ball mill, which leads to a much shorter grinding period required to achieve a similar grind. The shaded area indicates the net energy used by each device during the tests. The size specific energy intensity was calculated as the energy required to generate new material finer than 53 μm, and this is reported in Table 6.2. For the fine grind the size specific grinding energy is very similar, but for the ultrafine grind the stirred mill size specific energy was approximately 15% lower than the ball mill under the conditions tested. The feed and product particle size distributions are presented in Section 6.3.1 along with the bulk mineralogy of the ore.

6.2.3 Details of plant samples

Three samples were taken from the fine grinding circuit of a UG2 concentrator located in the southern section of the Western Limb of the Bushveld Complex. The circuit is a tailings treatment plant, which could also be described as a tertiary mill-float circuit with a nominal throughput of 220 tph. It is located after a gravity circuit in which spirals are used to recover some of the chromite. This does not have a major effect on the composition of the tailings stream, which still contains over 60% chromite after the spirals, however the size distribution is significantly affected by the desliming process that is required to prepare the feed for the spirals. The circuit configuration and sampling points are indicated in Figure 6.3. The open circuit configuration with a single pass through the ball mill is not unusual for UG2 ore, to avoid recirculation and overgrinding of dense chromite (Hay and Roy, 2010; Rule and Schouwstra, 2011). There were no sampling points on the cyclone overflow nor ball mill discharge, so the particle shape characteristics of the ball mill discharge have to be inferred from the IsaMill feed. The slurry density of the ball mill feed sample was low at 47%, and that of the IsaMill samples was typical for such devices at 51%. A mass balance was not performed over the circuit, and these samples were only used for a preliminary assessment of particle shape within the circuit.

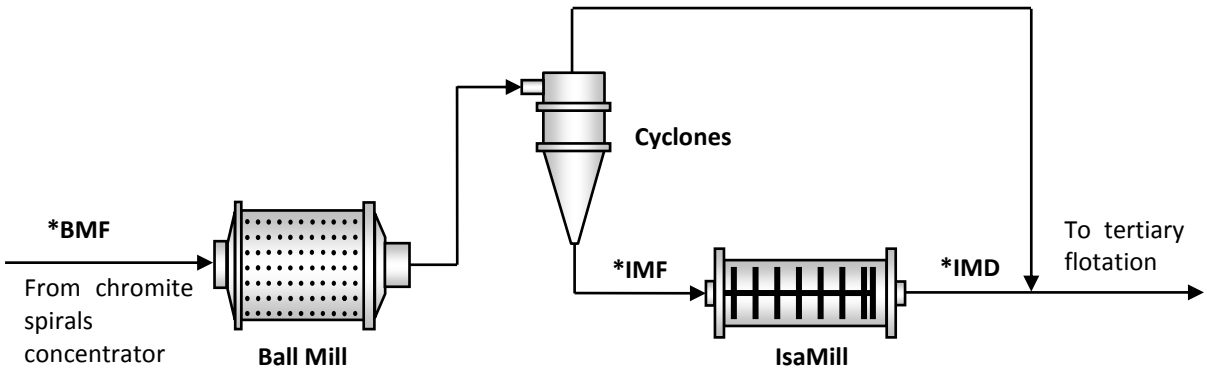

Figure 6.3: Flow diagram of the UG2 concentrator fine grinding circuit – the three sampling points are indicated with an asterisk.

6.2.4 Mineralogical and particle shape analysis

After drying and de-lumping, each sample was representatively split into ~300 g aliquots. These were then wet screened at 75, 53, 38 and 25 µm. The -25 µm samples were then screened through a 10 µm cloth in an ultrasonic bath. The +75 µm fractions were dry screened to determine the remainder of the particle size distribution (PSD). From analysis of the PSDs, the fractions to be analysed with QEMSCAN were selected, and each of these was split using a micro-riffler to 4 g aliquots that were mounted in resin and prepared as vertical sections for analysis. The FEG QEMSCAN 650F was used. The blocks for the laboratory test-work were analysed using the particle mineral analysis (PMA) setting, with EDS mapping of the particles at pixel spacings between 0.44 µm (-10 µm samples) and 4.88 µm (+150 µm fraction of the laboratory mill feed). As this work indicated that most of the particles were liberated mineral grains, the plant samples were run with a simpler, quicker measurement setting, with BSE images used for the shape and dimensions of the particle, and EDS only measured at the particle centroid. For PGM liberation analysis of the laboratory ultra-fine grinds in the two mill types, unsized samples (representatively split) were prepared for analysis using the trace mineral search setting on QEMSCAN. Unsized samples were used for this analysis due to the scarcity and fineness of PGM grains within the ore. For typical Auto-SEM-EDS analysis, measurement of sized-fractions is preferred as this allows for adjustment of the field size and image resolution to suit the properties of the particles being analyzed. The use of sized-fractions can also reduce the stereological bias associated with 2-D liberation measurements, provided that appropriate size filters are applied to exclude small cross sections which are likely taken from the surface of a larger particle. However, in a trace mineral search for PGM grains, a large number of fields are rapidly scanned based on BSE thresholds, and only particles containing bright phases (i.e., PGMs), are then mapped with EDS at a high resolution. As PGM grains coarser than 20 microns are very rare in South African PGM ores, a high resolution is appropriate for analysis of these

grains, even when they are locked within much coarser particles. In addition, the time and monetary resources required to "find" a certain number of PGM grains in an unsized sample is already substantial. To have to find a comparable number of PGMs in three fractions of a sized-sample would likely triple these costs. Inductively Coupled Plasma with Optical Emission Spectroscopy (ICP-OES) assays were used for QEMSCAN data validation.

6.3 Results

6.3.1 Particle size distributions and bulk mineralogy

The particle size distributions of the various samples are shown in Figure 6.4, and the bulk mineralogy for the laboratory and plant samples is presented in Table 6.3. For the laboratory test work, the PSDs are broad with a shallow slope, although the ball mill PSDs are steeper than those of the stirred mill. The shallow stirred mill PSDs with a coarse tail are possibly due to the media size being too fine to cause breakage of the top size ore particles. The high pulp density used (74%) may have also contributed to the broad distributions for the laboratory SMD. It should be noted that in continuous stirred milling devices with internal classification a steeper particle size distribution would be expected (Ye et al., 2010). The plant samples have steeper PSDs than the lab samples due to classification/de-sliming up stream.

The size range for the laboratory test work was selected to compare the two mill types in a size region where there is some overlap between the applicability of the two mill types, approaching the limiting product fineness of ball mills, with a relatively coarse feed size for stirred mills. The high reduction ratio possible with batch grinding at the lab scale is not necessarily representative of plant devices, but this was intended to emphasise any differences in liberation or particle shape produced.

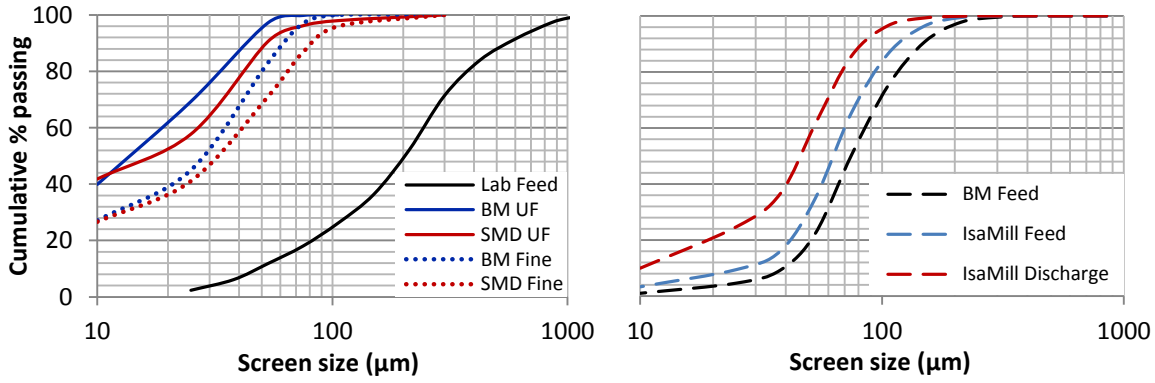

Figure 6.4: Particle size distributions of samples milled in the laboratory (left) and samples taken from the plant (right) as determined by screening.

The bulk mineralogy obtained with QEMSCAN is presented in Table 6.3. The ranges of values presented is fairly typical of UG2 ore (Penberthy, 2001), with the low standard error for the plant samples suggesting that the non-rigorous sampling approach was not introducing significant bias to the mineralogical measurements. The plant ore samples have higher chromite content and less alteration silicates, the latter likely due to a relatively high recovery of the naturally floatable alteration silicates such as talc during primary and secondary flotation stages.

Table 6.3: QEMSCAN bulk mineralogy for the laboratory and plant samples, based on the average of 5 samples and 3 samples respectively. The mineral groups indicated are used for the QEMSCAN false colour images to facilitate interpretation of roundness distributions presented in Figures 6.6, 6.7 and 6.11.

Mineral groups	Mineral	Laboratory		Plant	
		Mean wt.%	St. Error	Mean wt.%	St. Error
Chromite	Chromite	61.58	1.24	69.56	0.85
BMS	BMS	0.21	0.02	0.03	0.01
Plagioclase	Plagioclase	15.71	0.48	7.15	0.23
Pyroxene	Orthopyroxene	16.05	0.95	20.19	0.66
	Clinopyroxene	1.22	0.10	0.81	0.03
Alteration silicates	Amphibole	0.99	0.11	0.26	0.02
	Chlorite	1.29	0.10	0.34	0.02
	Serpentine	0.24	0.02	0.06	0.01
	Talc	0.27	0.06	0.01	0.00
Other	Mica	0.40	0.05	0.16	0.02
	Olivine	1.56	0.17	0.78	0.07
	Other	0.49	0.05	0.64	0.06

6.3.2 Particle shape characterisation

For a qualitative assessment of the typical sample shape characteristics, SEM back scattered electron (BSE) images of the -25/+10 µm fraction of IsaMill and laboratory ball mill progeny are provided in Figure 6.5. The images presented in Figure 6.5 show the wide range of particle shapes present in a particular sample. Most of the particles appear to have smooth faces, with sharp edges and corners. Nano-SEM images from the other samples showed similar shape characteristics. For these images, a small pinch of powder was sprinkled on a patch of resin, and the field to capture was selected arbitrarily, so the images are not necessarily representative of the bulk samples. A qualitative comparison based on images of this type is likely to be subjective and inconclusive; however these images complement the information from the more rigorous quantitative Auto-SEM-EDS information presented in Figures 6.6 and 6.7. If the 3-D images were

to indicate a high proportion of flaky particles, this would be important to consider during interpretation of the 2-D shape characterisation results. The peaks of the roundness frequency distributions presented in Figures 6.6 and 6.7 lie between roundness values of 0.3 and 0.6, which appears to be reasonable based on the Nano-SEM images.

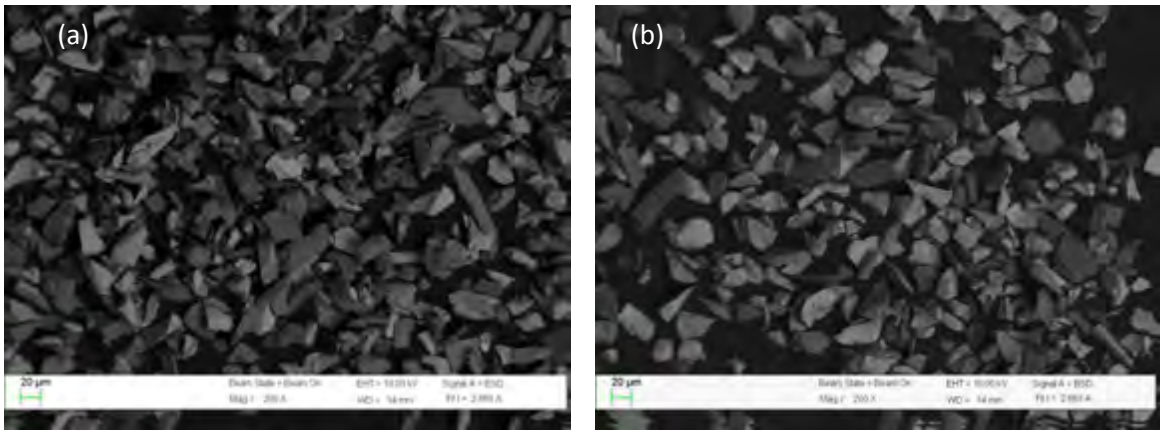

Figure 6.5: Nano-SEM images of the -25/+10 µm fractions of: (a) the laboratory ball mill fine sample; (b) the IsaMill discharge sample.

The data from the -75/+53 µm fractions were selected for presentation in Figure 6.6 because it is the fraction from the laboratory testwork with the highest variation in shape. The same fraction was selected for the plant samples (Figure 6.7), both for comparison with the laboratory data, and because it represents a major portion of each plant sample. The normal distribution with mean 0.49 and standard deviation 0.14 is included as a reference point in both figures. The mean roundness values for these and other size fractions are presented in Table 6.4a, along with the number of particles analysed, standard deviation (of the distribution) and standard error (standard deviation of the mean) in Table 6.4b.

The image grid insets in Figures 6.6 and 6.7 show false colour images classified by roundness to facilitate interpretation of the roundness distributions. The inset indicates that most of the rounded particles are chromite, but it is important to refer to the distribution and acknowledge that this does not necessarily mean that most of the chromite particles are rounded, as in this case rounded categories only account for a very small portion of the particles in the sample. Previously, the shape characteristics of chromite and silicates were reported independently for some of these fractions (Little et al., 2015, Paper 1). However, below 75 µm, there was seen to be no significant difference between the shape characteristics of the chromite and silicates, so the data presented here are for all particles.

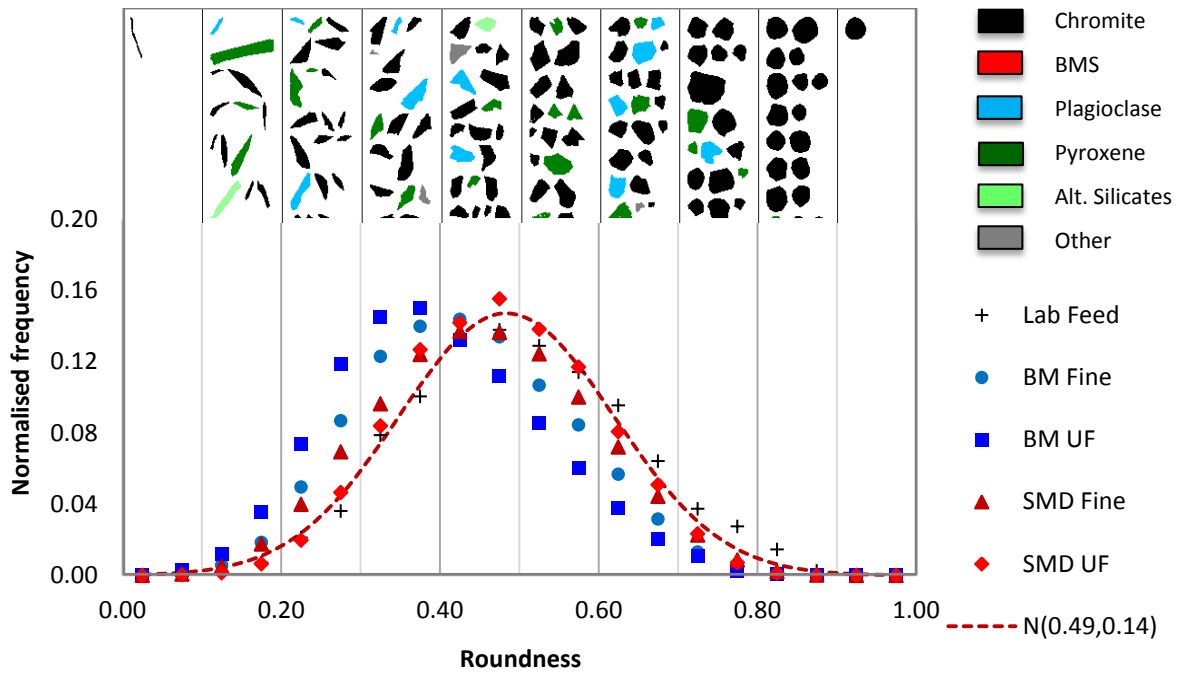

Figure 6.6: Roundness frequency distributions for the -75/+53 µm fractions of the laboratory test work samples. The image grid inset of UG2 particle false colour images illustrates typical characteristics of particles in each roundness category.

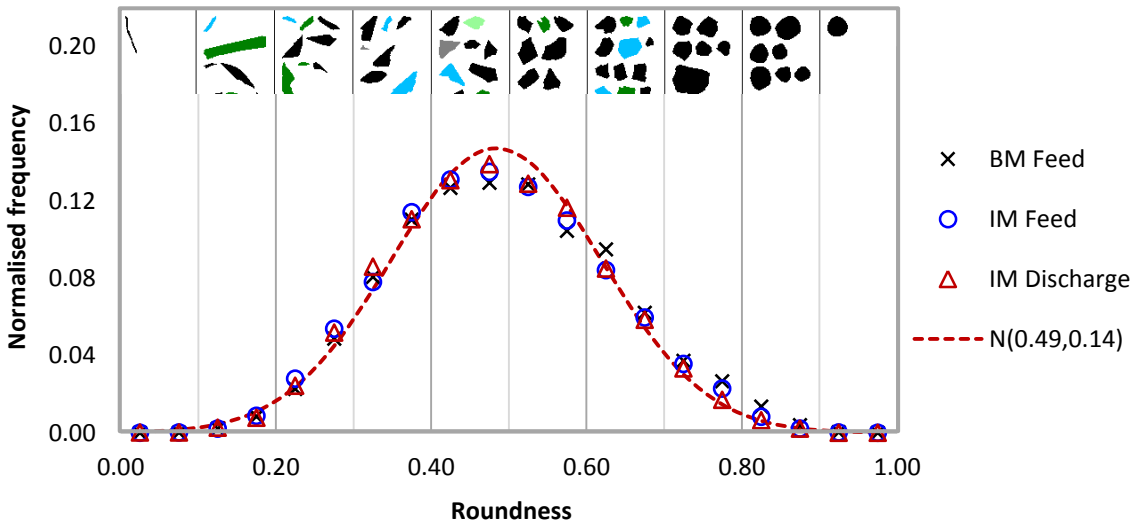

Figure 6.7: Roundness frequency distributions for the -75/+53 µm fractions of the plant samples.

In Figure 6.6 the ball mill ultrafine grind is seen to have the most angular-elongated particles, followed by the ball mill fine grind. The laboratory feed has the most rounded particles. The roundness distributions of the finer size fractions (Table 6.4) show less variation between samples, with the finest size class having very similar roundness distributions. Figure 6.7 indicates no difference between the shape characteristics of particles in the -75/+53 µm size

fraction of the plant samples. This is consistent with the other size fractions (Table 6.4), which only show slight variation between samples, although the finer fractions have lower mean roundness values indicating a shift towards more elongated and angular particles. These observations are discussed in more detail with reference to the breakage mechanisms in Section 6.4.1.

The descriptor roundness is good at differentiating between round particles and non-rounded particles, but it does not clearly distinguish between smooth elongated particles and highly irregular particles with low *aspect ratios*. Little et al. (2015, Paper 1) developed shape classes using roundness and *aspect ratio* in conjunction to achieve an additional level of classification, which would indicate significant differences in roughness, without the need for resolution-dependent perimeter measurements. Figure 6.8 illustrates the sample shape characteristics based on this classification system, which complements the data presented in Figures 6.6 and 6.7, indicating that the proportions of particles in the 'elongated smooth' and 'angular' categories are minor, and have minimal variation across samples. The use of this shape classification system clarifies that the less-rounded distribution for the ball mill ultrafine sample is due to the particles being more elongated rather than particles being more rough or angular.

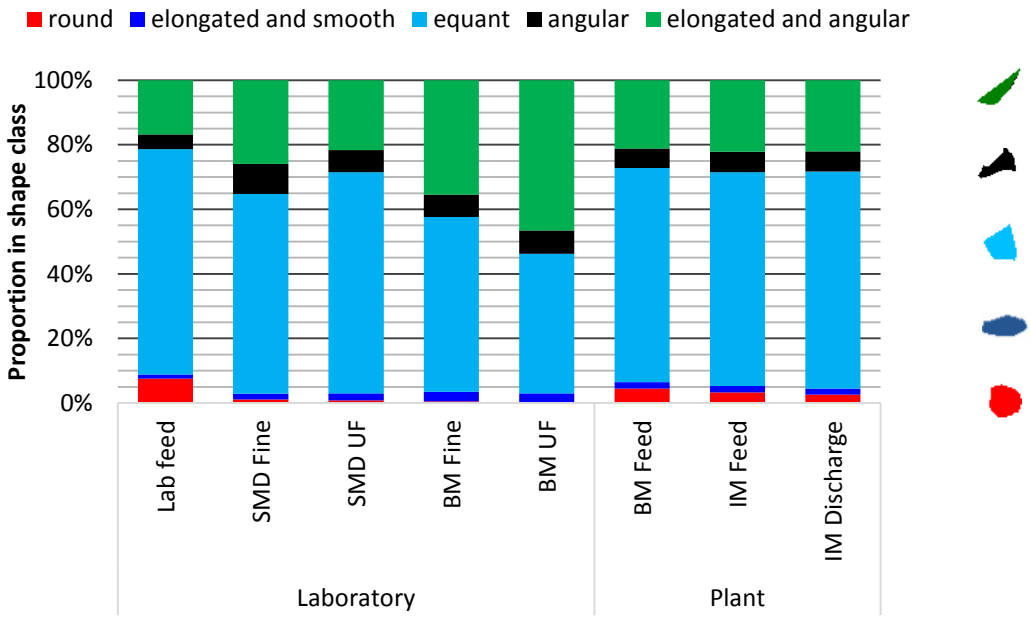

Figure 6.8: Alternative shape characterisation approach based on using roundness and aspect ratio in conjunction after Little et al. (2015, Paper 1). Data presented for the -75/+53 µm fraction.

Table 6.4a: Size-by-size data showing mean roundness for each sample.

		Size fraction (µm)				
	Sample	**+75**	**-75/+53**	**-53/+25**	**-25/+10**	**-10/+0**
Laboratory	Lab Feed	0.59	0.52	0.48	0.45	0.47
	BM Fine	-	0.43	0.46	0.39	0.46
	BM UF	-	0.40	0.47	0.46	0.46
	SMD Fine	-	0.46	0.47	0.45	0.45
	SMD UF	-	0.48	0.49	0.48	0.46
Plant	BM Feed	0.50	0.49	0.49	0.41	0.42
	IsaMill Feed	0.48	0.49	0.49	0.43	0.44
	IsaMill Discharge	0.49	0.48	0.50	0.45	0.42

Table 6.4b: Size-by-size data showing number of particles included in each analysis, standard deviation and standard error (standard deviation of the mean).

			Size fraction (µm)				
	Sample		**+75**	**-75/+53**	**-53/+25**	**-25/+10**	**-10/+0**
Laboratory	Lab Feed	n	17339	712	4965	19168	76240
		St. Dev	0.15	0.14	0.14	0.14	0.15
		S.E	0.001	0.005	0.002	0.001	0.001
	BM Fine	n	-	8764	5001	9984	98925
		St. Dev	-	0.13	0.14	0.14	0.14
		S.E	-	0.001	0.002	0.001	0.000
	BM UF	n	-	3334	10984	18635	150146
		St. Dev	-	0.13	0.13	0.13	0.14
		S.E	-	0.002	0.001	0.001	0.000
	SMD Fine	n	-	17688	11889	2828	84177
		St. Dev	-	0.13	0.13	0.13	0.14
		S.E	-	0.001	0.001	0.003	0.000
	SMD UF	n	-	8910	11164	21674	104251
		St. Dev	-	0.12	0.12	0.12	0.14
		S.E	-	0.001	0.001	0.001	0.000
Plant	BM Feed	n	5832	5694	7896	15217	21143
		St. Dev	0.15	0.14	0.13	0.14	0.15
		S.E	0.002	0.002	0.001	0.001	0.001
	IsaMill Feed	n	6552	5733	7679	18166	31204
		St. Dev	0.14	0.14	0.13	0.14	0.15
		S.E	0.002	0.002	0.001	0.001	0.001
	IsaMill Discharge	n	6662	4792	24434	28168	65567
		St. Dev	0.13	0.14	0.12	0.13	0.14
		S.E	0.002	0.002	0.001	0.001	0.001

6.3.3 Valuable mineral liberation

For this work, the ultrafine grinds of the ball mill and stirred mill were selected for analysis of PGM liberation. This was based on associated flotation test work that showed significantly higher PGE recoveries for the stirred mill ultrafine grind than the ball mill ultrafine grind with similar solids recoveries and total concentrate grades. In the case of UG2 ore, PGM liberation data are generally considered in conjunction with the association of PGM with BMS as this has a significant impact on particle hydrophobicity and thus floatability (Chetty et al., 2009; Nel et al., 2004; Penberthy, 2001; Rule and Schouwstra, 2011). Similarly, exposure of a small PGM or BMS grain to the surface of a particle can impact its hydrophobicity and chance of bubble attachment.

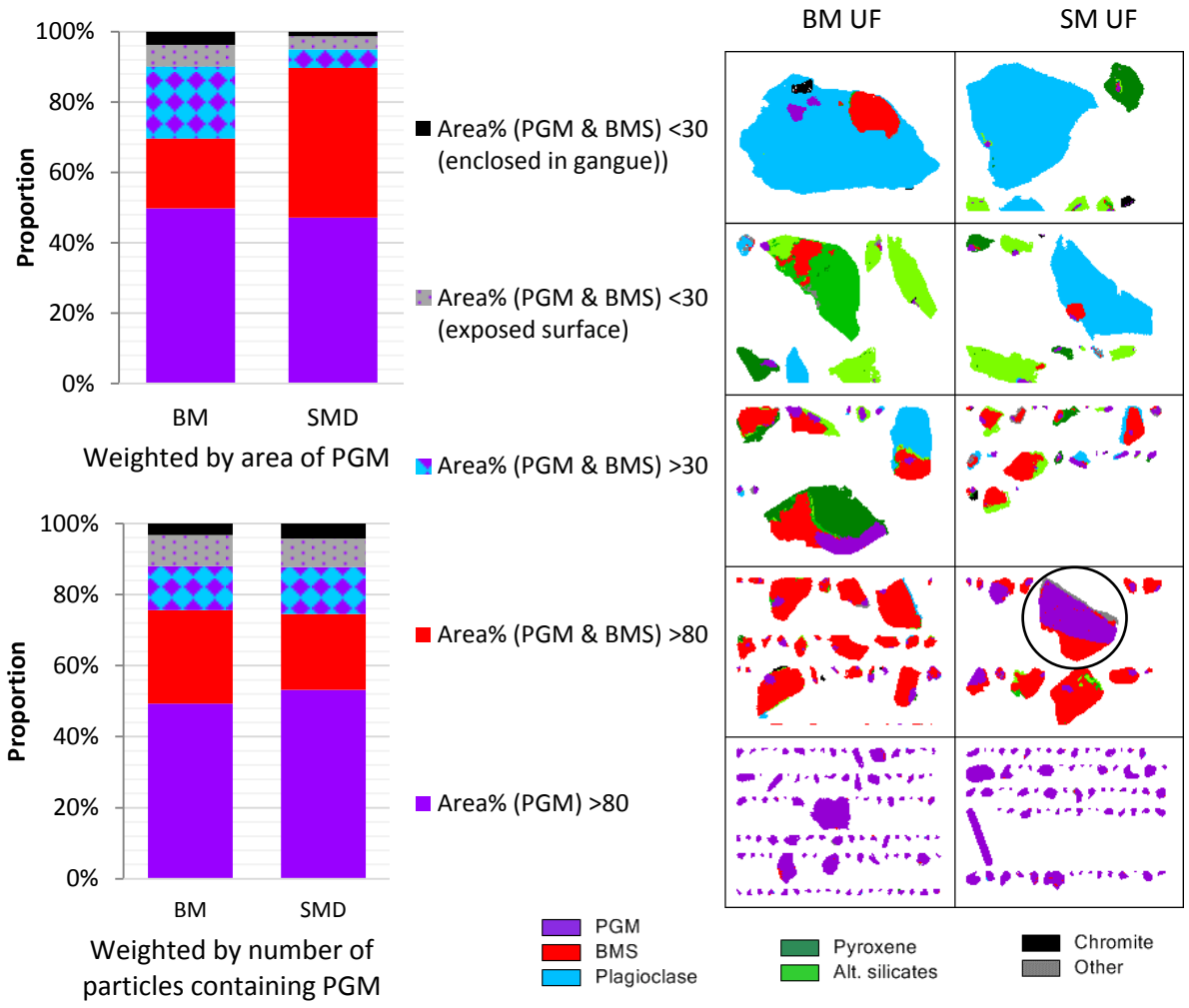

Figure 6.9: PGM liberation and associations for the laboratory ultra-fine grinds. The circle indicates a large PGM grain associated with BMS, which caused the large apparent difference between the area-weighted proportions of PGMs associated with BMS. BM UF: n = 217, SMD UF: n = 188.

The categories presented in Figure 6.9 are based on the combined fractional area of PGM and BMS, although all particles considered contain one or more PGM grains. The two bar charts

show the difference in the deportment of PGM within these categories depending on whether the proportions are weighted according to the area of PGM, or the number of particles containing PGM.

The liberation characteristics of the BMS are reported in Figure 6.10, weighted by area of BMS, with the liberation categories based on fractional area of BMS. This analysis is for all BMS grains, not only those that are associated with PGM.

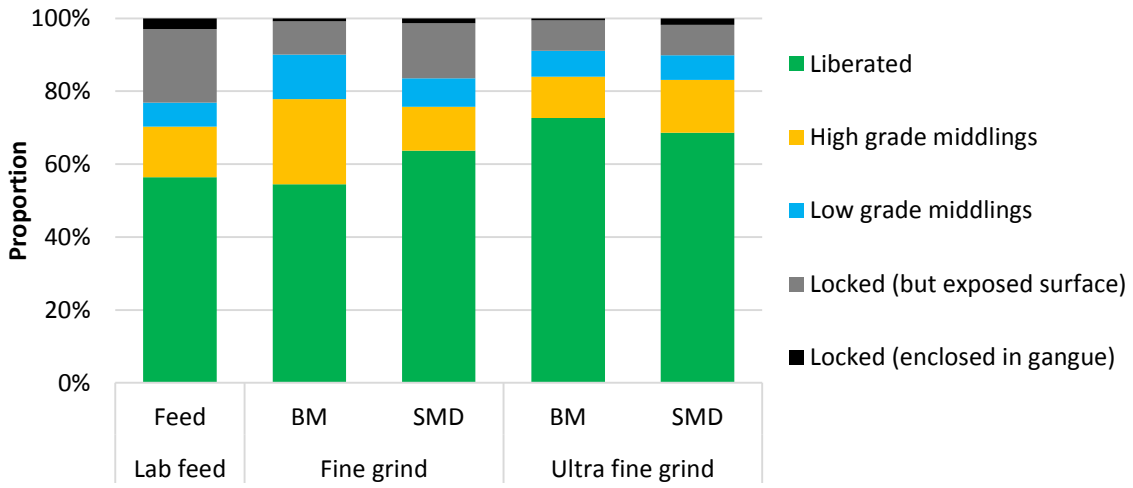

Figure 6.10: BMS liberation for the laboratory feed, fine and ultra-fine grinds of the two mill types.

In Figure 6.9, the stirred mill ultrafine grind initially appears to have a considerably higher combined PGM – BMS liberation than the ball mill, however when considering the contribution of one or two large grains to the area-based statistics, it is evident that this difference would not be statistically significant. This is reinforced by the similarity between the proportions in each category based on number of particles containing PGMs. Larger numbers of particles would be preferable to provide a higher level of confidence in PGM liberation data, but finding PGM grains in feed samples with PGE grades of 4 g/t requires extended periods of machine time, so 100 grains are generally used to provide an indication of liberation characteristics (Becker et al., 2008; Solomon et al., 2011). The BMS liberation data are likely to have less associated uncertainty due to the higher abundance of BMS grains relative to PGMs. The degree of association between PGM and BMS in UG2 ore can vary significantly (Penberthy, 2001), but for this ore there is a high degree of association between PGM and BMS which is evident in Figure 6.9.

Based on the fine BMS grain size distribution (Penberthy, 2001), the liberation of BMS in the coarse laboratory feed sample would be expected to be much lower than what was observed. With a reduction ratio of approximately 10, grinding to a product size distribution similar to the

BMS grain size distribution, a more pronounced increase in liberation after grinding would then be expected. This is an indication of the major role played by phase boundary fracture during primary grinding leading to early liberation of the base metal sulfides, a phenomenon explored by Little et al. (2016, Paper 2). The same phenomenon has a significant impact on PGM liberation, as values similar to those observed for the ultra-fine grinds in Figure 6.9 have been reported at a coarse grind comparable to the laboratory feed. Chetty et al. (2009) analysed 4513 PGM grains from samples of the primary rougher feed with a grind of 40% passing 75 µm. 50% of PGM (by area) was liberated, and 10% was associated with base metal sulfides in composites. This suggests that the ore texture and the strength of phase boundaries between mineral grains have a greater impact on valuable mineral liberation than the mechanisms through which energy is imparted to the particles, which is in agreement with observations of Vizcarra et al. (2010) and Napier-Munn (2014).

6.4 Discussion

6.4.1 Particle shape and mineral liberation: Insight into breakage mechanisms

In many studies, differences in progeny shape characteristics are attributed to the degree of abrasion, with more rounded particles indicative of a greater proportion of abrasion - chipping away topographical features having a smoothening effect (Cleary and Morrison, 2016; Kaya et al., 2002; Pourghahramani, 2012; Roufail, 2011; Vizcarra et al., 2011b; Ye et al., 2010).

Kaya et al. (2002) milled samples of coal and quartz in a variety of mill types, concluding that shape is controlled by the nature of the ore, the type of comminution device and the time spent in the grinding device. They observed that high energy devices yield products with a high portion of newly created, irregular particles, while low energy devices with a repeated breakage action and prolonged exposure to the grinding environment leads to more rounded particles. Based on this logic, and the illustration in Figure 6.1, the high energy intensity stirred mill with less than one tenth of the grinding time of the ball mill would have more angular progeny than the ball mill.

On the other hand, Sinnott et al. (2006) used DEM simulations to investigate energy dissipation in two vertical stirred mills considering energy dissipation in terms of contributions of shear and normal contacts. For both the pin mill and tower mill (with helical screw impeller), they concluded that “the average rate of shear energy absorption is about a factor of three higher than for the normal energies, indicating that comminution is dominated by attrition and abrasion” (Sinnott et al., 2006: 1549). This conclusion is dependent on a definition of attrition and abrasion relating to a shear based grinding action rather than the definition based on the gradual erosion of the particle surface (Gao and Forssberg, 1995). In low energy intensity

stirred mills such as the Tower mill, the lack of distinction between the two definitions is perhaps irrelevant. However, in high intensity mills such as the SMD, the shear-induced stresses within the particles may be adequate to cause massive fracture rather than localised fracture (gradual erosion). In these instances the lack of distinction between the two definitions of abrasion can be misleading (Resabel et al., 2014).

Nevertheless, based on the literature both the extended grinding time in the ball mill and the high shear environment in the stirred mill would be expected to lead to a significant degree of abrasion (gradual erosion of particles) within both mill types. However, the laboratory feed has the most rounded particles, nearly all of which are chromite grains that were liberated from the silicate matrix by phase boundary fracture (Little et al., 2016, Paper 2). The decrease in proportion of rounded particles during grinding in both the ball mill and stirred mill indicates that most progeny particles are produced by complete fracture of the mother particles, with minimal evidence of the abrasion mechanism as defined by Gao and Forssberg (1995). Initially-rounded chromite grains break into smooth sharp fragments of chromite, rather than experiencing a gradual erosion of the grains' surfaces leading to smaller rounded grains with a bimodal size distribution. As the -75/+53 μm fraction is effectively the top size fraction of the laboratory mill products, this is the size range where evidence of an abrasion-dominated grinding environment would be expected in the form of a significant proportion of rounded particles. Hogg (1999) describes the occurrence of attrition (abrasion) as due to small stresses which only exceed a critical value locally, i.e. at the edges of a particle. The apparent increase in particle strength with decreasing particle size has been explained as due to fewer flaws and micro-cracks (Gao and Forssberg, 1995, 1989; King, 2001). This reasoning could also be applied to explain the high angularity of fine particles as fewer flaws and micro-cracks (and grain boundaries) would lead to less local weaknesses on the surfaces of fine particles. Small stresses would then be less likely to exceed a critical value locally, so only stresses with sufficient energy to cause massive fracture would be effective.

Although there is minimal evidence of the conventionally defined abrasion mechanism in both fine grinding devices, there is a difference in the progeny shape characteristics between the two mill products at the laboratory scale. This is likely due to differences in the degree of normally applied impact or compression forces and tangential shear forces, with impact producing more elongated fragments in the ball mill, and shear leading to breakage of any elongated fragments to more equant fragments in the stirred mill. The apparent increase in progeny elongation with time in the ball mill was an unexpected observation. To explore this further, data from a previous study by Khonthu (2012) with a similar UG2 ore sample in the same laboratory mill were considered. Ceramic grinding media were also used in these tests, which were for shorter

grinding periods than those used in this study. Khonthu's QEMSCAN data were re-evaluated to obtain roundness distributions for comparison with those from this study, which are presented in Figure 6.11. This suggests that there is a trend of increasing particle elongation with increased grinding time in the ball mill, for the -75/+53 µm size fraction. This is difficult to explain, as coarse elongated or flaky particles would be expected to be weaker than more compact rounded particles, and thus more likely to break with increased grinding time. However, Bbosa et al. (2006) used the split Hopkinson pressure bar to investigate the energy absorbed by different particle types under impact loading, and showed that rounded particles had a greater probability of fracture than angular particles because they absorb more energy for a given loading.

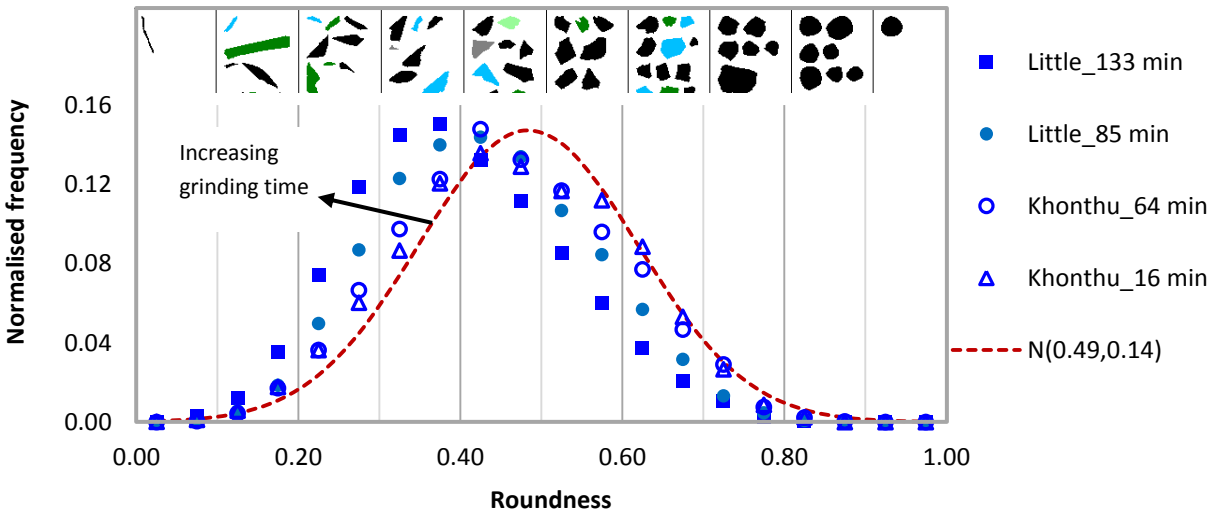

Figure 6.11: The effect of grinding time in the ball mill on product roundness distribution in the -75/+53 µm fraction.

The findings from the plant samples do not directly support the laboratory scale investigation, although neither are they contradictory. The shape characteristics of the ore going into the plant-scale ball mill and IsaMill, and coming out of the IsaMill are very similar, and these are close to the shape characteristics of particles in the laboratory feed, as well as progeny from the laboratory stirred mill. Although fine and ultra-fine grinding in the laboratory ball mill led to more elongated particles, Figure 6.11 suggests that shorter milling times in the laboratory ball mill produces progeny with shape characteristics more similar to those of the plant samples.

In general, there was only minor variation in both particle shape and mineral liberation between the two mill products at similar grinds. This suggests that in the case of UG2 ore, particle shape is predominantly a function of ore texture, with liberated grains of individual

minerals breaking into particles with similar shape distributions in both stirred mills and ball mills.

6.5 Conclusions

The large difference in energy intensity between the two types of milling devices does not severely impact the progeny shape characteristics. The exception to this observation was the laboratory ball mill progeny in the top size fraction of the product, which became more elongated with increasing grinding time in the batch laboratory mill. The same trend was not evident in the finer size fractions. The product particles from both fine grinding devices were either similar or more angular than the feed particles, with very small proportions of rounded grains. The term 'abrasion' associated with the mechanism through which large particles in an autogenous mill become more rounded, has connotations that may be misleading when applied to fine grinding. That is to say, that if breakage is caused by shear, one cannot infer that the dominant breakage mechanism will involve gradual erosion of particles, with localised breakage on particle edges.

In the case of UG2 ore, both particle shape and liberation are mostly controlled by the ore properties, particularly the texture. Analysis of texture, shape and liberation are important to characterize the relationship between energy input, particle size distribution and liberation, in order to fully utilise the benefits of early liberation and reduce operating costs. The findings of this work suggest that at the plant-scale, UG2 ore particle shape characteristics within any particular size class are not significantly affected by grinding in an open circuit ball mill or stirred mill. This may be of interest for operators of UG2 ore concentrators with a ball mill and optional IsaMill grinding stage prior to secondary rougher flotation. Differences in flotation circuit performance when the IsaMill is on- or off-line, are unlikely to be attributable to effects of particle shape.

6.6 Acknowledgements

This work is based on research supported in part by the National Research Foundation of South Africa (Grant Number 86054). Any opinions, findings and conclusions or recommendations expressed in any publication generated by the NRF supported research is that of the author(s), and the NRF accepts no liability whatsoever in this regard. The authors would like to acknowledge the South African Minerals to Metals Research Institute (SAMMRI) and the South African Department of Science and Technology for funding the work.

6.7 References

Bbosa, L., Powell, M.S., Cloete, T.J., 2006. An investigation of impact breakage of rocks using the split Hopkinson pressure bar. J. South African Inst. Min. Metall. 106, 291–296.

Becker, M., Mainza, A.N., Powell, M.S., Bradshaw, D.J., Knopjes, B., 2008. Quantifying the influence of classification with the 3 product cyclone on liberation and recovery of PGMs in UG2 ore. Miner. Eng. 21, 549–558. doi:10.1016/j.mineng.2007.11.001

Chetty, D., Gryffenberg, L., Lekgetho, T.B., Molebale, I.J., 2009. Automated SEM study of PGM distribution across a UG2 flotation concentrate bank: Implications for understanding PGM floatability. J. South. African Inst. Min. Metall. 109, 587–593.

Cleary, P.W., Morrison, R.D., 2016. Comminution mechanisms, particle shape evolution and collision energy partitioning in tumbling mills. Miner. Eng. 86, 75–95. doi:10.1016/j.mineng.2015.12.006

Cleary, P.W., Sinnott, M., Morrison, R., 2006. Analysis of stirred mill performance using DEM simulation: Part 2 – Coherent flow structures, liner stress and wear, mixing and transport. Miner. Eng. 19, 1551–1572. doi:10.1016/j.mineng.2006.08.013

Frances, C., Le Bolay, N., Belaroui, K., Pons, M.-N., 2001. Particle morphology of ground gibbsite in different grinding environments. Int. J. Miner. Process. 61, 41–56. doi:10.1016/S0301-7516(00)00025-9

Gao, M., Forssberg, E., 1995. Prediction of product size distributions for a stirred ball mill. Powder Technol. 84, 101–106.

Gao, M.W., Forssberg, E., 1989. The effect of powder filling on selection and breakage functions in batch grinding. Powder Technol. 59, 275–283. doi:10.1016/0032-5910(89)80086-5

Gu, Y., Schouwstra, R.P., Rule, C., 2014. The value of automated mineralogy. Miner. Eng. 58, 100–103. doi:10.1016/j.mineng.2014.01.020

Guven, O., Çelik, M.S., 2015. Can roughness of particles be tuned to reach maximum flotation recoveries?, in: MEI Flotation '15. Cape Town.

Hay, M.P., Roy, R., 2010. A case study of optimising UG2 flotation performance. Part 1: Bench, pilot and plant scale factors which influence Cr2O3 entrainment in UG2 flotation. Miner. Eng. 23, 855–867. doi:10.1016/j.mineng.2010.05.002

Hogg, R., 1999. Breakage mechanisms and mill performance in ultrafine grinding. Powder Technol. 105, 135–140.

Hoşten, Ç., Özbay, C., 1998. A comparison of particle bed breakage and rod mill grinding with regard to mineral liberation and particle shape effects. Miner. Eng. 11, 871–874. doi:10.1016/S0892-6875(98)00074-0

Jankovic, A., 2003. Variables affecting the fine grinding of minerals using stirred mills. Miner. Eng. 16, 337–345. doi:10.1016/S0892-6875(03)00007-4

Kaya, E., Hogg, R., Kumar, S.R., 2002. Particle Shape Modification in Comminution. KONA 20, 188–195.

Khonthu, T., 2012. Investigation of the flotation behaviour of ball mill and IsaMill products. University of Cape Town.

King, R.P., 2001. Modeling & Simulation of Mineral Processing. Butterworth-Heinemann, Oxford.

Little, L., Becker, M., Wiese, J., Mainza, A.N., 2015. Auto-SEM particle shape characterisation: Investigating fine grinding of UG2 ore. Miner. Eng. 82, 92–100. doi:10.1016/j.mineng.2015.03.021

Little, L., Mainza, A.N., Wiese, J.G., Becker, M., 2016. Using mineralogical and particle shape analysis to investigate enhanced mineral liberation through phase boundary fracture. Powder Technol. 301, 794-804. Doi:10.1016/j.potec.2016.06.05

Mudd, G.M., 2012. Key trends in the resource sustainability of platinum group elements. Ore Geol. Rev. 46, 106–117. doi:10.1016/j.oregeorev.2012.02.005

Napier-Munn, T., 2014. Is progress in energy-efficient comminution doomed? Miner. Eng. Article in. doi:10.1016/j.mineng.2014.06.009

Nel, E., Theron, J., Martin, C., Raabe, H., 2004. PGM Ore Processing at Impala's UG-2 Concentrator in Rustenburg, South Africa. SGS Mineral Services.

Palaniandy, S., Azizli, K.A.M., Hussin, H., Hashim, S.F.S., 2008. Effect of operational parameters on the breakage mechanism of silica in a jet mill. Miner. Eng. 21, 380–388. doi:10.1016/j.mineng.2007.10.011

Penberthy, C.J., 2001. The effect of mineralogical variation in the UG2 chromitite on recovery of platinum-group elements. University of Pretoria.

Pourghahramani, P., 2012. Effects of ore characteristics on product shape properties and breakage mechanisms in industrial SAG mills. Miner. Eng. 32, 30–37. doi:10.1016/j.mineng.2012.03.005

Radziszewski, P., 2013. Assessing the stirred mill design space. Miner. Eng. 41, 9–16. doi:10.1016/j.mineng.2012.10.012

Rahimi, M., Dehghani, F., Rezai, B., Aslani, M.R., 2012. Influence of the roughness and shape of quartz particles on their flotation kinetics. Int. J. Miner. Metall. Mater. 19, 284–289. doi:10.1007/s12613-012-0552-z

Resabel, V.J., 2014. A method using 2-D images obtained from SEM-based image analysis system to model mineral liberation in regrind stirred mills, in: MEI Process Mineralogy '14. Cape Town.

Roufail, R.A., 2011. The effect of stirred mill operation on particles breakage mechanism and their morphological features. The University of British Columbia.

Rule, C., 2010. Stirred milling — new comminution technology in the PGM industry, in: The 4th International Platinum Conference, Platinum in Transition "Boom or Bust." pp. 71–78.

Rule, C., 2011. Stirred milling at Anglo American Platinum, in: International Conference on Autogenous Grinding, Semiautogenous Grinding and High Pressure Grinding Roll Technology.

Rule, C., Schouwstra, R.P., 2011. Process mineralogy delivering significant value at Anglo Platinum concentrator operations, in: 10th International Congress for Applied Mineralogy. Trondheim, pp. 1–5.

Sinnott, M., Cleary, P.W., Morrison, R., 2006. Analysis of stirred mill performance using DEM simulation: Part 1 – Media motion, energy consumption and collisional environment. Miner. Eng. 19, 1537–1550. doi:10.1016/j.mineng.2006.08.012

Solomon, N., Becker, M., Mainza, A., Petersen, J., Franzidis, J.-P., 2011. Understanding the influence of HPGR on PGM flotation behavior using mineralogy. Miner. Eng. 24, 1370–1377. doi:10.1016/j.mineng.2011.07.015

Tavares, L.M., 2009. Analysis of particle fracture by repeated stressing as damage accumulation. Powder Technol. 190, 327–339. doi:10.1016/j.powtec.2008.08.011

Ulusoy, U., Yekeler, M., Hiçyılmaz, C., 2003. Determination of the shape, morphological and wettability properties of quartz and their correlations. Miner. Eng. 16, 951–964. doi:10.1016/j.mineng.2003.07.002

Varinot, C., Hiltgun, S., Pons, M.-N., Dodds, J., 1997. Identification of the fragmentation mechanisms in wet-phase fine grinding in a stirred bead mill. Chem. Eng. Sci. 52, 3605–3612.

Vizcarra, T.G., Wightman, E.M., Johnson, N.W., Manlapig, E.V., 2010. The effect of breakage mechanism on the mineral liberation properties of sulphide ores. Miner. Eng. 23, 374–382. doi:10.1016/j.mineng.2009.11.012

Vizcarra, T.G., Wightman, E.M., Johnson, N.W., Manlapig, E.V., 2011. The effect of breakage method on the shape properties of an iron-oxide hosted copper–gold ore. Miner. Eng. 24, 1454–1458. doi:10.1016/j.mineng.2011.07.007

Weerasekara, N.S., Powell, M.S., Cleary, P.W., Tavares, L.M., Evertsson, M., Morrison, R.D., Quist, J., Carvalho, R.M., 2013. The contribution of DEM to the science of comminution. Powder Technol. 248, 3–4. doi:10.1016/j.powtec.2013.05.032

Wills, B.A., Napier-Munn, T., 2006. Wills' Mineral Processing Technology, 7th ed. Elsevier Science & Technology Books.

Ye, X., Gredelj, S., Skinner, W., Grano, S.R., 2010. Regrinding sulphide minerals — Breakage mechanisms in milling and their influence on surface properties and flotation behaviour. Powder Technol. 203, 133–147. doi:10.1016/j.powtec.2010.05.002

Paper 5: Investigating the effects of particle shape on chromite entrainment at a platinum concentrator

Little, L., Wiese, J., Becker M., Mainza, A. N., Ross, V., 2016. Minerals Engineering. Article in press.

Keywords: Entrainment, particle shape

Abstract

In flotation, entrainment is undesirable as it results in the recovery of hydrophilic gangue particles which reduces the concentrate grade. For UG2 ore, a South African platinum group mineral (PGM) ore, entrainment is particularly problematic because it leads to the recovery of chromite in the final concentrate which can cause severe problems in the smelter. It is therefore important to understand all factors affecting entrainment. These factors include froth characteristics, as well as particle size distribution and density, which have been studied widely. Theoretically, they should also include shape, as shape affects drag coefficients of particles and thus hindered settling rates of particles within plateau borders. In this study, detailed mineral-specific shape characterisation with Quantitative Evaluation of Minerals by Scanning Electron Microscopy (QEMSCAN) was used to assess the effect of particle shape on chromite entrainment during flotation of UG2 ore at a South African platinum concentrator. This plant-scale study suggests that shape does affect entrainment, with more rounded particles showing higher entrainment than angular, elongated particles.

6.8 Introduction

The Upper Group 2 chromitite ore (UG2), from the Bushveld Complex in South Africa accounts for 40% of global platinum group element (PGE) reserves (Mudd, 2012). The run of mine ore contains 50 – 80% chromite ($FeCr_2O_4$). Following flotation, the concentrate is sent for further smelting and refining to produce the valuable PGE metal. Given the detrimental effects of high spinel (chromite) in the smelter, a practical upper limit of 2.5% Cr_2O_3 is usually imposed on concentrate quality (Hay and Roy, 2010). The issue of chromite entrainment to the concentrate, has led to particular interest in understanding chromite recovery by entrainment and methods to reduce this (Alvarez-Silva et al., 2014; Eksteen et al., 2011; Hay and Roy, 2010; Hay, 2010; Jones and Geldenhuys, 2011; Jones, 2005; Leroy et al., 2011; McFadzean et al., 2015; Wesseldijk et al., 1999). Entrainment is widely accepted to be the dominant mechanism of chromite recovery during UG2 ore flotation, particularly in the size range below 45 μm.

Entrainment is a non-selective physical process through which fine particles are transported into the froth and recovered in the flotation concentrate. Wang et al. (2015) provide a review of the literature on flotation entrainment, describing the various mechanisms of interest, and both theoretical and empirical models that have been developed to predict/simulate entrainment. There is a direct relationship between entrainment and water recovery, which is mostly dependent on froth characteristics, and is a key parameter in most models. Apart from factors that affect froth characteristics, there are those that affect drainage within the plateau borders. Particle mass, i.e. size and density, has a significant effect, and is accounted for in most recent models. Theoretically, particle shape should also have an effect, but it is not incorporated in most models. The theory behind particle and fluid flow within the plateau borders has been explored by Neethling and Cilliers (2009, 2002), who considered effects of both dispersion and hindered settling.

Although the effect of particle shape on flotation has been studied in various fundamental studies (Koh et al., 2009; Rahimi et al., 2012; Verrelli et al., 2012a, 2014; Vizcarra et al., 2011a) the effect on entrainment has received little attention, with previous batch flotation test work producing contradictory results (van de Ruit et al., 2014; Kirjavainen, 1996, 1992; Wiese et al., 2015). Kirjavainen (1992) and Wiese et al. (2015) used a similar approach, comparing entrainment rates of pure hydrophilic minerals with different shape characteristics in laboratory flotation experiments. Kirjavainen (1992) compared entrainment rates of quartz and mica, with mica showing the higher degree of entrainment. He developed an empirical model incorporating shape factor, particle mass, water recovery and slurry viscosity which fitted his laboratory experimental data well, but was not validated with additional data. Kirjavainen used the dynamic shape factor and Wadell's sphericity factor, based on the modal volume diameter

and modal Stokes diameter of each sample. These were measured with Coulter analysis and gravitational sedimentation respectively. This does have the benefit of being a 3-D shape characterisation approach, but attempting to decouple effects of size and shape would be difficult with this method. Wiese et al. (2015) compared entrainment of ballotini, mica, talc, vermiculite and wollastonite, with the elongated wollastonite showing significantly higher solids per unit water recovered than the other minerals. The small difference between the mica and ballotini was not consistent with Kirjavainen's model and observations. In previous work, the authors of the current study - van de Ruit et al., (2014) - used a different approach to Kirjavainen and Wiese comparing shape distributions of hydrophilic chromite particles within feed and concentrate samples of laboratory flotation tests with UG2 ore. The work suggested that the shape characteristics of particles within a flotation feed did not affect the likelihood of entrainment of those particles. However, for all three of these laboratory based studies, the possibility exists that the shallow froths are not a realistic representation of industrial flotation. This led to the consideration of an industrial scale flotation operation with deep froths and multiple flotation stages for this work.

One of the likely reasons why the effect of particle shape on entrainment has received such minimal attention is the scarcity of appropriate methods for quantifying the shape of fine particulate samples below 75 μm (Varinot et al., 1997). Indirect 3-D methods such as that used by Kirjavainen (1992) are limiting in that one can only obtain an average shape factor for a sample, which "has been shown to be an ineffective approach" (International Organisation for Standardisation, 2008: 1). Micro- and nano-X-CT has the potential to be useful for such studies, but the technology is not widely available, and has other practical limitations (Vonlanthen et al., 2015). 2-D shape characterisation methods based on dynamic image analysis are applied more widely (Ulusoy and Igathinathane, 2014; Ulusoy and Yekeler, 2014; Westermann, n.d.), however these do not have sufficiently high resolution for accurate measurement of particles below 53 μm. Auto-SEM EDS has a higher resolution than camera based devices, and shape information can be considered as a by-product of routine mineralogical analyses carried out with these devices.

In the ISO standard for quantitative representation of shape, it is acknowledged that problems of shape and morphology are typically 3-D problems, as is the case for the problem of entrainment, however most of the document is based on 2-D analysis due to the widespread use of image analysis methods (International Organisation for Standardisation, 2008). 2-D shape characterisation does have limitations relating to stereology – a particle that appears round in 2-D may be a rod, and a particle appearing to be needle-shaped may be a flake. However, the benefit of 2-D analysis is that shape descriptors can be measured for thousands of particles in a

sample, which enables the presentation of shape characteristics as a distribution. This is particularly appropriate for mineral samples containing irregular particles with a wide range of shape characteristics. Furthermore, provided that the orientation of the particles being measured is random, the 2-D distribution measured will be highly reproducible. This, along with issues relating to resolution and uncertainty was addressed by Little et al. (2015, Paper 1).

This work uses a novel approach to assess the effects of particle shape on entrainment at an industrial scale. Observations based on this study alone are unlikely to produce generalizable conclusions, but if the methodology is applied more widely, this study could make a significant contribution towards closing the gap in understanding relating to effects of particle shape on entrainment in flotation.

6.9 Methodology

For this investigation, samples were taken from a 150 t/h flotation circuit at a South African UG2 ore concentrator. A simplified flow diagram of the circuit is provided in Figure 6.12. The streams selected for sampling included the Primary Rougher Feed (PRF), High Grade re-cleaner Concentrate (HGC), Low Grade re-cleaner Concentrate, Primary Rougher Tails (PRT), and Secondary Rougher Tails (SRT). The rationale for the selection was to take a black-box approach and determine whether there was a significant overall effect of shape on entrainment.

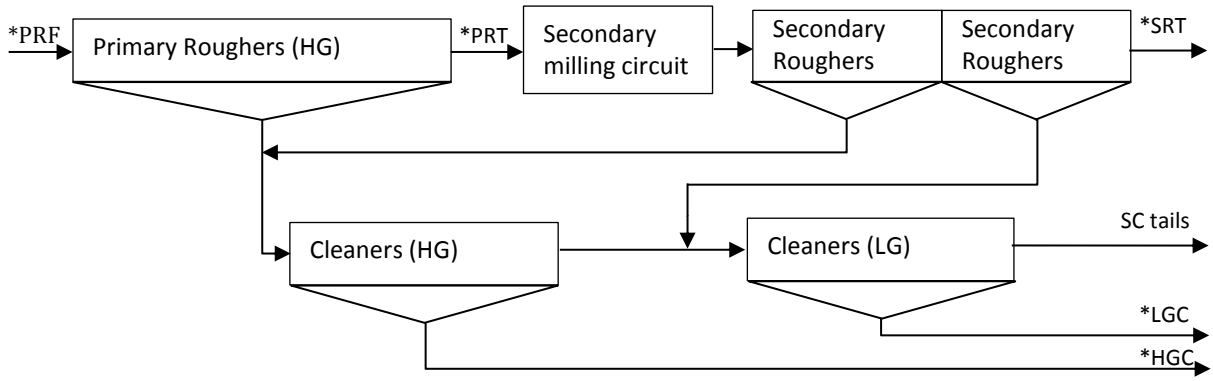

*Figure 6.12: Simplified flow diagram of the flotation circuit investigated – precise feed points and recycles within the cleaning circuit are not shown. *Samples collected.*

The plant had an effective level control system, with set points for froth depths varying from 14 cm – 20 cm for rougher cells and 20 cm – 25 cm for cleaner cells, depending on the variation of conditions with position throughout the circuit. During sampling, the control system indicated that the operating points (relating to the flotation circuit) were close to the set points, and the circuit was stable, indicating that it was at steady-state. The plant targets an overall mass pull of 0.35% for the high grade concentrate and 0.8% for the low grade concentrate, which were used

to estimate the HGC and LGC solids recoveries respectively. These were also used along with the measured slurry densities from the samples to estimate water recoveries.

This was considered to be an exploratory study, with no direct financial impact, and no major risk associated with the findings. Furthermore, the work focuses on the shape of chromite particles, and chromite is a major phase in the ore, and thus it is not likely to demonstrate significant variability over short time periods. Based on the fine particle size, the high chromite grade, and roundness distributions for both the feed and concentrate samples, it was estimated using two approaches outlined by Napier-Munn, (2015, pp. 544-555), that only 700 mg of sample would be sufficient to have a 95% confidence of +/-1% relative error in the portion of chromite with a roundness greater than 0.6, in the -25/+10 μm size fraction. For these reasons, coupled with the stable operating performance of the plant, a rigorous sampling campaign did not seem justifiable, and grab samples were deemed sufficient for the purpose of this study. From the excellent agreement of the chromite shape distributions presented in the results section, this sampling approach was adequate.

Although sample variability with time was not considered to be a major source of error, the potential for segregation within a pipe due to density and particle shape was considered. The primary rougher feed, secondary rougher tails and concentrate samples were taken with the automated representative sample-cutters used for metal accounting, set on manual. The primary rougher tailing sample was taken with a pelican sample-cutter. Approximately 7 kg of each sample was collected, which is well above Gy's safety line. Each sample was dried and split into 300 g aliquots using a rotary splitter. Each of these was screened to obtain the particle size distribution (PSD) using a $\sqrt{2}$ sieve series. Screening at 10 μm was carried out with a 30 cm x 40 cm filter cloth in an ultrasonic bath, rinsing with approximately 30 L of water over a period of 3 hours. Based on the PSDs, the following size fractions were selected for assay (ICP-OES for Cr and Si) and auto-SEM-EDS (QEMSCAN) analysis: -106/+53 μm; -53/+25 μm; -25/+10 μm; and -10 μm. As 106 μm was the top size of the concentrate samples, the +106 μm fractions of the feed and tails were not included in the entrainment analysis, and were only sent for chromite assay for the entrainment mass balance.

Blocks for QEMSCAN were prepared as vertical sections for measurement with the Particle Mineral Analysis (PMA) setting on a FEG QEMSCAN 650F. Close to 10 000 chromite particles were analysed for the concentrates, and over 30 000 chromite particles for the feeds and tails samples. The QEMSCAN software, iDiscover®, was then used to filter particle images according to size, mineral type, and the shape descriptor 'roundness', which is defined in Equation 6.2. Fe_{max} is the maximum Feret diameter.

$$Roundness = \frac{4 \cdot Area}{\pi \cdot {Fe_{max}}^2} \qquad 6.2$$

Roundness distributions of chromite particles reporting to concentrate and tails samples were then compared for equivalent, narrow size fractions. The shape characterisation methodology applied is described in more detail by Little et al. (2015, Paper 1), in which it was demonstrated that there was no preferential orientation of particles within the QEMSCAN blocks leading to significant bias of the 2-D measurements. i.e. particles were found to be randomly oriented. It was also shown that the descriptor roundness is not dependent on image resolution in the manner of perimeter-dependent shape descriptors.

6.10 Results and Discussion

6.10.1 The effect of particle size on entrainment

In earlier work, particle size was identified as a key confounding variable in determining the effect of shape on entrainment (van de Ruit et al., 2014). The first step in this analysis was therefore to consider the effect of particle size on entrainment. The approach used will also be useful to illustrate the principle applied to particle shape in Section 6.10.2. Particle size distributions for the five streams investigated are provided in Figure 6.13.

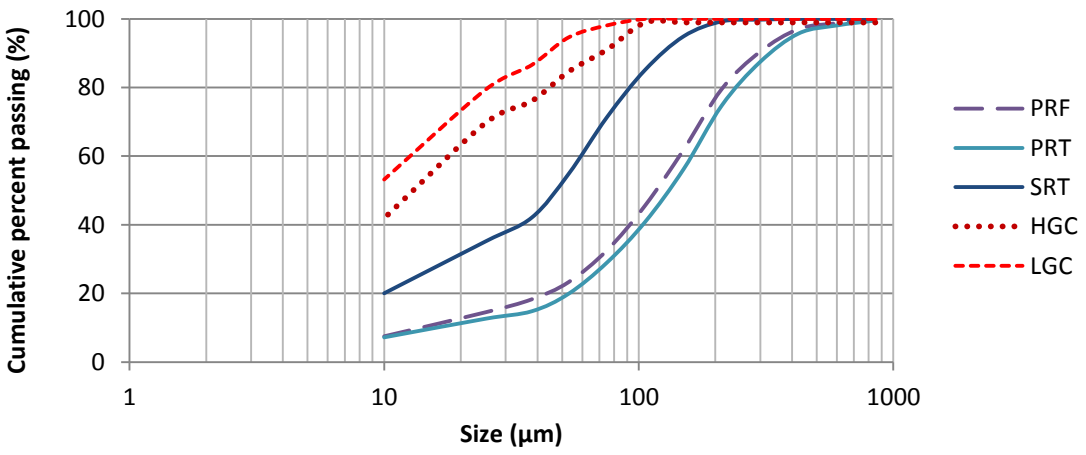

Figure 6.13: Particle size distributions obtained by screening for the various samples investigated.

The concentrates are shown to have significantly finer distributions than the feed and tails samples indicative of an effect of size on both liberation and recovery by true flotation, as well as recovery by entrainment. Dividing the continuous distribution into discrete size classes enables the calculation of an entrainment factor for each size class, as demonstrated by Yianatos

et al. (2008). The definition for the size dependent entrainment factor (EF_i) is shown in Equation 6.3, where RG_i is the recovery of gangue in size class *i*, and R_w is the water recovery.

$$EF_i = \frac{R_{Gi}}{R_w} \quad 6.3$$

Tables 6.5 (a) and (b) show the data used to calculate EF_i for the high grade and low grade concentrates. The results are shown in Figure 6.14. Entrainment factors were estimated based on chromite recovered to the concentrates relative to the secondary rougher tails. This was because a full mass balance indicating the relative proportions of chromite recovered in the primary and secondary roughers was not available, so it is assumed that the bulk of the entrainment occurs in the secondary roughers due to the much finer grind size.

Table 6.5(a): Generic data and parameters used to calculate EF_i.

	Units	**SRT**	**HGC**	**LGC**
Solids recovery	%	98.85	0.35	0.80
% solids	%	26.85	19.9	8.01
Water recovery (R_w)	%	96.1	0.52	3.41

Table 6.5(b): Fractional data used to calculate EF_i.

	PSD (m_i) %			**Cr_2O_3 grade (x_i) %**			**Cr_2O_3 deportment (x_i*m_i) %**			**EF_i**	
Size class (i)	**SRT**	**HGC**	**LGC**	**SRT**	**HGC**	**LGC**	**SRT**	**HGC**	**LGC**	**HGC**	**LGC**
-106/+53 µm	30	14	5	26.1	1.28	2.24	7.93	0.18	0.12	0.02	0.004
-53/+25 µm	20	15	15	25.1	1.14	1.50	4.92	0.17	0.23	0.02	0.01
-25/+10 µm	15	28	26	25.7	1.40	2.53	3.88	0.39	0.66	0.07	0.04
-10/+0 µm	20	42	53	22.7	3.94	8.00	4.55	1.65	4.26	0.24	0.22

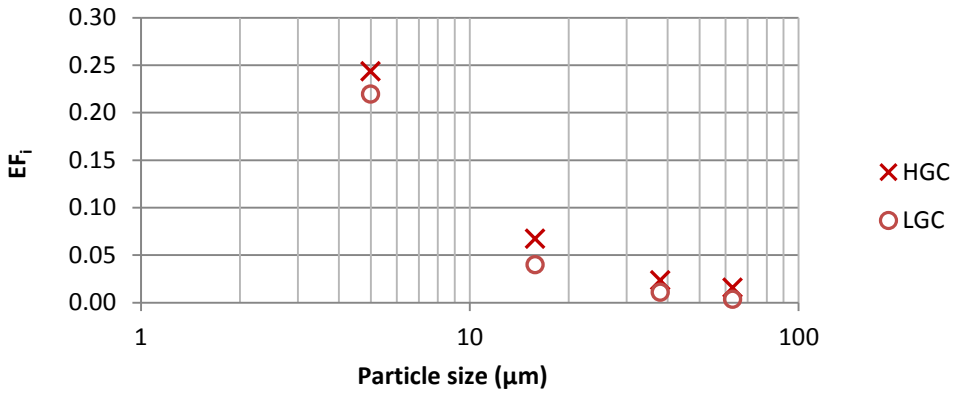

Figure 6.14: The variation of entrainment factor, EF_i with particle size, based on assay data for Cr_2O_3 in four size fractions. Refer to Table 6.5 for data and parameters.

The negative exponential relationship observed between size and entrainment is consistent with other studies (Yianatos and Contreras, 2010; Zheng et al., 2006). Particle size has a large effect on entrainment, with finer particles following the entrained water more easily, and coarser particles with more mass settling under gravity. From this it is apparent that in order to determine the effects of shape on entrainment, independently, the shape distribution of particles in the concentrate should only be compared to particles of the same size in the feed. This was done by initially focusing on an individual screened size fraction (-25/+10 µm) in Section 6.10.2, and then virtually dividing this fraction into considerably narrower size intervals, using the QEMSCAN software, for all five samples (Section 6.10.3).

For the particle shape investigation, results for the -25/+10 µm fraction were selected for analysis, as a size fraction showing a moderate degree of entrainment. The -10 µm fraction with the highest entrainment was not selected for two reasons. Firstly, the entrainment of very fine particles is less likely to be affected by shape than that of slightly larger particles. Secondly, the FEG QEMSCAN used in this study has a maximum resolution of 0.5 µm per pixel, so limitations due to resolution would affect the shape measurements of the finer particles. Although roundness is less dependent on image resolution than some other shape descriptors, roundness distributions appear to be affected by resolution for particles with cross-sectional areas composed of fewer than 30 pixels, equating to an equivalent circle diameter (ECD) of about 3 µm at a 0.5 µm pixel spacing (Little et al., 2015, Paper 1).

Detailed analysis of coarser fractions was not considered for this entrainment study as at these sizes there was a possibility that the contribution of chromite grains being recovered by true flotation would become significant relative to the much lower recovery of chromite by entrainment. This would be possible through association of chromite with naturally floatable gangue or base metal sulfides. However, with a median chromite grain size in the region of 170

µm, and a high degree of phase boundary fracture, most of the chromite below 75 µm is fully liberated, and entrainment is the dominant mechanism of chromite recovery in the case of UG2 ore (Alvarez-Silva et al., 2014; Hay and Roy, 2010). Within the -25 µm fraction the error introduced to this study through inclusion of particles that are not necessarily 100% liberated is therefore not likely to be significant.

The size distributions of chromite within the -25/+10 µm fraction are shown in Figure 6.15. The finer tail of the distribution below 10 µm could be due to a combination of factors, including the difference between screen size and equivalent circle diameter, (i.e. shape effects), screening inefficiencies, and the fact that the 2-D particle cross-sections do not necessarily go through the widest/longest axis of a particle in the third dimension. Although the difference in size distribution between the fractions of the concentrate, feed and tails is significantly reduced, the concentrate samples still have a finer distribution than the feed and tails samples.

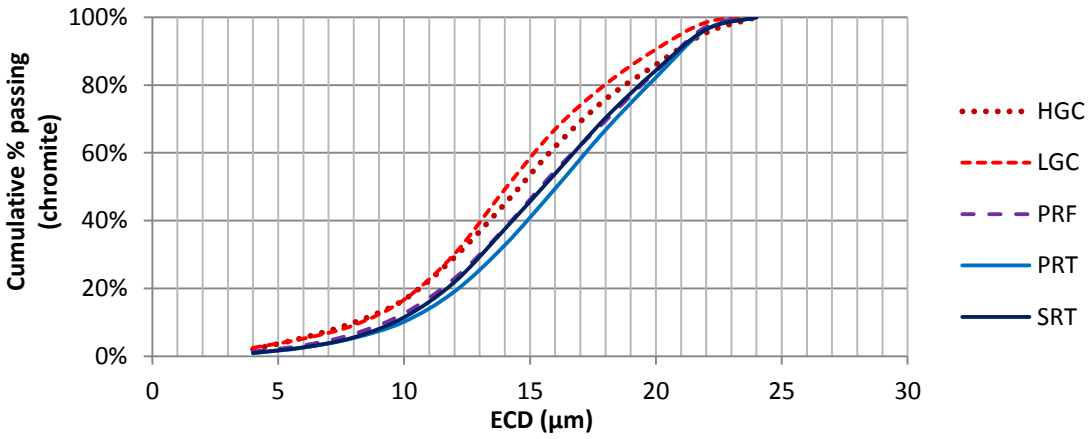

Figure 6.15: Particle size distributions of the chromite grains within the -25/+10 µm fractions from the various samples, used for the particle shape investigation. ECD – Equivalent circle diameter.

6.10.2 The effect of particle shape on entrainment

The roundness frequency distributions (weighted by mass) of liberated chromite within the -25/+10 µm fraction of the various samples collected are presented in Figure 6.16. Some of the sample statistics for the distributions are presented in Table 6.6. The distributions for the feed and two tails samples are very similar, while the distributions for the concentrates are shifted to the right indicating more rounded particles, and fewer angular, elongate particles.

Table 6.6: Sample statistics for chromite particles in the -25/+10 µm size fractions.

	HGC	LGC	PRF	PRT	SRT
No. of particles (n)	8941	12149	30516	32529	39545
Mean roundness	0.489	0.490	0.428	0.434	0.437
Standard deviation	0.132	0.134	0.142	0.144	0.143
Standard error	0.0014	0.0012	0.0008	0.0008	0.0007

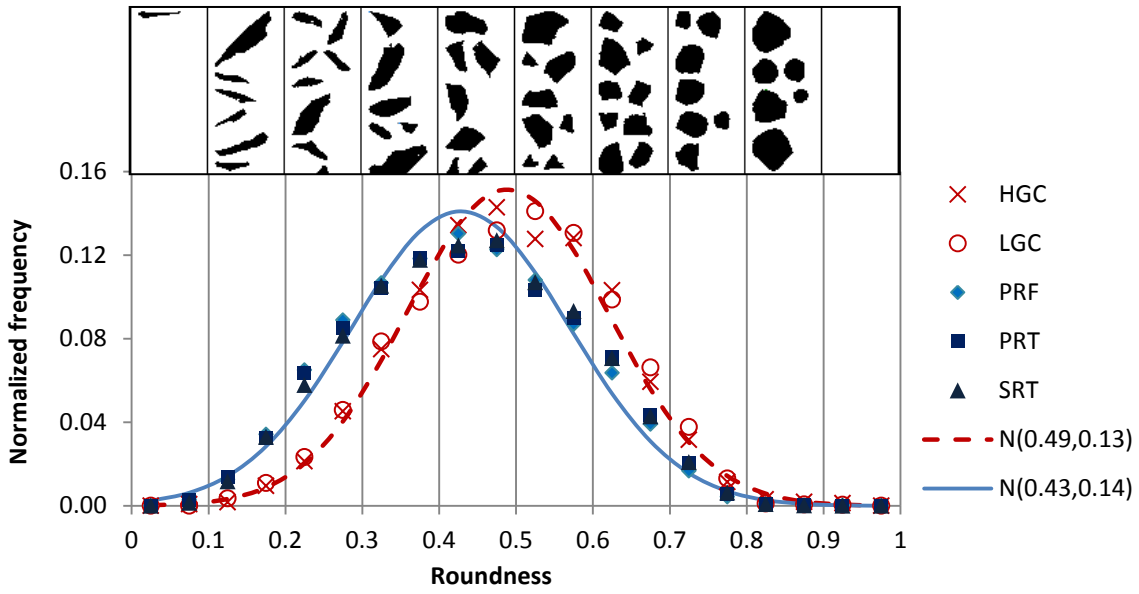

Figure 6.16: Roundness frequency distributions of chromite particles in the -25/+10 µm fractions of feed, concentrate, and tails samples. The upper inset illustrates the variation in roundness of various chromite particles. N (0.49, 0.14) represents a normal distribution with mean of 0.49 and standard deviation of 0.14. See Table 6.6 for more details.

In Section 6.10.1, a continuous size distribution was divided into *i* size classes, and an entrainment factor for each size class (EF_i) was calculated. Similarly, the *roundness* distributions shown in Figure 6.16 can be divided into *j* discrete *roundness* classes, and the entrainment factor for each *roundness* class (EF_{ij}) can be calculated using Equation 6.4. This is demonstrated in Table 6.7, for the -25/+10 size class, with the obtained relationship illustrated in Figure 6.17.

$$EF_{ij} = \frac{R_{Gij}}{R_w} = \frac{m_{cj}}{m_{fj}} \cdot EF_i \qquad 6.4$$

Table 6.7: Fractional data used to calculate EF_{ij}, for i = -25/+10 µm.

Shape class (j)	m_j			EF_{ij}	
	SRT	HGC	LGC	HGC	LGC
0 - 0.2	0.046	0.012	0.014	0.017	0.013
0.2 - 0.3	0.139	0.066	0.069	0.032	0.020
0.3 -0.4	0.223	0.178	0.176	0.054	0.032
0.4 - 0.5	0.251	0.277	0.252	0.074	0.040
0.5 - 0.6	0.200	0.256	0.271	0.086	0.054
0.6 - 0.7	0.113	0.162	0.165	0.096	0.058
0.7 - 1.0	0.028	0.049	0.053	0.118	0.076

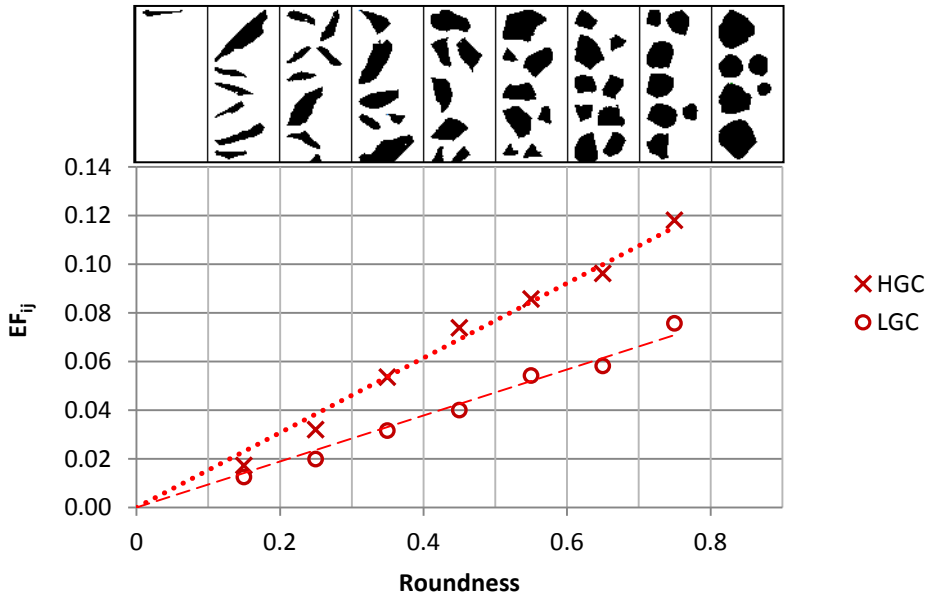

Figure 6.17: The variation of entrainment factor EF_{ij}, with roundness, for i = -25/+10, EF_i = 0.067 and 0.040 for the HGC and LGC respectively.

The relationship between entrainment factor and *roundness* illustrated in Figure 6.17 complements the data presented in Figure 6.16, indicating a linear increase in entrainment factor with increasing *roundness*. A comparison of Figure 6.14 and Figure 6.17 shows that the difference in entrainment between the most irregularly shaped particles and rounded particles within the -25/+10 µm size class, is roughly equivalent to the difference in entrainment between 45 µm particles and 10 µm particles.

This was not the result expected based on the literature (Kirjavainen, 1992; Wiese et al., 2015). Due to the observations presented by van de Ruit et al. (2014), the possibility was considered that this result could have been influenced by the difference in size distributions within the -25/+10 µm size fraction, as was shown in Figure 6.15. Section 6.10.3 aims to eliminate possible

effects due to variation of shape with size, and the possibility that the shape distributions may have been influenced by physical screening in the near-size regions.

6.10.3 Decoupling the effects of size and shape

This analysis relied on the use of a *roundness* categoriser in conjunction with a categoriser for equivalent circle diameter, as well as the use of filters to select 100% liberated chromite particles. The image grid presented in Figure 6.18 illustrates the approach. For each 2 µm ECD interval, the *roundness* frequency distribution was obtained and normalised. The mean *roundness* for each interval was then plotted in Figure 6.19 for the feed, tails and concentrate samples. Figure 6.19 corroborates the findings from Section 6.10.2, showing little variation of *roundness* with size, but higher mean *roundness* of the concentrates across the size range.

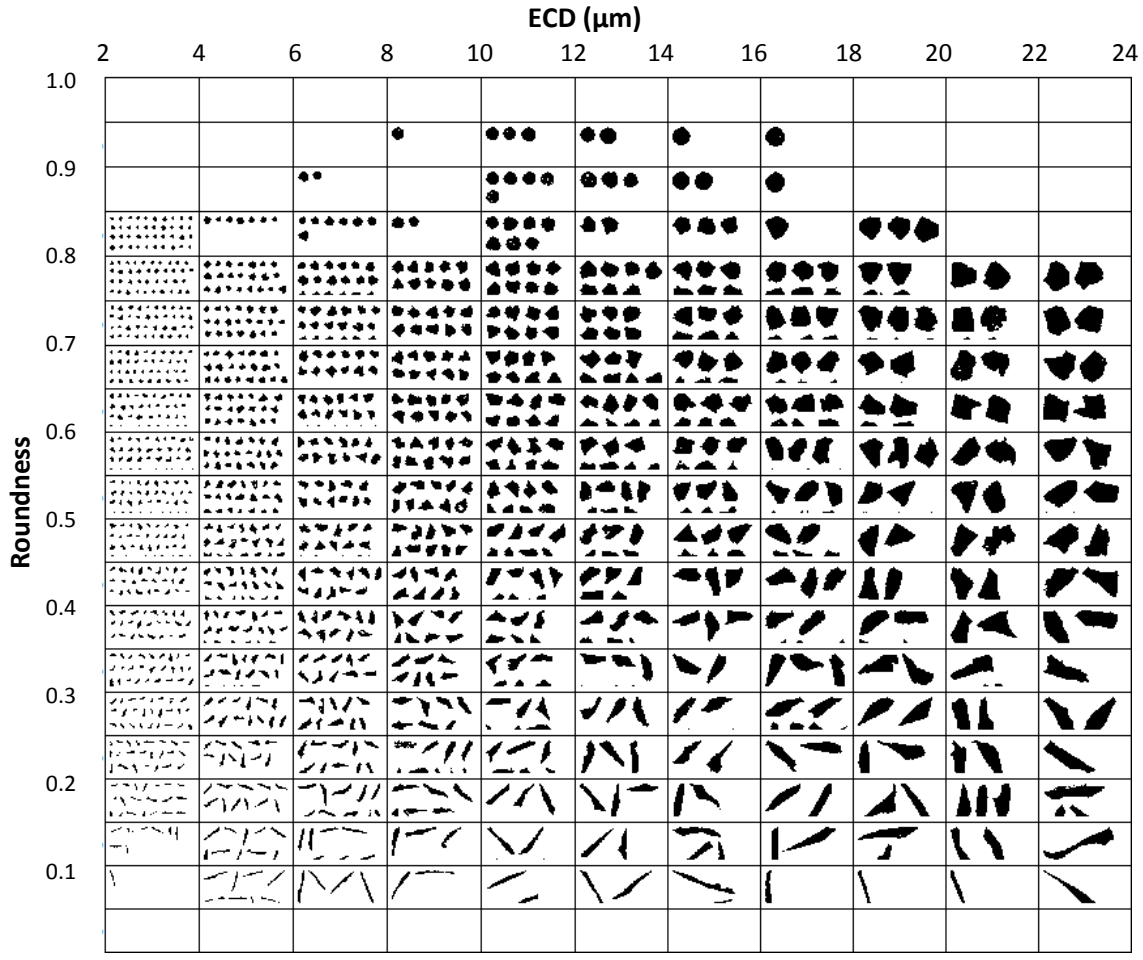

Figure 6.18: Illustration of the approach used to decouple chromite particle size and shape – classify particles into narrow sub-classes according to size, then determine the roundness frequency distribution for each sub-class.

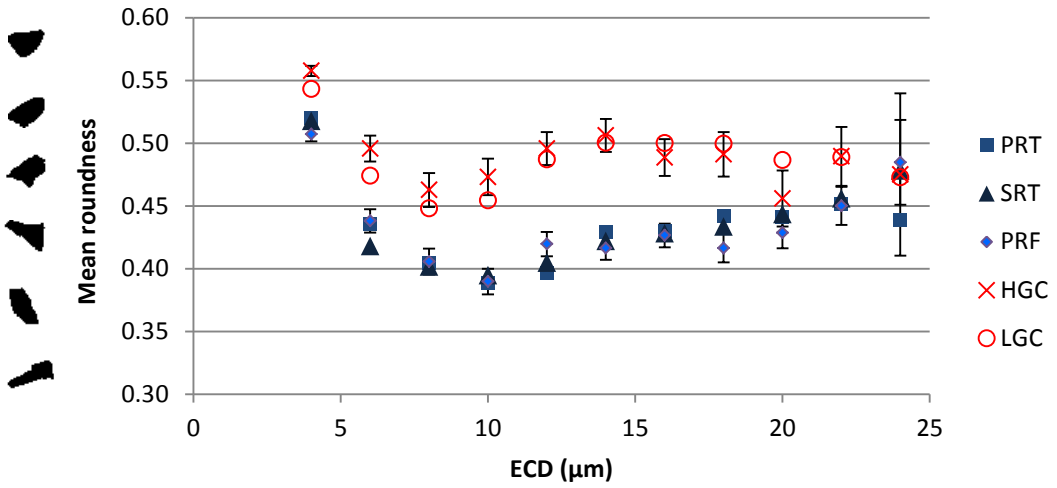

Figure 6.19: Variation of the mean roundness of chromite particles with particle size in the feed, tails and concentrate samples, indicating that more rounded particles show higher entrainment than angular particles with the same equivalent diameter. Error bars show 95% confidence intervals.

The evidence that shape is having an effect on entrainment is fairly convincing, however, the effect observed is not what was expected based on previous work reported in the literature (Kirjavainen, 1992; Wiese et al., 2014). This is an exploratory study - standing alone, the conclusions from this work do not present convincing evidence of the effect of particle shape on entrainment. However the new approach presented in this study could play a crucial role in clarifying these effects if applied more widely. More fundamental studies would also be useful to understand the mechanisms through which shape affects entrainment, with particular consideration of transport mechanisms of hydrophilic particles from the pulp phase into the froth phase. Possible explanations to be explored further relate to variation in particle hydrophilicity with shape, and variability in shape within the flotation cells relative to the streams due to bulk flow phenomena rather than transport within the froth. It is plausible that variation in surface hydrophilicity due to particle shape does not only affect particle-bubble attachment of hydrophobic particles, but also affects the behaviour of hydrophilic particles as they approach the froth interface, with more rounded particles being less hydrophilic, and thus more readily transported into the froth (M. Rudolph, personal communication, Nov. 2015). Alternatively, the observations from this study could be due to a bulk flow phenomenon, with more rounded particles concentrating within the flotation cells relative to the feed and tails streams, leading to a higher recovery of the more rounded particles to the concentrate (D. Deglon, personal communication, Dec. 2015)

6.11 Conclusions

This study of a 150 t/h UG2 platinum concentrator with multiple flotation stages has demonstrated that entrained chromite particles in the concentrate streams are more rounded than similarly sized particles in the feed and tails streams. These findings are not necessarily generalizable, and further work will be required to explain them as they are contradictory to previous work reported in the literature. These effects have implications for entrainment modelling, as well as being of particular interest for those UG2 platinum concentrators that have both a stirred mill (IsaMill) and ball mill within the secondary grinding circuit. Whether the IsaMill is on- or off-line, may be having an effect on the particle shape distribution as well as the particle size distribution, with implications for both true flotation and entrainment.

Aside from the findings relating to entrainment, the paper demonstrates a practical approach to investigating effects of particle shape in minerals processing operations. For example, a similar approach could be applied to assess the effects of particle shape on hydrocyclone performance, reflux classifier separations, and settling within thickeners.

6.12 Acknowledgements

This work is based on the research supported in part by the National Research Foundation of South Africa (Grant Number 86054). Any opinions, findings and conclusions or recommendations expressed in any publication generated by the NRF supported research is that of the author(s), and that the NRF accepts no liability whatsoever in this regard.

The authors would like to acknowledge the South African Minerals to Metals Research Institute (SAMMRI) and the South African Department of Science and Technology for funding the project.

6.13 References

Alvarez-Silva, M., Wiese, J., O'Connor, C.T., 2014. An investigation into the role of froth height and depressant dosage in the recovery of chromite in the flotation of UG2 ore using a laboratory column. Miner. Eng. 55, 125–131. doi:10.1016/j.mineng.2013.10.005

Eksteen, J.J., Van Beek, B., Bezuidenhout, G. A., 2011. Cracking a hard nut: An overview of Lonmin's operations directed at smelting of UG2-rich concentrate blends. J. South. African Inst. Min. Metall. 111, 681–690.

Hay, M.P., 2010. A case study of optimising UG2 flotation performance part 2: Modelling improved PGM recovery and Cr2O3 rejection at Northam's UG2 concentrator. Miner. Eng. 23, 868–876. doi:10.1016/j.mineng.2010.05.015

Hay, M.P., Roy, R., 2010. A case study of optimising UG2 flotation performance. Part 1: Bench, pilot and plant scale factors which influence Cr2O3 entrainment in UG2 flotation. Miner. Eng. 23, 855–867. doi:10.1016/j.mineng.2010.05.002

International Organisation for Standardisation, 2008. Representation of results of particle size analysis - Part 6: Descriptive and quantitative representation of particle shape and morphology. ISO 9276 - 6. Geneva.

Jones, R.T., 2005. An overview of Southern African PGM smelting, in: Nickel and Cobalt 2005 Challenges in Extraction and Production, 44th Annual Conference of Metallurgists. Calgary, Alberta, Canada, pp. 147–178.

Jones, R.T., Geldenhuys, I.J., 2011. The pros and cons of reductive matte smelting for PGMs. Miner. Eng. 24, 495–498. doi:10.1016/j.mineng.2011.03.007

Kirjavainen, V.M., 1992. Mathematical model for the entrainment of hydrophilic particles in froth flotation. Int. J. Miner. Process. 35, 1–11.

Kirjavainen, V.M., 1996. Review and analysis of factors controlling the mechanical flotation of gangue minerals. Int. J. Miner. Process. 46, 21–34. doi:10.1016/0301-7516(95)00057-7

Koh, P.T.L., Hao, F.P., Smith, L.K., Chau, T.T., Bruckard, W.J., 2009. The effect of particle shape and hydrophobicity in flotation. Int. J. Miner. Process. 93, 128–134. doi:10.1016/j.minpro.2009.07.007

Leroy, S., Dislaire, G., Bastin, D., Pirard, E., 2011. Optical analysis of particle size and chromite liberation from pulp samples of a UG2 ore regrinding circuit. Miner. Eng. 24, 1340–1347. doi:10.1016/j.mineng.2011.06.006

Little, L., Becker, M., Wiese, J., Mainza, A.N., 2015. Auto-SEM particle shape characterisation: Investigating fine grinding of UG2 ore. Miner. Eng. 82, 92–100. doi:10.1016/j.mineng.2015.03.021

Lotter, N.O., Monnapula, R., Oliveira, J., Fragomeni, D., Bradshaw, D.J., 2011. Formulation and Plant Trial of a Mixed Collector Suite For Eland Platinum, in: 43rd Annual Meeting of the Canadian Mineral Processors. Ottawa, pp. 161–183.

McFadzean, B., Pani, S., Wiese, J., O'Connor, C.T., 2015. The interactive effects of chemical and process parameters on the flotation performance of a UG2 ore. Miner. Eng. 70, 92–98. doi:10.1016/j.mineng.2014.08.016

Mudd, G.M., 2012. Key trends in the resource sustainability of platinum group elements. Ore Geol. Rev. 46, 106–117. doi:10.1016/j.oregeorev.2012.02.005

Napier-Munn, T.J., 2015. Statistical Methods for Mineral Engineers, How to design Experiments and Analyse Data. JKMRC, Brisbane, Australia.

Neethling, S.J., Cilliers, J.J., 2002. The entrainment of gangue into a flotation froth. Int. J. Miner. Process. 64, 123–134. doi:10.1016/S0301-7516(01)00067-9

Neethling, S.J., Cilliers, J.J., 2009. The entrainment factor in froth flotation: Model for particle size and other operating parameter effects. Int. J. Miner. Process. 93, 141–148. doi:10.1016/j.minpro.2009.07.004

Rahimi, M., Dehghani, F., Rezai, B., Aslani, M.R., 2012. Influence of the roughness and shape of quartz particles on their flotation kinetics. Int. J. Miner. Metall. Mater. 19, 284–289. doi:10.1007/s12613-012-0552-z

Ulusoy, U., Igathinathane, C., 2014. Dynamic image based shape analysis of hard and lignite coal particles ground by laboratory ball and gyro mills. Fuel Process. Technol. 126, 350–358. doi:10.1016/j.fuproc.2014.05.017

Ulusoy, U., Yekeler, M., 2014. Dynamic image analysis of calcite particles created by different mills. Int. J. Miner. Process. 133, 83–90. doi:10.1016/j.minpro.2014.10.006

van de Ruit, L., Becker, M., Wiese, J., Mainza, A., 2014. A mineralogical investigation of the effect of particle shape on chromite entrainment for a UG2 ore, in: XXVII International Mineral Processing Congress, Santiago, Chile. Santiago.

Varinot, C., Hiltgun, S., Pons, M., Dodds, J., 1997. Identification of the fragmentation mechanisms in wet-phase fine grinding in a stirred bead mill. Chem. Eng. Sci. 52, 3605–3612.

Verrelli, D.I., Bruckard, W.J., Koh, P.T.L., Schwarz, M.P., Follink, B., 2012a. Influence of particle shape and roughness on the induction period for particle-bubble attachment, in: XXVI International Mineral Processing Congress (IMPC). New Delhi, India, pp. 5665–5676.

Verrelli, D.I., Bruckard, W.J., Koh, P.T.L., Schwarz, M.P., Follink, B., 2014. Particle shape effects in flotation. Part 1: Microscale experimental observations. Miner. Eng. 58, 80–89. doi:10.1016/j.mineng.2014.01.004

Vizcarra, T.G., Harmer, S.L., Wightman, E.M., Johnson, N.W., Manlapig, E.V., 2011. The influence of particle shape properties and associated surface chemistry on the flotation kinetics of chalcopyrite. Miner. Eng. 24, 807–816. doi:10.1016/j.mineng.2011.02.019

Vonlanthen, P., Rausch, J., Ketcham, R.A., Putlitz, B., Baumgartner, L.P., Grobéty, B., 2015. High-resolution 3D analyses of the shape and internal constituents of small volcanic ash particles: The contribution of SEM micro-computed tomography (SEM micro-CT). J. Volcanol. Geotherm. Res. 293, 1–12. doi:10.1016/j.jvolgeores.2014.11.016

Wang, L., Peng, Y., Runge, K., Bradshaw, D., 2015. A review of entrainment: Mechanisms, contributing factors and modelling in flotation. Miner. Eng. 70, 77–91. doi:10.1016/j.mineng.2014.09.003

Wesseldijk, Q.I., Reuter, M.A., Bradshaw, D.J., Harris, P.J., 1999. The flotation behaviour of chromite with respect to the beneficiation of UG2 ore. Miner. Eng. 12, 1177–1184.

Westermann, J., n.d. Particle Characterization with Dynamic Image Analysis. Retsch Technol. Whitepaper 1–8.

Wiese, J., Becker, M., Yorath, G., O'Connor, C., 2015. An investigation into the relationship between particle shape and entrainment. Miner. Eng. 83, 211–216. doi:10.1016/j.mineng.2015.09.012

Wiese, J., Becker, M., Yorath, G., O'Connor, C.T., 2014. An investigation into the relationship between particle shape and entrainment, in: XXVII International Mineral Processing Congress, Santiago, Chile.

Yianatos, J., Contreras, F., 2010. Particle entrainment model for industrial flotation cells. Powder Technol. 197, 260–267. doi:10.1016/j.powtec.2009.10.001

Yianatos, J.B., Moys, M.H., Contreras, F., Villanueva, a., 2008. Froth recovery of industrial flotation cells. Miner. Eng. 21, 817–825. doi:10.1016/j.mineng.2007.12.012

Zheng, X., Johnson, N.W., Franzidis, J.-P., 2006. Modelling of entrainment in industrial flotation cells: Water recovery and degree of entrainment. Miner. Eng. 19, 1191–1203. doi:10.1016/j.mineng.2005.11.005

Chapter 7

CONCLUDING DISCUSSION

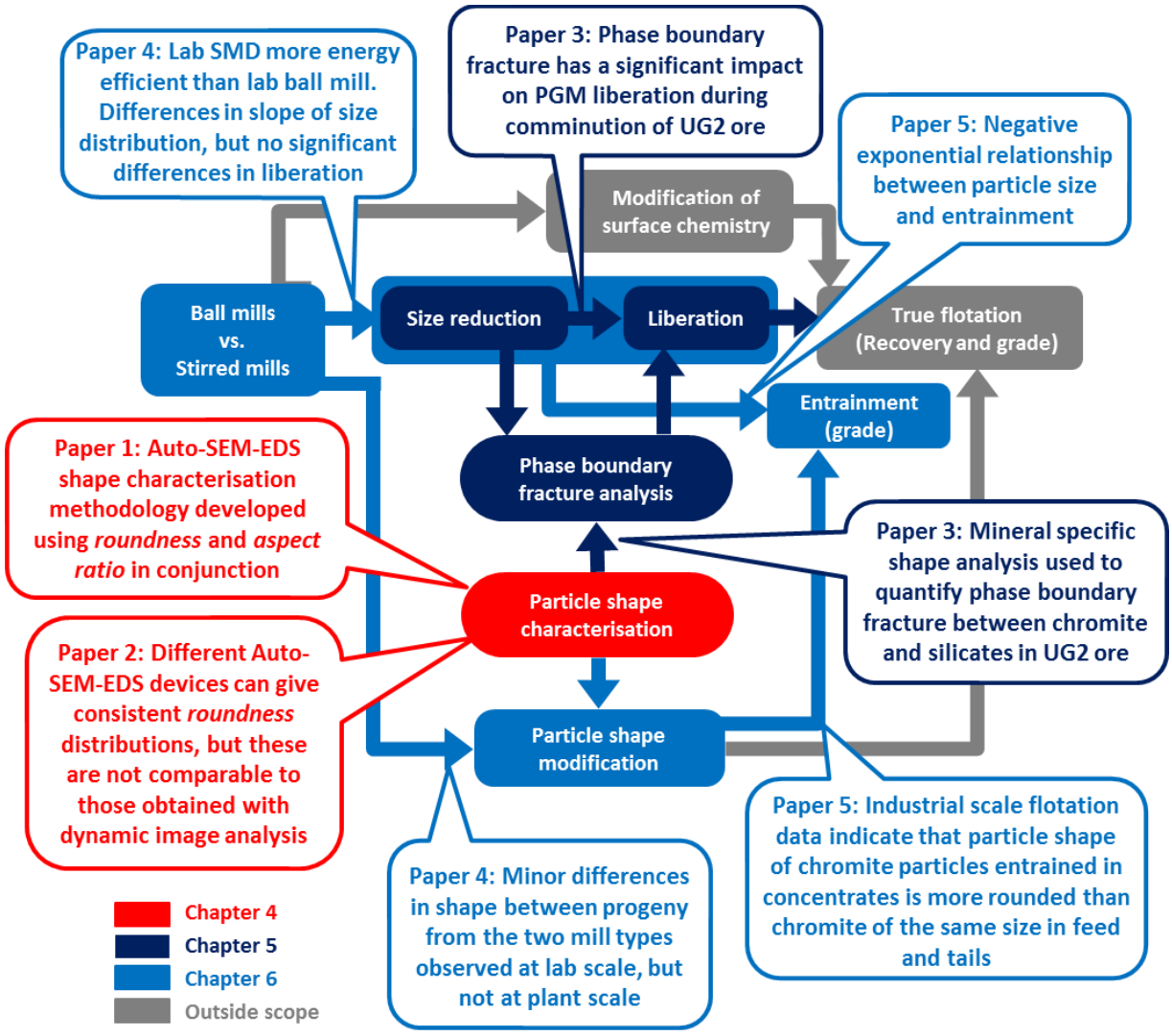

This diagram is based on the thesis scope outlined in Chapter 1. It summarises the results from the various aspects of the research and illustrates the connectivity between them.

In this chapter, the general outcomes of this thesis are first assessed in terms of the objectives relating to the development and demonstration of a methodology for Auto-SEM-EDS shape characterisation. The four hypotheses that guided the research are then examined with consideration of the key questions which were posed in Chapter 2. Finally the potential contributions of this body of work to the field of minerals processing are then assessed, and ideas and recommendations for further work are proposed.

7.1 Achievement of objectives

The first objective of this study was to develop a simple, meaningful, quantitative approach for Auto-SEM-EDS particle shape characterisation that is suitable for fine particles. This was successfully achieved and was documented in Chapter 4.

The second objective of this thesis was to demonstrate how this shape characterisation methodology can contribute towards the understanding of:

(a) Fracture mechanisms and the link between phase boundary fracture and liberation;
(b) The modification of shape during fine grinding in ball mills and stirred mills;
(c) The effects of particle shape on entrainment during flotation.

This objective was met through Papers 3, 4 and 5, with appropriate modifications of the shape characterisation methodology applied depending on the specific requirements associated with each task. For example, in Paper 3, assessment of the *roundness-aspect ratio* frequency distribution matrix for different particle types indicated that a single *roundness* value of 0.7 would be adequate to distinguish the majority of spherical chromite grains that had been liberated by detachment from other particle types. This demonstrated a novel application for mineral specific shape characterisation, which could make a valuable contribution towards the quantitative assessment of phase boundary fracture.

Paper 4 documented the application of the shape characterisation methodology to the study of fine grinding in ball mills and stirred mills, with observations based on both laboratory and plant-scale data. Preliminary work (Paper 1, Chapter 4.3) indicated that there were no significant differences in particle roughness for the different mill products, so presentation of the full *roundness-aspect ratio* frequency distribution matrix was not considered necessary for each sample. The shape characteristics of 8 samples (36 fractions) were assessed, and as the *roundness* distributions of all fractions closely followed the normal distribution, only the mean and standard deviations were reported for the majority of the samples.

Finally, for analysis of the effects of particle shape on entrainment, Paper 5 addressed issues associated with the use of the shape characterisation methodology in an application where

effects of both particle shape and size may need to be decoupled. An approach was presented in which particles are classified into narrow intervals based on equivalent circle diameter, and then the *roundness* distribution is obtained for each size interval. Although the accuracy of the size information is limited due to the 2-D sectional data, the relative comparison was considered adequate to confirm that the shape characteristics between feed and concentrate particles were different, and that this was not simply an artefact of the effect of particle size on entrainment. It was suggested that this approach would be useful for studying effects of shape on the performance of classification devices such as hydrocyclones.

7.2 Discussion of hypotheses

Hypothesis 1: Shape characterisation

1. The use of aspect ratio in conjunction with roundness will provide a quantitative, invariant shape characterisation technique that will be appropriate for the analysis of fine mineral particles (-75 μm) because neither descriptor depends on perimeter measurement.

The work presented in Chapter 4 supports this hypothesis. *Roundness* and *aspect ratio* are quantitative descriptors that are appropriate for 2-D shape characterisation of fine particulate samples, provided that clear, representative images of the particles have been obtained. The key questions associated with this hypothesis are addressed here:

- **How can Auto-SEM-EDS data best be used to characterise particle shape for minerals processing applications?**

The two descriptors *roundness* and *aspect ratio* can be applied in a variety of ways depending on the desired outcome - they can be used independently or in conjunction to either produce a 3-D frequency distribution/matrix, or to produce discrete shape categories. Presenting image grids in conjunction with frequency distributions is useful to assist with qualitative interpretation of the data.

  - How do *circularity* and *roundness* vary with resolution?

The commonly used descriptor, *circularity,* was found to be highly dependent on image resolution. Therefore, the rarely used descriptor, *roundness*, which is invariant with respect to image resolution, was selected as a preferred alternative. It is nevertheless recommended that images with resolutions lower than 20 pixels/particle should be excluded from shape analyses (Section 4.4).

- Is bias introduced to the 2-D shape measurements through preferential orientation of the particles being scanned, or are they randomly orientated?

Orthogonal sections from the same block of particles mounted in resin gave highly repeatable roundness distributions, indicating that the orientation of the particles within the blocks was random, and thus that the 2-D frequency distributions were indicative of the particulate sample's 3-D shape characteristics. However, 2-D measurements of a sample should be supported by a basic qualitative assessment of the 3-D particle morphology to indicate whether the majority of particles are highly flaky. If samples comprise highly flaky particles, 2-D measurements may be inappropriate (Section 4.8.2). In this thesis, secondary electron SEM images of 3-D particles indicating morphology were used for qualitative support of the observations made based on 2-D measurements.

- Are the differences observed between shape distributions statistically and practically significant?

Initial estimates of the error associated with statistical parameters such as the mean indicated that differences of less than 0.003 could be considered statistically significant at the 95% confidence level with over 10 000 particles analysed. However, differences of this magnitude were not considered practically significant (Paper 1, Section 4.3.2). An alternative method of estimating the uncertainty was therefore applied in Paper 2: The roundness frequency distributions obtained for three blocks were treated as repeat measurements of each sample, and the 'mean' distribution was then reported with 95% confidence intervals estimated at each point of the distribution (Paper 2, Section 4.9.2).

- How do these shape descriptors compare for different Auto-SEM-EDS systems such as the QEMSCAN and Mineralogic, and optical based systems such as the CAMSIZER XT?

Dissimilar image-capture mechanisms and image processing routines lead to differences in shape measurements, but these are less severe for *roundness* than for *circularity*. The descriptor a*spect ratio* requires consideration of the precise definitions of the 'length' and 'width' measurements used, as these can vary significantly for different systems (Section 4.13).

- How do the descriptors respond to differences in image processing techniques and perimeter algorithms?

Variation in perimeter measurement algorithms significantly impacts circularity measurements obtained with different devices. *Maximum Feret diameter* and *area* are more standard

measurements, which contribute to the invariance of *roundness*. Perimeter measurements are also much more sensitive to variation in image processing routines than maximum Feret diameter and *area* measurements.

Finally, in a complementary section in Chapter 4 (Sections 4.16 - 4.18) stereology and effects of different weighting parameters for shape distributions were discussed. In Paper 1, shape distributions were weighted by particle count based on previous work reported in the literature. However, this approach leads to the properties of the more numerous fine particles, or fine cross-sections in a sample measurement, receiving a high weighting, which may lead to exaggerated effects of resolution or sample preparation method (i.e. screening or cyclosizing). Weighting the distributions by area or mass (incorporating density) may therefore be preferable, but particle images should then be virtually filtered by equivalent circle diameter - near the top and at the bottom of each size fraction - to ensure that the largest particles of different shapes are weighted equally.

Hypothesis 2: Phase boundary fracture

2. During breakage of UG2 ore, phase boundary fracture between the chromite and silicates leads to enhanced liberation of the finely grained PGMs at a coarse size, because a significant portion of the PGMs occur along the weakly bonded chromite-silicate phase boundaries. The extent of this phenomenon can be inferred from the conservation of shape of the spherical chromite grains in conjunction with other techniques.

The work presented in chapter 5 supports this hypothesis. The extent of phase boundary fracture was estimated using a variety of methods, including a novel approach based on the conservation of chromite grain shape. The findings, based on all of these methods, indicated extensive phase boundary fracture and complete liberation-by-detachment of chromite grains. The key questions that were posed to address this hypothesis and the associated research findings are discussed hereafter:

- **Given the fine grain size distribution of PGMs in UG2 ore, is the liberation of PGMs typically observed at UG2 processing plants consistent with theory of random uniform isotropic fragmentation?**

Significant PGM liberation is achieved at a much coarser grind than would be required if breakage was random. Using theory developed by Barbery (1991), and PGM data presented by Chetty et al. (2009) and Penberthy (2001), it was shown that if breakage of UG2 ore was random, grinding down to as fine as 3 μm (median size) would be required to attain the same

degree of liberation which is currently achieved with median product sizes in the region of 75 µm.

- Can differences in particle shape in comminution products be related to the primary ore texture, and hence be linked to breakage along grain boundaries and liberation?

There is a clear relationship between the shape characteristics of the major mineral components and the primary texture of UG2 ore. The spherical chromite grains are loosely bonded within the silicate matrix, and are largely liberated by detachment producing particles with higher sphericity than other particle types within the ore.

- What descriptor or combination of descriptors will enable differentiation between the visibly liberated, spherical chromite grains and other particle types?

A spherical shape class with a minimum roundness value of 0.7 appeared to give the best differentiation between chromite grains liberated by detachment and other particle types as measured with Auto-SEM-EDS.

- Can phase boundary fracture be quantified based on the conservation of chromite grain shape?

Conservation of grain shape provides a quantitative indication of the extent to which phase boundary fracture has led to the complete detachment of spherical chromite grains from the primary silicate matrix.

- Are the findings from this method consistent with other methods for estimating phase boundary fracture?

The approaches to quantifying phase boundary fracture are all based on different metrics, so these cannot be compared directly. However the outcome from all methods consistently indicates that phase boundary fracture significantly affects PGM liberation during comminution of UG2 ore in typical concentrators.

Hypothesis 3: Fine grinding breakage mechanisms

3. The significant differences in energy intensity between ball mills and stirred mills, and the dissimilar ratio of normally opposed contact forces to tangential shear forces within the two mill types will lead to significant differences in the shape characteristics between ore particles produced within the two mills.

The laboratory data presented in Chapters 4 and 6 supports this hypothesis. However the plant data presented in Chapter 6 does not. This is discussed here through consideration of the key questions:

- **How do progeny particle shape and mineral liberation characteristics compare for ball mills and stirred mills at the laboratory scale, and are these consistent with observations made at plant-scale?**

The significant difference in energy intensity between the two mill types neither severely impacted the shape characteristics nor the valuable mineral liberation of the progeny. There was, however, an exception to this observation. The ball mill ultra-fine grinding product (80% passing 33 μm) had a significantly higher proportion of elongated particles than the other fine grinding product samples. This was speculated to be due to more rounded particles having a greater probability of fracture than angular particles because they absorb more energy during loading (Bbosa et al., 2006). Perhaps this effect only became apparent within the laboratory ball mill because it had a much lower energy intensity than both the plant ball mill (which used steel grinding media rather than ceramic grinding media), and the high-intensity stirred mills.

In general, the fine grinding products were either similar in shape or more angular than the fine grinding feed sample, indicating that the degree of abrasion in the fine grinding devices was not greater than that in the primary grinding circuit.

- Do the particle shape characteristics of the major mineral components differ?

Before fine grinding, significant differences were observed between the shape characteristics of the composites, liberated chromite, and liberated silicates, and this was linked to phase boundary fracture (Chapter 5). After fine grinding in the two mill types, the shape distributions of the major gangue minerals, which were close to 100% liberated, were very similar (Paper 1). From this observation, it was inferred that the fact that chromite does not have cleavage whereas the primary silicates in UG2 ore have prismatic cleavage did not significantly impact the roundness distributions of these mineral components after fine grinding.

- Do the particle shape characteristics vary with size?

There appear to be some trends in the variation of shape characteristics with size, but these are not consistent for all of the mill products that were assessed. For the plant samples and laboratory feed sample, the coarser size fractions (-75/+53 μm; -53/+25 μm) had significantly higher mean roundness than the finer fractions (-25/+10 μm; -10/+0 μm). For the laboratory samples the variation in mean roundness with size appears to be random.

- Is there a correlation between the particle shape characteristics and grinding time in the batch mills?

From the literature, an increase in grinding time was expected to result in an increase in the degree of abrasion, and thus the roundness of particles (Kaya et al., 2002). This was not observed, and in the case of the ball mill the particles became more elongated. This highlights the limitations in current understanding of fine grinding breakage mechanisms, particularly relating to the definition of abrasion and how it is linked to particle shape. The degree of abrasion in fine grinding is likely to be dependent on both ore characteristics and mill operating conditions, so the findings from this study are not necessarily generalizable. However this work indicates the requirement for increased shape characterisation of mineral particles in fine grinding applications in order to improve understanding of fine grinding breakage mechanisms.

Hypothesis 4: Effect of shape on entrainment

4. Particle shape will affect the drainage rates of chromite grains entrained within the plateau borders of the flotation froth, with more rounded particles draining more readily, leaving a higher concentration of more angular particles being recovered to the froth.

The data presented in Paper 5 does not support this hypothesis. This is discussed below in response to the key questions:

- **How does the particle shape of the chromite recovered to the concentrate compare to that in the feed and tails samples at both laboratory and plant-scale?**

At the platinum concentrator investigated in Paper 5, the chromite grains reporting to the concentrates were more rounded than those in the equivalent size fractions of the feed and tails. This observation was contradictory to the hypothesis, so particular attention was paid to the following key question:

- What is the effect of particle size on entrainment – is it a confounding variable?

A negative exponential relationship between size and entrainment was observed, which was consistent with the literature. Slight variation in roundness measurements with size indicated that size could be a confounding variable.

- How can the effect of shape be decoupled from the effect of size?

In order to ensure that the observed differences in shape between the samples was not simply an artefact of the effect of size, the measured samples were virtually classified into narrow size fractions (ECD intervals 2 μm wide). The roundness distributions and mean roundness for each

narrow size interval were then compared. This analysis indicated that the differences in shape between concentrate samples, and feed and tails samples were significant across the range of cross-sectional image sizes between 5 and 20 μm. Thus the difference in shape was not simply caused by the effect of size. An alternative explanation for the observations is therefore required, as they do not support the hypothesis that was proposed based on the literature. Two alternative explanations have been suggested:

a) The differences in shape distributions between the concentrate and feed and tails samples is due to a bulk flow phenomenon that leads to the concentration of more spherical particles within the flotation cells relative to in the feed and tails streams;
b) The effect of shape on hydrophobicity is not only relevant for particles that are considered hydrophobic (i.e. those that attach to bubbles), but also for those that are hydrophilic (i.e. those that do not actually attach to the bubbles). Less hydrophilic, more spherical particles may be more likely to cross the pulp froth interface and be recovered to the concentrates by entrainment.

This was not a fundamental study, so it is not possible to pinpoint the exact mechanisms responsible for the observed findings. Literature on this topic is limited, and these data constitute the first of their kind reported in the public field. For future work it would therefore be advisable to first assess more plant data in a similar manner to determine whether the findings from this study are generalizable. Historical Auto-SEM-EDS data should be adequate for this purpose. If the results are found to be generalizable, and if the differences are significant enough to justify additional fundamental research, appropriate experiments should then be designed to determine the mechanisms responsible.

7.3 The contribution of this thesis to minerals processing research

The novel shape characterisation methodology developed in this thesis can be applied to historical Auto-SEM-EDS data to build a substantial database that would contribute towards demystifying the effects of particle shape in minerals processing. The methodology developed has already been adopted by researchers at Mintek who are studying the effects of particle shape on various physical separations. Presentations of this work to international audiences (see page viii) have stimulated discussions about additional potential applications for the methodology.

Interpretability, invariance and automation were identified as important criteria for shape characterisation methodologies (Pirard, 1989). The approach developed in this thesis satisfies all three criteria:

- The illustrative approach of presenting shape data will make the particle shape information easier to interpret than that in most previous studies incorporating shape. This will persuade minerals processing researchers and practitioners who have no previous experience of particle shape characterisation to apply this methodology within their own work. It will also facilitate the more widespread application of Auto-SEM-EDS shape characterisation within minerals processing research.
- The invariance criterion was tested with respect to image resolution, different measurement devices and image processing algorithms. The selected shape descriptors, *roundness* and *aspect ratio,* were found to be less variable than *circularity*, the descriptor that has been used most widely in this field. However, for aspect ratio measurements, users are advised to report the exact definitions of the width and length parameters used.
- Auto-SEM-EDS devices are automated systems which produce data that are suited to statistical analysis.

The demonstration of the shape characterisation methodology included the following original contributions:

- A novel approach to quantify phase boundary fracture based on the conservation of grain shape;
- Confirmation that phase boundary fracture can severely enhance liberation of valuable minerals in traditional, industrial scale ball milling circuits;
- Evidence suggesting that the large difference in energy intensity between ball mills and stirred mills does not significantly impact product particle shape distributions of UG2 ore, and fine grinding does not lead to rounding of particles in either mill type;
- Evidence of differences in particle shape between entrained gangue particles of similar sizes in the feed, tails, and concentrate streams of an industrial scale concentrator, with the concentrate streams comprising more rounded particles.

The contributions relating to phase boundary fracture will revive interest in the measurement of phase boundary fracture in typical comminution operations, stimulating research in this field. Both the approach and the experimental data will be useful for liberation modelling efforts in which experimental evidence of the occurrence and extent of phase boundary fracture in typical grinding operations is required to validate and/or calibrate theoretical models. The latter contributions highlight the need for additional work to improve understanding of fine grinding breakage mechanisms, and effects of particle shape on entrainment

7.4 Recommendations for future work

A more robust understanding of particle shape effects in minerals processing can only be developed and usefully applied if measurements of shape characteristics become more routine. Although Auto-SEM-EDS is not widely used on-site, a large number of samples obtained from concentrators for many different ore types are analysed with Auto-SEM-EDS, sometimes on a routine basis. Particle shape characterisation can be carried out for any of these measurements apart from those based on line-scans for bulk mineralogical analysis. Without extensive test work, these databases could therefore be used to:

- Investigate the effects of shape on classification; UG2 ore would make a good case study for this with spherical dense chromite and more angular less dense silicates allowing for effects of shape, size and density to be decoupled;
- Rank the typical shape characteristics of different ore types over a range of sizes, and determine whether correlations exist between shape distributions of specific minerals, breakage parameters and ore textures;
- Further explore phase boundary fracture and liberation by detachment for other ore types, particularly those containing spinels such as chromite and magnetite, which are likely to be amenable to the conservation-of-shape approach. Previous literature studies in which certain ore types have been described that would likely be appropriate for such analysis include the Ernest Henry ore investigated by Vizcarra (2010), the chromite ore described by Hoşten and Özbay (1998), a chromite serpentine ore described by King (1992), and the iron ore described by Lewczuk (1988). The methodology may also be applicable to the liberation of globules of matte minerals during the regrinding of slags (Scharneck and Andrews, 2012);
- Determine whether the findings relating to the effect of shape on entrainment observed in Paper 5 are generalizable, and if so, investigate what mechanisms are responsible for the recovery of more rounded particles;

The basic understanding of shape effects to be developed based on 2-D Auto-SEM-EDS data should then be used to incorporate shape parameters within models used for design and optimisation of minerals processing.

In conclusion, a practical, robust, quantitative shape characterisation methodology was developed and demonstrated. The methodology is suitable for analysis of fine particulate ore samples measured with Auto-SEM-EDS devices, and it will be a useful precursor to the incorporation of effects of particle shape in minerals processing models. The shape characterisation methodology can also contribute towards mineral liberation modelling, through the novel conservation-of-shape approach to quantify phase boundary fracture.

Chapter 8

BIBLIOGRAPHY

Ahmed, M.M., 2010. Effect of comminution on particle shape and surface roughness and their relation to flotation process. Int. J. Miner. Process. 94, 180–191. doi:10.1016/j.minpro.2010.02.007

Albijanic, B., Nimal Subasinghe, G.K., Bradshaw, D.J., Nguyen, A. V., 2014. Influence of liberation on bubble–particle attachment time in flotation. Miner. Eng. 74, 156–162. doi:10.1016/j.mineng.2014.08.004

Alvarez-Silva, M., Wiese, J., O'Connor, C.T., 2014. An investigation into the role of froth height and depressant dosage in the recovery of chromite in the flotation of UG2 ore using a laboratory column. Miner. Eng. 55, 125–131. doi:10.1016/j.mineng.2013.10.005

Apling, A., Bwalya, M., 1997. Evaluating high pressure milling for liberation enhancement and energy saving. Miner. Eng. 10, 1013–1022. doi:10.1016/S0892-6875(97)00080-0

ASTM_International, 2010. ASTM F1877-05 Standard Practice for Characterization of Particles.

Bagheri, G.H., Bonadonna, C., Manzella, I., Vonlanthen, P., 2015. On the characterization of size and shape of irregular particles. Powder Technol. 270, 141–153. doi:10.1016/j.powtec.2014.10.015

Barbery, G., 1974. Determination of particle size distribution from measurements on sections. Powder Technol. 9, 231–240. doi:10.1016/0032-5910(74)80047-1

Barbery, G., 1987. Random sets and integral geometry in comminution and liberation of minerals, in: AIME Transactions. Soc. Min. Eng., pp. 96–102.

Barbery, G., 1991. Mineral liberation: measurement, simulation and practical use in mineral processing. Les Editions GB, Quebec.

Barret, P.J., 1980. The shape of rock particles, a critical review. Sedimentology 27, 291–303.

Baum, W., 2014. Ore characterization, process mineralogy and lab automation a roadmap for future mining. Miner. Eng. 60, 69–73. doi:10.1016/j.mineng.2013.11.008

Bbosa, L., Powell, M.S., Cloete, T.J., 2006. An investigation of impact breakage of rocks using the split Hopkinson pressure bar. J. South African Inst. Min. Metall. 106, 291–296.

Becker, M., 2009. The Mineralogy and Crystallography of Pyrrhotite from Selected Nickel and PGE Ore Deposits and its Effect on Flotation Performance. University of Pretoria.

Becker, M., Harris, P.J., Wiese, J.G., Bradshaw, D.J., 2009. Mineralogical characterisation of naturally floatable gangue in Merensky Reef ore flotation. Int. J. Miner. Process. 93, 246–255. doi:10.1016/j.minpro.2009.10.004

Becker, M., Mainza, A.N., Powell, M.S., Bradshaw, D.J., Knopjes, B., 2008. Quantifying the influence of classification with the 3 product cyclone on liberation and recovery of PGMs in UG2 ore. Miner. Eng. 21, 549–558. doi:10.1016/j.mineng.2007.11.001

Becker, M., Yorath, G., Ndlovu, B., Harris, M., Deglon, D., Franzidis, J.-P., 2013. A rheological investigation of the behaviour of two Southern African platinum ores. Miner. Eng. 49, 92–97. doi:10.1016/j.mineng.2013.05.007

Bengtsson, M., Lee, E., Evertsson, C.M., 2010. Influence of throw and compression ratio on particle shape – A full scale investigation and laboratory tests. Miner. Eng. 23, 549–557. doi:10.1016/j.mineng.2009.12.009

Bezuidenhout, G.A., Eksteen, J.J., Akdogan, G., Bradshaw, S.M., De Villiers, J.P.R., 2013. Pyrometallurgical upgrading of PGM-rich leach residues from the Western Platinum base metals refinery through roasting. Miner. Eng. doi:10.1016/j.mineng.2013.04.002

Bond, F.C., 1958. Grinding ball size selection. Min. Eng. 592–595.

Bowman, E.T., Soga, K., Drummond, W., 2001. Particle shape characterisation using Fourier descriptor analysis. Géotechnique 51, 545–554. doi:10.1680/geot.2001.51.6.545

Bridgwater, J., Utsumi, R., Zhang, Z., Tuladhar, T., 2003. Particle attrition due to shearing—the effects of stress, strain and particle shape. Chem. Eng. Sci. 58, 4649–4665. doi:10.1016/j.ces.2003.07.007

Bruckard, W.J., Sparrow, G.J., Woodcock, J.T., 2011. A review of the effects of the grinding environment on the flotation of copper sulphides. Int. J. Miner. Process. 100, 1–13. doi:10.1016/j.minpro.2011.04.001

Cabri, L.J., Rudashevsky, N.S., Rudashevsky, V.N., Gorkovetz, V.Y., 2008. Study of native gold from the Luopensulo deposit (Kostomuksha area, Karelia, Russia) using a combination of electric pulse disaggregation (EPD) and hydroseparation (HS). Miner. Eng. 21, 463–470. doi:10.1016/j.mineng.2008.02.006

Califice, A., Michel, F., Dislaire, G., Pirard, E., 2013. Influence of particle shape on size distribution measurements by 3D and 2D image analyses and laser diffraction. Powder Technol. 237, 67–75. doi:10.1016/j.powtec.2013.01.003

Chandramohan, R., Holtham, P., Powell, M., 2010. the Influence of Particle Shape in Rock Fracture. XXV Int. Miner. Process. Congr. 3163–3171.

Chapman, N.A., Shackleton, N.J., Malysiak, V., O'Connor, C.T., 2011. The effect of using different comminution procedures on the flotation of Platinum-Group Minerals. Miner. Eng. 24, 731–736. doi:10.1016/j.mineng.2011.01.001

Chaponda, B., 2011. Effect of operating variables on IsaMill performance using Platinum bearing Ores. University of Cape Town.

Charikinya, E., 2015. Characterising the effect of microwave treatment on bio-leaching of coarse, massive sulphide ore particles. Stellenbosch University.

Chetty, D., Gryffenberg, L., Lekgetho, T.B., Molebale, I.J., 2009. Automated SEM study of PGM distribution across a UG2 flotation concentrate bank: Implications for understanding PGM floatability. J. South. African Inst. Min. Metall. 109, 587–593.

Cleary, P.W., 2001. Recent advances in DEM modelling of tumbling mills. Miner. Eng. 14, 1295–1319. doi:10.1016/S0892-6875(01)00145-5

Cleary, P.W., Morrison, R.D., 2016. Comminution mechanisms, particle shape evolution and collision energy partitioning in tumbling mills. Miner. Eng. 86, 75–95. doi:10.1016/j.mineng.2015.12.006

Cleary, P.W., Sinnott, M., Morrison, R., 2006. Analysis of stirred mill performance using DEM simulation: Part 2 – Coherent flow structures, liner stress and wear, mixing and transport. Miner. Eng. 19, 1551–1572. doi:10.1016/j.mineng.2006.08.013

Coetzee, L.L., Theron, S.J., Martin, G.J., Merwe, J.-D. Van Der, Stanek, T.A., 2011. Modern gold deportments and its application to industry. Miner. Eng. 24, 565–575. doi:10.1016/j.mineng.2010.09.001

Cropp, A.F., Goodall, W.R., Bradshaw, D.J., 2013. The Influence of Textural Variation and Gangue Mineralogy on Recovery of Copper by Flotation from Porphyry Ore – A Review. AusIMM GeoMet 2013 Proc. 279–291.

Dal Martello, E., Bernardis, S., Larsen, R.B., Tranell, G., Di Sabatino, M., Arnberg, L., 2012. Electrical fragmentation as a novel route for the refinement of quartz raw materials for trace mineral impurities. Powder Technol. 224, 209–216. doi:10.1016/j.powtec.2012.02.055

Das, R., Cleary, P.W., 2010. Effect of rock shapes on brittle fracture using Smoothed Particle

Hydrodynamics. Theor. Appl. Fract. Mech. 53, 47–60. doi:10.1016/j.tafmec.2009.12.004

Diez, D.M., Barr, C.D., Cetinkaya-Rundel, M., 2012. OpenIntro Statistics.

Dumm, T.F., Hogg, R., 1990. Characterization of particle shape, in: Proceedings of International Symposium on Respirable Dust in the Mineral Industries. pp. 283–288. doi:10.1007/978-1-4614-4310-0

Durney, T.E., Meloy, T.P., 1986. Particle shape effects due to crushing method and size. Int. J. Miner. Process. 16, 109–123.

Dworzanowski, N.I., 2014. Maximizing haematite recovery within a fine and wide particle-size distribution using wet high-intensity magnetic separation. J. South African Inst. Min. Metall. 114, 559–567.

Ekmekçi, Z., Bradshaw, D.J., Allison, S.A., Harris, P.J., 2003. Effects of frother type and froth height on the flotation behaviour of chromite in UG2 ore. Miner. Eng. 16, 941–949. doi:10.1016/j.mineng.2003.08.001

Eksteen, J.J., Van Beek, B., Bezuidenhout, G.A., 2011. Cracking a hard nut: An overview of Lonmin's operations directed at smelting of UG2-rich concentrate blends. J. South. African Inst. Min. Metall. 111, 681–690.

Engelbrecht, J.A., Woodburn, E.T., 1975. The effect of froth height, aeration rate and gas precipitation on flotation. J. South African Inst. Min. Metall. 76, 125–132.

Erb, H., van de Vijfeijken, M., Hanuman, Y., Rule, C., Swart, W.C.E., Lehto, H., Keikkala, V., 2015. An initial review of the metallurgical performance of the HIGmillTM in a primary milling application in the hard rock mining industry, in: SAG Conference. Canadian Institute of Mining and Metallurgy, Vancouver, pp. 1–12.

Evans, C.L., Wightman, E.M., Manlapig, E.V., Coulter, B.L., 2011. Application of process mineralogy as a tool in sustainable processing. Miner. Eng. 24, 1242–1248. doi:10.1016/j.mineng.2011.03.017

Fandrich, R., Gu, Y., Burrows, D., Moeller, K., 2007. Modern SEM-based mineral liberation analysis. Int. J. Miner. Process. 84, 310–320. doi:10.1016/j.minpro.2006.07.018

Fandrich, R.G., Bearman, R.A., Boland, J., Lim, W., 1997. Mineral liberation by particle bed breakage. Miner. Eng. 10, 175–187.

FEI, 2015a. FEI [WWW Document]. URL http://www.fei.com/products/sem/mla/ (accessed 2.11.15).

FEI, 2015b. FEI [WWW Document]. URL http://www.fei.com/products/sem/qemscan/ (accessed 2.11.15).

Frances, C., Le Bolay, N., Belaroui, K., Pons, M.-N., 2001. Particle morphology of ground gibbsite in different grinding environments. Int. J. Miner. Process. 61, 41–56. doi:10.1016/S0301-7516(00)00025-9

Gao, M., Forssberg, E., 1995. Prediction of product size distributions for a stirred ball mill. Powder Technol. 84, 101–106.

Gao, M.W., Forssberg, E., 1989. The effect of powder filling on selection and breakage functions in batch grinding. Powder Technol. 59, 275–283. doi:10.1016/0032-5910(89)80086-5

Garboczi, E.J., Liu, X., Taylor, M.A., 2012. The 3-D shape of blasted and crushed rocks: From 20μm to 38mm. Powder Technol. 229, 84–89. doi:10.1016/j.powtec.2012.06.012

Garcia, D., Lin, C.L., Miller, J.D., 2009. Quantitative analysis of grain boundary fracture in the breakage of single multiphase particles using X-ray microtomography procedures. Miner. Eng. 22, 236–243. doi:10.1016/j.mineng.2008.07.005

Gaudin, A.M., 1939. Principles of Mineral Dressing. McGraw-Hill Book Company, Inc., New York.

Gay, S.L., 2004. Simple texture-based liberation modelling of ores. Miner. Eng. 17, 1209–1216. doi:10.1016/j.mineng.2004.06.032

Glencore Technology, 2016. IsaMill [WWW Document]. URL http://www.isamill.com/ (accessed 8.8.16).

Goodall, W.R., 2008. Characterisation of mineralogy and gold deportment for complex tailings deposits

using QEMSCAN®. Miner. Eng. 21, 518–523. doi:10.1016/j.mineng.2008.02.022

Goodall, W.R., Scales, P.J., 2007. An overview of the advantages and disadvantages of the determination of gold mineralogy by automated mineralogy. Miner. Eng. 20, 506–517. doi:10.1016/j.mineng.2007.01.010

Goodall, W.R., Scales, P.J., Butcher, A.R., 2005. The use of QEMSCAN and diagnostic leaching in the characterisation of visible gold in complex ores. Miner. Eng. 18, 877–886. doi:10.1016/j.mineng.2005.01.018

Gottlieb, P., Wilkie, G., Sutherland, D., Ho-Tun, E., Suthers, S., Perera, K., Jenkins, B., Spencer, S., Butcher, A., Rayner, J., 2000. Using quantitative electron microscopy for process mineralogy applications. J. Mineral. 52, 24 – 25.

Grano, S., 2009. The critical importance of the grinding environment on fine particle recovery in flotation. Miner. Eng. 22, 386–394. doi:10.1016/j.mineng.2008.10.008

Grano, S.., Lauder, D.., Johnson, N.., Ralston, J., 1997. An investigation of galena recovery problems in the Hilton concentrator of Mount Isa Mines Limited, Australia. Miner. Eng. 10, 1139–1163.

Greet, C.., Small, G.., Steinier, P., Grano, S.., 2004. The Magotteaux Mill: investigating the effect of grinding media on pulp chemistry and flotation performance. Miner. Eng. 17, 891–896.

Grobler, J.D., Bosman, J.B., 2011. Gravity separator performance evaluation using Qemscan® particle mineral analysis. J. South. African Inst. Min. Metall. 111, 401–408.

Gu, Y., Schouwstra, R.P., Rule, C., 2014. The value of automated mineralogy. Miner. Eng. 58, 100–103. doi:10.1016/j.mineng.2014.01.020

Guven, O., Çelik, M.S., 2015. Can roughness of particles be tuned to reach maximum flotation recoveries?, in: MEI Flotation '15. Cape Town.

Guven, O., Ozdemir, O., Karaagaclioglu, I.E., Çelik, M.S., 2015. Surface morphologies and floatability of sand-blasted quartz particles. Miner. Eng. 70, 1–7. doi:10.1016/j.mineng.2014.08.007

Hay, M.P., 2010. A case study of optimising UG2 flotation performance part 2: Modelling improved PGM recovery and Cr2O3 rejection at Northam's UG2 concentrator. Miner. Eng. 23, 868–876. doi:10.1016/j.mineng.2010.05.015

Hay, M.P., Roy, R., 2010. A case study of optimising UG2 flotation performance. Part 1: Bench, pilot and plant scale factors which influence Cr2O3 entrainment in UG2 flotation. Miner. Eng. 23, 855–867. doi:10.1016/j.mineng.2010.05.002

Hay, M.P., Schroeder, G., 2005. Use of the SUPASIM flotation model in optimising Impala's UG2 circuit. Miner. Eng. 18, 772–784. doi:10.1016/j.mineng.2005.01.028

Hennart, S.L.A., Wildeboer, W.J., van Hee, P., Meesters, G.M.H., 2009. Identification of the grinding mechanisms and their origin in a stirred ball mill using population balances. Chem. Eng. Sci. 64, 4123–4130. doi:10.1016/j.ces.2009.06.031

Heywood, H., 1945. No Title. Trans. Inst. Min. Met. 15, 373.

Hicyilmaz, C., Ulusoy, U., Bilgen, S., Yekeler, M., 2005. Flotation responses to the morphological properties of particles measured with three-dimensional approach. Int. J. Miner. Process. 75, 229–236. doi:10.1016/j.minpro.2004.08.019

Hill, E., 2014. Zeiss Mineralogic Mining - Ore Process Optimization. Carl Zeiss White Pap.

Hogg, R., 1999. Breakage mechanisms and mill performance in ultrafine grinding. Powder Technol. 105, 135–140.

Holt, C.B., 1981. The Shape of Particles Produced by Comminution , A Review. Powder Technol. 28, 59–63.

Hoşten, Ç., Özbay, C., 1998. A comparison of particle bed breakage and rod mill grinding with regard to mineral liberation and particle shape effects. Miner. Eng. 11, 871–874. doi:10.1016/S0892-6875(98)00074-0

International Organisation for Standardisation, 2008. Representation of results of particle size analysis - Part 6: Descriptive and quantitative representation of particle shape and morphology. ISO 9276 - 6.

Geneva.

Jankovic, A., 2003. Variables affecting the fine grinding of minerals using stirred mills. Miner. Eng. 16, 337–345. doi:10.1016/S0892-6875(03)00007-4

Johnson, N.W., 1972. The Flotation Behaviour of Some Chalcopyrite Ores. PhD, JKMRC, University of Queensland. University of Queensland.

Jones, R.T., 2005. An overview of Southern African PGM smelting, in: Nickel and Cobalt 2005 Challenges in Extraction and Production, 44th Annual Conferences of Metallurgists. Calgary, Alberta, Canada, pp. 147–178.

Jones, R.T., Geldenhuys, I.J., 2011. The pros and cons of reductive matte smelting for PGMs. Miner. Eng. 24, 495–498. doi:10.1016/j.mineng.2011.03.007

Kashiwaya, K., Noumachi, T., Hiroyoshi, N., Ito, M., Tsunekawa, M., 2012. Effect of particle shape on hydrocyclone classification. Powder Technol. 226, 147–156. doi:10.1016/j.powtec.2012.04.036

Kawatra, K., 2006. Advances in Comminution, 1st ed. Society for Mining, Metallurgy and Exploration, Inc., Littleton, Colorado.

Kaya, E., Hogg, R., Kumar, S.R., 2002. Particle Shape Modification in Comminution. KONA 20, 188–195.

Kelly, E.G., Spottiswood, D.G., 1990. The breakage function; What is it really? Miner. Eng. 3, 405–414.

Khonthu, T., 2012. Investigation of the flotation behaviour of ball mill and IsaMill products. University of Cape Town.

King, R.P., 1978. Determination of particle size distribution from measurements of sections. Powder Technol. 21, 147–150.

King, R.P., 1982. Determination of the distribution of size of irregularly shaped particles from measurements on sections or projected areas. Powder Technol. 32, 87–100.

King, R.P., 1984. Measurement of particle size distribution by image analyser. Powder Technol. 39, 279–289. doi:10.1016/0032-5910(84)85045-7

King, R.P., 1992. Techniques for estimating the amount of grain-boundary fracture during comminution of mineralogical materials, in: Kawatra, K. (Ed.), Comminution- Theory and Practice. Soc. Min. Eng., pp. 1–16. doi:10.1016/B978-0-7020-2797-0.00001-1

King, R.P., 1993. Comminution research - a success story that has not yet ended., in: Proceedings XVIII International Mineral Processing Congress. pp. 39–45.

King, R.P., 1994. Linear stochastic models for mineral liberation. Powder Technol. 81, 217–234. doi:10.1016/0032-5910(94)02886-9

King, R.P., 2001. Modeling & Simulation of Mineral Processing. Butterworth-Heinemann, Oxford.

King, R.P., Schneider, C.L., 1998. Mineral liberation and the batch comminution equation. Miner. Eng. 11, 1143–1160. doi:10.1016/S0892-6875(98)00102-2

Kingman, S.W., Rowson, N.A., 1998. Microwave treatment of minerals-a review. Miner. Eng. 11, 1081–1087. doi:10.1016/S0892-6875(98)00094-6

Kirjavainen, V.M., 1992. Mathematical model for the entrainment of hydrophilic particles in froth flotation. Int. J. Miner. Process. 35, 1–11.

Kirjavainen, V.M., 1996. Review and analysis of factors controlling the mechanical flotation of gangue minerals. Int. J. Miner. Process. 46, 21–34. doi:10.1016/0301-7516(95)00057-7

Koh, P.T.L., Hao, F.P., Smith, L.K., Chau, T.T., Bruckard, W.J., 2009. The effect of particle shape and hydrophobicity in flotation. Int. J. Miner. Process. 93, 128–134. doi:10.1016/j.minpro.2009.07.007

Komabayashi, T., Spångberg, L.S.W., 2008. Comparative analysis of the particle size and shape of commercially available mineral trioxide aggregates and Portland cement: a study with a flow particle image analyzer. J. Endod. 34, 94–8. doi:10.1016/j.joen.2007.10.013

Kröner, S., Doménech Carbó, M.T., 2013. Determination of minimum pixel resolution for shape analysis: Proposal of a new data validation method for computerized images. Powder Technol. 245, 297–313.

doi:10.1016/j.powtec.2013.04.048

Krumbein, W.C., 1941. Measurement and Geological Significance of Shape and Roundness of Sedimentary Particles. J. Sediment. Res. 11, 64–72.

Kursun, H., Ulusoy, U., 2006. Influence of shape characteristics of talc mineral on the column flotation behavior. Int. J. Miner. Process. 78, 262–268. doi:10.1016/j.minpro.2005.11.003

Kwitko-Ribeiro, R., 2011. New sample preparation developments to minimize mineral segregation in process mineralogy, in: 10th International Congress for Applied Mineralogy. Trondheim, pp. 411 – 417.

Laslett, G.M., Sutherland, D.N., Gottlieb, P., Allen, N.R., 1990. Graphical assessment of a random breakage model for mineral liberation. Powder Technol. 60, 83–97. doi:10.1016/0032-5910(90)80135-L

Lätti, D., Adair, B.J.I., 2001. An assessment of stereological adjustment procedures. Miner. Eng. 14, 1579–1587. doi:10.1016/S0892-6875(01)00176-5

Lau, R., Chuah, H.K.L., 2013. Dynamic shape factor for particles of various shapes in the intermediate settling regime. Adv. Powder Technol. 24, 306–310. doi:10.1016/j.apt.2012.08.001

Leigh, G.M., Lyman, G.J., Gottlieb, P., 1996. Stereological estimates of liberation from mineral section measurements: A rederivation of Barbery's formulae with extensions. Powder Technol. 87, 141–152. doi:10.1016/0032-5910(95)03080-8

Leroy, S., Dislaire, G., Bastin, D., Pirard, E., 2011. Optical analysis of particle size and chromite liberation from pulp samples of a UG2 ore regrinding circuit. Miner. Eng. 24, 1340–1347. doi:10.1016/j.mineng.2011.06.006

Lewczuk, L., 1988. Mineralogical and Liberation Study of the Iron Ore Mill Products, in: Process Mineralogy VIII. The Minerals, Metals & Materials Society, pp. 227–234.

Lin, C.L., Miller, J.D., 2005. 3D characterization and analysis of particle shape using X-ray microtomography (XMT), in: SME Annual Meeting. Salt Lake City, pp. 61–69. doi:10.1016/j.powtec.2005.04.031

Lisso, M., 2013. Evaluating the effect of operating variables on energy consumption in stirred mills. University of Cape Town.

Little, L., Becker, M., Wiese, J., Mainza, A.N., 2015, Paper 1. Auto-SEM particle shape characterisation: Investigating fine grinding of UG2 ore. Miner. Eng. 82, 92–100. doi:10.1016/j.mineng.2015.03.021

Little, L., Mainza, A.N., Wiese, J.G., Becker, M., 2016, Paper 3. Using mineralogical and particle shape analysis to investigate enhanced mineral liberation through phase boundary fracture. Powder Technol. 301, 794–804.

Little, L., Wiese, J., Becker, M., Mainza, A., Ross, V., 2016, Paper 5. Investigating the effects of particle shape on chromite entrainment at a platinum concentrator. Miner. Eng. 96-97, 46–52. doi:10.1016/j.mineng.2016.06.003

Lotter, N.O., 2011. Modern Process Mineralogy: An integrated multi-disciplined approach to flowsheeting. Miner. Eng. 24, 1229–1237. doi:10.1016/j.mineng.2011.03.004

Lotter, N.O., Bradshaw, D.J., Becker, M., Parolis, L.A.S., Kormos, L.J., 2008. A discussion of the occurrence and undesirable flotation behaviour of orthopyroxene and talc in the processing of mafic deposits. Miner. Eng. 21, 905–912. doi:10.1016/j.mineng.2008.02.023

Lotter, N.O., Kormos, L.J., Oliveira, J., Fragomeni, D., Whiteman, E., 2011. Modern Process Mineralogy: Two case studies. Miner. Eng. 24, 638–650. doi:10.1016/j.mineng.2011.02.017

Lydall, M., 2009. Backward linkage development in the South African PGM industry: A case study. Resour. Policy 34, 112–120. doi:10.1016/j.resourpol.2009.01.001

Mailula, T.D., Bradshaw, D.J., Harris, P.J., 2003. The effect of copper sulphate addition on the recovery of chromite in the flotation of UG2 ore. J. South African Inst. Min. Metall. African Inst. Min. Metall. 143–146.

Mainza, A., Powell, M.S., Knopjes, B., 2004a. A comparison of different cyclones in addressing challenges in the classification of the dual density UG2 platinum ore, in: International Platinum Conference

"Platinum Adding Value." The South African Institute of Mining and Metallurgy, pp. 95 – 102.

Mainza, A., Powell, M.S., Knopjes, B., 2004b. Differential classification of dense material in a three-product cyclone. Miner. Eng. 17, 573–579. doi:10.1016/j.mineng.2004.01.023

Mainza, A.N., 2006. Contribution to the understanding of the three-product cyclone on the classification of a dual density platinum ore. University of Cape Town.

Makvandi, S., Beaudoin, G., McClenaghan, B.M., Layton-Matthews, D., 2014. The surface texture and morphology of magnetite from the Izok Lake volcanogenic massive sulfide deposit and local glacial sediments, Nunavut, Canada: Application to mineral exploration. J. Geochemical Explor. doi:10.1016/j.gexplo.2014.12.013

Manouchehri, H.R., 2015. Towards sustainability by bridging the gap in comminution - from finely crushed ore to stirred media milling, in: SAG Conference. Canadian Institute of Mining and Metallurgy, Vancouver, pp. 1–16.

Matrox, 2016. Matrox Imaging Library Overview [WWW Document]. URL http://www.matrox.com/imaging/en/products/software/mil/ (accessed 5.17.16).

McFadzean, B., Pani, S., Wiese, J., O'Connor, C.T., 2015. The interactive effects of chemical and process parameters on the flotation performance of a UG2 ore. Miner. Eng. 70, 92–98. doi:10.1016/j.mineng.2014.08.016

Medalia, A., 1970. Dynamic shape factors for particles. Powder Technol. 4, 117–138.

Meloy, T.P., 1990. Shape characterization of particles - problems and progress, in: Advanced Materials - Application of Mineral and Metallurgical Processing Principles. Soc. Min. Eng., pp. 195 – 203.

Metso, 2016. SMD [WWW Document]. URL http://www.metso.com/products/grinding/stirred-media-detritors-smd/ (accessed 8.8.16).

Micromeritics, 2016. No Title [WWW Document]. URL http://www.particulatesystems.com/Products/Particle-Insight-Dynamic-Image-Analyzer.aspx (accessed 8.4.16).

Mollon, G., Zhao, J., 2014. 3D generation of realistic granular samples based on random fields theory and Fourier shape descriptors. Comput. Methods Appl. Mech. Eng. 279, 46–65. doi:10.1016/j.cma.2014.06.022

Mudd, G., 2015. Producing more from less [WWW Document]. CSIRO, Resour. Issue 07. URL http://www.csiro.au/en/Research/MRF/Areas/Resourceful-magazine/Issue-07/Producing-more-from-less# (accessed 6.20.16).

Mudd, G.M., 2012. Key trends in the resource sustainability of platinum group elements. Ore Geol. Rev. 46, 106–117. doi:10.1016/j.oregeorev.2012.02.005

Napier-Munn, T., 2014. Is progress in energy-efficient comminution doomed? Miner. Eng. Article in. doi:10.1016/j.mineng.2014.06.009

Napier-Munn, T.J., 2015. Statistical Methods for Mineral Engineers, How to design Experiments and Analyse Data. JKMRC, Brisbane, Australia.

Ndlovu, B., Becker, M., Forbes, E., Deglon, D., Franzidis, J.-P., 2011. The influence of phyllosilicate mineralogy on the rheology of mineral slurries. Miner. Eng. 24, 1314–1322. doi:10.1016/j.mineng.2011.05.008

Neethling, S.J., Cilliers, J.J., 2002. The entrainment of gangue into a flotation froth. Int. J. Miner. Process. 64, 123–134. doi:10.1016/S0301-7516(01)00067-9

Neethling, S.J., Cilliers, J.J., 2009. The entrainment factor in froth flotation: Model for particle size and other operating parameter effects. Int. J. Miner. Process. 93, 141–148. doi:10.1016/j.minpro.2009.07.004

Nel, E., Theron, J., Martin, C., Raabe, H., 2004. PGM Ore Processing at Impala's UG-2 Concentrator in Rustenburg, South Africa. SGS Mineral Services.

Omran, M., Fabritius, T., Mattila, R., 2015. Thermally assisted liberation of high phosphorus oolitic iron ore: A comparison between microwave and conventional furnaces. Powder Technol. 269, 7–14.

doi:10.1016/j.powtec.2014.08.073

Oxford_Instruments, 2012. Oxford Instruments [WWW Document]. URL http://www.oxford-instruments.com/OxfordInstruments/media/nanoanalysis/brochures and thumbs/OI_EDS_INCAMineral_Brochure.pdf (accessed 2.11.15).

Ozcan, O., Ruhland, M., Stahl, W., 2000. The effect of pressure, particle size and particle shape on the shear strength of very fine mineral filter cakes. Int. J. Miner. Process. 59, 185–193. doi:10.1016/S0301-7516(99)00064-2

Palaniandy, S., Azizli, K.A.M., Hussin, H., Hashim, S.F.S., 2008. Effect of operational parameters on the breakage mechanism of silica in a jet mill. Miner. Eng. 21, 380–388. doi:10.1016/j.mineng.2007.10.011

Payton, E.J., Mills, M.J., 2011. Stereology of backscatter electron images of etched surfaces for characterization of particle size distributions and volume fractions: Estimation of imaging bias via Monte Carlo simulations. Mater. Charact. 62, 563–574. doi:10.1016/j.matchar.2011.04.003

Pease, J.D., Curry, D.C., Barns, K.E., Young, M.F., Rule, C., 2006a. Transforming flowsheet design with inert grinding media - the IsaMill, in: Proceedings of 38th Annual Meeting of the Canadian Mineral Processors. CIMMP, Ottawa, pp. 231–249.

Pease, J.D., Curry, D.C., Young, M.F., 2006b. Designing flotation circuits for high fines recovery. Miner. Eng. 19, 831–840. doi:10.1016/j.mineng.2005.09.056

Pease, J.D., Young, M.F., Curry, D., Johnson, N.W., 2004. Improving fines recovery by grinding finer, in: Metallurgical Plant Design and Operating Strategies 2004. AUSIMM, Perth, WA, pp. 65 – 78. doi:10.1179/037195510X12816242170852

Penberthy, C.J., 2001. The effect of mineralogical variation in the UG2 chromitite on recovery of platinum-group elements. University of Pretoria.

Pérez-Barnuevo, L., Pirard, E., Castroviejo, R., 2013. Automated characterisation of intergrowth textures in mineral particles. A case study. Miner. Eng. 52, 136–142. doi:10.1016/j.mineng.2013.05.001

Petruk, W., 1988. Ore characteristics that affect breakage and mineral liberation, in: Process Mineralogy VIII. The Minerals, Metals & Materials Society, pp. 181–193.

Petruk, W., 1995. Some relationships between mineral textures and extractive metallurgy, in: Process Mineralogy XIII. The Minerals, Metals & Materials Society.

Petruk, W., 2000. Applied mineralogy in the mining industry. Elsevier Science, Oxford.

Pillay, K., 2015. Mineralogical effects on the dense medium separation of low grade nickel ore. University of Cape Town.

Pirard, E., 1990. Applications of shape analysis in ore beneficiation, in: Process Mineralogy IX: Applications to Mineral Beneficiation, Metallurgy, Gold, Diamonds. TMS, pp. 205–218.

Pirard, E., 2004. Image Measurements, in: Francus, P. (Ed.), Image Analysis, Sediments and Paleoenvironments. Springer, Dordrecht, The Netherlands, pp. 76–77.

Pons, M.-N., Vivier, H., 1990. Crystallization monitoring by quantitative image analysis. Anal. Chim. Acta 238, 243–249. doi:10.1016/S0003-2670(00)80543-7

Pons, M.N., Vivier, H., Belaroui, K., Bernard-Michel, B., Cordier, F., Oulhana, D., Dodds, J. a., 1999. Particle morphology: From visualisation to measurement. Powder Technol. 103, 44–57. doi:10.1016/S0032-5910(99)00023-6

Pons, M.-N., Vivier, H., Delcour, V., Authelin, J.-R., Paillères-Hubert, L., 2002. Morphological analysis of pharmaceutical powders. Powder Technol. 128, 276–286. doi:10.1016/S0032-5910(02)00177-8

Pourghahramani, P., 2012. Effects of ore characteristics on product shape properties and breakage mechanisms in industrial SAG mills. Miner. Eng. 32, 30–37. doi:10.1016/j.mineng.2012.03.005

Powell, M.S., Mainza, A.N., 2012. Step Change – a Staircase Rather Than a Giant Leap, in: XXVI International Mineral Processing Congress (IMPC). Gecamin, New Delhi, India, pp. 4259–4268.

Powell, M.S., Morrison, R.D., 2007. The future of comminution modelling. Int. J. Miner. Process. 84, 228–

239. doi:10.1016/j.minpro.2006.08.003

Radziszewski, P., 2013. Assessing the stirred mill design space. Miner. Eng. 41, 9–16. doi:10.1016/j.mineng.2012.10.012

Rahimi, M., Dehghani, F., Rezai, B., Aslani, M.R., 2012. Influence of the roughness and shape of quartz particles on their flotation kinetics. Int. J. Miner. Metall. Mater. 19, 284–289. doi:10.1007/s12613-012-0552-z

Ralph, B., Kurzydłowski, K.J., 1997. The philosophy of microscopic quantification. Mater. Charact. 38, 217–227. doi:10.1016/S1044-5803(97)00051-X

Resabel, V.J., Manlapig, E., Evans, C.L., Wightman, E.M., 2014. A method using 2-D images obtained from SEM-based image analysis system to model mineral liberation in regrind stirred mills, in: MEI Process Mineralogy '14. Cape Town.

Retsch Technology, 2016. Camsizer XT [WWW Document]. URL http://www.retsch-technology.com/rt/products/dynamic-image-analysis/camsizer-xt/function-features/? (accessed 1.13.16).

Rickman, D., Lohn-Wiley, B., Knicely, J., Hannan, B., 2016. Probabilistic solid form determined from 2D shape measurement. Powder Technol. 291, 466–472. doi:10.1016/j.powtec.2015.10.044

Roufail, R.A., 2011. The effect of stirred mill operation on particles breakage mechanism and their morphological features. The University of British Columbia.

Rule, C., 2010. Stirred milling — new comminution technology in the PGM industry, in: The 4th International Platinum Conference, Platinum in Transition "Boom or Bust." pp. 71–78.

Rule, C., 2011. Stirred milling at Anglo American Platinum, in: International Conference on Autogenous Grinding, Semiautogenous Grinding and High Pressure Grinding Roll Technology.

Rule, C., 2015. Pushing the Boundaries of Feed Size with IsaMill inert grinding, in: SAG Conference. Canadian Institute of Mining and Metallurgy, Vancouver, pp. 1–17.

Rule, C., Schouwstra, R.P., 2011. Process mineralogy delivering significant value at Anglo Platinum concentrator operations, in: 10th International Congress for Applied Mineralogy. Trondheim, pp. 1–5.

Russ, J.C., 1995. The Image Processing Handbook, 2nd ed. CRC Press, Raleigh, North Carolina.

Safari, M., Harris, M., Deglon, D., 2014. The Effect of Energy Input on the flotation kinetics of galena in an oscillating grid flotation cell, in: XXVII International Mineral Processing Congress, Santiago, Chile. Gecamin, Santiago, pp. 1–10.

Savassi, O.N., Alexander, D.J., Franzidis, J.P., Manlapig, E.V., 1998. An empirical model for entrainment in industrial flotation plants. Miner. Eng. 11, 243–256. doi:10.1016/S0892-6875(98)00003-X

Scharneck, Y., Andrews, L., 2012. The use of QEMSCAN techniques to characterize entrained matte in platinum furnace slags, in: Ninth International Conference on Molten Slags, Fluxes and Salts. Pyro.co.za, Beijing, China, p. W114.

Schubert, H., 1999. On the turbulence-controlled microprocesses in flotation machines. Int. J. Miner. Process. 56, 257–276. doi:10.1016/S0301-7516(98)00048-9

Schubert, H., 2008. On the optimization of hydrodynamics in fine particle flotation. Miner. Eng. 21, 930–936. doi:10.1016/j.mineng.2008.02.012

Shi, F., Morrison, R., Cervellin, A., Burns, F., Musa, F., 2009. Comparison of energy efficiency between ball mills and stirred mills in coarse grinding. Miner. Eng. 22, 673–680. doi:10.1016/j.mineng.2008.12.002

Sinnott, M., Cleary, P.W., Morrison, R., 2006. Analysis of stirred mill performance using DEM simulation: Part 1– Media motion, energy consumption and collisional environment. Miner. Eng. 19, 1537–1550. doi:10.1016/j.mineng.2006.08.012

Solomon, N., Becker, M., Mainza, A., Petersen, J., Franzidis, J.-P., 2011. Understanding the influence of HPGR on PGM flotation behavior using mineralogy. Miner. Eng. 24, 1370–1377. doi:10.1016/j.mineng.2011.07.015

Solomon, N., Mainza, A., Becker, M., Petersen, J., Ross, V., Franzidis, J.-P., 2010. Effects of high pressure grinding rolls on platinum-bearing ores and the flotation response as compared to the conventional ball mill, in: XXV International Mineral Processing Congress (IMPC) 2010 Proceedings. Brisbane, Australia, pp. 1249–1263.

Song, S., Campos-Toro, E.F., López-Valdivieso, A., 2013. Formation of micro-fractures on an oolitic iron ore under microwave treatment and its effect on selective fragmentation. Powder Technol. 243, 155–160. doi:10.1016/j.powtec.2013.03.049

Spencer, S., Sutherland, D., 2000. Stereological Correction of Mineral Liberation Grade Distributions Estimated By Single Sectioning of Particles. Image Anal. Stereol. 19, 175–182. doi:10.5566/ias.v19.p175-182

Sutherland, D., 2007. Estimation of mineral grain size using automated mineralogy. Miner. Eng. 20, 452–460. doi:10.1016/j.mineng.2006.12.011

Tavares, L.M., 2009. Analysis of particle fracture by repeated stressing as damage accumulation. Powder Technol. 190, 327–339. doi:10.1016/j.powtec.2008.08.011

Tescan, 2012. Tescan [WWW Document]. URL http://www.tescan.com/en/products/tima/tima-lm (accessed 2.11.15).

Tonzetic, I., 2015. Quantitative analysis of iron ore using SEM based technologies, in: Iron Ore: Mineralogy, Processing and Environmental Issues.

Triffett, B., Bradshaw, D.J., 2008. The role of morphology and host rock lithology on the flotation behaviour of molybdenite at Kennecott Utah Copper, in: 9th International Congress for Applied Mineralogy. Brisbane, Australia, pp. 465–473.

Triffett, B., Veloo, C., Adair, B.J.I., Bradshaw, D., 2008. An investigation of the factors affecting the recovery of molybdenite in the Kennecott Utah Copper bulk flotation circuit. Miner. Eng. 21, 832–840. doi:10.1016/j.mineng.2008.03.003

Ulusoy, U., Hiçyılmaz, C., Yekeler, M., 2004. Role of shape properties of calcite and barite particles on apparent hydrophobicity. Chem. Eng. Process. 43, 1047–1053. doi:10.1016/j.cep.2003.10.003

Ulusoy, U., Igathinathane, C., 2014. Dynamic image based shape analysis of hard and lignite coal particles ground by laboratory ball and gyro mills. Fuel Process. Technol. 126, 350–358. doi:10.1016/j.fuproc.2014.05.017

Ulusoy, U., Kursun, I., 2011. Comparison of different 2D image analysis measurement techniques for the shape of talc particles produced by different media milling. Miner. Eng. 24, 91–97. doi:10.1016/j.mineng.2010.05.011

Ulusoy, U., Yekeler, M., 2005. Correlation of the surface roughness of some industrial minerals with their wettability parameters. Chem. Eng. Process. Process Intensif. 44, 555–563. doi:10.1016/j.cep.2004.08.001

Ulusoy, U., Yekeler, M., 2014. Dynamic image analysis of calcite particles created by different mills. Int. J. Miner. Process. 133, 83–90. doi:10.1016/j.minpro.2014.10.006

Ulusoy, U., Yekeler, M., Hiçyılmaz, C., 2003. Determination of the shape, morphological and wettability properties of quartz and their correlations. Miner. Eng. 16, 951–964. doi:10.1016/j.mineng.2003.07.002

Unland, G., Al-Khasawneh, Y., 2009. The influence of particle shape on parameters of impact crushing. Miner. Eng. 22, 220–228. doi:10.1016/j.mineng.2008.08.008

van de Ruit, L., Becker, M., Wiese, J., Mainza, A., 2014. A mineralogical investigation of the effect of particle shape on chromite entrainment for a UG2 ore, in: XXVII International Mineral Processing Congress, Santiago, Chile. Santiago.

Varinot, C., Hiltgun, S., Pons, M.-N., Dodds, J., 1997. Identification of the fragmentation mechanisms in wet-phase fine grinding in a stirred bead mill. Chem. Eng. Sci. 52, 3605–3612.

Vashisth, S., Bennington, C.P.J., Grace, J.R., Kerekes, R.J., 2011. Column Flotation Deinking: State-of-the-art and opportunities. Resour. Conserv. Recycl. 55, 1154–1177. doi:10.1016/j.resconrec.2011.06.013

Vermeulen, L.., Howat, D.D., 1989. A sampling procedure validated. J. South African Inst. Min. Metall. 89, 365–370.

Verrelli, D.I., Bruckard, W.J., Koh, P.T.L., Schwarz, M.P., Follink, B., 2012. Influence of particle shape and roughness on the induction period for particle-bubble attachment, in: XXVI International Mineral Processing Congress (IMPC). New Delhi, India, pp. 5665–5676.

Verrelli, D.I., Bruckard, W.J., Koh, P.T.L., Schwarz, M.P., Follink, B., 2014. Particle shape effects in flotation. Part 1: Microscale experimental observations. Miner. Eng. 58, 80–89. doi:10.1016/j.mineng.2014.01.004

Verrelli, D.I., Koh, P.T.L., Bruckard, W.J., Schwarz, M.P., 2012. Variations in the induction period for particle–bubble attachment. Miner. Eng. 36-38, 219–230. doi:10.1016/j.mineng.2012.03.034

Vizcarra, T.G., 2010. The Effect of Comminution Mechanism on Particle Properties: Consequences for Downstream Flotation Performance. University of Queensland.

Vizcarra, T.G., Harmer, S.L., Wightman, E.M., Johnson, N.W., Manlapig, E.V., 2011a. The influence of particle shape properties and associated surface chemistry on the flotation kinetics of chalcopyrite. Miner. Eng. 24, 807–816. doi:10.1016/j.mineng.2011.02.019

Vizcarra, T.G., Wightman, E.M., Johnson, N.W., Manlapig, E.V., 2010. The effect of breakage mechanism on the mineral liberation properties of sulphide ores. Miner. Eng. 23, 374–382. doi:10.1016/j.mineng.2009.11.012

Vizcarra, T.G., Wightman, E.M., Johnson, N.W., Manlapig, E.V., 2011b. The effect of breakage method on the shape properties of an iron-oxide hosted copper–gold ore. Miner. Eng. 24, 1454–1458. doi:10.1016/j.mineng.2011.07.007

Vonlanthen, P., Rausch, J., Ketcham, R.A., Putlitz, B., Baumgartner, L.P., Grobéty, B., 2015. High-resolution 3D analyses of the shape and internal constituents of small volcanic ash particles: The contribution of SEM micro-computed tomography (SEM micro-CT). J. Volcanol. Geotherm. Res. 293, 1–12. doi:10.1016/j.jvolgeores.2014.11.016

Wadell, H., 1935. Volume, shape, and roundness of quartz particles. J. Geol. 43, 250–279.

Walker, C.I., Hambe, M., 2015. Influence of particle shape on slurry wear of white iron. Wear 332-333, 1021–1027. doi:10.1016/j.wear.2014.12.029

Wang, L., Peng, Y., Runge, K., Bradshaw, D., 2015. A review of entrainment: Mechanisms, contributing factors and modelling in flotation. Miner. Eng. 70, 77–91. doi:10.1016/j.mineng.2014.09.003

Weerasekara, N.S., Powell, M.S., Cleary, P.W., Tavares, L.M., Evertsson, M., Morrison, R.D., Quist, J., Carvalho, R.M., 2013. The contribution of DEM to the science of comminution. Powder Technol. 248, 3–4. doi:10.1016/j.powtec.2013.05.032

Wesseldijk, Q.I., Reuter, M.A., Bradshaw, D.J., Harris, P.J., 1999. The flotation behaviour of chromite with respect to the beneficiation of UG2 ore. Miner. Eng. 12, 1177–1184.

Westermann, J., n.d. Particle Characterization with Dynamic Image Analysis. Retsch Technol. Whitepaper 1–8.

Wiese, J., Becker, M., Yorath, G., O'Connor, C., 2015. An investigation into the relationship between particle shape and entrainment. Miner. Eng. 83, 211–216. doi:10.1016/j.mineng.2015.09.012

Wiese, J., Becker, M., Yorath, G., O'Connor, C.T., 2014. An investigation into the relationship between particle shape and entrainment, in: XXVII International Mineral Processing Congress, Santiago, Chile.

Wiese, J., Harris, P., Bradshaw, D., 2005. The influence of the reagent suite on the flotation of ores from the Merensky reef. Miner. Eng. 18, 189–198. doi:10.1016/j.mineng.2004.09.013

Wills, B.A., Napier-Munn, T., 2006. Wills' Mineral Processing Technology, 7th ed. Elsevier Science & Technology Books.

Xiao, X., Zhang, G., Feng, Q., Xiao, S., Huang, L., Zhao, X., Li, Z., 2012. The liberation effect of magnetite fine ground by vertical stirred mill and ball mill. Miner. Eng. 34, 63–69. doi:10.1016/j.mineng.2012.04.004

Xie, H.Y., Zhang, D.W., 2001. Stokes shape factor and its application in the measurement of spherity of non-spherical particles. Powder Technol. 114, 102–105. doi:10.1016/S0032-5910(00)00269-2

Xu, W., Dhawan, N., Lin, C.L., Miller, J.D., 2013. Further study of grain boundary fracture in the breakage of single multiphase particles using X-ray microtomography procedures. Miner. Eng. 46-47, 89–94. doi:10.1016/j.mineng.2013.03.016

Ye, X., Gredelj, S., Skinner, W., Grano, S.R., 2010. Regrinding sulphide minerals — Breakage mechanisms in milling and their influence on surface properties and flotation behaviour. Powder Technol. 203, 133–147. doi:10.1016/j.powtec.2010.05.002

Yekeler, M., Ulusoy, U., Hiçyılmaz, C., 2004. Effect of particle shape and roughness of talc mineral ground by different mills on the wettability and floatability. Powder Technol. 140, 68–78. doi:10.1016/j.powtec.2003.12.012

Yianatos, J., Contreras, F., 2010. Particle entrainment model for industrial flotation cells. Powder Technol. 197, 260–267. doi:10.1016/j.powtec.2009.10.001

Yianatos, J.B., Moys, M.H., Contreras, F., Villanueva, a., 2008. Froth recovery of industrial flotation cells. Miner. Eng. 21, 817–825. doi:10.1016/j.mineng.2007.12.012

Zeiss_Microscopy, n.d. Zeiss Microscopy [WWW Document]. URL http://www.zeiss.co.za/microscopy/en_za/products/scanning-electron-microscopes/mineralogic-systems.html (accessed 2.11.15).

Zheng, X., Johnson, N.W., Franzidis, J.-P., 2006. Modelling of entrainment in industrial flotation cells: Water recovery and degree of entrainment. Miner. Eng. 19, 1191–1203. doi:10.1016/j.mineng.2005.11.005

Zhu, J.Y., Tan, F., Scallon, K.L., Zhao, Y.L., Deng, Y., 2005. Deinking selectivity (Z -factor): a new parameter to evaluate the performance of flotation deinking process. Sep. Purif. Technol. 43, 33–41. doi:10.1016/j.seppur.2004.09.011

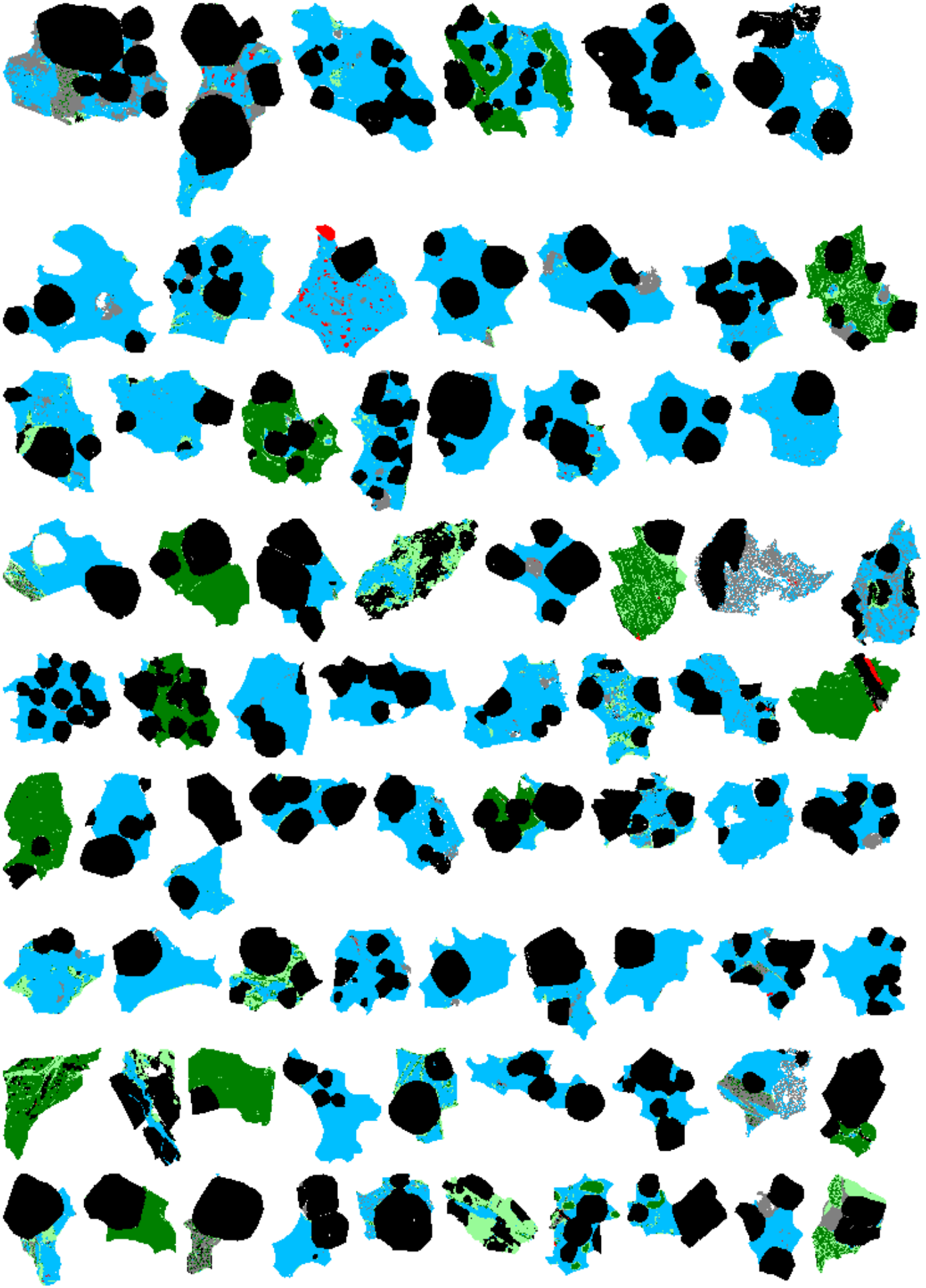

APPENDICES

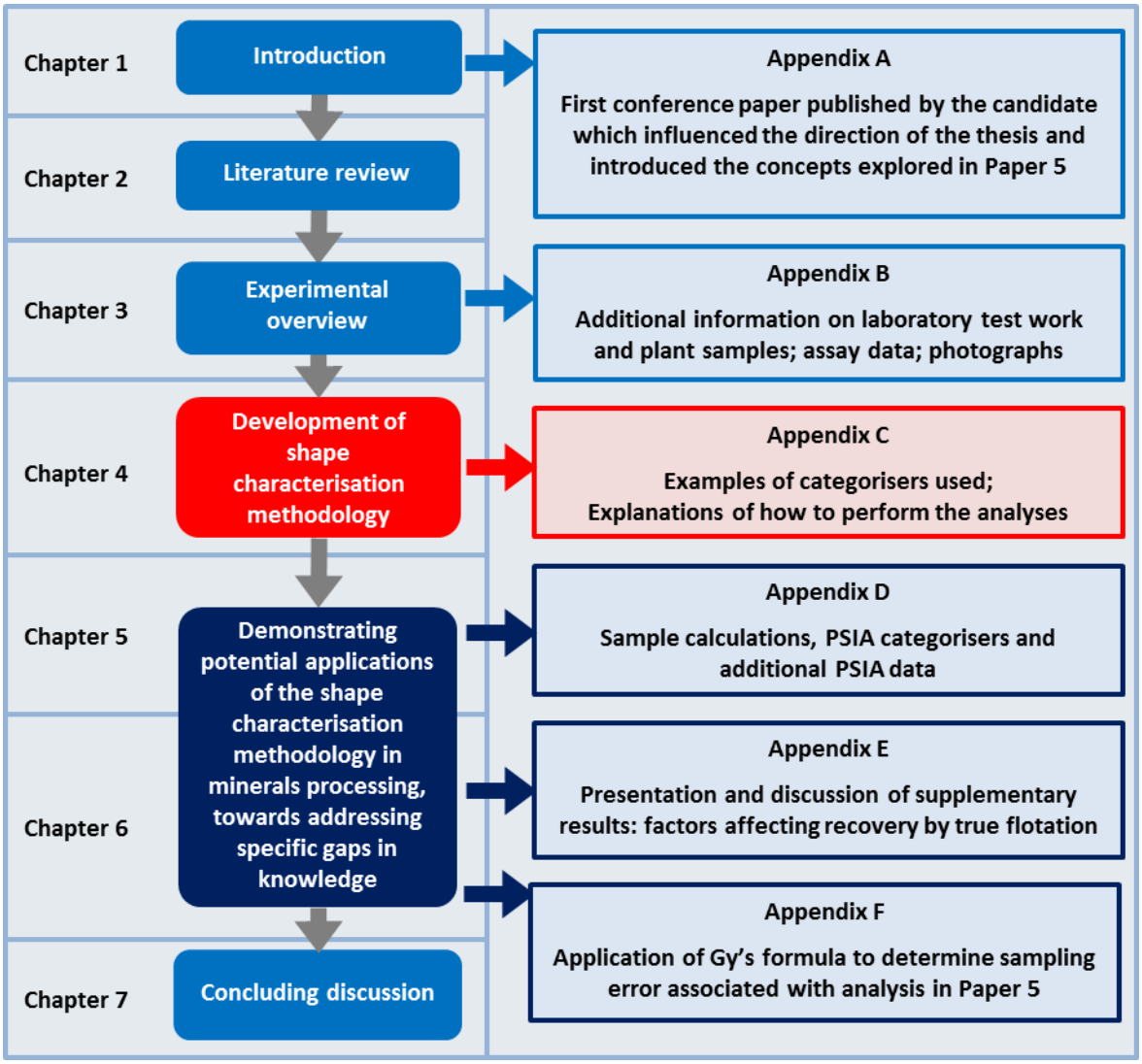

Illustration of how the appendices have been structured; each appendix is complementary to a specific chapter of the thesis.

Appendix A

Paper 0: A mineralogical investigation of the effect of particle shape on chromite entrainment for a UG2 ore

---

Published in: Proceedings of the XXVIIth International Mineral Processing Congress, Santiago, Chile, 2014, Gecamin.

Abstract

UG2 chromitite ore is a complex, highly disseminated platinum ore from the Bushveld Complex in South Africa, with typical platinum group mineral (PGM) grain sizes below 15µm. The introduction of stirred mills to the platinum industry has enabled grinding to finer product sizes, which has improved liberation and recovery of the finely grained PGMs. However, reduction in particle size leads to an increase in chromite entrainment in the flotation concentrate, which has a negative impact on the subsequent smelting process. Factors such as particle size, froth structure, solids concentration and water recovery have all been identified as impacting entrainment, but whether particle shape also has a significant effect is unclear. The purpose of this study was to determine whether the recovery of chromite particles by entrainment during the flotation of UG2 ore is affected by particle morphology.

A laboratory vertical stirred mill with inert ceramic media was used for grinding UG2 ore which was then floated in a batch flotation cell. Flotation feed and concentrate samples were analysed using QEMSCAN to quantify the angularity and aspect ratio distributions of the particles. The stirred mill product was found to have relatively broad aspect ratio and angularity distributions, with the major mineral components (chromite and silicates) having very similar shape characteristics. Analysis of flotation feed and concentrate samples suggested that particle shape does not have a significant effect on chromite entrainment.

A.1 Introduction

The Bushveld Complex in South Africa hosts most of the world's platinum group mineral resources within three ore bodies, the Merensky Reef, Upper Group 2 Chromitite (UG2) and Platreef. A detailed survey of global PGE resources in 2010 reported that 70.9% of the world's PGE resources are within the Bushveld Complex, of which UG2 ore contributes about 60% (Mudd, 2012).

UG2 ore contains up to 75% chromite by mass, which is interlocked with silicates, mainly orthopyroxene and plagioclase. Head grades vary between 2 and 9 g/t (4E-PGE) with the majority between 3 and 5 g/t (Hay & Roy, 2010; Rule & Schouwstra, 2011; Mudd, 2012). UG2 ore is a challenging ore to process due to the fine PGM grains (<10μm) which, unlike Merensky ore, do not have a high association with the base metal sulfides. In order to liberate these finely grained PGMs for flotation, stirred mills are used for fine grinding. The large portion of chromite in the ore introduces additional challenges to both the comminution and flotation circuits.

The comminution challenge is due to the high density of the chromite (SG ~5) relative to the silicates (SG ~2.6 – 3) in the ore which leads to inefficiencies in classification, causing a high circulating load of fine chromite particles. This leads to the loss of PGMs locked in coarse silicate particles that report to cyclone overflow, a reduction in the mill's capacity for fresh feed, and energy being wasted in over-grinding chromite (Mainza et al., 2004a).

The challenge for the flotation circuit is to minimize the chromite recovery in the concentrate because of the problems it causes in the smelter (Hay & Roy 2010). This study was set out to address the latter problem, but the methodology used has potential as a technique to monitor the former.

Chromite is dense and naturally hydrophilic, so it is generally not recovered to the concentrate by true flotation. However, at fine particle sizes (-45 microns) chromite particles are recovered to the concentrate by entrainment. Hay and Roy (2010) describe the ability to predict chromite recovery and identify potential areas for its reduction as having a significant impact on a project's financials and subsequently, plant design.

Entrainment is the mechanism by which hydrophilic particles are transported into the froth within the water that forms lamella between bubbles. The main factors affecting entrainment are particle size, density, froth structure, water recovery and solids concentration. Entrainment has been observed to have a linear relationship with water recovery for fine particles (Engelbrecht and Woodburn, 1975). In the development of various entrainment models, authors have suggested that particle morphology would have an effect on entrainment, but this

was only accounted for within a 'froth structure factor' (Kirjavainen, 1996; Savassi et al., 1998). In de-inking for paper recycling, fiber length has been shown to affect entrainment, with long fibers moving higher up in the flotation froth leading to increased entrainment (Zhu et al., 2005). In a concurrent study investigating entrainment rates of spherical ballotini and various single minerals with different shape characteristics, Wiese et al. (2014) have shown that more angular, elongated particles have a higher degree of entrainment than regular or spherical particles.

Particle morphology is difficult to characterize fully, with a wide number of different techniques and descriptors used. In the past it was difficult to take enough measurements to be statistically representative but automated technology enables analysis of thousands of particles, and thus the ability to represent shape characteristics of a sample as a distribution (Pourghahramani, 2012; Vizcarra, 2011). The advantage of automated scanning electron microscopy (auto-SEM) is that it gives direct measurements of the morphology on a mineral basis. A weakness is that the measurements are two-dimensional, so stereological errors may be introduced. Three dimensional methods used include resistance to flow through a packed bed, and rheological studies (Hicyilmaz et al., 2005; Khonthu, 2012; Wiese et al., 2014). The auto-SEM approach has been used to show that different mill types can affect the morphology of progeny particles, and that particle angularity affects particle-bubble attachment and thus recovery by true flotation. There do not appear to be any reports in the literature of these techniques being used to investigate comminution with stirred mills, nor the effect of particle shape on entrainment. QEMSCAN, which provides information such as mineral composition, liberation and particle shape characteristics, is used in this study to investigate the effect of particle shape on entrainment of chromite during flotation of a UG2 ore.

This study is a subsection of an investigation of the relationship between fine-grinding and flotation performance using mineralogy. The overall aim is to analyze particle characteristics caused by different mill types in terms of mineral liberation and association, particle size distribution (PSD) and particle morphology, and use these to link various flotation responses to causes within the comminution circuit.

A.2 Methodology

The experimental set-up was designed to produce similar flotation conditions at the laboratory scale to those used in industry. The approach was to compare angularity distributions of flotation feed and concentrate to determine whether particles with certain shape characteristics within the feed have a greater chance of reporting to the concentrate by entrainment than others.

UG2 primary mill discharge was used as the feed sample, with a top size of 1.12 mm. It was blended and rigorously split into 3 kg samples using a rotary splitter. Each sample was then milled in a batch laboratory scale vertical stirred mill. A milling time of 9 minutes and 10 seconds corresponding to an energy input of 18 kWh/t was used to obtain a grind with a P80 of 43µm and a P50 of 20 µm. A Fluke Power Logger was used to measure the energy input. After milling, the slurry was washed from the media and placed in an 8 L modified Leeds float cell.

The flotation reagents used were sodium isobutyl xanthate at a dosage of 150 g/t, a guar depressant at 200 g/t, and a polyglycol frother at 40 g/t. Additional flotation tests with excess depressant (500 g/t) were performed to estimate the degree of entrainment, under the assumption that all of the naturally floatable gangue is depressed at this dosage (Wiese et al., 2005, 2009). The impeller speed was 1200 rpm, and the air flow rate was 13 l/min to give a Jg of 0.65 cm/s. Four concentrates were collected over 2, 4, 6 and 8 minute periods consecutively, with scraping every 15 seconds. Synthetic plant water was used in the mill slurry, for washing the media and as make-up water during the flotation tests to simulate typical plant conditions. The recipe for the synthetic plant water used is detailed by Wiese et al. (2005). Water and mass recoveries were measured and recorded.

Flotation feed, concentrate and tails samples were dried and weighed. Mass - water recoveries were used to ascertain the repeatability of the flotation tests, and to determine the degree of entrainment as described by Wiese et al. (2005). The concentrates from the 200 g/t tests were combined and split using a micro-riffler into samples for assay, sizing and QEMSCAN. The stirred mill product was split into 5 size fractions for QEMSCAN, but only the -10 µm and +53/-75 µm fractions are included in this report. More than 90% of the concentrate was finer than 10 µm, so this was not sized. QEMSCAN samples were prepared as vertical-cross-sections to prevent the settling of dense chromite from causing bias in the results. The blocks were analysed using the Particle Mineral Analysis setting on a QEMSCAN 650F, with over 100 000 particles scanned in each fraction. There were at least 20 000 liberated chromite particles in each fraction after processing to screen out touching particles and particles less than 1 µm, as these images are typically composed of one or two pixels. The resolution was set at 0.5 µm/pixel for the -10 µm size fraction, and 3 µm/pixel for the +53/-75 µm fraction. Mineral data validation was performed by comparison of the QEMSCAN calculated assays with chemical assays.

The QEMSCAN software enables the classification of particles into different categories based on mineral composition, size, shape factor, aspect ratio, degree of liberation, and a number of other characteristics. The QEMSCAN ‘shape factor’ is described as the ratio of the square of the perimeter to the area of the particle, so this factor was divided by 4π to give angularity, the

inverse of circularity. Aspect ratio was calculated as the ratio of the longest axis of a particle to the widest perpendicular axis of that particle. Figure A.1 demonstrates classification of flotation feed particles into different groups using the QEMSCAN image grid, based on their angularities and aspect ratios.

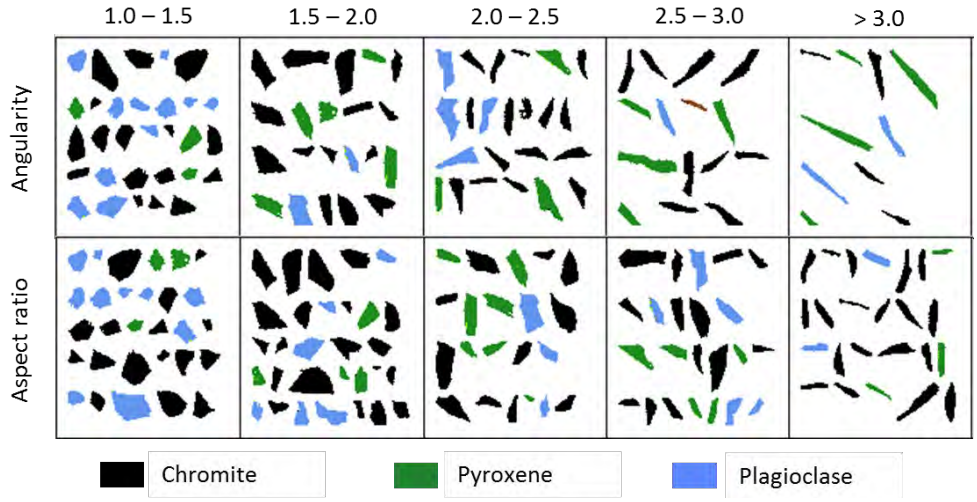

Figure A.1: QEMSCAN images of particles in the +53/-75 µm size class of the stirred mill product, categorised by both angularity and aspect ratio

Of the two descriptors, angularity has the advantage of being able to differentiate between irregularly shaped particles and smooth ones of similar aspect ratios; however it is dependent on the image resolution, so comparisons in angularity can only be accurate for particle images composed of a similar number of pixels, or for samples with very similar size distributions scanned at the same resolution. It appears that the QEMSCAN perimeter measurement counts the number of pixels around the edge of the particle, and multiplies this by the pixel spacing. For particle images composed of a few pixels, this can lead to angularity values less than one for non-rounded particles. For example an image of only 5 pixels will generally present an angularity value of $5/(5x4\pi) = 0.4$. This can lead to the impression that particles become more rounded with increasing fineness. As aspect ratio is less dependent on image resolution, it was used instead of angularity for the comparison of fine chromite particles in the feed and concentrate.

The frequency distributions were plotted based on particle count, i.e. the number of particles in each class rather than the mass of particles in each class, to reduce the dependence of the shape distributions on size.

A.3 Results and Discussion

Flotation performance

The bulk mineral compositions of the UG2 ore feed and concentrate are shown in Figure A.2. The 4-PGE grades of the feed and concentrate were 6 g/t and 200 g/t respectively, with a PGM recovery of 90%. The degree of entrainment was calculated from the gradient of the solids recovery vs water recovery plot at excess depressant dosage (Figure A.3), followed by subtraction of the mass of base metal sulfides recovered (true flotation). This gave a value of 0.03 grams of entrained solid per gram of water recovered. Assuming that the degree of entrainment was the same for the excess (500 g/t) and normal (200 g/t) depressant dosage tests, then 53% of the solids recovered in the normal (200g/t) depressant dosage test was recovered by true flotation.

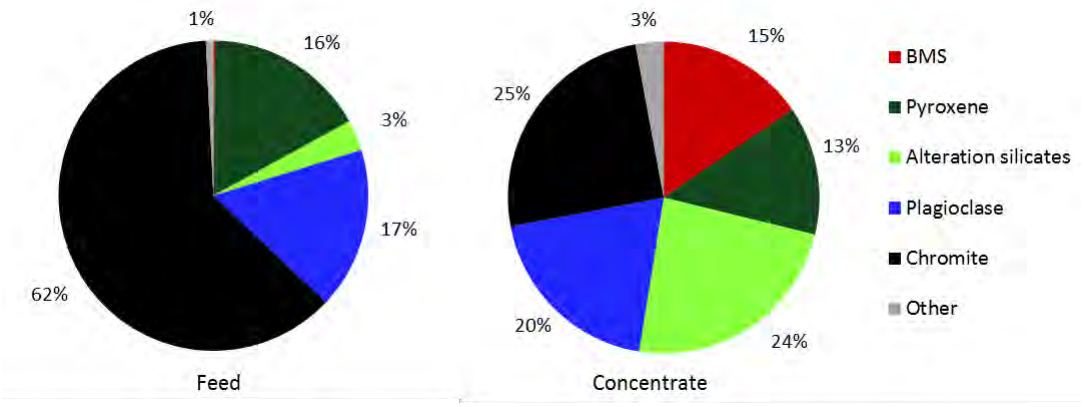

Figure A.2: Bulk mineralogy of the feed and concentrate for the 200g/t test. BMS represents the base metal sulfides (chalcopyrite, pentlandite, pyrrhotite), and alteration silicates represents talc, chlorite, amphibole and serpentine.

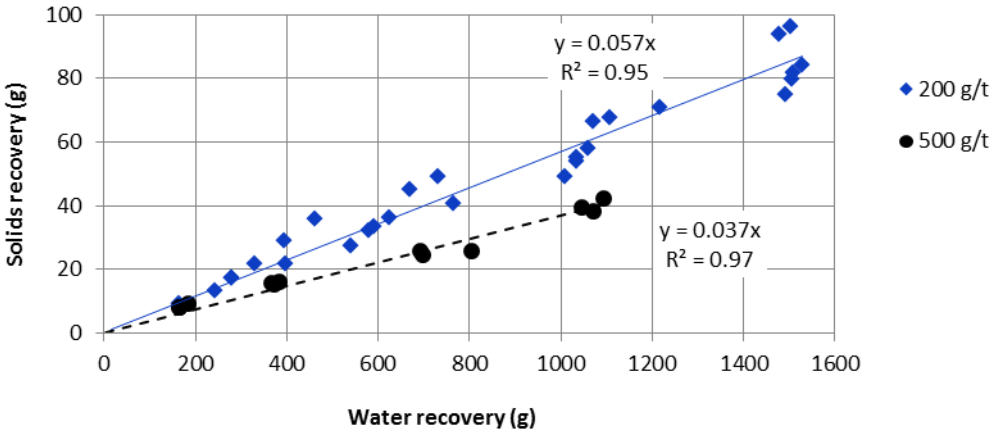

Figure A.3: Cumulative solids vs cumulative water recoveries for replicate flotation tests

Shape characterisation of the flotation feed

Figure A.4 shows the aspect ratio and angularity distributions of liberated (>90% area) chromite and silicate particles in the -75/+53 µm fraction of the stirred mill product, along with fitted beta distribution curves. These suggest that the breakage mechanisms within the mill are consistent for both the chromite and silicate minerals, producing fairly angular particles with a relatively high proportion of elongated particles.

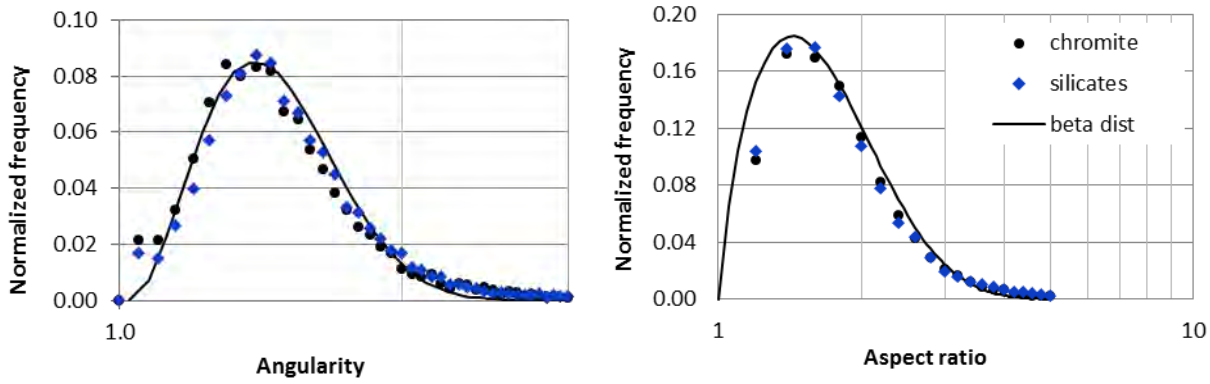

Figure A.4: Angularity and aspect ratio frequency distributions of liberated chromite and silicate particles in the +53 µm size fraction of the mill product

Effect of particle morphology on entrainment

Particle size is known to affect entrainment, and in this study the chromite entrained in the concentrate was considerably more fine than the chromite in the corresponding size class (-10µm) of the feed, as shown in Figure A.5. The initial plot of cumulative aspect ratio distributions of chromite in the feed and concentrates is shown in the same figure.

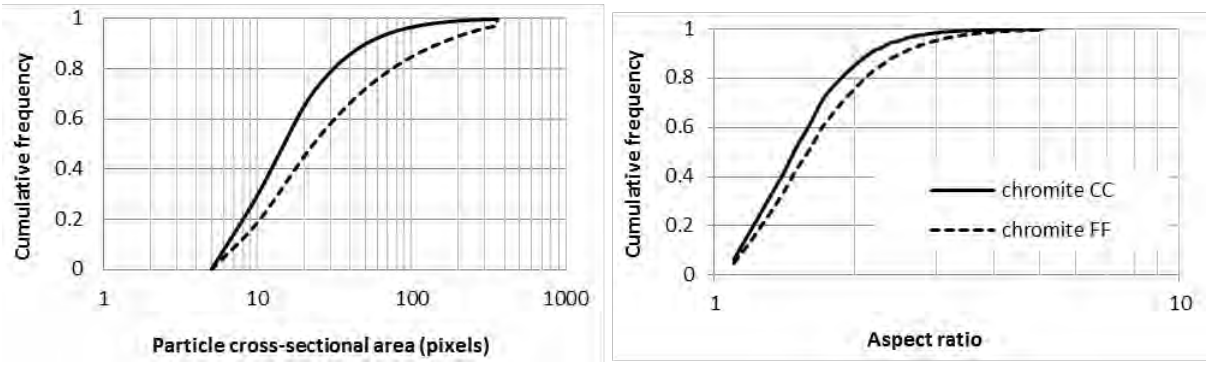

Figure A.5: Particle size and aspect ratio cumulative frequency distributions of liberated chromite particles in the -10 µm fraction of the flotation feed (FF) and combined concentrate (CC). A cross-sectional area of 100 pixels corresponds to an equivalent diameter of 8 µm

Figure A.5 suggests that size could be a confounding variable in the study, as the chromite particles in the concentrate are both more rounded and finer than those in the feed. The

relationship between particle image size (pixels) and mean aspect ratio is investigated further in Figure A.6. Particles in both the feed and concentrate were grouped into narrow size classes, and the mean aspect ratio of each size class was calculated. A strong positive correlation between size and mean aspect ratio is observed, particularly for fine particles. This suggests that the difference in particle size distribution between the chromite in the feed and concentrate could be responsible for the observed difference in aspect ratio distributions.

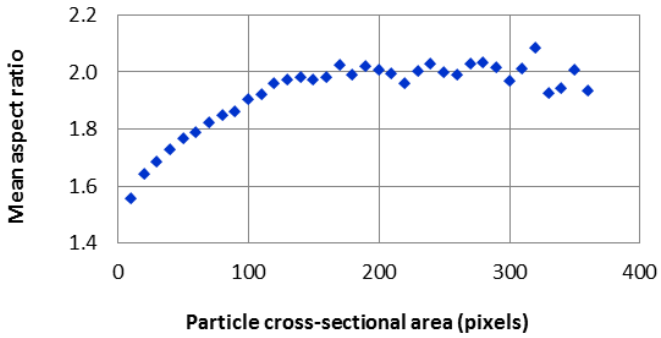

Figure A.6: Variation of mean aspect ratio with particle size (pixels).

In an effort to investigate the effect of shape independent of size, the particles in the -10 μm fraction were divided into two sub-fractions using the QEMSCAN software, as shown in Figure A.7. The fine fraction (<40 pixels, equivalent sphere diameter of 5 μm) is considered most appropriate as it only shows a slight difference between the feed and concentrate size distributions. The new aspect ratio distributions of chromite in the feed and concentrate with particle areas below 40 pixels are very similar suggesting that the effect of shape on entrainment is of no practical significance. The slight difference still observed is expected to be due to the slight difference remaining in the PSDs. This suggests that under constant froth conditions, particle morphology does not have an effect on entrainment, with more elongated particles having an equal likelihood of being entrained as regularly shaped ones.

In a concurrent study, Wiese et al. (2014) compared the degree of entrainment obtained when separate samples of angular wollastonite and spherical ballotini were floated independently, and found that the wollastonite had a higher degree of entrainment than the ballotini, even though the ballotini was finer. It is possible that the difference between the two studies can be explained by froth stability. If particle shape affects froth stability, it could have an indirect effect on the degree of entrainment.

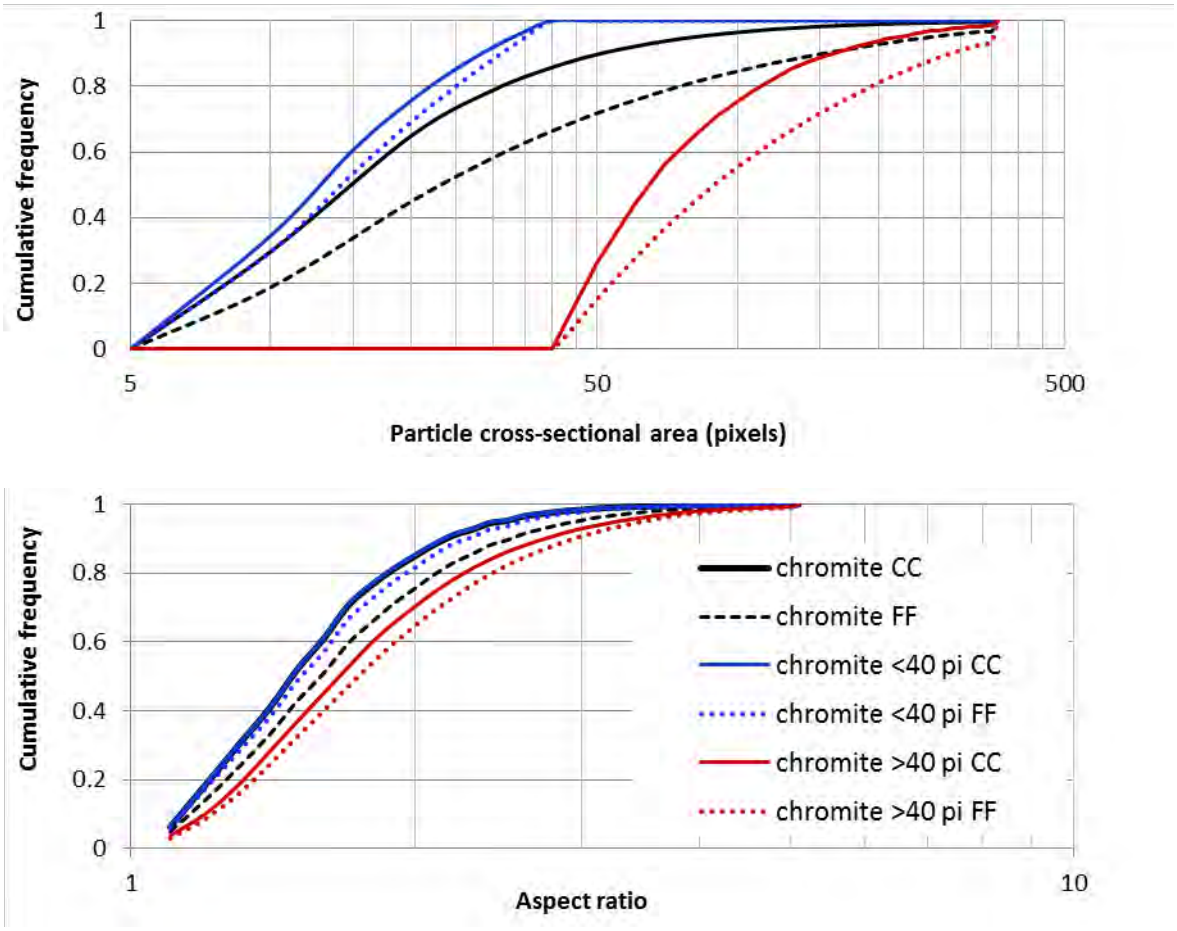

Figure A.7: Particle size and aspect ratio cumulative frequency distributions comparing liberated chromite particles in the -10 µm fractions of the flotation feed (FF) and combined concentrate (CC) of the +/- 40 pixel (5 µm) sub-fractions.

A.4 Conclusions

When fine grinding UG2 ore in a batch stirred mill, there is no significant difference in particle angularity of the major mineral components, despite differences in friability of these minerals.

Below an equivalent diameter of about 8 µm, it was observed that chromite particles become less elongated with decreasing size. It was therefore necessary to take the particle size distribution of each sample into consideration for comparison of the feed and concentrate shape characteristics. For sub-fractions with similar size distributions there was minimal difference in aspect ratio distributions between chromite particles in the feed and concentrate. This shows that during flotation of UG2 ore, the shape characteristics of the chromite particles in the feed have no effect on their entrainment.

A.5 Acknowledgements

The authors would like to thank the South African Minerals to Metals Research Institute (SAMMRI), the Department of Science and Technology, South Africa (DST) and the South African

National Research Foundation (NRF) for funding; and Anglo American Technical Operations for providing the stirred mill that was used.

A.6 References

Becker, M., Mainza, A. N., Powell, M. S., Bradshaw, D. J., & Knopjes, B. (2008). Quantifying the influence of classification with the 3 product cyclone on liberation and recovery of PGMs in UG2 ore. Minerals Engineering, 21(7), pp. 549–558.

Hay, M. P., & Roy, R. (2010). A case study of optimising UG2 flotation performance. Part 1: Bench, pilot and plant scale factors which influence Cr2O3 entrainment in UG2 flotation. Minerals Engineering, 23(11-13), pp. 855–867.

Hicyilmaz, C., Ulusoy, U., Bilgen, S., & Yekeler, M. (2005). Flotation responses to the morphological properties of particles measured with three-dimensional approach. International Journal of Mineral Processing, 75(3-4), pp. 229–236.

Khonthu, T. (2012). Investigation of the flotation behaviour of ball mill and IsaMill products. University of Cape Town.

Kirjavainen, V. M. (1996). Review and analysis of factors controlling the mechanical flotation of gangue minerals. International Journal of Mineral Processing, 46(1-2), pp. 21–34.

Leroy, S., Dislaire, G., Bastin, D., & Pirard, E. (2011). Optical analysis of particle size and chromite liberation from pulp samples of a UG2 ore regrinding circuit. Minerals Engineering, 24(12), pp. 1340–1347.

Mudd, G. M. (2012). Key trends in the resource sustainability of platinum group elements. Ore Geology Reviews, 46, pp. 106–117.

Pourghahramani, P. (2012). Effects of ore characteristics on product shape properties and breakage mechanisms in industrial SAG mills. Minerals Engineering, 32, pp. 30–37.

Rule, C., & Schouwstra, R. P. (2011). Process mineralogy delivering significant value at Anglo Platinum concentrator operations. In 10th International Congress for Applied Mineralogy (pp. 1–5).

Savassi, O. N., Alexander, D. J., Franzidis, J. P., & Manlapig, E. V. (1998). An empirical model for entrainment in industrial flotation plants. Minerals Engineering, 11(3), pp. 243–256.

Vizcarra, T. G., Wightman, E. M., Johnson, N. W., & Manlapig, E. V. (2011). The effect of breakage method on the shape properties of an iron-oxide hosted copper–gold ore. Minerals Engineering, 24(13), pp. 1454–1458.

Wiese, J., Harris, P., & Bradshaw, D. (2005). The influence of the reagent suite on the flotation of ores from the Merensky reef. Minerals Engineering, 18(2), pp. 189–198.

Wiese, J., Becker, M., Yorath, G. & O'Connor, C.T. (2014) A fundamental investigation into the relationship between particle shape and entrainment. Submitted for the 14th International Minerals Processing Conference

Zhu J.Y., Tan, F. Scallon, K.L. Zhao, Y.L. Deng, Y. (2005) Deinking selectivity (Z-factor): a new parameter to evaluate the performance of flotation deinking process, Separation and Purification Technology, 43 (1), pp. 33- 41.

Appendix B: Additional information on experimental test work

B.1 Sample preparation (laboratory feed samples)

The bulk laboratory mill feed sample (primary ball mill discharge), weighed 288 kg. This bulk sample was dried and then screened at 1.12 mm to remove the coarse particles and some debris. The coarse fraction removed weighed 8 kg, equivalent to 2.8% of the original sample. The remaining 280 kg sample was blended and split using a 10-way rotary splitter into representative 1 kg samples as illustrated in Figure B.1. A PSD of the feed was obtained by screening, and feed samples were prepared for mineralogical analysis. The feed PSD is shown in Section 3.3 in comparison with the PSDs of the two mill products at the two target grinds.

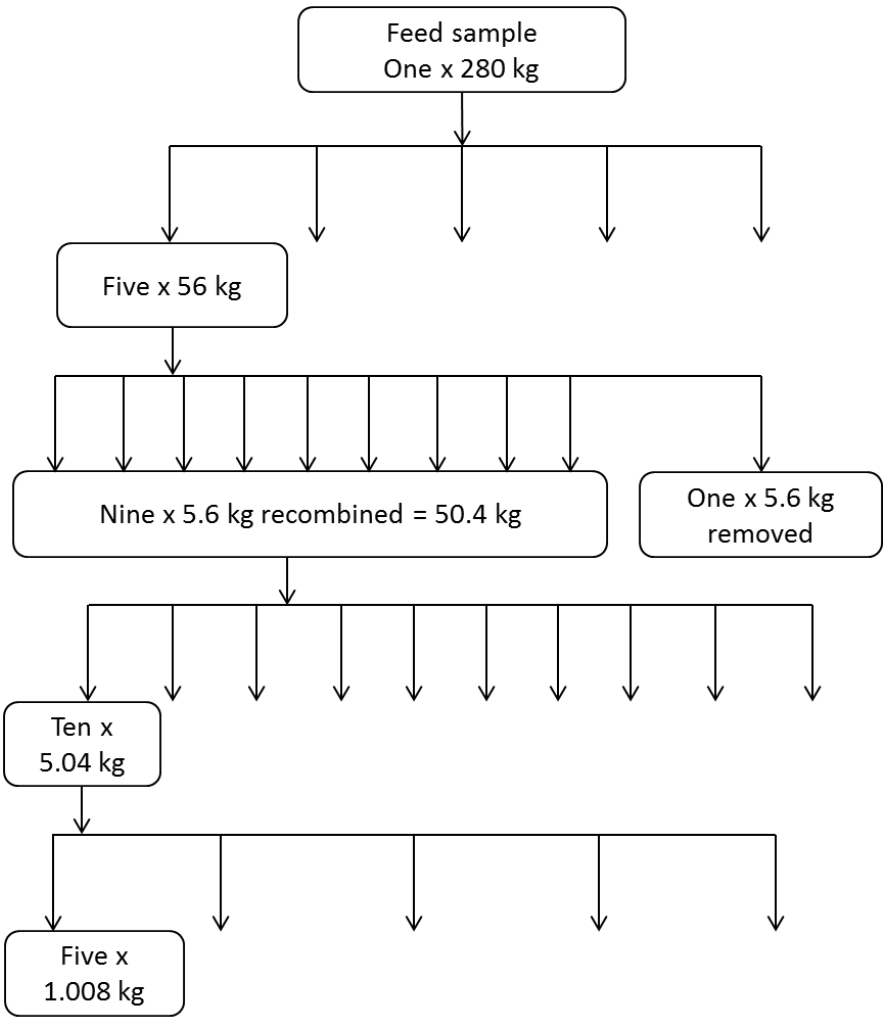

Figure B.1: Splitting procedure to obtain 250 representative 1 kg samples which were then randomly recombined to form 3 kg samples prior to milling

B.2 Comminution experimentation

The specifications of the laboratory ball mill and SMD are presented in Table B.1, a summary of which was presented in Paper 4, Chapter 6, Table 6.3.

Table B.1: Milling specifications for the ball mill and SMD used

Specification	Units	SMD	Ball mill
Mode of operation	NA	Batch	Batch
Media type	NA	Zirconia toughened alumina	Alumina
Media diameter (graded charge)	mm	5	12, 19, 25, 32
Mill volume	L	6.5	21.2
Bulk volume of media	L	3.54	5.4
Mass of media	kg	8.35	11.87
Media density	kg/m^3	3.83	3.6
Mass of ore sample	kg	3.0	3.0
Volume of water	L	1.06	1.70
Impeller speed	rpm	535	NA
Mill speed	% critical	NA	70
Mill diameter	mm	219	300
Impeller diameter	mm	161	NA
Power draw under these conditions	W	702	275
No-load power (no media or water)	W	354	245
Net power	W	348	30
Milling time – fine grind	min	6	85
Milling time - UF grind	min	9.2	133
Size specific energy intensity (-53µm) fine grind	kWh/t	17.7	22.7
Size specific energy intensity (-53µm) UF grind	kWh/t	53.2	68.1

Milling Procedure

For both mill types, the dry media, 3 kg ore sample, and synthetic plant water (for flotation) were added to the mill chamber. The mill was switched on and run for the required time period, and then switched off. For the stirred mill, after milling the impeller was disconnected to enable lifting of the mill chamber. The contents of the mill chamber were poured over a 2 mm screen, and the slurry was washed from the media until the beads were clean, while ensuring that the

total slurry volume collected was less than 8 L (for flotation). The beads were dried in an oven before the next test.

For the ball mill, after milling, the lid was removed and the mill was tilted to pour out the contents of the mill over a perforated bucket. The slurry was washed through the holes in the perforated bucket into a normal bucket below, and the media was retained in the top bucket and rinsed thoroughly. The major difference between the ball mill and stirred mill test work was that the grinding time in the ball mill was approximately 10 times longer than that of the stirred mill.

As energy efficiency is of key interest in comminution, a Fluke power logger was used to measure the power draw and no-load power draw of both mill types. This device was set to record measurements at three second intervals throughout the duration of an experiment. Three repeat grinds for each mill type were measured, and showed good repeatability. Both mills were batch operated, of a similar scale, with the same feed size distribution, which provides a reasonable basis for comparison of energy efficiency.

Grinding curves and energy measurements

The grinding curves based on P80 and P50 of the stirred mill and ball mill are shown in Figures B.2 and B.3 respectively. Initial stirred mill tests included experimenting with different media sizes, media densities, milling times and impeller pin lengths, so the grinding curve for the selected conditions is not extensive. However, once the two grinds were established for the stirred mill, the grinding curve for the ball mill was used to determine the milling times required to obtain equivalent grinds based on both P50 and P80. The grinding time to give equivalent P50 based on the Malvern data was selected. The PSDs based on screening data were reported in the main body of this thesis as the sized samples sent for assays and mineralogy were separated by screening. The screening PSDs indicated that the products obtained with the two mill types were not equivalent which was perhaps due to the differences in particle shape. The SMD grinding curves based on P50 and P80 indicate that the coarse particles in the feed have a lower breakage rate than the median sized particles.

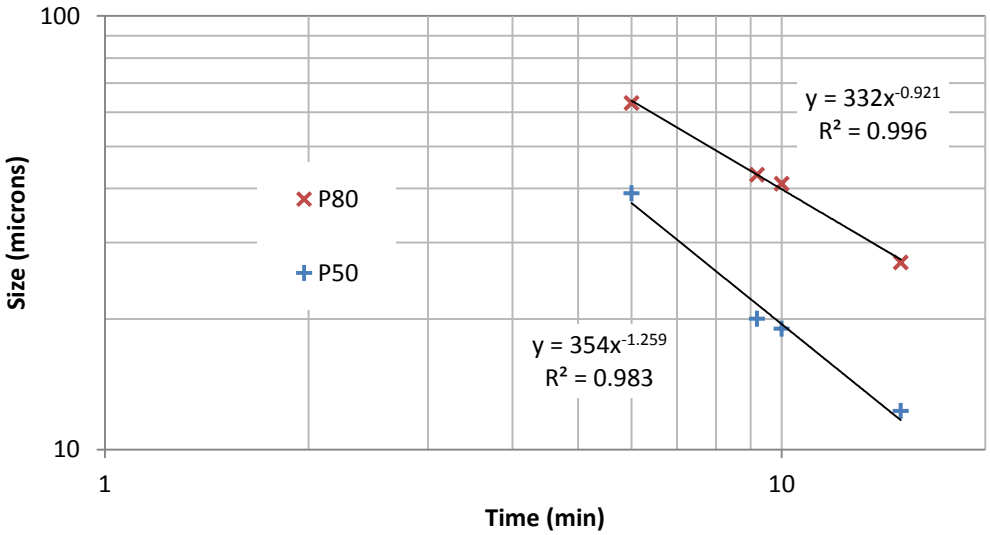

Figure B.2: SMD grinding curve showing reduction in P50 and P80 with time.

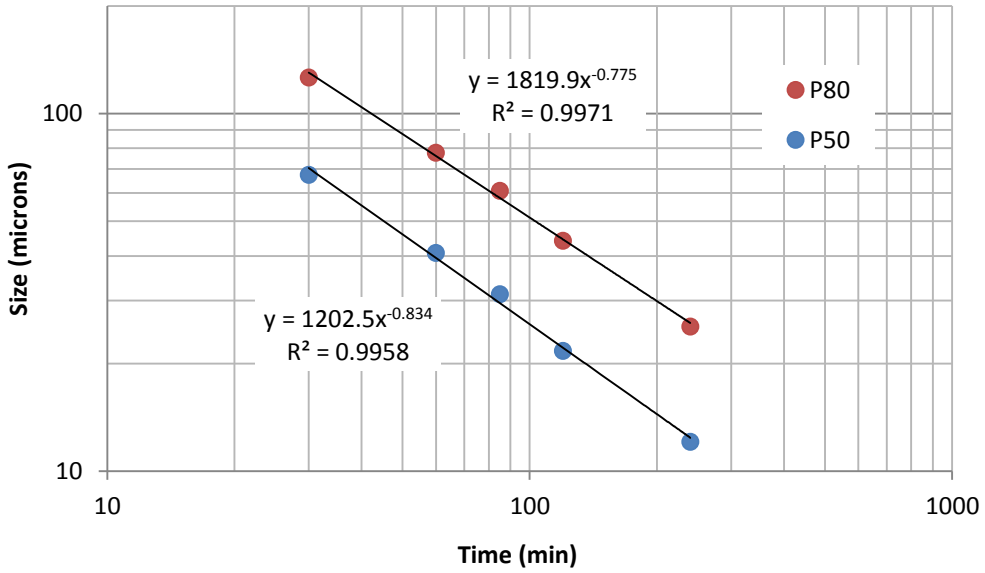

Figure B.3: Ball mill grinding curve showing reduction in P50 and P80 with time.

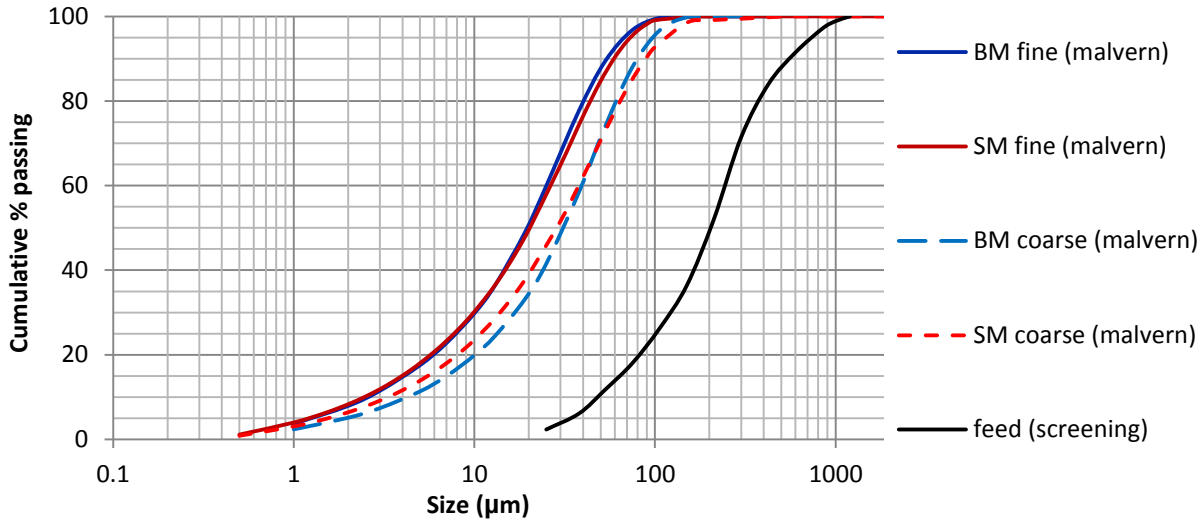

Figure B.4: The Malvern PSDs of the ball mill and SMD products at the two target grinds

B.3 Flotation experimentation

The flotation tests were carried out in an 8L modified Leeds float cell following the standard University of Cape Town procedure for platinum group mineral flotation (Wiese et al., 2005). After reagent dosage and conditioning for the required time period, four concentrates were collected by scraping of froth every 15 seconds for intervals of 2, 4, 6 and 8 minutes consecutively, which is 20 minutes in total. After each test the concentrates were vacuum-filtered and then oven dried. The flotation tails were drained from the float cell into a bucket and then pressure-filtered and oven dried.

Level was controlled throughout the tests by addition of synthetic plant water, which was also used to wash the froth-scraper and float cell lip between scrapes. The water bottles, concentrate collection pans, filter paper and dried concentrate samples were weighed before and after each test to enable calculation of water and solids recoveries to each concentrate. The impeller speed was set at 1200 rpm, and the air flow rate at 13 L/min – intended to give a J_g of 0.65 cm/s. However, the rotameter was not recalibrated for this work, and it was discovered that the previous calibration was inaccurate, so the flow rate used was actually 7.9 L/min, with a J_g of 0.42 cm/s. The reagents used, along with dosages and conditioning times are reported in table B.2, in sequence of addition.

Table B.2: Details of the reagent suite

Reagent type	Reagent name and description	Dosage (g/t)	Dosage (ml) (vol. of 1% soln.)	Conditioning time (min)
Collector	SIBX (Sodium isobutyl xanthate)	150	45	2
Depressant	Sendep369 (a guar depressant)	0, 200, 500	0, 60, 150	2
Frother	XP200 (a polyglycol frother)	40	12	1

All of the reagents were prepared as 1% solutions with distilled water. The SIBX solution was freshly prepared each morning by dissolving 2.00 g of powder in distilled water, pouring it into a 200 ml volumetric flask, diluting up to the 200 ml mark with distilled water, and then mixing thoroughly by inverting the flask. For Sendep369, 5.00 g of powder were dissolved in 150 ml of water by stirring with a magnetic stirrer for 1 hour. The resulting solution was then poured into a 500 ml volumetric flask and made up to the mark with distilled water. Finally, 1.00 g of frother (XP200) was diluted in a 100 ml volumetric flask.

Synthetic plant water

Synthetic plant water was used in all experiments including the initial water used in the mill, cleaning out the mill and media, and make up water in flotation. The synthetic plant water was prepared by dissolving various salts in distilled water to produce a solution with a fixed ionic strength. The recipe used is shown in table B.3 and was developed for research in PGM flotation as a control, firstly to mimic the ionic strength of plant water at some PGM plants, and to provide a constant basis for comparison between different experiments (Wiese 2005). The ionic concentrations present in the synthetic plant water are reported by Wiese et al. (2005).

Table B.3: The required quantities of salts to be added to 40L of distilled water to make synthetic plant water

Salt	Molecular formula	Mass (g)
Hydrated magnesium sulphate	$MgSO_4.7H_2O$	24.60
Hydrated magnesium nitrate	$Mg(NO_3)_2.6H_2O$	4.28
Hydrated calcium nitrate	$Ca(NO_3)_2.4H_2O$	9.44
Anhydrous Calcium chloride	$CaCl_2$	4.44
Sodium chloride	NaCl	14.24
Anhydrous sodium carbonate	Na_2CO_3	1.20

B.5 Assays and Mineralogy

QEMSCAN sample preparation procedure

200 g aliquots of the mill product/flotation feed samples selected for QEMSCAN were wet screened at 53 and 25 µm. The -25 µm fraction was then further screened in an ultrasonic bath for six hours through 10 µm cloth. The flotation concentrate samples were very fine, mostly less than 10 µm, so these were generally scanned unsized, except for the stirred mill coarse concentrates. These were screened at 10 µm to generate more +10 µm particle images to use in the investigation of effect of shape on entrainment.

After drying, the screened samples were split using a micro-riffler into 4 g aliquots. These were mixed with an equivalent mass of graphite from the size class below that of the sample, except for the -25/+10 µm and -10 µm size fractions which were mixed with -25 µm graphite. The graphite was added to provide spacing between the sample particles to minimize touching particles, and to help with electron conductivity. The mixed graphite and sample were then added to labelled ice-cube moulds. Resin was added to each sample in the mould, and mixed thoroughly by stirring in a figure of eight pattern. The blocks were then placed in a vacuum chamber for 10 minutes, and then 5 more minutes to release trapped air bubbles, and finally, they were cured under pressure overnight.

Figure B.5: Samples to be made into blocks for vertical sections in ice-cube moulds

After curing, the blocks were removed from the moulds and sliced into thin vertical sections which were then remounted into 30 mm round mounts, with printed labels inserted at the top. Once the new blocks had cured, they were polished in a number of stages, starting with a rough grind and getting smoother and smoother until the last 1 µm polish step. Between each grind, the samples are gently washed with soap to remove loose grains. Afterwards, they are cleaned again in an ultrasonic bath, and wiped with ethanol, and then dried in an oven at 30°C for an

hour. The quality of the final polish was then checked using an optical microscope before carbon coating of the samples in an Emitech carbon evaporator. The carbon coat is to diffuse electrons off the surface of the sample during scanning.

Assay plan and Mineralogical analyses

Tables B.4 and B.5 show the samples assayed by ICP-OES and fire assay for 4E PGEs. The assays were conducted at Mintek analytical services division in Johannesburg. Inductively coupled plasma optical emission spectrometry (ICP-OES) was performed to quantify the major elemental constituents in each sample. Of these, the chrome grades of the feeds, concentrates and tails were used to determine chromite grades and recoveries to assess entrainment. The ICP-OES results for the main elements were also used for parity charts to verify the QEMSCAN mineralogy data (see Figure B.6). The QEMSCAN analyses were carried out at UCT using the FEI QEMSCAN 650F. Tables B6 and B7 show the samples selected for QEMSCAN analysis.

The QEMSCAN bulk mineralogical analysis (BMA) is a line scan setting to determine the bulk mineralogy of the ore. Particle Mineral Analysis (PMA) scans all of the particles within a given field, providing shape information on a mineral basis, and mineral associations and liberation data for the major mineral constituents. The trace mineral search (TMS) setting is used to search for trace minerals, and only particles that contain a specific mineral are scanned.

In this project, most of the samples were run on PMA for particle shape information on a mineral basis. TMS was used to search for the base metal sulphide minerals, to determine their liberation in the mill feed, and each mill product, and for the PGM mineral liberation analysis presented in Paper 4.

After scanning, iDiscover pre-processors were used to filter out touching particles, particle fragments <1 micron, and fine particle composites. The number of particles remaining for each sample is reported in the final column of Tables B.6 and B.7. The QEMSCAN sample preparation procedure is described in the following section.

Table B.4: Assay plan for laboratory SMD and ball mill (BM) flotation feeds, concentrates and tails for both grinds and all three depressant dosages.

Mill type	Grind	Dep. Dosage	Float Feed		Concentrates		Tails	
			ICP-OES	PGE-FA	ICP-OES	PGE-FA	ICP-OES	PGE-FA
SMD	Coarse	0	x5 size fractions	3	4	1	1	1
		200			4	2	2	2
		500			4	0	2	2
	Fine	0	x5 size fractions		4	1	1	1
		200			1 (comb)	2	2	2
		500			0	0	2	2
BM	Coarse	0	x 4 size fractions		4	2	2	2
		200			4	2	2	2
		500			4	0	2	2
	Fine	0	x 4 size fractions		4	1	2	2
		200			16	2	6	2
		500			4	0	2	2
Total			18	3	68	13	26	22

Table B.5: Assay and QEMSCAN plan for plant samples- variation due to differences in PSDs, and purpose of the data. QEMSCAN of 8 PRF size fractions was for assessment of phase boundary fracture of the chromite and silicates. The SRT sample was split into five fractions for PGE to differentiate between PGE losses in the -10 and -25/+10 µm fractions.

		No. of size fractions selected for each analysis		
Concentrator	Sample name	QEMSCAN	4E-PGE (Fire assay)	Cr (ICP-OES)
ETTP	BM Feed	3	3	3
	IsaMill Feed	3	3	3
	IsaMill Discharge	4	4	4
EPA	PRF	8	4	8
	PRT	4	4	5
	SRT	4	5	5
	HGC	4	4	6
	LGC	4	4	5
Total		34	31	39

Table B.6: Laboratory samples selected for QEMSCAN analyses using BMA, TMS and PMA

Sample	Size fractions	QEMSCAN setting	Resolution (µm/pixel)	Minimum particle count (PMA)
Mill Feed	-1000/+212	PMA	4.84	1889
	-212/+150	BMA, TMS, PMA	4.88	4158
	-150/+106	BMA, TMS, PMA	4.59	6112
	-106/+75	BMA. TMS,PMA	3.99	22110
	-75	BMA, TMS, PMA	1.97	27941
Mill products (float feeds)	+53	TMS, PMA	2.93	21650
	-53/+25	TMS, PMA	1.95	28201
	-25/+10	TMS, PMA	1.95/0.44	19233
	-10	TMS, PMA	0.98/0.44	42226
BM UF and SMD UF (float feeds)	Unsized	TMS for PGMs	0.44	188 (PGMs)
SMD UF, 200g/t dep. (C1+C2+C3+C4)	Unsized	PMA	0.44	40605
BM UF, 200g/t dep. (C1+C2+C3+C4)	Unsized	PMA	0.44	47880
BM F, 200g/t dep. (C1+C2+C3+C4)	Unsized	PMA	0.44	50230
SMD F, 200g/t dep. (C1+ 2)	+10	PMA	0.44	21458
	-10	PMA	0.44	43321
SMD F, 200g/t dep. (C3+C4)	+10	PMA	0.44	7742
	-10	PMA	0.44	46023
BM F, no dep. C1	Unsized	PMA	0.44	49204
BM F, no dep. C4	Unsized	PMA	0.44	46150

**All PMA analyses were carried out with EDS mapping*

Table B.7: Plant samples selected for QEMSCAN analysis using PMA setting

Concentrator	Sample	Size fractions	QEMSCAN PMA setting	Resolution (µm/pixel)	Particle count
ETTP	BM feed	+75	centroid	3.66	5832
		-75/+53		2.93	13212
		-53/+0		0.95	44256
	IsaMill feed	+75	centroid	3.66	6552
		-75/+53		2.93	13669
		-53/+0		0.95	57049
	IsaMill discharge	+75	centroid	3.66	6662
		-75/+53		2.93	13064
		-53/+25		1.83	43576
		-25/+0		0.95	94908
EPA	PRF	-1000/+212	EDS mapping	4.84	2054
		-212/+150		4.84	4158
		-150/+106		4.84	7559
		-106/+75		3.66	13264
		-75/+53		2.93	9519
		-53/+25		1.83	12570
		-25/+10	centroid	0.44	75358
		-10/+0		0.44	150682
	PRT	-1000/+106	centroid	4.84	1820
		-106/+53		2.93	14571
		-53/+25		1.83	5254
		-25/+10		0.44	76147
		-10/+0		0.44	61619
	SRT	-1000/+106	centroid	4.84	2222
		-106/+53		2.93	13522
		-53/+25		1.83	4880
		-25/+10		0.44	82358
		-10/+0		0.44	74010
	HGC	-106/+53	EDS mapping	2.93	39910
		-53/+25		1.83	99554
		-25/+10	centroid	0.44	201188
		-10/+0		0.44	350292
	LGC	-106/+53	EDS mapping	2.93	50633
		-53/+25		1.83	99436
		-25/+10	centroid	0.44	214100
		-10/+0		0.44	343869

B.6 Raw flotation data, assay data and QEMSCAN data validation

The data presented here includes all of the assays which were carried out during the course of the test work, although only a relatively small proportion of these relate to data examined within the main body of this thesis. In particular, most of the flotation data is only relevant to Appendix E in which the flotation performance of the laboratory fine grinding products is presented and discussed.

The laboratory flotation test work is described in Table B.8, which indicates the codes used to differentiate between repeat tests. The mean total solids and total water recovered for the repeat tests is also presented. There were two frothers used in these tests, XP200 and DOW 200. This was initially not expected to significantly affect the froth because they were believed to be very similar. However, a difference in total water recovery was observed for the two frothers, so samples from the XP200 tests were sent for PGE assay where consistency for the comparison of the flotation performance of the two mill products was considered most important. The concentrate samples from the remaining repeat tests were then combined for ICP-OES assay (e.g. LL C1& SS C1 → BM F 0 C1). The solids and water recoveries for these tests are provided in Tables B.9 and B.10, followed by the associated assay data in Tables B.11 and B.12. Assays from the plant samples are then presented in Table B.13.

Table B.8: The codes used to differentiate between flotation repeats. Note, repeat codes in bold were carried out with the frother XP 200, while others were carried out with the frother Dow 200.

Mill Test	Depressant dosage (g/t)	Flotation Repeat codes	Mean solids recovered (g)	Mean water recovered (g)	S.E. solids (g)	S.E. water (g)
BM F	0	LL, SS, **UU, DDD**	123.14	1529.28	7.20	78.43
	200	MM, QQ, **WW, XX**	58.29	1323.15	1.38	52.36
	500	NN, PP, **VV, CCC**	27.92	953.27	5.53	129.98
BM UF	0	HH, KK, RR, **AAA, BBB**	155.07	1667.96	2.44	14.00
	200	GG, JJ, OO, **YY, ZZ**	78.13	1372.83	3.76	59.78
	500	FF, II, TT, **EEE, FFF**	36.75	786.92	4.89	3.72
SMD F	0	**Q, R, X, Z**	101.93	1421.68	2.49	68.69
	200	**G, H, K, M, N, DD**	53.58	1311.52	1.53	54.10
	500	**I, U, CC**	24.16	920.94	1.96	61.57
SMD UF	0	**O, P, W, V**	109.62	1369.74	5.28	58.80
	200	**D, J, S, T, EE**	73.81	1454.89	3.56	64.74
	500	**F, V, AA, BB**	36.40	1074.17	1.02	14.05

Table B.9: Mean solids and water recoveries of the repeated tests for each flotation concentrate of the ball mill grinding testwork

Grind	Depressant dosage (g/t)	Sample	Time, min	Solids g	Water g	Cum solids, g	Cum Water, g
BM F	0 g/t	C1	2	37.78	260.98	37.78	260.98
		C2	6	36.53	389.70	74.31	650.68
		C3	12	32.65	513.55	106.95	1164.23
		C4	20	26.53	535.76	133.48	1699.99
		T				2874.52	
BM F	200 g/t	C1	2	12.33	258.00	12.33	258.00
		C2	6	13.53	318.35	25.85	576.35
		C3	12	19.17	449.51	45.03	1025.85
		C4	20	21.08	485.43	66.10	1511.29
		T				2941.90	
BM F	500 g/t	C1	2	11.28	256.89	11.28	256.89
		C2	6	5.79	215.31	17.07	472.20
		C3	12	8.15	337.96	25.22	810.15
		C4	20	8.60	379.73	33.82	1189.88
		T				2974.18	
BM UF	0 g/t	C1	2	45.84	327.38	45.84	327.38
		C2	6	40.86	402.66	86.70	730.03
		C3	12	38.20	532.13	124.90	1262.16
		C4	20	30.93	533.10	155.83	1795.26
		T				2852.17	
BM UF	200 g/t	C1	2	21.64	314.96	21.64	314.96
		C2	6	19.35	351.35	40.99	666.31
		C3	12	23.83	451.73	64.82	1118.04
		C4	20	24.39	477.11	89.21	1595.15
		T				2918.79	
BM UF	500 g/t	C1	2	19.09	274.96	19.09	274.96
		C2	6	8.55	218.21	27.64	493.17
		C3	12	10.82	301.40	38.46	794.57
		C4	20	11.91	339.27	50.37	1133.84
		T				2957.63	

Table B.10: Mean solids and water recoveries of the repeated tests for each flotation concentrate of the SMD grinding testwork

Grind	Depressant dosage (g/t)	Sample	Time, min	Solids g	Water g	Cum solids, g	Cum Water, g
SMD F	0 g/t	C1	2	26.33	205.27	26.33	205.27
		C2	6	27.50	314.75	53.83	520.02
		C3	12	26.37	448.13	80.20	968.15
		C4	20	21.73	453.52	101.93	1421.68
		T				2906.08	
SMD F	200 g/t	C1	2	10.86	250.08	10.86	250.08
		C2	6	10.24	264.43	21.09	514.51
		C3	12	15.20	378.80	36.29	893.31
		C4	20	17.29	418.22	53.58	1311.52
		T				2954.42	
SMD F	500 g/t	C1	2	6.70	181.07	6.70	181.07
		C2	6	4.86	184.48	11.56	365.54
		C3	12	5.89	249.44	17.45	614.98
		C4	20	6.71	305.96	24.16	920.94
		T				2983.84	
SMD UF	0 g/t	C1	2	27.80	210.31	27.80	210.31
	O	C2	6	27.81	286.45	55.60	496.75
		C3	12	28.94	415.81	84.54	912.56
		C4	20	25.07	457.18	109.62	1369.74
		T				2898.39	
SMD UF	200 g/t	C1	2	15.63	260.27	15.63	260.27
	S	C2	6	14.50	286.30	30.12	546.58
	EE	C3	12	21.21	434.59	51.33	981.17
		C4	20	22.48	473.72	73.81	1454.89
		T				2934.19	
SMD UF	500 g/t	C1	2	8.32	171.11	8.32	171.11
	AA	C2	6	7.20	203.98	15.53	375.09
	V	C3	12	9.71	355.96	25.23	731.06
		C4	20	11.16	343.12	36.40	1074.17
		T				2971.60	

Table B.11: 4-E-PGE assay data for the laboratory flotation from the Mintek analytical services report. Project No: ASC – 00000043-10, Date Received 14/07/2014. Note that Rhodium has a low bias on this method.

Sample description	Repeat	Au ppm	Pd ppm	Pt ppm	Rh ppm
O conc	1	0.37	21.3	49.3	8.89
S conc	1	0.79	38.9	86.8	16.1
EE conc	1	0.73	39.4	90.6	16.8
X conc	1	0.57	30.8	69.4	11.9
DD conc	1	0.97	50.3	111	20.3
M conc	1	1.03	59.3	127	23.4
AAA conc	1	0.58	24.7	64.1	9.72
AAA conc	2	0.51	23.6	60.5	9.23
BBB conc	1	0.43	20.0	47.8	7.92
YY conc	1	0.89	38.3	85.0	14.9
ZZ conc	1	0.62	35.5	80.3	14.4
UU conc	1	0.68	25.4	62.9	10.2
WW conc	1	1.11	55.2	121	21.7
XX conc	1	1.10	52.0	117	20.7
XX conc	2	1.06	52.4	117	20.1
WW tails	1	<0.1	0.24	0.38	<0.1
WW tails	2	<0.1	0.24	0.39	<0.1
XX tails	1	<0.1	0.25	0.41	<0.1
CCC tails	1	<0.1	0.29	0.46	<0.1
VV tails	1	<0.1	0.29	0.48	<0.1
O tails	1	<0.1	0.15	0.31	<0.1
O tails	2	<0.1	0.16	0.34	<0.1
S tails	1	<0.1	0.14	0.28	<0.1
EE tails	1	<0.1	0.13	0.24	<0.1
AA tails	1	<0.1	0.10	0.20	<0.1
V tails	1	<0.1	0.16	0.33	<0.1
X tails	1	<0.1	0.17	0.32	<0.1
DD tails	1	<0.1	0.18	0.34	<0.1
M tails	1	<0.1	0.18	0.37	<0.1
CC tails	1	<0.1	0.21	0.36	<0.1
I tails	1	<0.1	0.19	0.36	<0.1
AAA tails	1	<0.1	0.20	0.32	<0.1
BBB tails	1	<0.1	0.22	0.34	<0.1
YY tails	1	<0.1	0.21	0.35	<0.1
YY tails	2	<0.1	0.23	0.38	<0.1
ZZ tails	1	<0.1	0.23	0.39	<0.1
EEE tails	1	<0.1	0.29	0.54	0.1
FFF tails	1	<0.1	0.28	0.51	0.11
UU tails	1	<0.1	0.24	0.37	<0.1
DDD tails	1	<0.1	0.22	0.35	<0.1

Table B.12: ICP-OES assay data for the laboratory flotation feed samples. From the Mintek analytical services report. Project No: ASC–00000043-10, Date Received 14/07/2014. Note that Rhodium has a low bias on this method. Sample naming convention: Mill type (BM, SMD), fine or ultrafine grind (F, UF), size fraction.

Sample name	Mg %	Al %	Si %	Ca %	Ti %	V %	Cr %	Mn %	Fe %	Ni %
BM F +53	8.42	7.37	9.82	1.51	0.47	0.22	19.8	0.16	16	0.1
BM F -53/+25	7.54	8.41	10.6	2.21	0.45	0.21	19.2	0.15	15.3	0.1
BM F -25/+10	7.2	8.6	11	2.58	0.43	0.2	18.3	0.15	14.7	0.11
BM F -10	7.17	8.38	11.5	2.58	0.42	0.18	16.1	0.14	13.7	0.13
BM UF +53	8.92	6.61	10.8	1.35	0.5	0.2	18.3	0.16	15.5	0.11
BM UF -53/+25	8.04	7.6	10.2	1.82	0.45	0.21	18.8	0.15	15.4	0.1
BM UF -25/+10	7.24	8.38	10.4	2.32	0.44	0.21	19	0.15	15.2	0.12
BM UF -10	7.26	8.44	11.5	2.61	0.42	0.19	16.7	0.14	14	0.13
BM UF -10	7.32	8.49	11.6	2.65	0.43	0.19	16.7	0.14	13.9	0.14
SMD F +75	8.37	6.23	10.8	1.5	0.4	0.18	16.9	0.16	14.8	0.097
SMD F +75	8.56	6.39	11.2	1.51	0.41	0.18	17.3	0.17	15.2	0.094
SMD F-75/+53	7.51	7.66	7.88	1.38	0.48	0.24	21.9	0.16	17	0.1
SMD F -53/+25	7.31	8.29	9.93	2.14	0.46	0.21	19.8	0.15	15.5	0.095
SMD F -25/+10	6.92	8.6	11.5	2.87	0.41	0.19	17.3	0.17	14	0.11
SMD F -10	7.24	8.65	12.3	2.97	0.43	0.18	16	0.14	13.4	0.12
SMD F 200 C1+C2 -10	8.59	6.42	16.2	2.77	0.32	0.1	9.34	0.11	11.9	1.15
SMD F 200 C1+C2 +10	8.56	3.71	15.6	2.28	0.18	<0.05	3.32	0.074	15.9	4.96
SMD F 200 C3+C4 -10	10.2	5.64	19.3	2.47	0.29	0.084	7.39	0.11	9.5	0.28
SMD F 200 C3+C4 +10	13.8	2.42	24.1	2.33	0.18	<0.05	1.21	0.1	7.79	0.46
SMD F 200 C3+C4 +10	14	2.46	24.7	2.36	0.19	<0.05	1.22	0.1	7.94	0.47

Table B12 (continued)

Sample name	Mg %	Al %	Si %	Ca %	Ti %	V %	Cr %	Mn %	Fe %	Ni %	Cu %
SMD F 0 C1	12.9	2.98	22.8	1.92	0.20	<0.05	2.77	0.10	8.51	0.68	0.72
SMD F 0 C1	12.7	2.95	22.4	1.87	0.20	<0.05	2.80	0.10	8.46	0.68	0.71
SMD F 0 C2	12.6	3.67	22.3	2.01	0.23	<0.05	3.63	0.11	8.94	0.76	0.097
SMD F 0 C3	11.9	4.71	21.2	2.48	0.26	0.065	4.96	0.12	9.19	0.45	<0.05
SMD F 0 C4	11.1	5.21	20.2	2.65	0.29	0.076	5.74	0.12	9.40	0.27	<0.05
SMD F 200 C1	7.57	6.28	13.5	2.69	0.30	0.10	8.11	0.10	14.0	2.63	1.67
SMD F 200 C2	9.72	5.49	17.8	2.43	0.27	0.086	6.38	0.10	10.7	1.29	0.20
SMD F 200 C3	10.8	5.16	19.6	2.67	0.27	0.078	6.06	0.11	9.54	0.44	0.061
SMD F 200 C4	11.4	5.07	20.6	2.55	0.27	0.076	5.93	0.11	9.20	0.25	<0.05
SMD F 500 C1	6.69	6.90	12.4	2.84	0.31	0.12	8.69	0.10	14.4	2.68	2.25
SMD F 500 C2	7.49	6.90	13.3	2.96	0.31	0.10	8.33	0.10	13.1	2.83	0.44
SMD F 500 C2	7.38	6.89	13.3	3.02	0.31	0.10	8.17	0.10	12.9	2.73	0.44
SMD F 500 C3	8.22	7.37	15.0	3.09	0.34	0.11	9.11	0.11	12.3	1.22	0.14
SMD F 500 C3	8.10	7.32	14.7	3.08	0.33	0.12	9.06	0.11	12.2	1.21	0.14
SMD F 500 C4	8.24	7.44	15.0	2.99	0.34	0.12	9.01	0.11	11.4	0.60	0.067
SMD UF 0 C1	12.4	3.24	22.6	1.90	0.20	<0.05	3.23	0.098	8.64	0.68	0.73
SMD UF 0 C2	12.3	3.67	21.9	1.99	0.22	0.056	3.85	0.11	8.82	0.73	0.089
SMD UF 0 C3	11.9	4.52	20.7	2.39	0.26	0.074	5.23	0.12	9.44	0.45	<0.05
SMD UF 0 C4	10.8	5.26	20.0	2.68	0.28	0.079	6.05	0.13	9.49	0.25	<0.05
BM F 0 C1	13.1	2.72	22.6	1.76	0.20	<0.05	2.74	0.11	8.78	0.67	0.50
BM F 0 C2	12.5	3.77	21.8	2.21	0.24	0.054	4.08	0.13	9.11	0.48	0.066
BM F 0 C3	11.5	4.61	20.5	2.46	0.28	0.069	5.41	0.13	9.48	0.27	<0.05
BM F 0 C3	11.4	4.60	20.5	2.61	0.27	0.071	5.36	0.13	9.45	0.27	<0.05
BM F 0 C4	11.5	5.33	18.7	2.68	0.30	0.085	6.55	0.13	9.94	0.19	<0.05
BM F 0 C4	11.4	5.28	18.6	2.67	0.30	0.087	6.49	0.13	9.93	0.19	<0.05
BM F 200 C1	8.38	5.69	13.2	2.21	0.28	0.091	7.13	0.10	13.6	2.10	1.70
BM F 200 C2	10.5	5.21	17.6	2.39	0.28	0.084	6.59	0.11	10.6	0.77	0.14
BM F 200 C3	10.7	5.13	18.0	2.37	0.28	0.088	6.34	0.11	9.57	0.28	<0.05
BM F 200 C4	11.2	5.09	19.1	2.44	0.28	0.081	6.22	0.12	9.56	0.19	<0.05
BM F 500 C1	7.09	7.49	12.0	2.83	0.35	0.13	10.2	0.12	14.7	1.83	1.62
BM F 500 C1	7.11	7.35	12.0	2.89	0.34	0.13	10.4	0.12	14.8	1.88	1.62
BM F 500 C2	8.10	7.05	12.8	2.76	0.34	0.12	9.70	0.12	13.6	1.80	0.36
BM F 500 C3	8.24	7.41	13.5	2.82	0.35	0.13	9.99	0.12	12.8	0.81	0.13
BM F 500 C4	8.62	7.36	14.2	2.94	0.35	0.13	10.2	0.13	12.5	0.51	0.070
BM UF 0 C1	12.2	3.94	20.7	2.16	0.23	0.067	4.93	0.12	9.52	0.40	0.41
BM UF 0 C2	12.1	3.94	20.3	2.01	0.24	0.070	4.64	0.13	9.17	0.42	0.068
BM UF 0 C2	12.3	4.01	21.0	2.03	0.24	0.061	4.68	0.12	9.35	0.44	0.066
BM UF 0 C3	11.6	4.72	19.4	2.29	0.27	0.078	5.85	0.13	9.77	0.29	<0.05
BM UF 0 C4	11.1	5.28	18.6	2.46	0.29	0.090	6.56	0.13	10.0	0.22	<0.05
BM UF 200 C1	8.24	6.68	13.8	2.77	0.33	0.12	10.3	0.12	13.7	1.23	0.86
BM UF 200 C2	10.4	5.62	17.4	2.47	0.29	0.10	7.79	0.12	11.1	0.65	0.092
BM UF 200 C3	10.6	5.42	17.5	2.40	0.28	0.096	7.33	0.12	10.2	0.27	<0.05
BM UF 200 C3	10.9	5.49	18.0	2.49	0.32	0.098	7.46	0.12	10.5	0.28	<0.05
BM UF 200 C4	10.8	5.31	18.4	2.52	0.29	0.096	7.32	0.13	10.3	0.18	<0.05
BM UF 500 C1	7.36	7.51	11.4	2.75	0.38	0.14	11.3	0.12	14.1	1.16	0.96
BM UF 500 C2	8.22	7.47	12.7	2.82	0.36	0.13	10.6	0.12	13.7	1.41	0.25
BM UF 200 C2	10.4	5.62	17.4	2.47	0.29	0.10	7.79	0.12	11.1	0.65	<0.05
BM UF 200 C3	10.6	5.42	17.5	2.40	0.28	0.096	7.33	0.12	10.2	0.27	<0.05
BM UF 200 C3	10.9	5.49	18.0	2.49	0.32	0.098	7.46	0.12	10.5	0.28	0.96
BM UF 200 C4	10.8	5.31	18.4	2.52	0.29	0.096	7.32	0.13	10.3	0.18	0.25
BM UF 500 C1	7.36	7.51	11.4	2.75	0.38	0.14	11.3	0.12	14.1	1.16	0.14
BM UF 500 C2	8.22	7.47	12.7	2.82	0.36	0.13	10.6	0.12	13.7	1.41	0.14

Table B.12 (continued)

	Mg %	Al %	Si %	Ca %	Ti %	V %	Cr %	Mn %	Fe %	Ni %	Cu %
BM UF 500 C3	8.11	7.63	13.3	3.20	0.36	0.14	12.4	0.13	13.4	0.64	0.088
BM UF 500 C3	8.15	7.51	13.5	3.31	0.36	0.14	12.5	0.13	13.6	0.64	0.092
BM UF 500 C4	8.24	7.35	13.8	3.26	0.36	0.14	12.4	0.13	13.1	0.39	0.052
BM UF 200 C1 (2)	8.18	6.55	13.7	3.01	0.33	0.12	10.9	0.12	13.9	1.18	0.87
BM UF 200 C2 (2)	9.95	5.38	17.6	2.82	0.29	0.10	8.44	0.12	11.3	0.63	0.086
BM UF 200 C3 (2)	10.4	5.37	18.8	2.77	0.29	0.097	8.08	0.12	10.7	0.27	<0.05
BM UF 200 C1 (3)	8.28	6.41	13.6	2.92	0.32	0.12	10.8	0.12	13.7	1.16	0.85
BM UF 200 C2 (3)	9.98	5.39	17.3	2.81	0.29	0.10	8.51	0.12	11.5	0.66	0.091
BM UF 200 C3(3)	10.7	5.35	18.6	2.96	0.29	0.093	8.20	0.12	10.8	0.35	<0.05
BM UF 200 C1 (4)	8.43	6.52	14.0	3.06	0.32	0.13	10.9	0.12	13.9	1.19	0.88
BM UF 200 C2 (4)	10.1	5.46	17.8	2.93	0.29	0.098	8.53	0.12	11.5	0.64	0.095
BM UF 200 C2 (4)	10.2	5.60	17.9	3.00	0.29	0.10	8.73	0.12	11.7	0.65	0.1
BM UF 200 C3 (4)	10.6	5.33	18.7	2.88	0.29	0.093	8.14	0.12	10.7	0.28	<0.05
BM UF 200 C3 (4)	10.7	5.33	18.5	2.87	0.29	0.097	8.22	0.12	10.9	0.28	<0.05
BM UF 200 C1 (5)	8.31	6.41	13.5	3.04	0.32	0.13	10.9	0.12	13.7	1.15	0.83
BM UF 200 C2 (5)	10.2	5.45	17.5	2.9	0.29	0.099	8.63	0.12	11.5	0.65	0.093
BM UF 200 C3 (5)	10.7	5.26	18.6	2.95	0.29	0.096	8.26	0.13	10.8	0.27	<0.05
O tails	7.27	8.25	10.5	2.79	0.44	0.20	18.2	0.15	15.3	0.098	<0.05
S tails	7.37	8.07	10.5	2.65	0.45	0.20	17.9	0.15	15.4	0.089	<0.05
EE tails	7.47	8.23	10.6	2.79	0.45	0.20	18.5	0.15	15.7	0.097	<0.05
AA tails	7.48	7.85	10.5	2.75	0.44	0.21	18.0	0.15	15.5	0.098	<0.05
V tails	7.49	8.11	10.6	2.78	0.44	0.20	18.2	0.15	15.4	0.094	<0.05
V tails	7.52	8.15	10.7	2.81	0.44	0.20	18.2	0.15	15.5	0.094	<0.05
X tails	7.00	8.45	10.0	2.15	0.43	0.21	18.3	0.14	15.7	0.13	<0.05
X tails	6.96	8.36	9.99	2.13	0.44	0.20	18.4	0.14	15.6	0.11	<0.05
DD tails	6.98	8.04	9.90	2.10	0.43	0.20	17.9	0.14	15.3	0.11	<0.05
M tails	7.49	8.11	10.4	2.24	0.44	0.20	18.4	0.15	15.8	0.11	<0.05
CC tails	7.48	8.07	10.6	2.24	0.44	0.21	18.3	0.15	15.8	0.10	<0.05
I tails	7.24	8.13	10.5	2.21	0.43	0.20	18.1	0.14	15.5	0.086	<0.05
AAA tails	7.34	8.35	10.5	2.22	0.45	0.20	19.0	0.15	16.3	0.13	<0.05
AAA tails	7.31	8.57	10.1	2.14	0.44	0.21	18.6	0.14	15.7	0.12	<0.05
BBB tails	7.12	8.53	10.4	2.25	0.45	0.21	18.6	0.15	15.9	0.12	<0.05
YY tails	7.44	8.53	10.7	2.25	0.45	0.20	18.5	0.15	15.9	0.15	<0.05
ZZ tails	7.42	8.40	10.9	2.25	0.44	0.21	18.3	0.15	15.8	0.13	<0.05
EEE tails	7.42	8.59	10.8	2.14	0.45	0.21	18.0	0.15	15.4	0.13	<0.05
FFF tails	7.51	8.26	10.9	2.22	0.44	0.20	18.4	0.15	16.0	0.12	<0.05
FFF tails	7.45	8.23	10.7	2.19	0.44	0.20	18.2	0.15	15.6	0.13	<0.05
UU tails	7.29	8.34	10.4	2.19	0.45	0.20	18.5	0.15	15.8	0.12	<0.05
DDD tails	7.42	8.41	10.6	2.33	0.45	0.21	18.8	0.15	16.1	0.10	<0.05
WW tails	7.46	8.31	11.0	2.35	0.44	0.20	18.4	0.15	15.8	0.096	<0.05
XX tails	7.41	8.08	10.4	2.17	0.44	0.20	18.1	0.15	15.6	0.11	<0.05
CCC tails	7.51	8.26	11.0	2.28	0.45	0.20	18.4	0.15	15.9	0.12	<0.05
CCC tails	7.49	8.31	10.8	2.21	0.44	0.19	18.1	0.15	15.6	0.11	<0.05
VV tails	6.87	7.58	10.1	2.07	0.41	0.19	16.7	0.13	14.5	0.10	<0.05
ZZ tails (2)	7.46	8.34	10.7	2.23	0.45	0.21	18.4	0.15	15.9	0.11	<0.05
ZZ tails (3)	7.53	8.33	10.7	2.27	0.44	0.20	18.6	0.15	16.1	0.11	<0.05
ZZ tails (4)	7.47	8.40	10.6	2.25	0.47	0.21	18.4	0.15	15.0	0.11	<0.05
ZZ tails (4)	7.57	8.40	10.8	2.34	0.45	0.20	18.6	0.15	15.0	0.11	<0.05
ZZ tails (5)	7.45	8.29	10.7	2.29	0.45	0.21	18.7	0.15	14.9	0.098	<0.05

Table B.13: Assay data from the plant samples, from Mintek Analytical Services test report, Project No: ASC-00000045-10, Date Received 21/10/2015.

Description	Rep	Cr2O3 %	SiO2 %	Au ppm	Pd ppm	Pt ppm	Rh ppm
Lucy PRT -1000/+106	1	25	22	<0.1	0.44	0.73	<0.1
Lucy PRT -1000/+106	2	25.1	22.2	<0.1	0.43	0.69	<0.1
Lucy PRT -106/+53	1	28.2	19.5	<0.1	0.2	0.46	<0.1
Lucy PRT -53/+25	1	22.6	21.6	<0.1	0.62	1.67	0.11
Lucy SRT -1000/+106	1	25.3	19.5	<0.1	0.32	0.62	<0.1
Lucy SRT -106/+53	1	26.1	18.9	<0.1	0.26	0.53	<0.1
Lucy SRT -53/+25	1	24.8	22	<0.1	0.23	0.53	<0.1
Lucy SRT -53/+25	2	25.3	22.2				
Lucy SRT -25/+10	1	25.7	19	<0.1	0.38	0.99	<0.1
Lucy SRT -10/+0	1	22.7	21.4	<0.1	0.32	0.78	<0.1
Lucy HGC -212/+53	1	1.28	37	3.92	244	397	88.8
Lucy HGC -53/+25	1	1.14	43.4	3.59	238	447	106
Lucy HGC -25/+10	1	1.4	42.3	3.23	226	415	96.5
Lucy HGC -25/+10	2	1.4	42.3				
Lucy HGC -10/+0	1	3.94	40.1	6.7	267	619	102
Lucy LGC -212/+53	1	2.24	44.8	1.39	49.9	101	21
Lucy LGC -53/+25	1	1.5	50.8	0.59	17.6	41.9	8.87
Lucy LGC -25/+10	1	2.53	46	0.46	9.57	22.4	4.13
Lucy LGC -10/+0	1	7.99	41.3	0.26	8.27	22.3	4.39
Lucy LGC -10/+0	2	8.01	41.6				
Lucy ETTP BMF -300/+75	1	23	23.2	<0.1	0.24	0.46	<0.1
Lucy ETTP BMF -300/+75	2			<0.1	0.22	0.43	<0.1
Lucy ETTP BMF -75/+53	1	33.6	12.6	<0.1	0.31	0.56	<0.1
Lucy ETTP BMF -53/+38	1	32.7	11	<0.1	0.15	0.37	<0.1
Lucy ETTP IMF -300/+75	1	21.9	23.6	<0.1	0.32	0.63	<0.1
Lucy ETTP IMF -75/+53	1	33	11.4	<0.1	0.12	0.28	<0.1
Lucy ETTP IMF -75/+53	2	33.2	11.6				
Lucy ETTP IMF -53/+0	1	33.2	10.5	<0.1	0.21	0.43	<0.1
Lucy ETTP IMD -300/+75	1	16.1	33.2	<0.1	0.26	0.46	<0.1
Lucy ETTP IMD -75/+53	1	32.4	11.2	<0.1	0.12	0.26	<0.1
Lucy ETTP IMD -53/+25	1	27.8	16.1	<0.1	0.13	0.34	<0.1
Lucy ETTP IMD -25/+0	1	30.1	14	<0.1	0.35	0.76	<0.1
Lucy ETTP IMD -25/+0	2	30.3	13.9	<0.1	0.31	0.65	<0.1

Table B.13 (continued)

Description	Rep	Cr2O3 %	SiO2 %
PRF -1000/+212	1	18.2	36.2
PRF -1000/+212	2	18.3	36.3
PRF -212/+150	1	29.3	21.0
PRF -150/+106	1	29.8	18.5
PRF -106/+75	1	29.6	19.0
PRF -75/+53	1	25.1	23.3
PRF -53/+25	1	25.1	25.9
PRF -53/+25	2	24.3	25.3
PRF -25/+10	1	23.0	26.5
PRF -10	1	18.7	30.4
PRT -25/+10	1	24.4	23.7
PRT -10/+0	1	20.6	27.3
HGC -212/+75	1	1.42	41.7
HGC -212/+75	2	1.40	41.2
HGC -75/+53	1	0.88	43.0
HGC -53/+38	1	1.01	45.1
HGC -38/+25	1	1.22	45.6
LGC -53/+38	1	1.61	53.1
LGC -38/+25	1	1.96	54.0
LGC -38/+25	2	1.95	53.6

QEMSCAN data validation

Mineralogical analysis with Auto-SEM-EDS is not fully automated and still requires considerable input from the user. In the case of the QEMSCAN, the user creates a SIP list (Species Identification Protocol) which determines the classification of minerals based on the BSE and EDS elemental concentrations associated with each pixel. Developing this list is no small task, and fortunately for this project a SIP list which had been developed for UG2 ore in previous research projects was available. One of the ways of checking that the minerals are being classified appropriately is to back-calculate a QEMSCAN assay value for each element based on the area proportion of each mineral measured, and the density and elemental composition thereof. These QEMSCAN assay values can then be compared to ICP-OES assays to determine whether the classification is appropriate. If there is a large disparity, the mineral definitions in the SIP list may need to be adjusted. Minor disparities may be addressed with slight adjustments to the elemental compositions of the classified minerals. This can reduce most of the variation in the analysis when applied to any single sample, however some variation is typically introduced when different samples are measured, or different size fractions of the same sample are measured. The parity chart in Figure B.6 shows the relationship between the QEMSCAN assay and ICP-OES assays for a range of samples (including different size fractions)

measured in this thesis. This variability is considered adequate for this study in which a very simple mineral list was used, and the bulk of the analysis simply required distinction between chromite and silicate minerals within the ore.

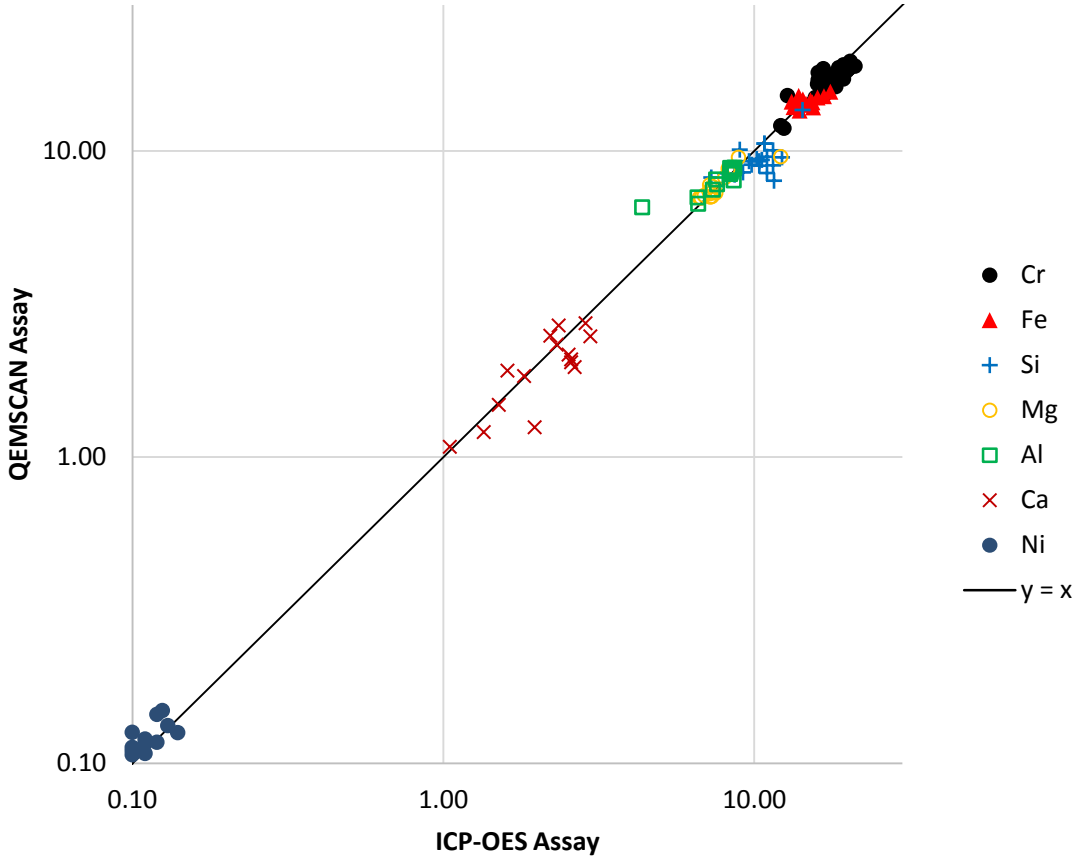

Figure B.6: Correlation between the QEMSCAN assay (calculated) and ICP-OES assay (measured) data for each size fraction of all of the feed samples measured by PMA with EDS mapping.

B.5 Gallery

Figures B.7 – B.10 comprise photographs taken at the Lonmin ETTP and EPA concentrators.

Figure B.7: (a) The ETTP IsaMill considered in this study. (b) Using a wire to unblock the outlet of the only sampling point for the IsaMill Discharge, prior to collecting the sample.

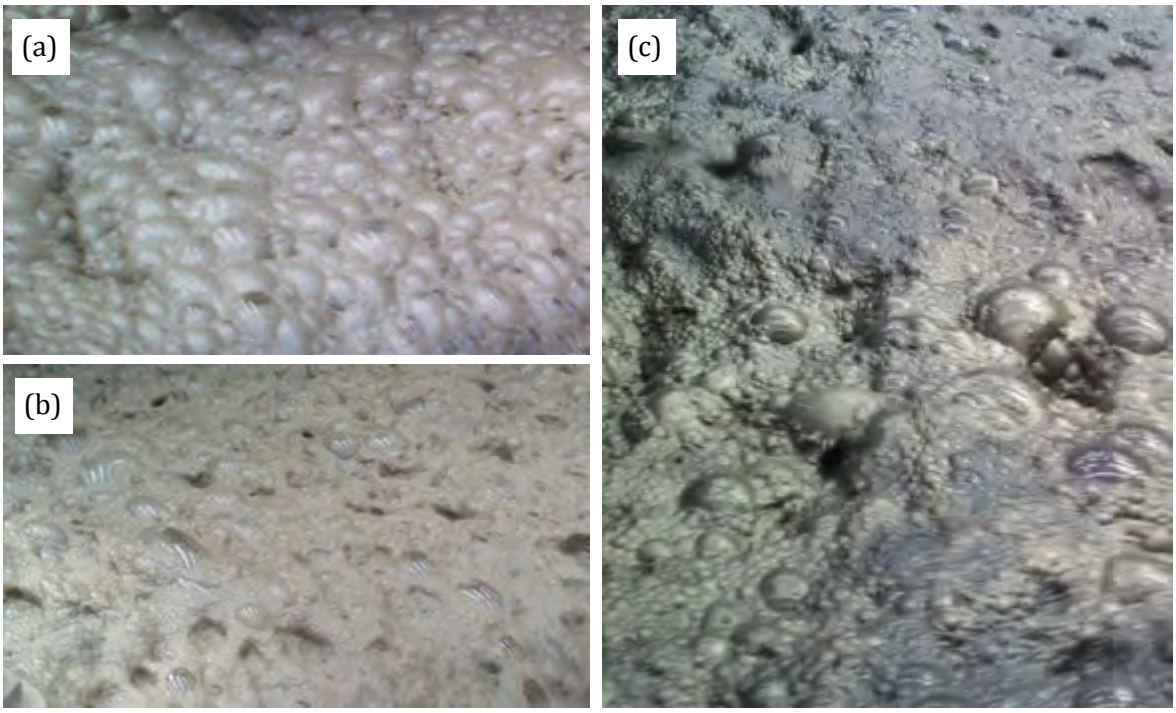

Figure B.8: Images of the froth at different stages in the circuit: (a) primary roughers, (b) secondary roughers, (c) high grade recleaners.

Figure B.9: The automated sample cutter used for sampling the high grade recleaner concentrate (HGC). The sample cutter (to the right of the stream) moves across the stream at a uniform speed, directing the collected sample to an additional splitter (Vezin sampler) which diverts the final cut into a bucket.

Figure B.10: The metal accounting sampling station for EPA.

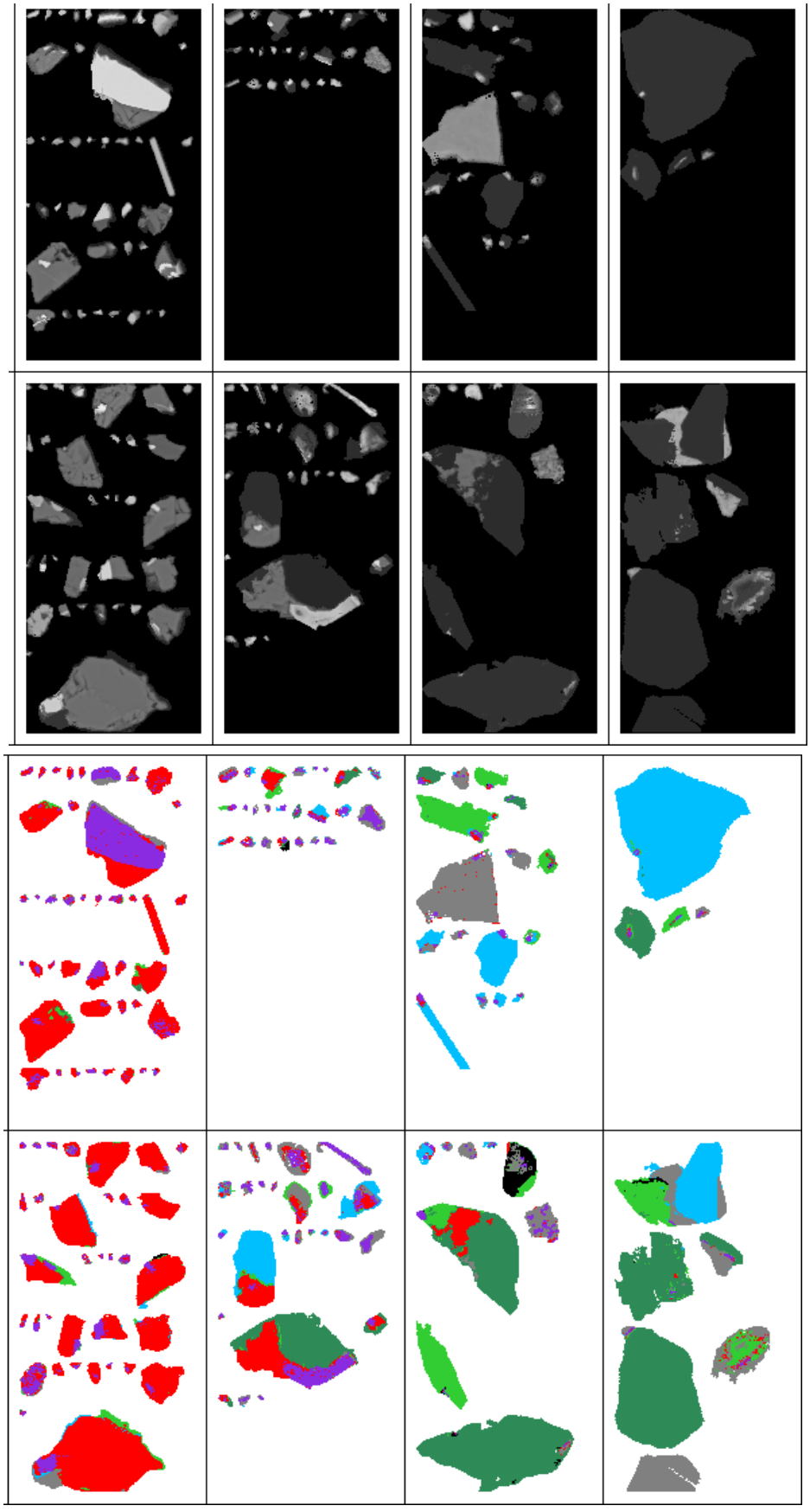

Figure B.11: Image grids showing BSE images and false colour images of the PGM grains analysed in the SMD UF (top row) and BM UF samples (bottom row)

Appendix C: Shape characterisation sample calculations

C.1 Examples of QEMSCAN (iDiscover) categorisers used

To create a categoriser with the iDiscover software, one can use a combination of predefined variables (eg. LongAxis), mathematical operators, and numbers. The predefined variables and parameters available for these categorisers are diverse, and include measurement settings (eg. PixelArea), mineralogy (eg. the proportion of a particle made up of chromite), and particle dimensions (eg. LongAxis). Examples of the categorisers used in this study for shape characterisation are outlined below.

ECD < 25:

host.Area*PixelArea*4/3.1416 < 25*25

equivalent to: (host.Area*PixelArea*4/3.1416)^0.5 < 25

'Area' represents the area of the particle in pixels, so multiplying by 'PixelArea' gives units for particle area of μm^2. Pi is not included in the software, so the value of 3.1416 is typed out.

This example represents a categoriser that will divide a population of particles into only two classes, those with an ECD less than 25 µm, and those with an ECD greater than or equal to 25 µm. To obtain an ECD distribution, a similar line of code is typed for each ECD interval to produce a single categoriser with multiple classes. It is valuable to always qualitatively check the performance of the categoriser created using the image grid function.

Roundness < 0.7:

Area*PixelArea*4/LongAxis/LongAxis/3.1416 < 0.7

The roundness categoriser used the most in this thesis had 20 roundness intervals between 0 and 1 in equal increments of 0.05.

Area*PixelArea*4/LongAxis/LongAxis/3.1416 <0.05
Area*PixelArea*4/LongAxis/LongAxis/3.1416 <0.1
Area*PixelArea*4/LongAxis/LongAxis/3.1416 <0.15
.
.
.
Area*PixelArea*4/LongAxis/LongAxis/3.1416 <1

New jaggedness categoriser presented in Section 4.15 (smooth category):

Roundness > 0.75 * Aspect ratio + 0.05

host.Area*PixelArea*4/LongAxis/LongAxis/3.1416 > 0.75*ShortAxis/LongAxis +0.05

C.2 How to plot shape descriptor frequency distributions

C.2.1 Shape distributions with iDiscover QEMSCAN

The population of particles of interest (false colour images) is first selected, and filtered as appropriate (i.e. a filter 'area > 20' will exclude any false colour images comprised of less than 20 pixels). To save time, multiple samples or fractions can be selected at once, and sorted using a categoriser based on sample information (eg. LocationName or FractionDescription). The data can then be exported using a 3-D chart report option. The three categorisers to be entered on the control panel will then be the categoriser differentiating between the samples of interest (eg. Location name), the shape descriptor categoriser (e.g. roundness described in section C.1), and the weighting parameter of choice (eg. ParticleCount or Area). The resultant data can then be exported to Microsoft Excel, and fitted with a normal distribution model. Note that sample statistics such as the mean and standard deviation can be calculated directly from the measured distribution and used to plot the 'fitted' normal distribution (or beta distribution if preferred for skewed distributions). Vizcarra (2010) did this backwards – he fitted beta distributions to his data, and then reported the mean and modal parameters corresponding to his fitted beta distributions. He also never reported alpha, beta, a, and b values which are key parameters of the beta distribution. The screen capture in Figure C.1 is of an Excel spreadsheet illustrating the calculation of the mean and standard deviation of the roundness frequency distribution (based on particle count), and the fitting of the normal distribution model to the experimental data.

	A	B	C	D	E	F	G	H	I	J
1			Experimental data					Fitted normal distribution		
2						calc for S.D		N(0.487,0.123)		
3		Roundness (x)	Particle count	Normalised distribution		(x-mean)^2		N =NORM.DIST (x,Mean,S.D,cumulative)		
4		0.025	0	0.000		0.213		0.003	0.000	
5		0.075	0	0.000		0.170		0.012	0.001	
6		0.125	5	0.001		0.131		0.043	0.002	
7		0.175	31	0.003		0.097		0.130	0.006	
8		0.225	112	0.012		0.069		0.336	0.017	
9		0.275	408	0.043		0.045		0.735	0.037	
10		0.325	786	0.082		0.026		1.364	0.068	
11		0.375	1066	0.112		0.013		2.146	0.107	
12		0.425	1371	0.144		0.004		2.861	0.143	
13		0.475	1475	0.155		0.000		3.231	0.162	
14		0.525	1395	0.146		0.001		3.093	0.155	
15		0.575	1107	0.116		0.008		2.509	0.125	
16		0.625	835	0.088		0.019		1.725	0.086	
17		0.675	525	0.055		0.035		1.005	0.050	
18		0.725	253	0.027		0.057		0.496	0.025	
19		0.775	123	0.013		0.083		0.208	0.010	
20		0.825	35	0.004		0.114		0.074	0.004	
21		0.875	7	0.001		0.151		0.022	0.001	
22		0.925	1	0.000		0.192		0.006	0.000	
23		0.975	0	0.000		0.238		0.001	0.000	
24		total	9535	1				20	1	
25										
26		n							9535	
27		Mean = SUMPRODUCT (B4:B23,D4:D23)							0.487	
28		S.D. = SQRT(SUMPRODUCT (D4:D23,F4:F23))							0.123	
29										
30										
31										
32										
33										
34										
35										
36										
37										
38										
39										

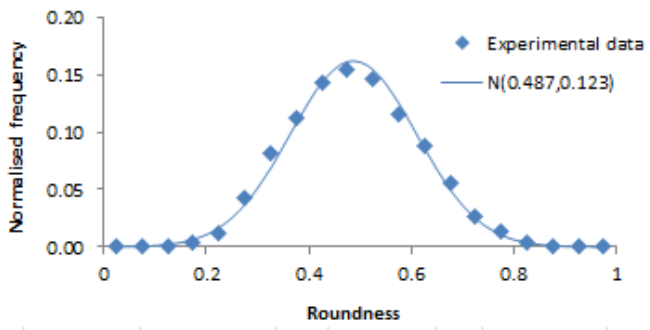

Figure C.1: Screen capture of excel spreadsheet illustrating the determination of the mean and standard deviation of a roundness frequency distribution, and the determination of the corresponding normal distribution model.

C.2.2 Plotting a roundness distribution with Mineralogic

For the determination of roundness distributions with the Mineralogic, the Maximum Feret diameter and area data for each particle was exported to Excel, and the roundness frequency distributions were then calculated based on this data. This would likely be easier with almost any program other than Excel, but the method that was applied in this work is described here for those who like to use Excel for everything,

The raw data is formatted with the information in each row corresponding to a different particle, and the information in each column corresponding to the measured properties of each particle (i.e. area, Maximum Feret Diameter). In a new column, the formula for the required descriptor (e.g. roundness) is entered with reference to the Maximum Feret diameter column and Area column. 20 bins (columns) are then prepared for the frequency distribution, each with an IF statement to display the particle area (for weighting by area) or 1 (for weighting by particle count) if the number in the roundness cell falls within the range of values for that bin. Copy-paste the formulae in each of these columns for all 1500+ rows corresponding to each particle). AutoSum the contents of each bin (column) to obtain the frequency distribution. The screen shot provided in Figure C.2 shows a screen capture from the spreadsheet for obtaining the circularity distribution (based on number of particles) for the Mineralogic measurement of block B of the -212/+150 µm fraction. The results from each of the three blocks (repeat measurements) were then collated and normalised, and then the average of the three was presented as a cumulative frequency distribution. The 95% confidence limits associated with each point on the distribution were estimated based on the standard deviation of the three repeats, the number of repeats, and the Z score of 1.96. A screen capture from the Mineralogic circularity data summary sheet is provided in Figure C.3.

	A	B	C	E	M	N	O	P	Q	R	S	T
1	ParticleID	Area µm²	Perimeter	Feret Max	Diameter	circularity	0	0.05	0.1	0.15	0.2	0.25
1527	6232520	847.67	317.01	70.73		0.1060		0	1	0	0	0
1528	6221443	10890.06	1138.15	277.21		0.1056		0	1	0	0	0
1529	6213865	4667.17	751.85	124.63		0.1037		0	1	0	0	0
1530	6213868	5220.64	844.28	136.21		0.0920		1	0	0	0	0
1531	6232274	6437.3	962.99	136.24		0.0873		1	0	0	0	0
1532	6231977	27260.04	2024.46	252.69		0.0836		1	0	0	0	0
1533	6216780	1460.98	479.99	82.39		0.0797		1	0	0	0	0
1534	6217077	15542.26	1591.39	218.91		0.0771		1	0	0	0	0
1535	6217091	4976.32	910.7	219.52		0.0754		1	=IF(AND($N1535>Q$1,$N1535<=R$1),1,0)			
1536	6213687	5100.97	960.76	130.21		0.0694		1	0	0	0	0
1537	6232608	598.35	376.38	54.35		0.0531		1	0	0	0	0
1538	6214274	6178.01	1447.44	141.32		0.0371	1	0	0	0	0	0
1539	6212339	9827.98	1844.69	201.76		0.0363	1	0	0	0	0	0
1540							2	8	17	30	42	63

Figure C.2: Screen capture of an excel spreadsheet illustrating the methodology used to calculate the shape descriptor frequency distributions from the raw data obtained with the Mineralogic and CAMSIZER XT.

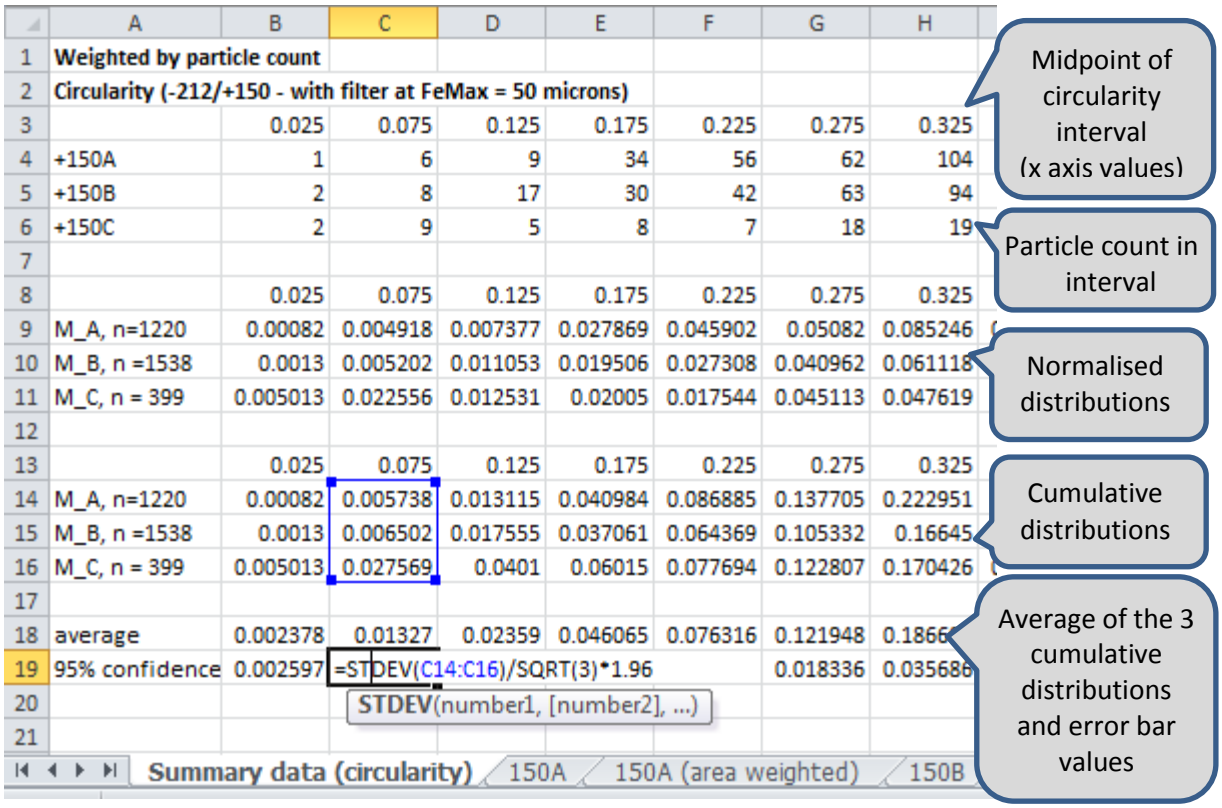

	A	B	C	D	E	F	G	H
1	Weighted by particle count							
2	Circularity (-212/+150 - with filter at FeMax = 50 microns)							
3		0.025	0.075	0.125	0.175	0.225	0.275	0.325
4	+150A	1	6	9	34	56	62	104
5	+150B	2	8	17	30	42	63	94
6	+150C	2	9	5	8	7	18	19
7								
8		0.025	0.075	0.125	0.175	0.225	0.275	0.325
9	M_A, n=1220	0.00082	0.004918	0.007377	0.027869	0.045902	0.05082	0.085246
10	M_B, n =1538	0.0013	0.005202	0.011053	0.019506	0.027308	0.040962	0.061118
11	M_C, n = 399	0.005013	0.022556	0.012531	0.02005	0.017544	0.045113	0.047619
12								
13		0.025	0.075	0.125	0.175	0.225	0.275	0.325
14	M_A, n=1220	0.00082	0.005738	0.013115	0.040984	0.086885	0.137705	0.222951
15	M_B, n =1538	0.0013	0.006502	0.017555	0.037061	0.064369	0.105332	0.16645
16	M_C, n = 399	0.005013	0.027569	0.0401	0.06015	0.077694	0.122807	0.170426
17								
18	average	0.002378	0.01327	0.02359	0.046065	0.076316	0.121948	0.1866
19	95% confidence	0.002597	=STDEV(C14:C16)/SQRT(3)*1.96				0.018336	0.035686
20								
21								

Figure C.3: Screen capture of an excel spreadsheet used to determine the 95% confidence intervals to plot the error bars for the cumulative frequency distributions presented in Figures 4.17 and 4.18. In the case of the Auto-SEM-EDS devices, these were obtained from measurements of three blocks, A, B & C. For the CAMSIZER XT, these were based on three repeat measurements.

C.2.3 Plotting a roundness distribution with the CAMSIZER XT

With the CAMSIZER XT, one can plot size distributions based on maximum Feret diameter or equivalent area diameter, and determine the average sphericity (circularity) for any number of particle size classes based on a range of size parameters. Or one can obtain a sphericity frequency distribution. However, it is typical for millions of particles to be analysed so the data for each particle is not stored, and furthermore, the CAMSIZER XT data is weighted by volume (for compatibility with screening). The volume weighting is based on the rotation of an equivalent ellipse of each particle silhouette around its long axis, which would lead to a heavier weighting of spherical particle images relative to elongated particle images than with area-weighting. In Paper 2, for comparison of the different devices it therefore made sense to by-pass most of the CAMSIZER XT software. Instead, from randomly selected images that had been captured, the parameters for each particle in the image were exported in a simple list format, and the same procedure that was described in C.2.2 was followed.

C.3 Plotting a *roundness–aspect ratio* normalised frequency distribution with iDiscover (QEMSCAN) and Microsoft Excel

Prepare roundness and aspect ratio categorisers. Select the population of particles of interest – if necessary applying filters such as the granulator (for determination of shape characteristics of unliberated grains). Select the 3-D chart report option on iDiscover, and with the control panel set the *roundness* categoriser to the x-axis and the *aspect ratio* categoriser to the y-axis. Use *particle count*, *mass* or *area* for the z-axis depending on preferred normalisation parameter. Copy data, and then paste in Excel. AutoSum the entire contents of the data grid, and normalise the distribution by dividing the value in each cell of the grid/matrix by the total particle count, mass or area obtained (depending on the normalisation parameter selected). This can then be simply plotted by selecting the entire contents of the data grid and then 'insert chart'(see Figure C.4. The surface contour chart was the option preferred in this thesis, with the number of contours adjusted by editing the major unit of the 'vertical axis', and the colours adjusted by right-clicking on the fill-colour of the legend entry and selecting the preferred colour.

	A	B	C	D	E	F	G	H	I	J	K	L	M	N	O	P	Q	R	S	T	U	V	W
1	**ParticleCount**										**roundness medium**												
2		**0.0**				**0.2**				**0.4**				**0.6**				**0.8**				**1.0**	
3		**0**	0	0	0	0	0	0	0	0	0	0	0	0	0	0	0	0	0	0	0	0	
4			0	0	0	0	0	0	0	0	0	0	0	0	0	0	0	0	0	0	0	0	
5			0	0	0	0	0	0	0	0	0	0	0	0	0	0	0	0	0	0	0	0	
6			0	0	0	0	0	0	0	0	0	0	0	0	0	0	0	0	0	0	0	0	
7		**0.2**	0	0	1	1	0	0	0	0	0	0	0	0	0	0	0	0	0	0	0	0	
8			0	0	1	3	0	0	0	0	0	0	0	0	0	0	0	0	0	0	0	0	
9			0	0	0	0	7	0	0	0	0	0	0	0	0	0	0	0	0	0	0	0	
10			0	0	0	1	6	9	2	0	0	0	0	0	0	0	0	0	0	0	0	0	
11		**0.4**	0	0	0	0	2	24	13	3	0	0	0	0	0	0	0	0	0	0	0	0	
12	**aspect ratio**		0	0	0	0	0	4	19	9	1	0	0	0	0	0	0	0	0	0	0	0	
13			0	0	0	0	0	5	13	29	17	3	0	0	0	0	0	0	0	0	0	0	
14			0	0	0	0	0	1	6	30	31	15	3	0	0	0	0	0	0	0	0	0	
15		**0.6**	0	0	0	0	0	0	2	13	32	34	21	1	0	0	0	0	0	0	0	0	
16			0	0	0	0	0	0	0	5	17	46	47	14	6	0	0	0	0	0	0	0	
17			0	0	0	0	0	0	0	0	6	32	41	46	18	2	0	0	0	0	0	0	
18			0	0	0	0	0	0	0	0	1	10	32	46	44	21	2	0	0	0	0	0	
19		**0.8**	0	0	0	0	0	0	0	0	0	4	10	22	63	61	26	2	0	0	0	0	
20			0	0	0	0	0	0	0	0	0	0	3	28	37	76	64	25	3	0	0	0	
21			0	0	0	0	0	0	0	0	0	1	1	10	17	44	89	52	14	1	0	0	
22			0	0	0	0	0	0	0	0	0	0	0	2	10	23	60	89	58	4	0	0	
23		**1**	0	0	0	0	0	0	0	0	0	0	1	2	3	2	11	32	36	6	1	0	
24																							1791
25						Normalised roundness - aspect ratio distribution																		
26										**roundness medium**													
27		**0.0**				**0.2**				**0.4**				**0.6**				**0.8**				**1.0**	
28																							
29																							
30				=D6/W24																			
31		**0.2**			0.00	0.00																	
32					0.00	0.00																	
33						0.00	0.00																
34						0.00	0.00	0.01	0.00														
35		**0.4**					0.00	0.01	0.01	0.00													
36								0.00	0.01	0.01	0.00												
37	**aspect ratio**							0.00	0.01	0.02	0.01	0.00											
38								0.00	0.00	0.02	0.02	0.01	0.00										
39		**0.6**							0.00	0.01	0.02	0.02	0.01	0.00									
40										0.00	0.01	0.03	0.03	0.01	0.00								
41											0.00	0.02	0.02	0.03	0.01	0.00							
42											0.00	0.01	0.02	0.03	0.02	0.01	0.00						
43		**0.8**										0.00	0.01	0.01	0.04	0.03	0.01	0.00					
44													0.00	0.02	0.02	0.04	0.04	0.01	0.00				
45												0.00	0.00	0.01	0.01	0.02	0.05	0.03	0.01	0.00			
46														0.00	0.01	0.01	0.03	0.05	0.03	0.00			
47		**1**											0.00	0.00	0.00	0.00	0.01	0.02	0.02	0.00	0.00		
48																							1

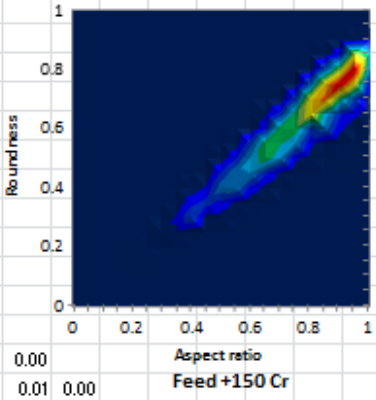

Figure C.4: Screen capture of a Microsoft Excel spread sheet used to obtain a normalised roundness – aspect ratio frequency distribution.

Appendix D: Phase boundary fracture calculations and supporting data

In Paper 3, Chapter 5, various methods for assessing phase boundary fracture were explored. None of the methods are perfect - all rely on a variety of assumptions. All of the methods depended on the assumed grain size distribution of the chromite in-situ, based on the rounded chromite grains (likely an underestimate). Thereafter, the conservation-of-shape approach was perhaps simplest, and the supporting information provided in Paper 3 should be sufficient to enable replication of the analysis. The other assumption for this method relates to the estimate of the proportion of rounded grains prior to breakage, and this may cause some difficulty depending on the performance of the 'granulator' for separating touching rounded grains within composites. Qualitative analysis using the image grid is advisable to check all of the proportions obtained. For the comparison to random breakage approach using Gay's liberation model, the supporting data and calculations are provided in Section D.1. Of all of the methods, the assessment of PSIA involved the most 'experimentation/trial and error', and the quality of some of the output is still questionable. D.2 therefore outlines what was done to determine the PSIA distributions presented in Chapter 5, and some additional PSIA data is presented and discussed.

D.1 Comparison to Gay's liberation model

The liberation data presented by Gay (2004) for the twelve liberation classes was combined into the three liberation classes used for this study, with the phase with the spherical grains allocated to represent chromite, and the matrix phase allocated to represent the primary silicates. The median particle sizes at which the theoretical liberation was calculated by Gay were then normalised (by dividing by 16) for comparison to the particle size distribution of the experimental data which was also normalised (by dividing the geometric mean of each size fraction by 170, the mean grain size of the chromite). The obtained data, which is highlighted in grey in Figure D.1 was then plotted for presentation in Figure 5.3.

Grain size was 16 pixels. Median chromite grain size was 220 microns									
Gay (2004) randomly estimated liberation distribution for Boolean texture									
		24	20	16	12	8	4		
	0	0	0	0	1	5.4	24.5		
	0-10	0.7	1.4	3.2	7.1	9.8	6.8		
	10-20	1.4	1.8	4.8	6.5	5.6	3.9		
	20-30	4.2	4.9	6.7	7.6	5.1	3.7		
	30-40	10.5	10.2	5.8	7.2	4.2	3.2		
	40-50	14.7	10.9	11.8	8.5	6.7	1		
	50-60	19.7	22.3	19.2	9.3	7.2	3.2		
	60-70	21.4	16.4	10.2	8.8	8.3	4		
	70-80	15.7	15.2	14.4	10.8	6.7	3.6		
	80-90	9.1	10.6	10.5	10	9.1	4.8		
	90-100	2.6	6.4	13.3	18	14.7	8.7		
	100	0	0	0	5.2	17.1	32.6		
Calculated based on Gay's data									
Relative size (x - axis)		1.94	1.62	1.00	0.97	0.65	0.32		
Upscaling to median size of 170		330	275	220	165	110	55		
liberated silicates (90 - 100%)		0.70	1.40	3.20	8.10	15.20	31.30		
chromite silicate composites (10 - 90%)		96.70	92.30	83.40	68.70	52.90	27.40		
liberated chromite (90 - 100%)		2.60	6.40	13.30	23.20	31.80	41.30		
liberated silicates +liberated chromite				0.165					
Measured for UG2 ore									
Relative size (x- axis)		2.97	2.10	1.48	1.05	0.74	0.52	0.37	0.26
Top size of fraction	600	425	300	212	150	106	75	53	38
Geometric mean of size fraction		505	357	252	178	126	89	63	45
liberated silicates (90 - 100%)		0.32	0.23	0.23	0.24	0.33	0.37	0.55	0.57
chromite silicate composites (10 - 90%)		0.28	0.19	0.14	0.06	0.03	0.02	0.03	0.04
liberated chromite (90 - 100%)		0.40	0.58	0.63	0.70	0.64	0.61	0.42	0.39
liberated silicates +liberated chromite					0.94				

Figure D.1: Data associated with the comparison-to-random fracture approach

D.2 Estimation of PSIA

Phase specific interfacial area in 2-D is defined as the locked perimeter of a mineral phase divided by the area of that mineral phase. Apparently the MLA software includes both of these parameters; however the QEMSCAN software does not. Even if it did, the work in this thesis on angularity/circularity shows how fickle perimeter measurements can be. The QEMSCAN software does include an estimate for phase specific surface area (perimeter over area), which is based on 1-D Mean intercept length measurements and stereological relationships (Figure D.2). For estimating the PSIA of chromite, this should be accurate because the chromite grains in-situ are mostly spherical. This PSSA was compared to PSSA calculated as perimeter/area in Paper 5; additional PSSA measurements are presented in Figure D.3. They are seen to give fairly consistent results for the range from 25 – 300 µm, but they diverge considerably at coarse sizes, perhaps due to the higher error associated with fewer particles.

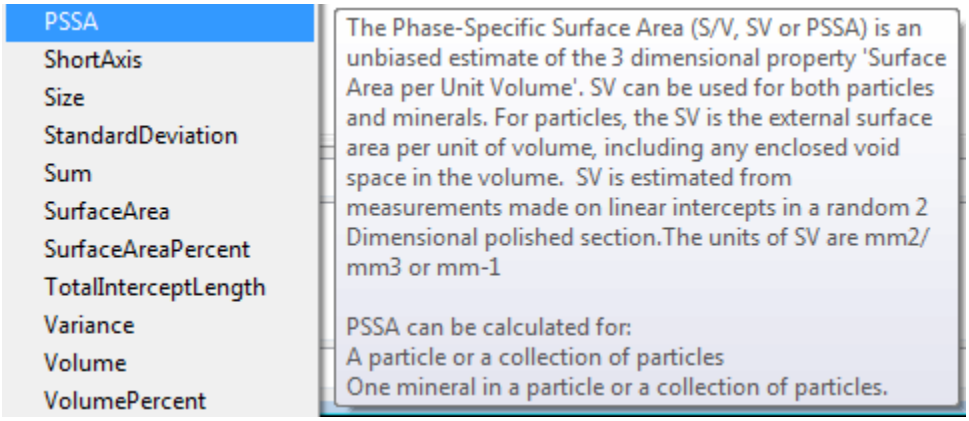

Figure D.2: iDiscover definition of PSSA.

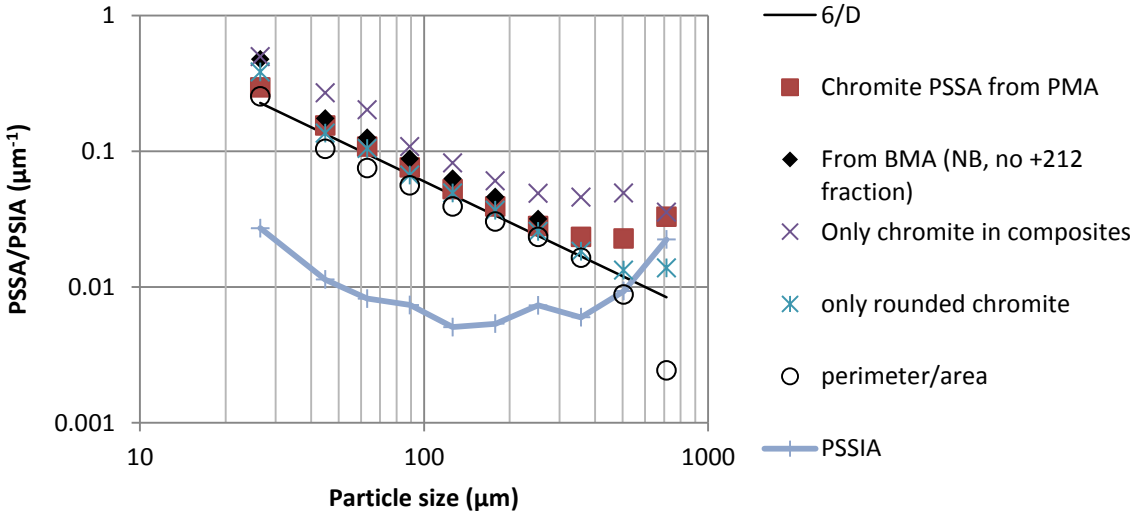

Figure D.3: Different estimates of PSSA which could be used for PSIA calculation. 'Chromite PSSA from PMA' is the QEMSCAN 'stereologically' correct estimate based on mean intercept length that was selected for the following analyses. 'From BMA' is the QEMSCAN applying the same relationship to 1-D line scan measurements rather than 2-D PMA measurements.

To determine the proportion of 'locked perimeter' to convert from PSSA to PSIA, the 'associations' parameter was applied as follows:

Chromite PSIA = Proportion of the total perimeter of chromite grains that is associated with other minerals rather than background, multiplied by the phase specific surface area of chromite. Note 'Associations' does not include associations with background unless explicitly stated (Figure D.4). The categoriser is therefore written as follows:

(Associations(Simple.Chromite)/(Associations(Simple.Chromite,Simple.Background) + Associations(Simple.Chromite))*PSSA(Simple.Chromite))/1000

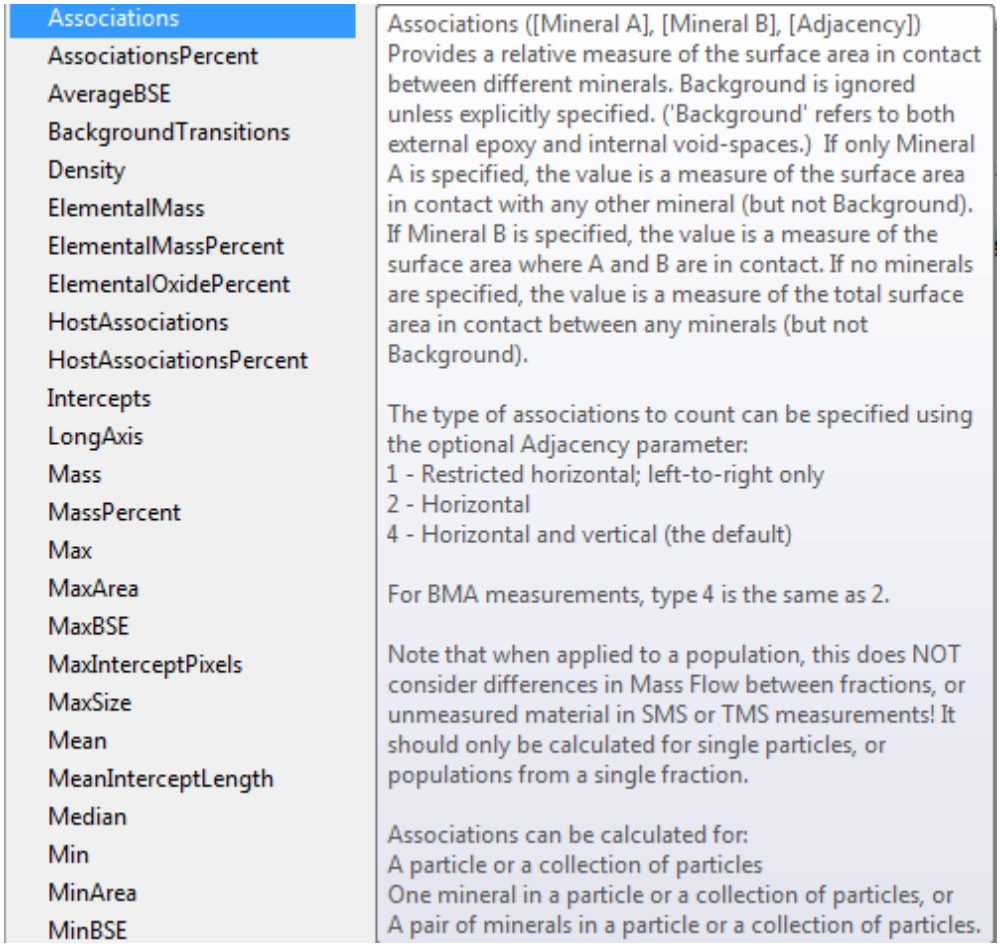

Figure D.4: iDiscover definition of 'Associations'.

To check the performance of this categoriser, the image grid function was used, and this is shown for a coarse fraction in Figure D.5. Applying the categoriser to individual particles (to classify them for the image grid) is not ideal as its value lies in applying it to a population of particles. However it is useful to have something to look at for this rather abstract measurement. From Figure D.5 the categoriser appears to be giving reasonable classification, with coarse liberated chromite grains having the lowest PSIA, and finely disseminated locked chromite grains having the highest PSIA. The PSIA relationship with size, observed in Figure D.3, is similar to relationships which have been reported in the past, such as that presented in Figure D.6 (Fandrich et al., 1997; King, 1992). Note that the units for Figure D.6 are mm^{-1}, while those in Figure D.3 are μm^{-1}, so the range of values for PSIA is of a similar magnitude. King (1992) justified the occurrence of the high PSIA at the finest particle size as due to a large degree of boundary region fracture leading to non-liberated fine particles. However, in this work this did not seem like a realistic explanation due to the apparently 'clean' phase boundary fracture, and the very high degree of liberation of chromite below 75 µm. The image grid in Figure D.7 was therefore used to qualitatively assess the PSIA results for the fine particles.

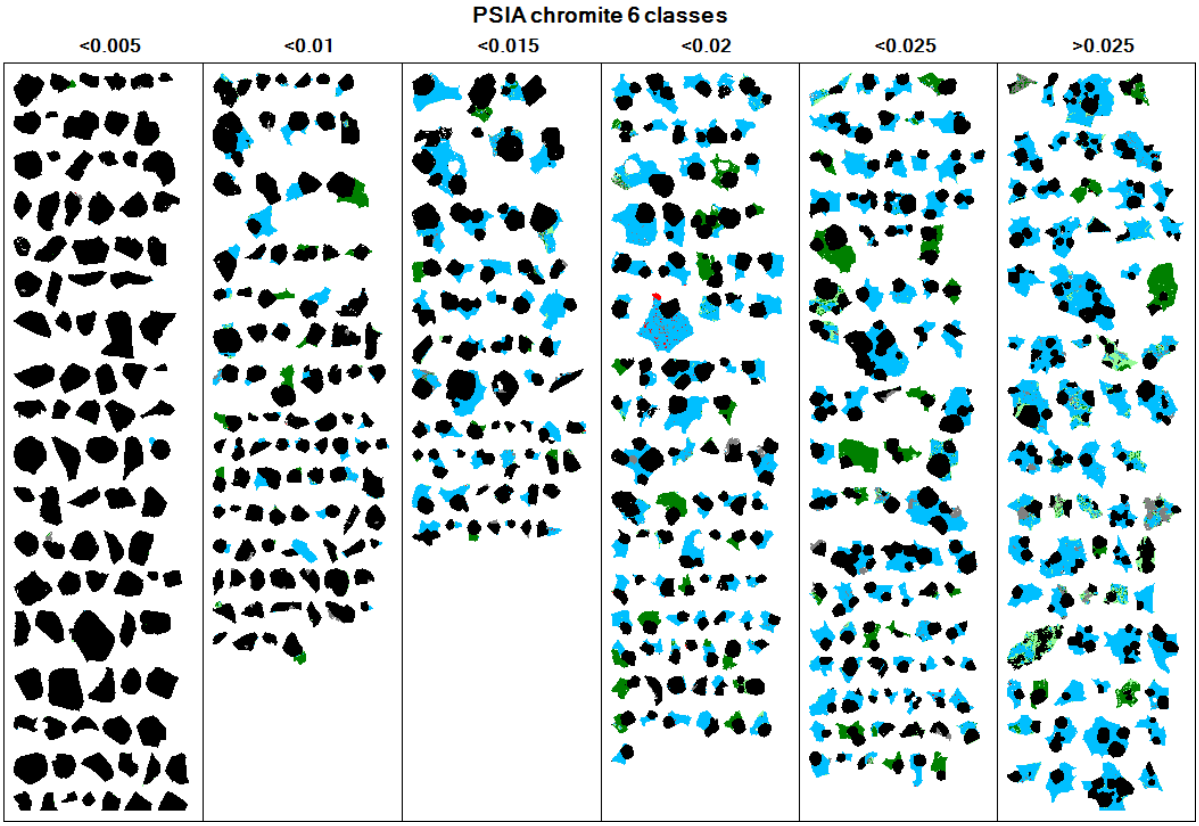

Figure D.5: Coarse UG2 ore particles (-1000/+212 µm) classified by chromite PSIA indicating that the categoriser is producing the expected relationship. PSIA categoriser values are in µm^{-1}.

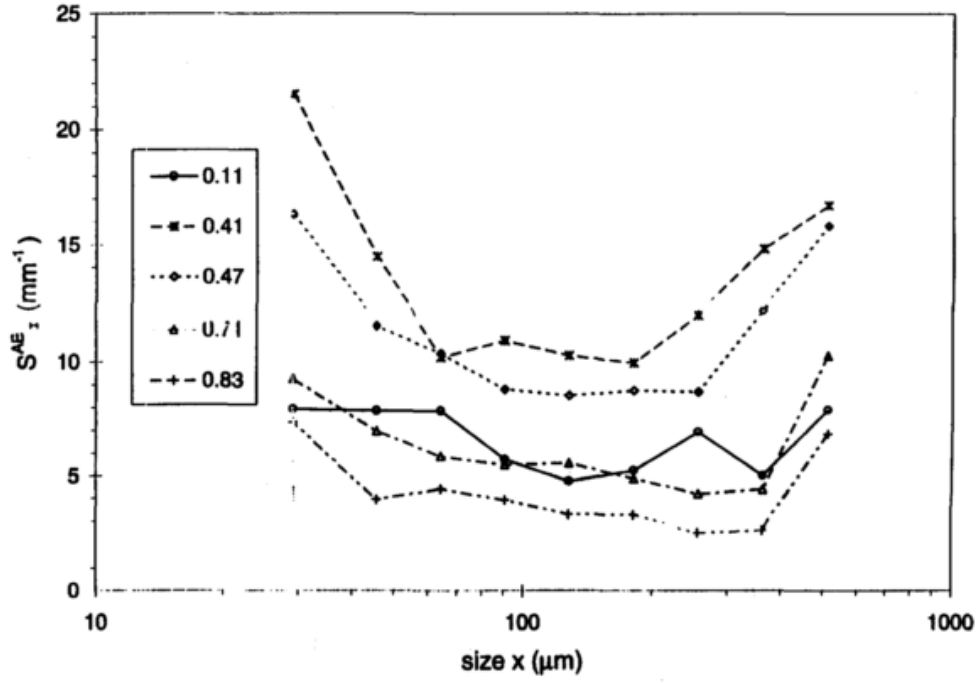

Figure D.6: Change in particle volume specific interfacial surface area with particle size (Fandrich et al., 1997)

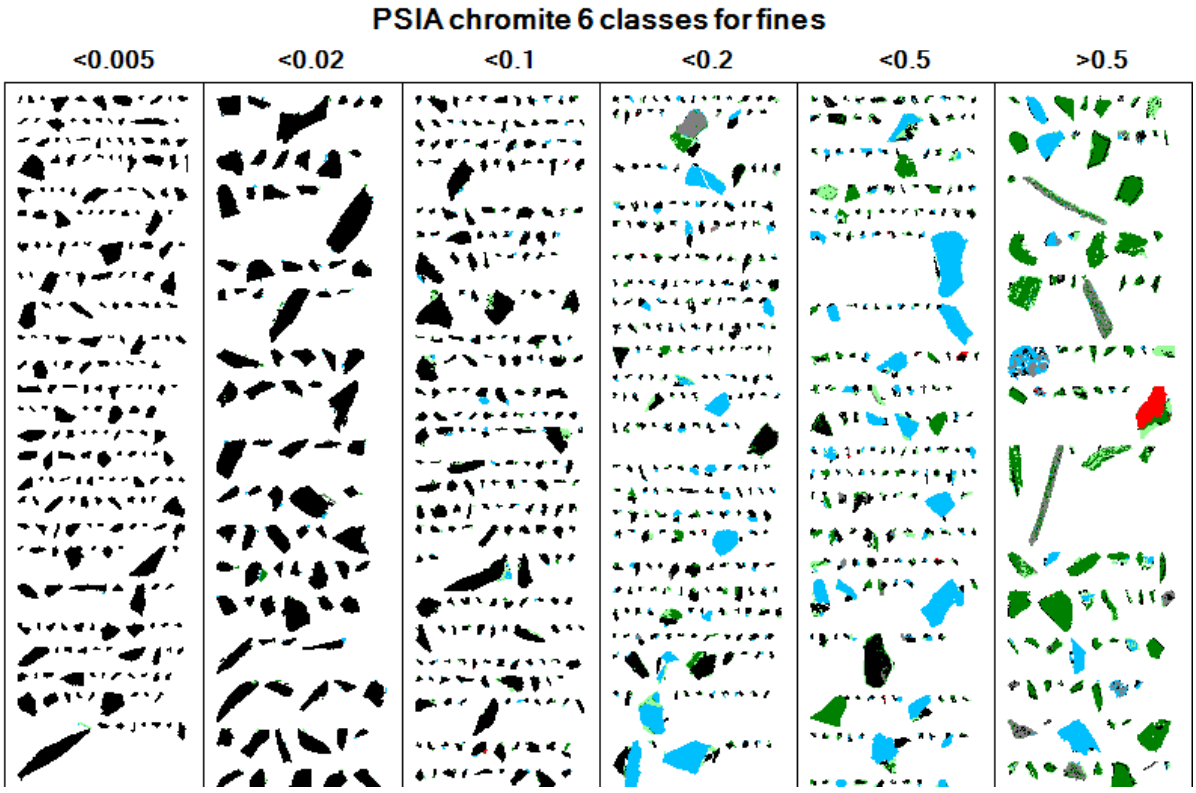

Figure D.7: Fine UG2 ore particles (-38/+0 µm) classified by chromite PSIA – much harder to visually confirm that the categoriser is performing as expected.

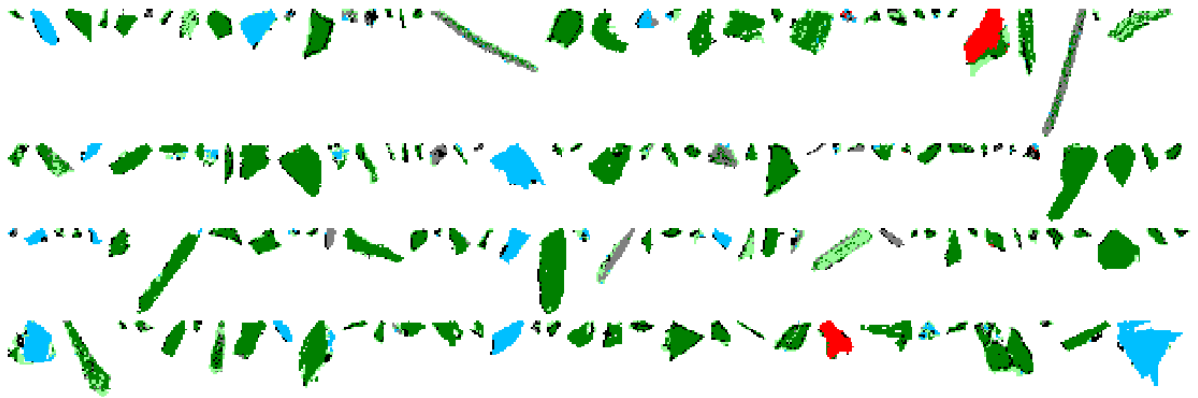

Figure D.8: A closer look at some of the particles which are responsible for the very high PSIA of chromite at fine particle sizes. Could this be due to boundary region fracture described by King, or is it perhaps an artefact of sample prep (touching particles), higher resolution, or poor mineral classification, or just the very high phase specific surface area associated with micron sized grains?

Figures D.7 and D.8 are not particularly enlightening as to whether the very high phase specific interfacial area of the fine fraction is evidence of boundary region fracture as described by King (1992). A few of the particles do appear to be touching particles that have not been adequately separated by the automatic touching-particle separation algorithms. However most of them appear to have single pixels that have been identified as chromite, which may or may not be a

true representation of fine chromite grains within the particles. The pixel spacing for the particle images presented in Figure D.8 was 2 μm. A spherical chromite grain of 2 μm in diameter would have a PSSA of 3 μm^{-1}. The associations categoriser determines the proportion of external pixels which are associated with other minerals, not the number of sides of a square pixel that are associated with other minerals. So for a grain comprising only one pixel which is adjoined to pixels of another mineral on only one side, the chromite grain would still read as a fully locked grain, with 100% of the boundary pixels associated with the other mineral. For this 2 μm grain mentioned above, the PSIA would then also be 3 μm^{-1}, even if it's supposed to be one quarter of that (which is still very high!). This error may contribute to the high PSIA measurements obtained at fine sizes and high resolutions. Note that the categoriser, when applied to a population of particles, is not determining PSIA on a particle-by-particle basis. If it was, this would be a significant concern because then fully liberated chromite grains would not be accounted for adequately.

Because of the large uncertainty associated with the (-38 μm) data point for the chromite in the laboratory feed sample, it was not presented as part of the PSIA distribution in Chapter 5 due to concern that it would lead to misleading interpretations without substantial additional supporting explanations. This proportion of particles also only accounts for 2.7% of the chromite within the sample. However, brief consideration was given to the chromite PSIA in the fine grinding test work, as the majority of particles in these samples are finer than 75μm. The PSIA distributions of chromite in the fine grinding products are presented in Figure D.9, with PSIA plotted against the median of the size fraction considered. The PSIA of the BMS for the same samples is presented in Figure D.10. These figures do not indicate a clear reduction in PSIA for a particular mill type across all size fractions, thus supporting the findings in Paper 4, Chapter 6. It is not possible to conclude that a greater degree of phase boundary fracture occurs in either mill type. Figure D.11 was plotted to indicate the degree of uncertainty associated with these measurements, with repeats for the SMD F sample presented. (This is the sample with the very high PSIA value for the -25/-10 μm fraction in Figure D.9). In general, the repeatability of these measurements appears to be better than was expected, however the high reading for the block A of the -25/-10 μm fraction indicates that significant variability can occur between sample blocks.

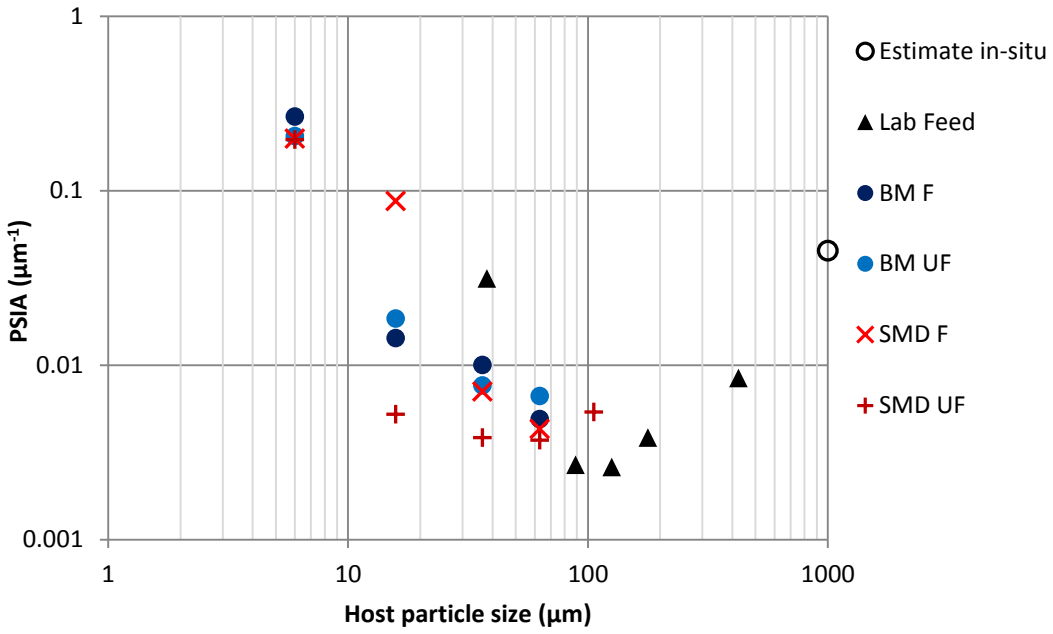

Figure D.9: Chromite PSIA after fine grinding in the ball mill and SMD

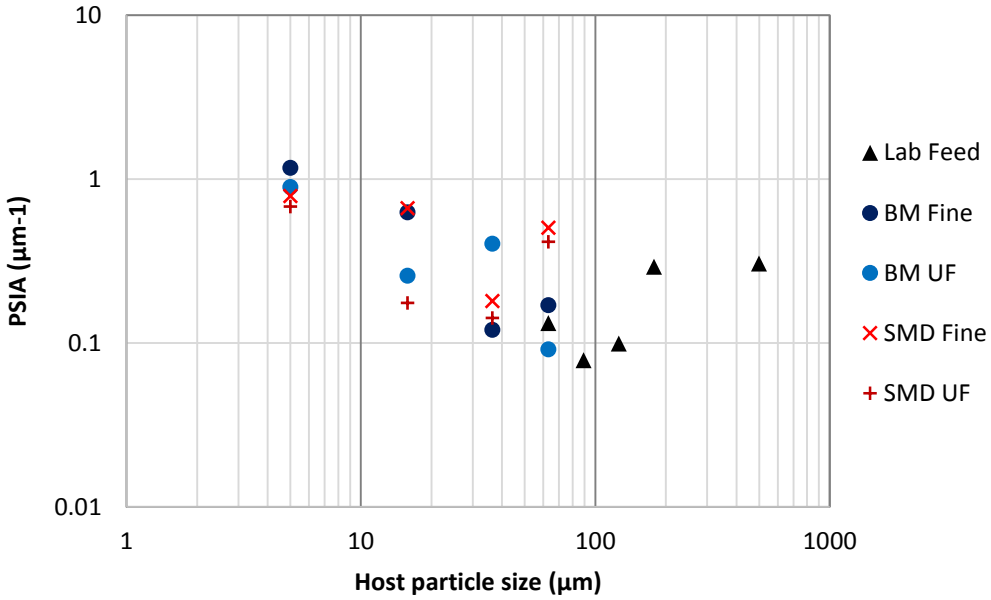

Figure D.10: BMS PSIA after fine grinding in the ball mill and SMD

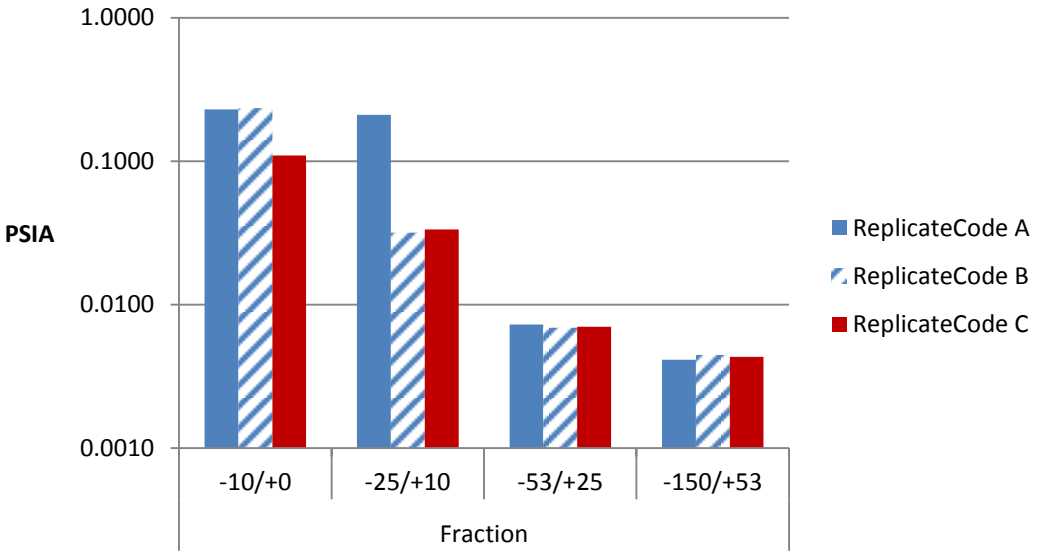

Figure D.11: Indication of the variability in chromite PSIA estimates based on replicate measurements for the SMD F sample

Resolution effects are also likely to contribute to the apparent increase in PSIA at the fine size fractions. Figure D.12 shows the PSIA of replicate blocks measured at two resolutions: 0.5 µm/pixel and 1 µm/pixel. Doubling the resolution appears to double the PSIA measurement. Overall, PSIA may have potential as a useful tool for estimating phase boundary fracture, but there appear to be many factors that can affect it, and these factors should be taken into consideration before drawing conclusions based on PSIA measurements.

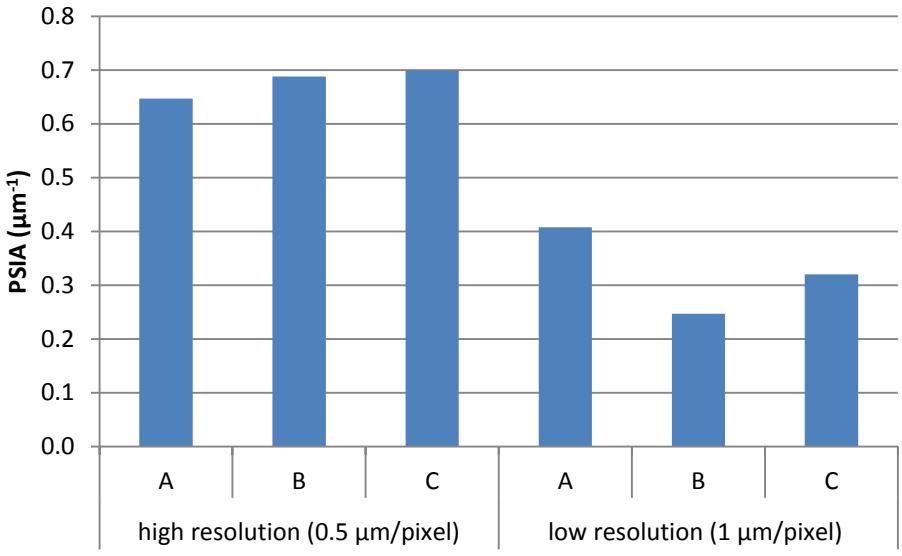

Figure D.12: PSIA measurements of the SMD UF grind -10 µm fraction with 3 repeated blocks at two different image resolutions.

Appendix E: Presentation and discussion of true flotation results

This body of work was initially intended to be incorporated within the thesis, but once particle shape characterisation became the main focus of the thesis, this part of the study no longer contributed directly towards addressing the main objectives of the thesis.

E.1 Fine grinding and PGE recovery

The literature review in Section 5.1.3, the plant data presented in Section 6.8, and the fine grinding laboratory data presented in Section 6.3 set the context for the laboratory flotation study. The main purpose of the flotation circuit is to recover as much of the valuable platinum group minerals as possible, at the highest possible grade. PGE grades and recoveries are the most important performance indicators for flotation in this study. Chromite recovery through entrainment is also an important factor for UG2 ore, and this was considered in Chapter 6.

The reagent suite was selected to simulate plant conditions at the time, with a nominal depressant dosage of 200 g/t. However, depressant dosages of 500 g/t and 0 g/t were also included in the test work. The excess depressant dosage (500 g/t) was to suppress the naturally floatable gangue for the entrainment study. The test work with no depressant was intended to achieve conditions that would maximise recovery irrespective of grade. The 4E-PGE recoveries and grades of the tests for both the fine and ultrafine grinds with both mill types and all three depressant dosages are compared in Figures E.1 and E.2 respectively.

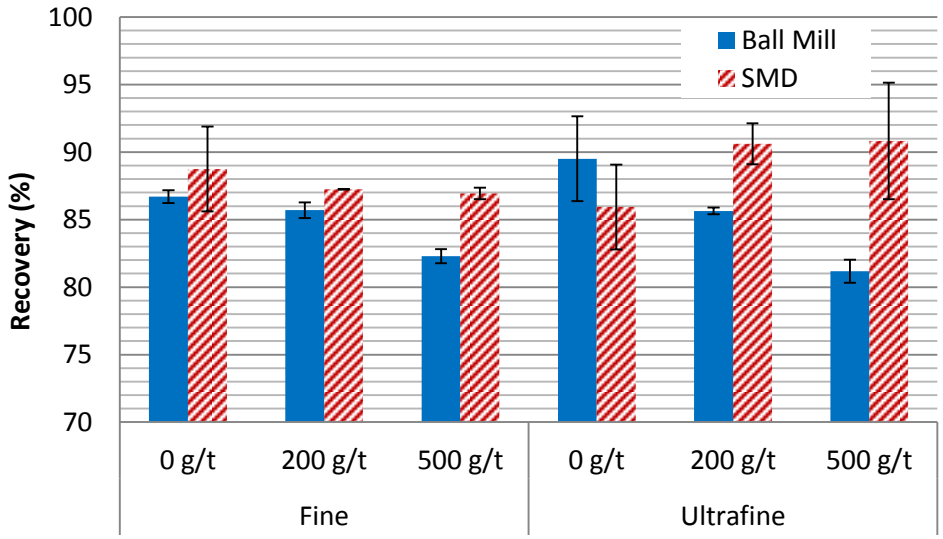

Figure E.1: Total 4E-PGE recoveries after flotation of the ball mill and stirred mill products at the two target grinds and three depressant dosages. Error bars show 95% confidence intervals.

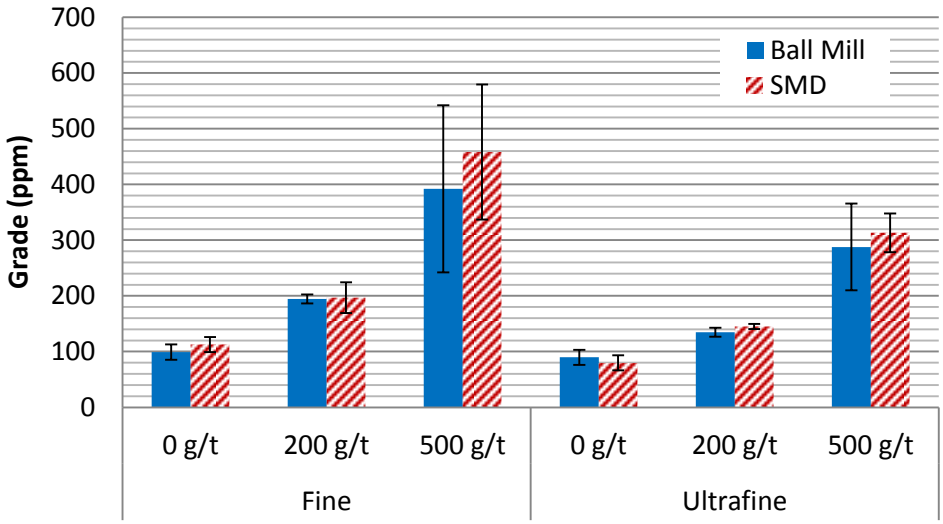

Figure E.2: 4E-PGE grades of combined concentrates after flotation of the ball mill and stirred mill products at the two target grinds and three depressant dosages. Error bars show 95% confidence intervals.

There is typically an inverse relationship between grade and recovery, with higher solids recoveries (mass pull) leading to higher recovery of valuable minerals at the cost of decreasing grade. In this test work, depressant dosage is seen to have the strongest effect on grade, followed by the grind, with zero depressant and the ultrafine grinds having the most stable froth and thus the highest mass pull (Figure E.4). This effectively accounts for the variation observed in PGM grade, as even with an upgrade ratio of 100, the bulk of the concentrate mass is still comprised of gangue minerals. The causes of the variation in recovery are less apparent. The PGE recovery of the ball mill products decreases with increasing depressant dosage and thus decreasing solids recovery, which could be attributed to the changes in froth conditions, or perhaps to an interaction of the depressant with the surfaces of the PGMs or minerals associated with them. This occurs at both grinds, and the finer grind did not necessarily improve the recovery attainable. The SMD product recoveries were not negatively affected by increasing depressant dosage, and the highest recoveries (above 90%) were attained for the ultrafine grind with depressant added.

The grade recovery relationship is typically illustrated on cumulative grade versus cumulative recovery plots, with the first concentrate collected over a short time period comprising fast floating material, and the cumulative grade decreasing as additional concentrates comprising a greater proportion of gangue are collected. An unconventional grade versus recovery plot is provided in Figure E.3, which does not show cumulative grade and recovery data over time, but rather summarises the overall grade and recovery achieved in the laboratory test work for the three depressant dosages and two target grinds. Rough estimates of the grade and recovery

attained at the EPA concentrator at the time of the survey are also provided. Note that this is simply to contextualise the laboratory data - the EPA data is not directly comparable to the laboratory data – the UG2 feed sample for the laboratory test work was taken a year before the EPA samples, the grind is different, and it is typical to achieve higher grades and recoveries in laboratory test work than it is on the plant.

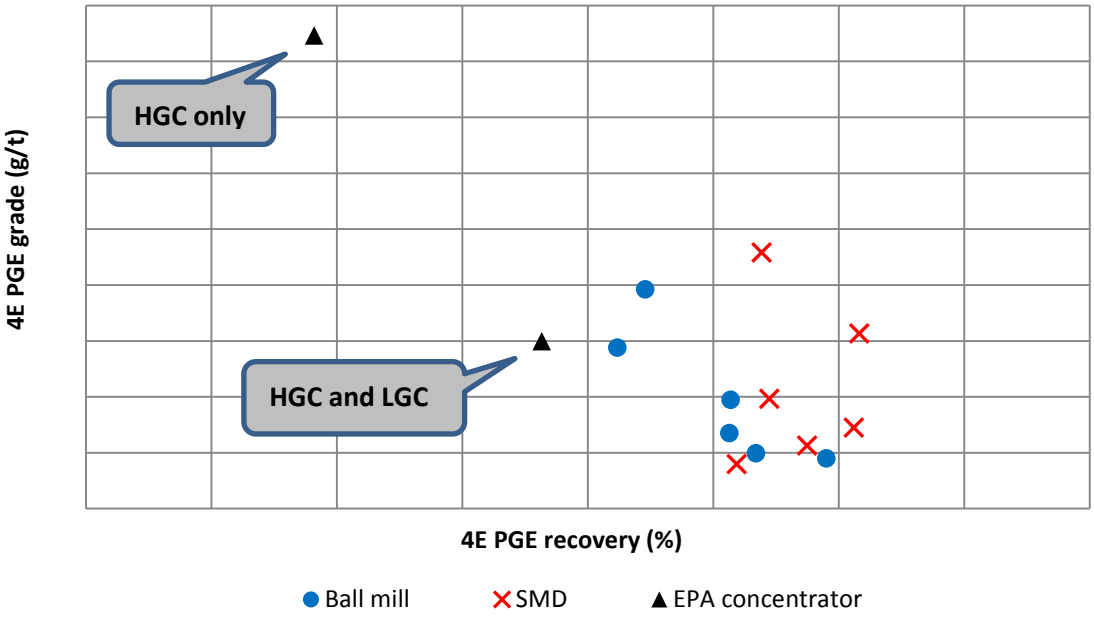

Figure E.3: Grade vs recovery for the laboratory flotation test work, with plant samples included for reference.

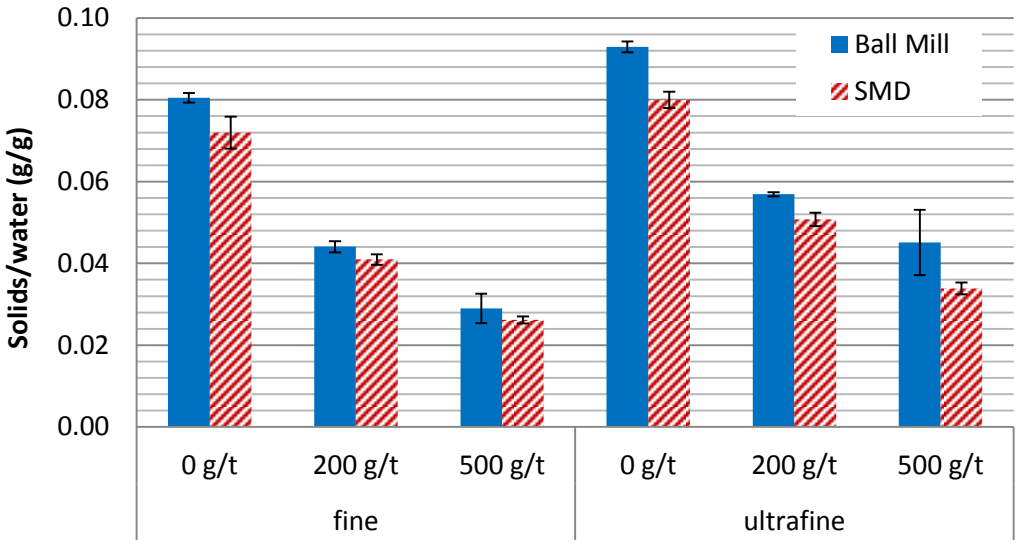

Figure E.4: Total solids per unit water recovered for the two target grinds and three depressant dosages. Error bars show 95% confidence intervals.

The differences observed in PGE recoveries for the two mill types do not appear to be attributable to liberation. Of the PGM liberation data presented in Section 6.3.3 for the SMD and ball mill ultrafine grinds, the narrow confidence limits that would be required to disprove the null hypothesis that there is no difference in liberation data based on PGM particle count would likely be unattainable at any reasonable confidence level. The liberation data weighted by area of PGMs, which is likely biased due to the low number of coarse PGMs measured, does suggest that the SMD produces a greater proportion of floatable PGMs (liberated and associated with base metal sulfides). Perhaps it could be speculated that this may reflect a real difference i.e. larger BMS - PGM particles are liberated at a coarser size in the SMD than in the ball mill, and that this in turn leads to less sensitivity of the particles containing PGMs towards other factors such as froth stability.

E.2 Particle shape and recovery by true flotation

For UG2 ore it would be difficult to detect any direct effects of particle shape on PGM flotation due to the extreme variability in nature and occurrence of the PGMs. The variability in PGM speciation, liberation, associations and grain size (illustrated in E.4) would be likely mask any effects of shape unless very large PGM datasets were available.

In the laboratory work, particle shape characteristics of the gangue could be affecting froth stability, with the more elongated particles in the ball mill ultra-fine grind possibly contributing to the slightly higher froth loadings observed for these flotation tests in Figure E.4. However, the slightly steeper, finer ball mill PSDs (illustrated in Figure 6.3), are more likely to be responsible for this difference.

For an indication of the effects of shape on true flotation, without attempting to decouple mineralogical effects, the roughness categoriser ‘jaggedness’ which was demonstrated in Section 4.15, was applied to the top size fraction of the high grade and low grade EPA concentrates as well as the corresponding size fraction of the PRF. This data is presented if Figure E.5. At this stage, the liberated chromite information was separated from the ‘other’ particles as it was considered the proportion most likely to confound the results with much smoother particles in this size range, and very different proportions of chromite within the feed and concentrates. Significant differences in liberated BMS or ‘other’ could then perhaps be attributed to effects of roughness on recovery by particle-bubble attachment. The data for the liberated BMS in the PRF was not presented due to an insufficient number of particles in this category. It should also be noted that the BMS does not represent an ideal control, because the speciation does change, with nearly all of the liberated chalcopyrite, pentlandite, galena and pyrite recovered to the high grade concentrate, and the slow floating pyrrhotite comprising the

majority of the liberated BMS in the low grade concentrate. Nevertheless, the difference in jaggedness between the BMS in each concentrate is minimal. The differences between the liberated chromite, liberated BMS and 'other' particle classes are more significant than the differences between the samples. The slightly higher roughness of the 'other' in the high grade concentrate than in the low grade concentrate could indicate the occurrence of the effect expected based on literature, with more rough particles showing higher particle-bubble attachment rates (Rahimi et al., 2012; Verrelli et al., 2012a, 2012b, 2014; Vizcarra et al., 2011a).

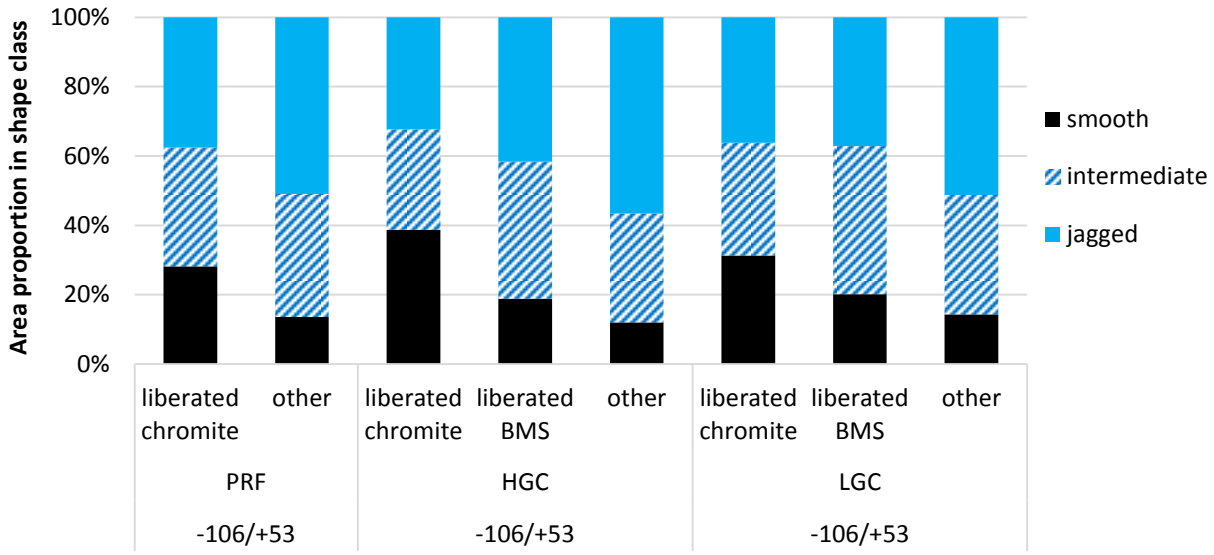

Figure E.5: Jaggedness shape classes (based on roundness and aspect ratio), for various particle categories in the EPA primary rougher feed, high grade concentrate and low grade concentrate. Data weighted by area, n > 400 for each category.

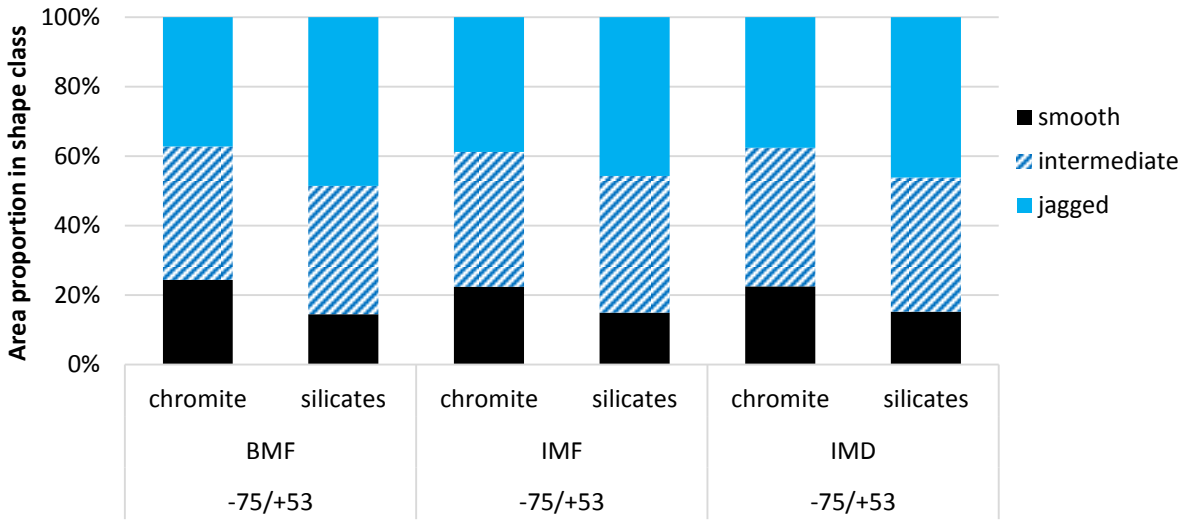

Figure E.6: Jaggedness shape classes for chromite and silicates in the ETTP ball mill feed, IsaMill feed and IsaMill discharge.

In order to contextualise the data relating to effect of shape on flotation, the comparative data for the ETTP ball mill and IsaMill samples is presented in Figure E.6. This data, along with that presented in Section 6.3, has indicated that the effects of fine grinding in different mill types is unlikely to significantly influence the flotation performance of UG2 ore through effects on particle shape or roughness. However, the effects of particle shape on entrainment still represent a gap in our understanding of particle behaviour within flotation, thus the analysis in Paper 5 and the recommendation for additional research on this topic.

E.3 Fine grinding, shape and chromite entrainment (laboratory data)

The data assessed in Paper 5 was based on the samples from the EPA concentrator. Some background information was omitted from Paper 5, which was brought to the authors' attention after publication. Of most significance was the lack of reference to the secondary cleaner tails stream and its flow-rate in the analysis. From a previous survey, the solids recovery to the secondary cleaner tails was approximately 5% (relative to the primary rougher feed flow rate). The shape characteristics of chromite particles within this stream could have been included in the analysis and this may have added additional insight towards decoupling entrainment within the roughers and entrainment within the cleaners. The fact that this stream was ignored in the analysis that was carried out will only have had a small impact on the magnitude of the estimated entrainment factors, and not on the trends observed. A disclaimer should have been included in the paper, highlighting that the magnitudes of the estimated entrainment factors used in the analysis are likely to have limited usefulness or applicability in future research. This is primarily due to the complex network of flows between the rougher and cleaner banks which leads to the fact that these banks are not "fully linked". These limitations do not invalidate the conclusions from the work, as these were dependent on the trends observed rather than the magnitude of the estimated entrainment factor values.

The corresponding data from the laboratory fine grinding and flotation test work is presented here for completeness, although due to the fineness of the recovered concentrates it does not contribute significantly to our understanding of the effect of shape on entrainment.

For the laboratory scale investigation, the entrainment factors for the two target grinds and three depressant dosages are presented in Figure E.7. As compared to the froth loading data in Figure E.4, the grind is seen to be the dominant variable affecting entrainment factor as opposed to the depressant dosage which had the dominant effect on froth loading. Again, the higher entrainment factors for the ball mill samples are likely due to the steeper, finer product particle size distributions.

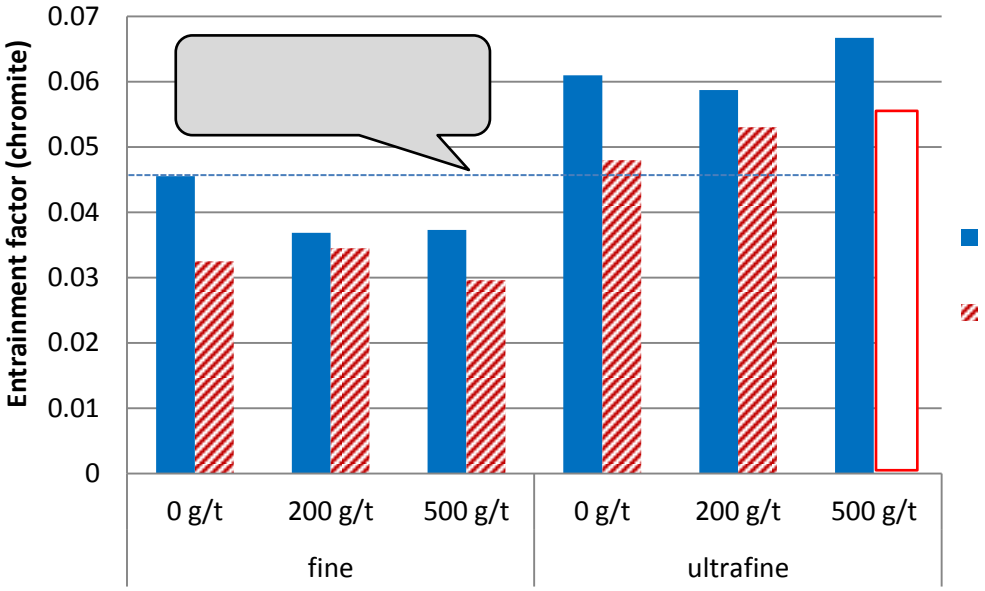

Figure E.7: The entrainment factor for chromite for the laboratory flotation tests with the two mill types, two target grinds and three depressant dosages. The SMD UF 500 g/t combined chromite assay sample was compromised through a mistake in the laboratory.

The approach applied in Section 6.10.3 was applied to the fine grinding and flotation test work data and the results are presented in Figure E.8. All the concentrate test data taken from a variety of depressant dosage and grinding conditions (shown in red) is compared to the feed data (blue). The data from EPA is also presented for comparative purposes. It is apparent that the laboratory data was insufficient to draw any conclusions relating to the effect of shape on chromite entrainment.

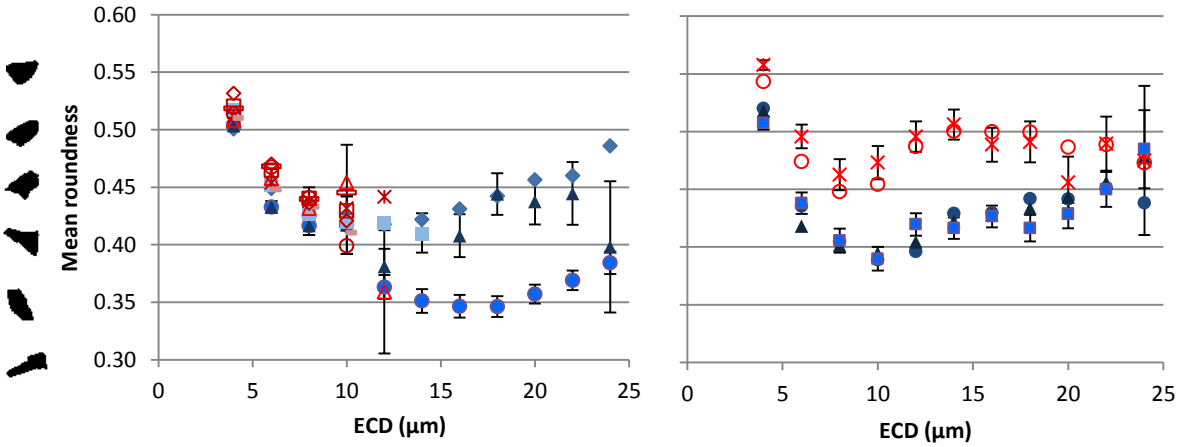

Figure E.8: Compilation of laboratory (left) and plant data (right), comparing the mean roundness of concentrates (red) to feeds and tails samples (blue). The number of particles analysed per data point varies between 60 and 3000, with error bars showing 95% confidence intervals.

E.3 Chromite recovery by true flotation

The chromite in UG2 ore is naturally hydrophilic and is therefore principally recovered by entrainment (Hay and Roy, 2010; Nel et al., 2004; Wesseldijk et al., 1999). In the literature, 50 μm has been considered the cut-off size above which mechanisms other than entrainment are likely responsible for particle recovery (Ekmekçi et al., 2003; Hay and Roy, 2010). The recovery of chromite in these fractions has previously been attributed to inadvertent activation of chromite or the occurrence of talc rimming rendering the chromite particles naturally floatable (Hay and Roy, 2010; Mailula et al., 2003; Wesseldijk et al., 1999). In the fine grinding laboratory test work for flotation tests with depressant, the concentrate samples had PSDs with over 95% passing 10 μm, so it was safe to assume that entrainment was the dominant mechanism of chromite recovery. In Section 6.13.1 considering the EPA concentrator data, the chromite recovered in the top size fractions of the concentrate (+53 μm) was minimal relative to that in the finer fractions, but still significant. Calculations performed for the size-by-size recovery indicated that this fraction accounted for 7.7% of the chromite recovered to the high grade concentrate, and 2.3% of the chromite recovered to the low grade concentrate. Samples from these fractions were therefore analysed using QEMSCAN with EDS particle mapping. The mode of occurrence of chromite within this fraction of the primary rougher feed and two concentrates is illustrated in Figure E.10. However, first it is important to note that the chromite recovery to the -106/+53 μm fraction constitutes a very small proportion of the total chromite recovered to the concentrates. This is emphasised in Figure E.9 which illustrates the relative proportions of chromite within the different size fractions of the HGC, LGC and SRT. If this diagram were to be used to illustrate recovery, the purple and blue bars representing the concentrate samples would need to be 100 times smaller as the total solids recover to the concentrate is close to 1%.

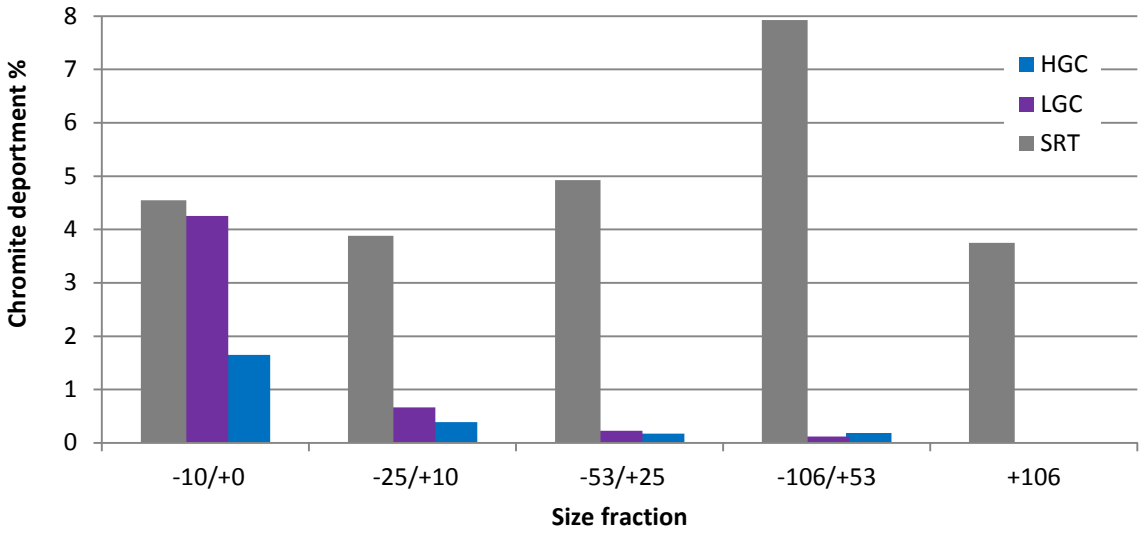

Figure E.9: Deportment of chromite in the secondary rougher tails, high grade concentrate, and low grade concentrate samples. Note, the lower values for the concentrate samples simply indicate the reduction in chromite grade- if the purple and blue bars were 100 times smaller they would more accurately represent the proportions of chromite recovered to the concentrate in each fraction.

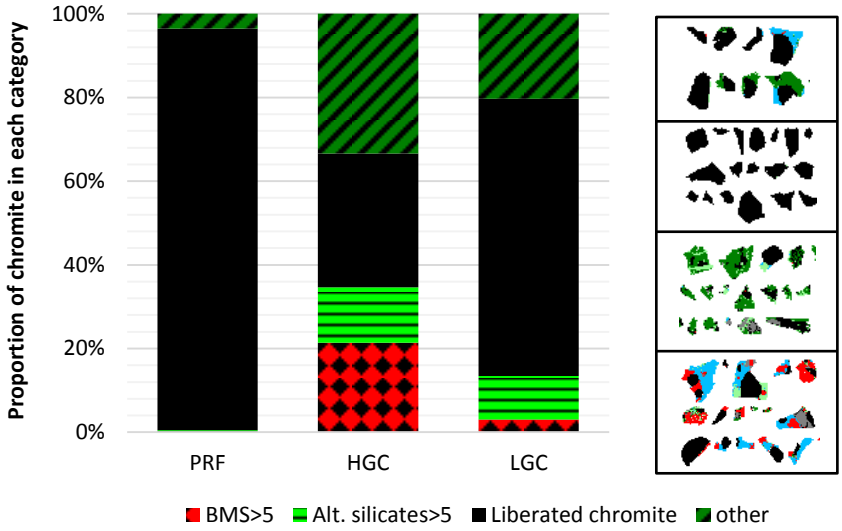

Figure E.10: Associations of chromite in the +53/-106 µm fractions of the EPA concentrator samples of the primary rougher feed (PRF), high grade concentrate (HGC), and low grade concentrate (LGC).

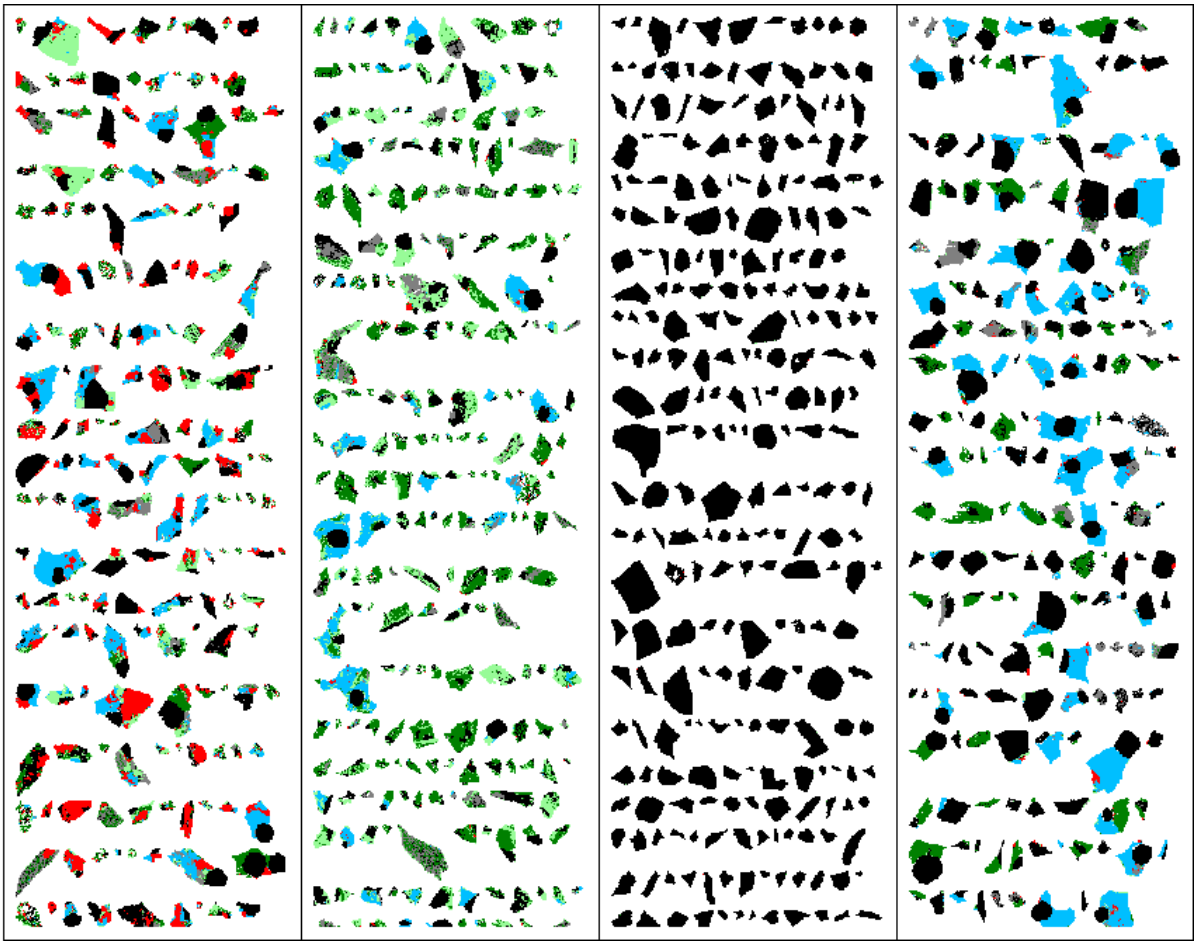

Figure E.11: Additional false colour images of particles containing chromite within the high grade concentrate classified into the same association groups in Figure E.10 for a qualitative description of these particles.

Figure E.10 shows that the majority of the chromite in the PRF is liberated, but as only less than 1% of the chromite in the PRF is recovered to the concentrates, the small proportion that is associated with other minerals has a much higher likelihood of being recovered to the concentrates. It is also important to bear in mind that 2-D typically underestimates 3-D liberation characteristics, so the proportion of chromite recovered to the high grade concentrate that is associated with either naturally floatable gangue or base metal sulfides is likely even higher. The high grade concentrate comprises fast floating, high grade particles and has a lower mass pull and residence time than the low grade concentrate. The recovery of coarse chromite by true flotation is therefore more likely to be responsible for the chromite recovered to the primary concentrate, and perhaps a combination of true flotation and other mechanisms such as entrapment for the low grade concentrate which is collected over a longer time period with a higher total mass pull.

E.4 Gallery: BSE and false colour images of particles after fine grinding

In publications there is often limited space to present photographs of particles. Nevertheless, these can convey valuable qualitative information, so some additional false colour and BSE images obtained during the analysis for Paper 4 are provided here. These illustrate the varied mode of occurrence of PGMs within the ore.

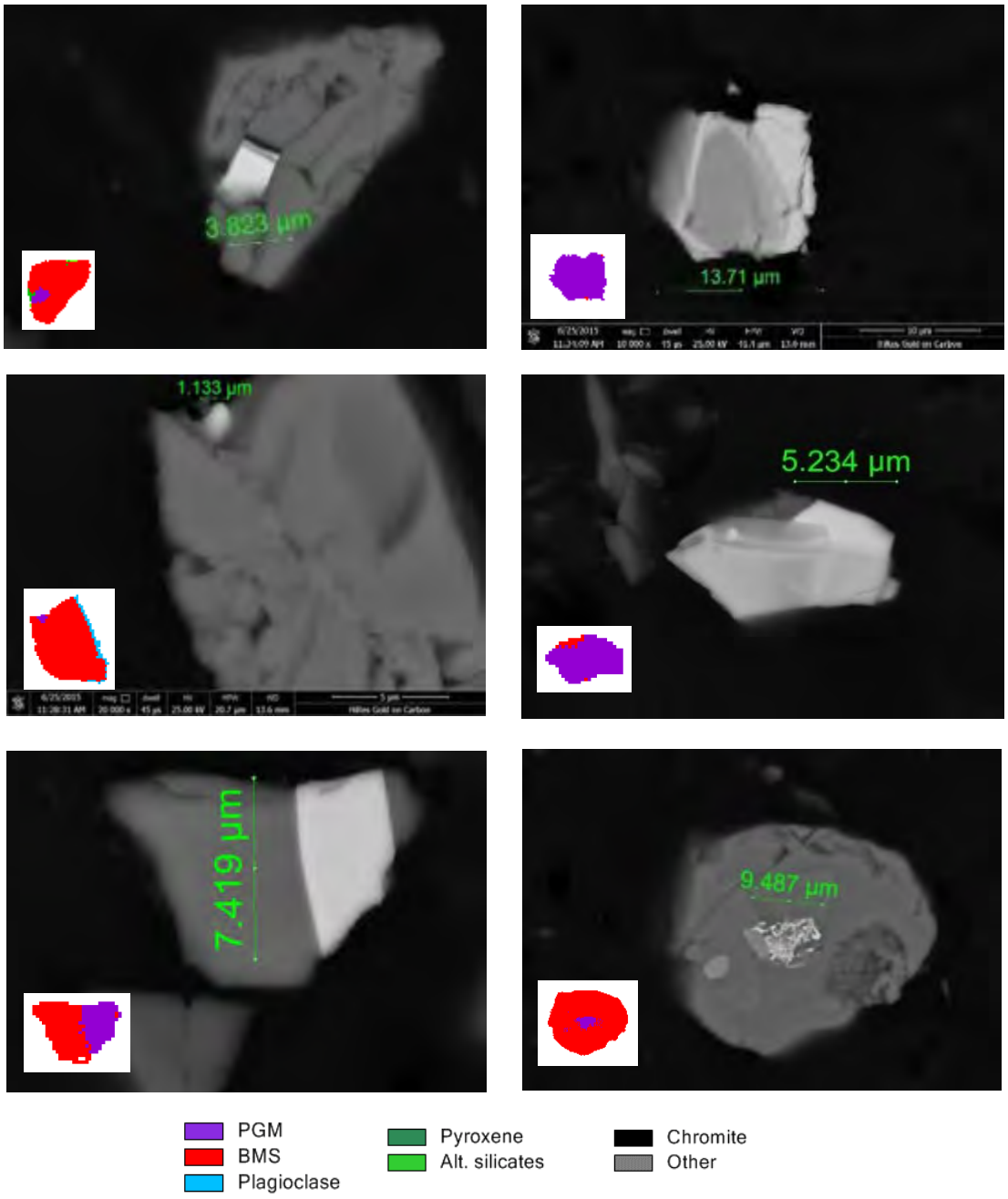

Figure E.11: Back scattered electron images taken with the FEG QEMSCAN 650F of the PGM grains identified within the ball mill ultra-fine grind (BM UF) product sample.

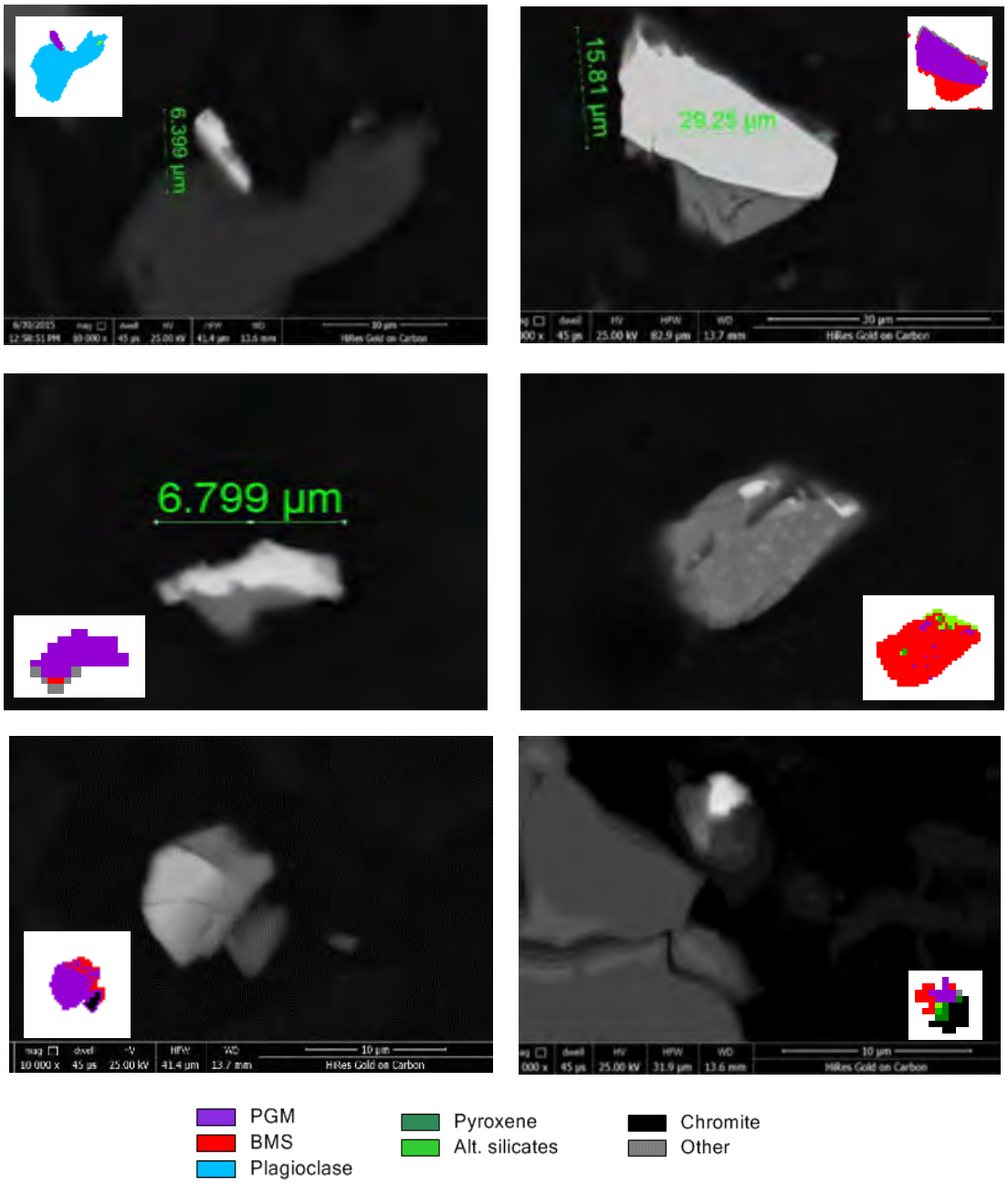

Figure E.12: Back scattered electron images taken with the FEG QEMSCAN 650F of the PGM grains identified within the SMD ultra-fine grind (SMD UF) product sample.

Appendix F: Assessment of sampling error for Paper 5

F.1 Application of Gy's formula for estimation of sampling error in EPA samples

In Paper 5, a concern was raised about whether the samples taken from the plant were large enough to have reduced the random error associated with sampling to an acceptable level. Gy's formula for particle size analysis was therefore applied retrospectively to the chromite shape entrainment analysis to determine whether the 300 g samples used for screening enabled adequate accuracy to determine whether the difference between shape of chromite in the -25/+10 μm for the primary rougher feed (PRF) and high grade concentrate (HGC) was significant at the 95% confidence level. The conclusions of this analysis were reported in the paper, and the supporting calculations are reported here.

The initial mass sampled from the plant was 5 – 12 kg for each sample. This was then split in a 10 way rotary splitter to obtain samples weighing approximately 300 g for wet and dry screening. The proportion of interest was a combination of size, grade and shape which has not been considered in previous work. However the formula presented by Napier Munn (2015, pp. 551), as derived by Barbery for size analysis was applied, with the value for P simply adjusted to incorporate size, shape and grade. The proportions of the total sample which were made up of chromite in the -25/+10 μm size class were found to be 3.52 and 0.855% for the PRF and HGC respectively. Note that the PRF has a much higher chromite grade, but also a much coarser size distribution than the HGC. The proportions of the chromite particles in these fractions with roundness values greater than 0.6 were 12.4% and 21.1% respectively. The proportions of the total sample made up of chromite particles in the -25/+10 μm size fractions, with a shape factor greater than 0.6 were therefore (3.52 * 12.4) and (0.855 *21.1) = 0.44% and 0.18% respectively. In order to determine the relative error associated with these proportions, the following formula was used (Napier Munn, 2015, pp. 551):

$$\sigma_{FE} = \sqrt{\frac{f\rho {d_m}^3}{MP}}$$

Where M = total mass of sample (300 g)

f = shape factor for material (typically estimated as 0.7 for quite rounded samples – another indication of the guesswork typically associated with shape)

ρ = density of material (3.9 $g.cm^{-3}$)

d_m = mean size of the size range of interest (0.00203 cm)

P = expected proportion of material in the size range of interest (0.0044 and 0.0018)

σ_{FE} = relative standard deviation of P

Using the above combination of estimates and measured values, σ_{FE} = 0.00013 and 0.0002 respectively. With M = 700 mg, these values are still under 1%, which is what led to the statement that was made in Chapter 5.xx. However the statement was perhaps misleading as it does not acknowledge that the proportions of interest (P) are also very small. The 95% confidence intervals for these proportions (based on 300 g sample mass) can be quoted as 0.44 +/-0.03% and 0.18 +/-0.04% for the PRF and HGC respectively. Unfortunately, these proportions are not actually the proportions on which we are basing our conclusions i.e. the 12.4% and 21.1% of the chromite particles in the specified size class which have roundness > 0.6. However, if we used these proportions for P, we would likely severely underestimate the error (2.5 x 10^{-5} and 3.7 x 10^{-5}% respectively). Rather, a more conservative estimate was obtained by determining the relative error associated with the proportion of the total samples comprising the particles of interest i.e. 0.03 * 0.44 = 6% and 0.04 * 0.18 = 22% respectively (quite large). Now 12.4% + 6%*12.4 = 13.2 % is the estimate for the upper 95% confidence limit on the proportion of rounded chromite in the -25/+10 μm size fraction of the PRF, and 21.1% - 22%*21.1 = 16.4 % is the estimate for the lower 95% confidence limit of the proportion of rounded chromite in the -25/+10 μm size fraction of the HGC. To phrase this properly, the null hypothesis that the chromite has the same shape characteristics in the PRF and HGC in the specified size class can be rejected at the 95% confidence level.